Fabrication of novel in-situ remediation tools for unconventional oil contamination

SEYYED MOHAMMADREZA DAVOODI

A DISSERTATION SUBMITTED TO
THE FACULTY OF GRADUATE STUDIES
IN PARTIAL FULFILLMENT OF THE REQUIREMENTS
FOR THE DEGREE OF
DOCTOR OF PHILOSOPHY

GRADUATE PROGRAM IN CIVIL ENGINEERING
YORK UNIVERSITY
TORONTO, ONTARIO

September 2022

ABSTRACT

The aftermath of unconventional oil (UO) accidents highlights the lack of preparedness of governments to deal with UO emergencies. Because bioremediation is considered slow process, physicochemical treatment processes are necessary in removing contaminants to constrain the spread of oil. In preliminary phase of study, bed systems for adsorption of oil compounds packed with modified dolomite were applied as pre-treatment for bioremediation systems. The high affinity of oil molecules to the active sites due to hydrophobic nature of dolomite surface, as well as low solubility of oil in water, resulted in rapid process of oil adsorption on external surface of modified dolomite. UO contaminated site contain high concentration of polyaromatic hydrocarbons (PAHs). Thus, the final phase of study focused on finding enzyme mixture for biodegradation of PAHs contaminated sites for water and soil treatment. In this regard, screening of indigenous bacteria, identification of involved enzymes, and biodegradation tests were carried out. Several combinations of the pre-selected strains were used to create most prompting consortium for enzyme production. To mimic *in situ* application of enzyme mixture, bioremediation of pyrene contaminated soil was carried out in soil column tests. The average values of pyrene removal after 6 weeks indicated that the enzyme cocktail can be an appropriate concentration for soil enzymatic bioremediation in the soil column system. A bioinspired device was fabricated as a sustainable remedial method. Our results showed that after 200 seconds of circulating the enzyme solution 100% of anthracene in 1.5 L of 4.6 mg/L was removed from the beaker side. In addition to the circulation of PAH degrading enzymes in hollow fiber lumens, aliphatic degrading enzymes confined in multilayer nanofibrous membrane systems play an important role in the removal of oily compounds. Based on our studies, modified polyimide aerogels were suitable to support enzyme immobilization. The degradation tests clearly showed that immobilized enzymes had biodegradation ability for model substrate in contaminated water. Our results confirmed that immobilization of cocktail enzyme mixture enhanced their storage stability, more than 45% of its residual activity at 15 ± 1 ºC for 16 days. This study could set the guideline for the enzymatic bioremediation of aromatic pollutants especially polycyclic aromatic hydrocarbons in highly contaminated soil and water body.

DEDICATION

TO MY PARENTS

For raising me to believe that anything was possible

TO MY SISTER

For making everything possible

TO MY TEACHERS

For giving me invaluable educational opportunities

ACKNOWLEDGEMENT

I would like to express my humble gratitude to my Ph.D. supervisor, **Professor Satinder Kaur Brar** for her guidance, suggestions, and valuable feedback during my doctoral training. And during the most difficult times when developing the project and writing this thesis, she gave me the moral support and the freedom I needed to move on. I want to equally express my regards to my co-supervisor, **Professor Richard Martel** who helped me in solving essential problems with multi-approach ideas. His constant motivation, support, and encouragement helped me to work with more freedom and passion. I would like to especially thanks to **Dr. Mehdrad Taheran** for his constant guidance and technical support.

I would like to thank **Prof. Emile Knystautas** for their constant support throughout my Ph.D. program.

A much and special thanks to my research partner **Dr. Saba Miri** for his valuable feedback and for a cherished time spent together in the lab. I would like to thank all the laboratory personnel from INRS, especially **Mr. Stephane Moise** for the instrument training. I would like to express my humble gratitude and genuinely like to thank my teammates and colleagues who supported me throughout my Ph.D. study, especially, **Dr. Lecka Joanna, Dr. Carlos Osorio Gonzalez, Dr. Rama Pulicharla, Dr. Pratik Kumar, Mr. Rahul Saini, Dr. Agnieszka Cupryś, Dr. Naghdi Mitra, Dr. Joseph Sebastian, Mr. Mohammad Hossein Karimi Darvanjooghi, Mrs. Gurpreet Kaur, Mrs. Noha Hasaneen, Mrs. Pratishtha Khurana, Mr. Xuhan Shu, Dr. Krishnamoorthy Hegde, Mrs. Mariana Valdez, Dr. Bikash Tiwari, Mr. Behnam Nayebi, Mrs. Shiva Akhtarian.** It would be incomplete without thanking my interns, **Mrs. Anupriya Ravula**, **Dr. Dheeraj Sharma,** and **Mr. Jose Alberto**, who assisted me during the project. Finally, I would like to give my sincerest thanks to my parents, and my sister who constantly supported and motivated me.

TABLE OF CONTENTS

LIST OF TABLES

LIST OF FIGURES

GRAPHICAL ABSTRACT

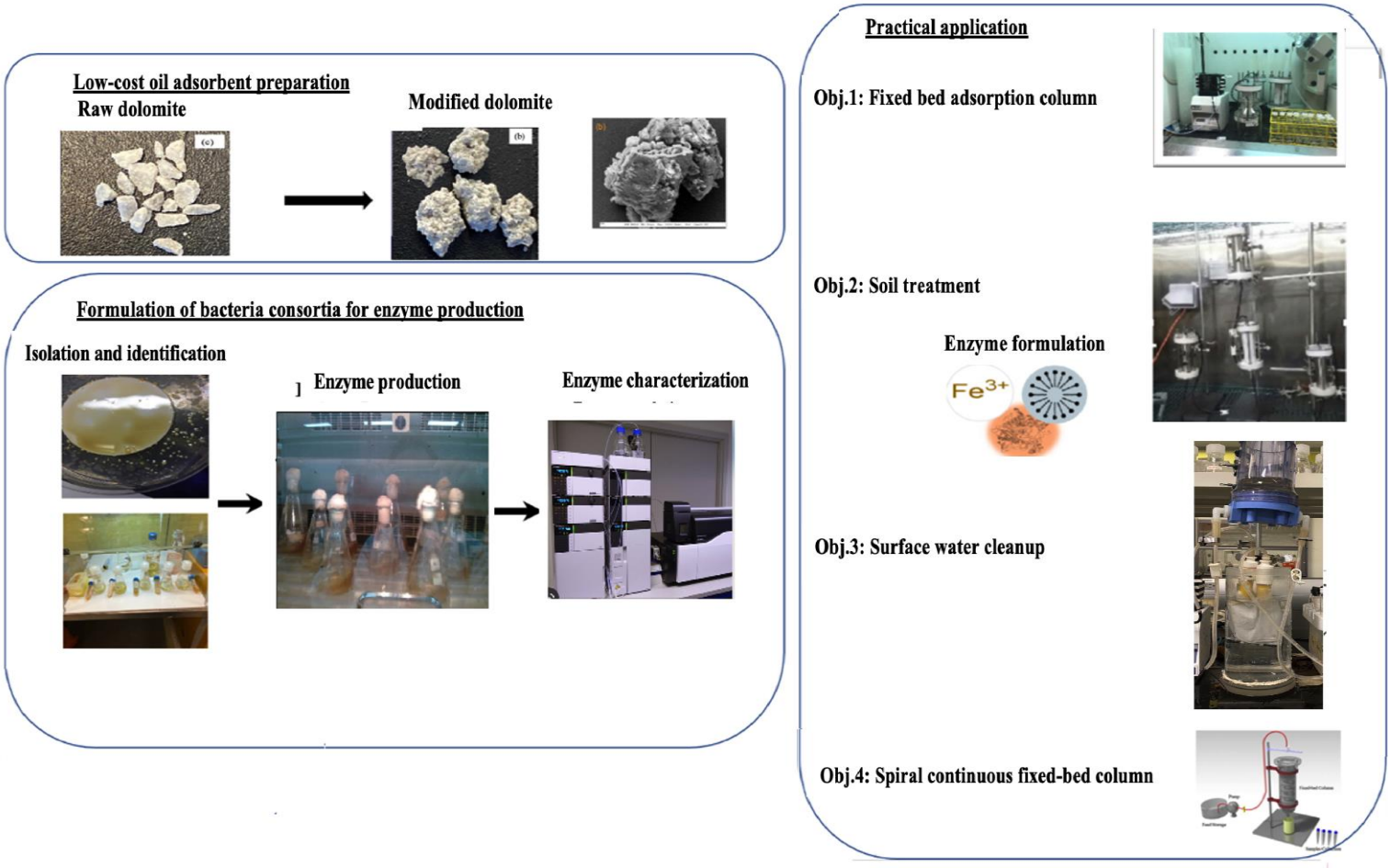

LIST OF PUBLICATIONS OF THIS THESIS

- **Patent and invention disclosure**

1. **Davoodi, S. M.,** Miri S., Brar SK. Enzyme Booster Technology (EnBooT) for advanced decontamination of petroleum hydrocarbons, Provisional filed. Invention disclosure submitted to York innovation office.

- **Peer-reviewed scientific articles from this thesis**

1. **Davoodi, S. M**., Miri, S., Taheran, M., Brar, S. K., Galvez-Cloutier, R., & Martel, R. (2020). Bioremediation of Unconventional Oil Contaminated Ecosystems under Natural and Assisted Conditions: A Review. Environmental Science & Technology, *54*(4), 2054-2067.
2. **Davoodi, S. M**., Taheran, M., Brar, S. K., Galvez-Cloutier, R., & Martel, R. (2019). Hydrophobic dolomite sorbent for oil spill clean-ups: Kinetic modeling and isotherm study. *Fuel*, *251*, 57-72.
3. **Davoodi, S. M.,** Brar, S. K., Galvez-Cloutier, R., & Martel, R. (2021). Performance of packed and fluidized bed columns for the removal of unconventional oil using modified dolomite. *Fuel*, *285*, 119191.
4. **Davoodi, S. M.,** Miri, S., Kaur Brar, S., Knystautas, E., & Martel, R. Simulation of Novel Jellyfish Type of Process for Bioremediation Application. *Available at SSRN 4140189*.
5. **Davoodi, S.M.,** Miri, S., Brar, R., Martel, R., 2022. Enzymatic biodegradation of Polyaromatic Hydrocarbons contaminated soil using cold-active enzymes: A soil column study. Environmental science & technology. Under review.
6. **Davoodi, S.M.,** Miri, S., Brar, R., Martel, R., 2022 Continuous fixed-bed column studies to remove polycyclic aromatic hydrocarbons by degrading enzymes immobilized on polyimide aerogels, *Journal of water processing. Under review.*

LIST OF CONFERENCES

1. Miri S., **Davoodi, S. M.,** Brar S.K, Kadri T. (2021). Enzymes: Catalysts to remediate Conventional and Unconventional Oils. 71st Canadian Chemical Engineering Conference, Montreal, Canada. October 24^{th} – 27^{th}.

2. **Davoodi, S.M,** Brar S.K, Martel R (2021). Removal of unconventional oil from stream water using bio-regenerated filter media after chemical De-emulsification. 43rd AMOP Technical Seminar on Environmental Contamination and Response, Jone 8th 2021 (Virtual Access). Chateau Lacombe Hotel, Edmonton, **Canada.**
3. 33rd CAWQ symposium, "Hydrophobic Dolomite for Emergent Cleanup of Unconventional Oil Spillage: Batch and Continuous Study", 27th Feb,2019
4. Miri S., **Davoodi, S. M.,** Brar S.K, Kadri T. (2021). Preliminary talk (Invitation). Enzymes: Catalysts to remediate Conventional and Unconventional Oils. 71st Canadian Chemical Engineering Conference, Montreal, Canada. October 24th – 27th. Oral presentation.
5. **Davoodi SM.,** Brar S.K, Martel R. (2022), SETAC North America 43st Annual Meeting. (Oral presentation). Nov 13-15th, 2022, Pittsburgh, United states.

- **Book chapters**

1. **Davoodi, S. M**., Darvanjooghi, M. H. K., & Brar, S. K. (2022). Perspectives on the use of modular systems for organic micropollutants removal. In Modular Treatment Approach for Drinking Water and Wastewater (pp. 33-53). Elsevier.

List of Abbreviations

AAD	Absolute average deviation
AF	Culture isolated from Ohio River;
ACW	Access Western Blend
API	American Petroleum Institute
ATR	Attenuated total reflectance
BTEX	Benzene, Toluene, Ethylbenzene, Xylene
BUD	Bioinspired Unconventional Decontamination
BBD	Box-Behnken design
COSR	Canada's oil sands region
CFSE	Carboxyfluorescein succinimidyl ester
C2,3D	Catechol dioxygenase,
CLB	Cold Lake Blende
KR	Culture isolated from Kalamazoo River
CYP	Cytochrome P450
Da	Dalton
DNAPL	Dense nonaqueous phase liquids
DCM	Dichloromethane
FDR	False discovery rate
FBCS	Fixed bed column system
FBC	Fluidized bed column
FTIR	Fourier-transform infrared spectroscopy
GC	Gas chromatography
GMOs	Genetically modified organisms
GF/C	Glass microfiber filters Grade
HMW	High molecular weight
HLB	Hydrophile–lipophile balance
HY	Hydroxy-2- naphthoate hydroxylase
LFD	Linear film-diffusion
LC-MS/MS	Liquid chromatography-Tandem mass spectrometry
MALDI-MS/MS	Matrix-assisted laser desorption/ionization mass spectrometry
NDH	Naphthalene dioxygenase
NAD(P)H	Nicotinamide adenine dinucleotide phosphate
ND	Not Determined
NB	Nutrition Broth

PCSP	Precipitated calcium carbonate sorbent powder
PAA	Poly (amic acid)
PAN	Polyacrilonirtile
PS	Polyester
PEI	Polyethylenimine
PCR	Polymerase chain reaction
PAH	Polynuclear aromatic hydrocarbon
PVDF	polyvinylidene fluoride
PCA	Principle Component Analysis
PA	Protocatechuic acid
PBC	Prudhoe Bay Crude
PSO	Pseudo-First-Order
PSO	Pseudo-Second-Order
PD	pyrene dioxygenase,
PPQ	Pyrroloquinoline quinone
RP	Redlich-Peterson
RNA	Ribonucleic acid
SEM	Scanning Electron microscopy
SD	Standard deviation
SFG	Sum frequency generation spectroscopy
SNE	Sum of normalized error
SQR	Sum of the square of the errors
TGA	Thermos gravimetric analysis
TPH	Total Petroleum Hydrocarbons
TEA	Triethylamine A67
TSB	Tryptic soy broth
USA	United States of America
WCS	Western Cadandia Select
XPS	X-ray photoelectron spectroscopy
XRD	X-ray powder diffraction
XMO	Xylene- monooxygenase
ZPC	zero potential charge

List of Symbols

a	Area under the breakthrough curve up to break point (mg min L^{-1})
A	Area of the column (cm^2)
t_b	Break point time (min)
A_T	The Temkin adsorption constant (L g^{-1})
B	Redlich-Peterson adsorption constant (L mg^{-1})
C	Constant of intraparticle diffusion model (mg g^{-1})
R^2	Correlation coefficient
d_p	Particle diameter of modified dolomite (mm)
c_p	Concentration of oil in the stagnant liquid phase (g L^{-1})
$c_{t,out}$	Concentration of oil in the effluent solution at any time (g L^{-1})
D_{ax}	Axial dispersion coefficient (cm)
D_m	Molecular diffusivity (cm^2 min^{-1})
C_O	Initial oil concentration (mg L-1)
k_F	Freundlich adsorption isotherm constant (mg g^{-1} $(L/g)^{1/n}$))
k_{film}	External mass transfer coefficient (cm min^{-1})
k_L	Langmuir constant (L g^{-1})
R	Oil removal percentage
D_{epp}	Apparent diffusion coefficient (cm^2/s)
β	Desorption Constant (g mg^{-1})
α	Initial oil sorption rate (mg g^{-1} min^{-1})
m	Adsorbent mass (g)
K_{WM}	Intra-particle transfer rate constant (mg g^{-1} $min^{-1/2}$)
i	Hydraulic gradient
K	Permeability Coefficient
$\bar{q}$	Average adsorbed-phase concentration of oil in the micopore (mg L^{-1})

$\bar{\bar{q}}$	Average adsorbed-phase concentration of oil over a particle (mg L^{-1})
F	Flow rate (mg/L)
R^2	Correlation coefficient
K_1	Pseudo-first-order rate constant (min^{-1})
K_2	Pseudo-second-order rate constant (g mg^{-1} min^{-1})
K_{TO}	Langmuir adsorption constant
K_{td}	Intraparticle diffusion rate constant (mg g^{-1} $min^{-1/2}$)
K_s	Constant related to the energy of the adsorption (L g^{-1})
h_1	Initial rate of sorption (min^{-1})
q_t	Amount of oil absorber at t (mg g^{-1})
q_e	Equilibrium sorption capacity (mg g^{-1})
$q_{e,meas}$	Experimental adsorption capacity at equilibrium (mg/g)
$q_{e,calc}$	Theoretically calculated adsorption capacity at equilibrium (mg/g)
q_m	Monolayer adsorption capacity
n	Number of observations in the experimental dat
C_O	Initial oil concentration ($g\ mL^{-1}$)
C_e	Equilibrium oil concentration ($g\ mL^{-1}$)
V	The volume of solution (L)
a	Particle size (cm)
R	Universal gas constant (8.314 j/mol.K)
C_p	Heat capacity (j/mol.'K)
K_c	Equilibrium constant for hydrogenation reaction
a_x	Concentration (mol/m^3)
$ierfc$	The error function
r	Radial position
D_{epp}	Apparent diffusion coefficient (cm^2/s)
f_{ax}	The relative fraction of sorbent particles

ρ	Density (kg/m^3)
β	The desorption Constant (g mg^{-1})
α	The initial oil sorption rate (mg g^{-1} min^{-1})
m	The adsorbent mass (g)
K_{WM}	Intra-particle transfers constant rate (mg g^{-1} min$^{-1/2}$)

CHAPTER ONE: INTRODUCTION & RESEARCH OBJECTIVES

PART 1- INTRODUCTION

It is a general understanding that unconventional oil is petroleum-extracted and processed into petroleum products using the unconventional method. Oil extracted from the oil sands is referred to as Bitumen. Due to its high viscosity, the bitumen is diluted with lighter petroleum products and benzene-containing diluents to produce diluted bitumen (hereafter mentioned as Dilbit). Currently, the majority of the Dilbit from the oil sands is sent to upgrading and refining facilities in Canada and the United States of America (U.S.A.) (Stout and Wang, 2017). In Canada, oil sands are found in the form of bitumen in three main geological zones, named Canada's oil sands region (COSR), including the Athabasca, Peace River, and Cold Lake which make up the third-largest proven oil reserves in the world, after Venezuela and Saudi Arabia. The technology of unconventional oil extraction from the rock, the costs of production, and the management of wastes and residues together with the oil transportation from sources are generally more complex and expensive than traditional petroleum, for example, in North Africa and the Persian Gulf. Oil generated by the Bakken shales is the other unconventional oil source of petroleum that is generally different from traditional crudes, for example, Texas crude oil. Bakken production has also increased in Canada since the 2004 discovery of the Viewfield Oil Field in Saskatchewan with the advent of horizontal drilling and hydraulic fracturing technologies.

Despite difficulties in extraction, production and ultimately the transport of crude oil, numerous oil industries are investigating these sources. This has increased the risk of incidents during the transportation of crude oils. It is the case in the U.S. with a light oil that has largely come from tight resource formations in regions of the Bakken Permian Basin with a prevision of 2 M barrels per day (bbl/day) in 2025 or Canada with bituminous sands (as Dilbit from Athabasca) with previsions exceeding the 3 M bbl/day in 2024. Multiple factors including aging infrastructure, ground failures, such as densifications, pipeline incidents, and increased rail transport, that uses unsafe tanker cars have increased the risk of unconventional oil spill incidents during the transportation of these hydrocarbons (EIA, 2008; Fielding et al., 2010; Gordon, 2012; Speight, 2013; Stout and Wang, 2017). With this rapid development of new supply sources, the other environmental problems associated with unconventional oils that have raised concerns over oil spills include waste generation and leakage from the streamer, underground tanks, and abandoned bitumen refinery sites. The aftermath of recent high-impact oil spill incidents (i.e., The

Northwestern Ontario derailment incident) highlights the lack of preparedness of governments to deal with unconventional oil emergencies (Fielding et al., 2010).

The inability to timely control the hazards; constrain the spread of oil, and efficiently protect polluted zones has been attributed to the differences between unconventional oil and traditional petroleum characteristics and their behavior in the environment. In order to address these issues, novel Dilbit/Bakken spill response techniques classified as chemical and physical/chemical have been recently applied to decrease the remediation time by: (1) limiting the movement of surface oil slicks using high-temperature oil booms, (2) reducing the water/oil interfacial tension using dispersants, (3) uptake of unconventional oil using superhydrophobic sorbents and magnetic particles applied in novel absorbent techniques, and (4) separating oil and water *in situ* without additional energy input using hydrophobic meshes. (Prendergast and Gschwend, 2014; Ridley, 2018) Moreover, the use of dispersants which makes water resources more toxic than oil has changed the scenario for spilled oil clean-up. Therefore, the removal of spilled oil from water resources is still a very topical issue (Hua et al., 2018). Coalescers for oil/water separation are not appropriate for dispersions that contain surfactants and electrolytes. Hence, among physicochemical methods, adsorption has attracted much attention in recent years. The manufacture and use of modular equipment for control and recovery of oil spills by engineered adsorption systems using granular activated carbon and organoclay is an example of this physicochemical method. Due to the low initial cost and low maintenance costs, packed bed systems are commonly used to perform separation processes in industrial processes, such as absorption, stripping, and distillation, and to carry out chemical reactions involving sold particulates either as a reactant or a catalyst. For environmental water treatment, many studies using packed beds for the adsorption of oil and VOCs from an aqueous phase are also well documented in the literature (Pintor et al., 2016; Refining, 1969; Wang, 2011).

Regarding the biological degradation of unconventional oil, traditional remediation such as organic amendments using activated sludge, dead plant biomass has been applied to enhance the biodegradation of asphaltene, resin fractions and high molecular weight (HMW) alkylated polynuclear aromatic hydrocarbon (PAH). However, it was generally thought that hydrocarbon-degrading microorganisms isolated from hydrocarbon polluted sites can only grow on the lighter components of bitumen/Bakken, not on the recalcitrant asphaltene, resin fractions, and HMW alkylated polynuclear aromatic hydrocarbon (PAH). Even though biodegradation of these

hydrocarbons has been extensively improved using bioaugmentation and biostimulation (such as organic/active sludge amendments), integrated methods and mechanisms including bioaugmentation, biostimulation, and phytoremediation are necessary to be applied to improve the performance of bioremediation of high concentrations of weathered hydrocarbons and bitumen. Other biotechnological approaches (such as genetically engineering bacteria, immobilization method, and enzyme remediation technology) and newly found potential microbes might also promote the degradation of recalcitrant components (Agamuthu et al., 2013).

In other to develop innovative efficient devices and/ or processes for the recuperation of oil and attenuation measures, there has been a great need to gain in-depth knowledge on the following aspects: (a) fate of dangerous compounds during environmental emergencies, (b) integrated methods for evaluating residual toxicity, (c) methods for understanding biological degradation while treating soils, and (d) the specific mechanism by which microorganisms degrade hydrocarbons, biodegradation patterns, the chemistry of transformation products, and their residual toxicity. (Davoodi et al., 2020)

PART 2- PROBLEM STATEMENT

Based on the literature review, certain problems have been identified for the current research work that should be addressed before formulating hypotheses and objectives. In recent years, remediation companies have applied a variety of technologies to clean up groundwater, soils, and sediments, including chemical methods, thermal treatments, and bioremediation. There is a risk of additional environmental impacts associated with conventional methods due to the production of certain intermediates during the process as well as their high cost and energy consumption. Compared to conventional methods, bioremediation has been found to be more effective, economical, and less damaging to the environment. In the literature, the biodegradation of petroleum hydrocarbons, particularly polyaromatic hydrocarbons, is well documented. In spite of this, most studies have reported a low rate of biodegradation.

Since enzymes transform the substrate in a minute timescale, the enzymatic method requires a shorter treatment period than the microbial method. Nevertheless, enzymatic biodegradation is hampered by inherent instability and high production costs. During these discussions, some technological bottlenecks were identified, and further research inputs were suggested for making

the overall treatment process more sustainable, economical, effective, and toxic-free. Moreover, bioremediation is more effective for confined contaminated areas such as shoreline pond or residential area. Thus, most of the physicochemical treatment processes are found to be effective in removing contaminants as pre remediation to constrain the spread of oil and accelerate the bioremediation and detoxification.

PART 3- CHALLENGES IN APPLICATION OF ENZYMATIC BIODEGRADATION

Based on the literature review, certain problems have been already defined and addressed for the current research work; however, some other issues need to be addressed before formulating the hypotheses and objectives. Different potential approaches for the bioremediation of unconventional oil were discussed in the literature. Some of the relevant problems associated with the current bioremediation practices that need timely attention are as follows:

1.3.1 Toxic intermediate and detection

Some bioremediation treatment methods resulted in the biotransformation of targeted contaminants into intermediate products despite being found effective in removing petroleum hydrocarbons. It should be noted that some of these intermediate products are more toxic than the initial parent compounds, which is why biotransformation is not always a preferred strategy for the management and remediation of pollutant contamination. Consequently, biodegradation should focus on mineralizing the target contaminate into harmless compounds. In order to detect intermediate products, there are two key points to consider:

A) Intermediate compounds may be volatile, semi-volatile, or nonvolatile, requiring a different detection method compared to their parent compounds. It is necessary to use more than two chromatography methods in this case. The first step in determining all the products formed during a reaction is through full scan mass detection. As a result, each compound can be detected according to its nature and according to the appropriate protocol.

B) Different samples exhibit different times and conditions for the formation of intermediates, so sampling should be performed at different times and under different conditions (e.g., without or

with shaking). To study the pathway of newly isolated bacteria, the formation of intermediates is critical.

1.3.2 Low efficiency of oil adsorbents at a high concentration of oil

One problem that arises in practicing the biological method is that toxicity prevents or slows metabolic reactions as well as the growth of the biomass needed to stimulate the rapid removal of contaminants. One potential solution is to remove the contaminant from the environment using non-chemical oil adsorbents and oxidants. Bioremediation is more effective for confined contaminated areas such as shoreline ponds or residential areas. Thus, most of the physicochemical treatment processes are found to be effective in removing contaminants as pre-remediation to accelerate the bioremediation and detoxification.

1.3.3 Challenges in the application of enzyme remediation methods

One of the major challenges in the commercial application of hydrocarbon-degrading enzymes is their inherent instability. The slow rate of bioremediation for unconventional crude oil might be addressed by using enzymes instead of the whole microorganism. Enzymatic technologies for the remediation of unconventional oils can be especially suitable for conditions where rapid bioremediation is needed to mitigate the adverse effects of indigenous microbes. A great deal of effort has been made to address issues regarding the application of enzymes for soil and water remediation. However, the production of purified target enzymes is a costly process; thus, recombinant strains are usually constructed to overproduce the specific enzymes.

There are two points that should be considered for the stability of produced enzyme. First of all, most of hydrocarbon-degrading enzymes such as oxidoreductases have some hydrophobic peptides since they are membrane-associated enzymes. Thus, extraction of them from the cell might affect their activity and it is necessary to mimic the condition in the membrane to enhance their activity after extraction. Secondly, these enzymes usually catalyze the exchange of electrons between donor and acceptor molecules. To perform this function, they employ redox-active centers (i.e., amino acid residues, metal ions, and coenzymes) that depend on co-factors. Other practical issues and challenges in the application of enzyme remediation methods such as cofactor regeneration rates, oxygen mass transfer, overoxidation, and substrate uptake. Moreover, redox

enzymes including oxygenases (e.g., monooxygenase and dioxygenase) require expensive cofactors, such as NAD(P)H and improved cofactor regeneration that increase the specific oxygenase activity of whole-cell oxygenase biocatalysts.

The above-mentioned problem together with the high hydrophobicity of contaminants such as PAHs that makes their diffusion from soil particles by hydraulic flow difficult, inspired researchers to combine two approaches for the adsorption and degradation of contaminants in soil via a phase transfer procedure. In other words, the release of substrates (e.g., PAHs) into the water from the soil particles is very slow because of the hydrophobicity of contaminants; however, innovative processes/devices can accelerate the mass transfer of contaminants and result in little contaminant left in aqueous phase and more of them can be released from the soil particles under the stress of equilibrium. A feasible method for contaminant to interphase transfer and subsequent degradation procedure by providing access for mass transfer and biocatalyst for degradation is crucial for contaminant removal.

PART 4- HYPOTHESES

Petrol hydrocarbons are organic contaminants that can be biodegraded by indigenous microorganisms due to their organic nature. However, due to the difficulties in biodegrading polyaromatic hydrocarbons, remediation alternatives such as oil adsorbents to remove oil from the environment as well as biotechnological improvements, such as enzyme encapsulation, immobilization and regeneration seem promising methods for increasing bioremediation efficiency. It is necessary to prove the following hypotheses in order to provide effective decontamination of polyaromatic hydrocarbons

Hypothesis I: Following the oil spill, other alternative methods are needed to constrain the spread of oil using oil adsorbent. *Dolomite is a locally available material, and the surface modification of dolomite sorbent particles can be carried out to obtain sorbents for Dilbit and Bakken oil removal.* Modified dolomite might outperform other filter media technologies in stand-alone applications for the removal of higher molecular weight hydrocarbons.

Hypothesis II: The practical application of oil adsorbents in large-scale water treatment is limited due to the difficulty of separating them from aqueous solution. To evaluate the effectiveness of prepared oil adsorbents, a continuous process must be developed. *Thus, both packed and fluidized bed treatment columns of low-cost chemical hydrophobic sorbents for removing unconventional*

oil from laboratory synthetic oil-in-water emulsions could ensure a proper interpretation of the laboratory results and determine the efficiency of the adsorption of contaminants. Modified dolomite should be designed for column operation. It should be placed in appropriately sized fluid contactor vessels in the same manner as granular activated carbon. Such adsorbents, if they can remove oil from water, can be very advantageous as they are low-cost locally available materials for effective water treatment.

Hypothesis III: The aftermath of UO accidents highlights the lack of preparedness of cities to deal with these emergencies that is attributed to UO different behavior in the environment compared to traditional petroleum. More notably, following the Kalamazoo River incident, local officials did not discover that pipeline was carrying UO and the submerged oil surprised them. Thus, devices/processes are needed to target oil below the water surface and provide common places for degraders and contaminants. Jellyfish, a marine animal with umbrella-shaped bells and trailing tentacles, may have a thing to teach us. Their tentacles covered with sticky substrates contain triggers that release the stingers. A jellyfish can catch food through a passive process, in which it floats into the pieces of food. Taking inspiration from nature to solve environmental issues is the idea behind the proposed biomimetics in our study. For oil recuperation and attenuation measures, a jellyfish type of process can be applied by developing multi-layer and hollow fiber membranes with immobilized enzymes via electrospinning for bioremediation application. *A synergistic effect between membrane adsorption, enzymatic degradation, and ultrafiltration can be applied for the removal of contamiannt from the column of water using jellyfish like device*.

Moreover, the inherent instability of oxidoreductases is one major challenge in the commercial application of dioxygenase enzymes. Since most oxidoreductases are membrane-associated enzymes, they contain some hydrophobic peptides, which can interfere with their activity when they are extracted from the cell. To increase their activity after extraction, various attempts can be made to mimic the membrane condition. Thus, jellyfish-like devices could protect the produced enzymes from surrounding environment. *Encapsulation of hydrocarbon-degrading enzyme using jellyfish built from multilayer membranes and hollow fiber membranes could facilitate the degradation of contaminations.*

Hypothesis IV: One challenge for *in-situ* application of enzymatic biodegradation for decontamination of soil is the instability of oxidoreductase enzymes. In oxidoreductases, electrons or redox equivalents are exchanged between donor and acceptor molecules. A variety of redox-active centers are employed by oxidoreductases to accomplish their physiological functions. Some of the most common redox centers are amino acid residues (e.g., tyrosine or cysteine), metal ions or complexes (e.g., Cu, Fe, Mo, Fe-S cluster, or heme), and coenzymes (e.g., FMN; FAD; or pyrroloquinoline quinone, or PPQ). *Formulation of synthetic bacterial consortia for more operational stability in soil as well as the addition of activators can enhance the effectiveness of enzymatic bioremediation methods for the land-based oil spills.* Coenzyme dependence and/or signature catalysis of target enzymes should be taken into account when designing enzyme formulations. In order to validate enzymatic biodegradation in soil, batch testing, soil columns, as well as 3D-tank testing are necessary. A soil column test or a tank test can be used to simulate in situ application of an enzyme mixture to predict the consequences of bioremediation. The formulated enzyme mixture could therefore be produced at different scales (bench to large scale) and applied to soil and groundwater (laboratory, pilot scale). As a result of the scale-up tests, laboratory results would be properly interpreted, and the efficiency of enzymatic bioremediation would be determined.

Hypothesis V: Other major challenges in the practical application of oxygenase are high production cost and their inherent instability. Immobilization improves enzymes resistance to a variety of operating conditions. Due to their prolonged availability and re-usability, immobilized enzymes are preferred over their free counterparts in biotechnological processes. An effective method for reducing costs is to immobilize enzymes as it enables efficient recovery, reuse, and recycling, as well as increased stability in harsh operating conditions such as high or low pH and temperature. In last phase of this project, *immobilization of target enzymes on polyimide aerogels can enhance the degradability of residual unconventional oil in the water. Moreover, a continuous fixed-bed process could be employed to resolve potential problems regarding the large-scale application of aerogel.*

PART 5- OBJECTIVES

To demonstrate that polyaromatic hydrocarbons can be effectively bioremediated, the following objectives have been investigated.

Objective 1: Synthesizing low-cost hydrophobic dolomite sorbent for oil spill clean-ups: Kinetic modeling and isotherm study

Objective 2: Investigate the feasibility of packed and fluidized bed treatment columns of hydrophobic dolomite granules for removing unconventional oil from laboratory synthetic oil-in-water emulsion.

Objective 3: Simulation of the jellyfish type process by developing multi-layer membranes with encapsulated hydrocarbon-degrading enzymes via electrospinning for bioremediation application.

Objective 4: Investigate the feasibility of enzymatic biodegradation of Polyaromatic Hydrocarbons contaminated soil using cold-active enzymes: A soil column study.

Objective 5: Investigate the feasibility of a continuous fixed-bed column to remove polycyclic aromatic hydrocarbons by degrading enzymes immobilized on polyimide aerogels.

PART 6- ORIGINALITY

The present study comprises of the following original concepts:

- ✓ This study for the first time presents the practical application of modified dolomite in large-scale water treatment using a continuous fixed-bed process. Moreover, a comparative analysis of results with other adsorbent materials has been reported.

- ✓ This study will improve existing water- and land-decontamination methods by developing microbial products for environmental cleanup, fabricating remediation tools by focusing on formulation and polymer processing to accelerate and encourage the removal of pollutants from affected sites.

- ✓ In addition, this study reported for the first time the enzymatic bioremediation of pyrene contaminated site soil with batch and column systems, as well as kinetic and tandem LC-MS/MS analyses of psychrozymes, microbial communities, and biotoxicity tests of the soil before and after bioremediation. Currently, no studies have been conducted on the

bioremediation of soil using psychrophilic enzyme cocktails for the complete detoxification of cold climate regions or the impact of microbial diversity prior to and following bioremediation treatment. The use of soil column tests can mimic the application of enzyme mixtures in situ, in order to simulate the essential characteristics of the environment and predict the effects of bioremediation on the environment. According to our knowledge, no studies have been conducted on the characterization and application of soil column systems for enzymatic biodegradation of petroleum hydrocarbons.

- ✓ Our lab study yielded positive results prompting us to proceed with fixed bed columns to develop an industrial process for enzymatic bioremediation. To the best of our knowledge, no study is available for the application of fixed bed columns with spiral baffles for enzymatic biodegradation of polyaromatic hydrocarbons as a viable remedial option. Our study method stands to be a much cheaper and more effective alternative which benefits environmental consultants looking for ways to meet cleanup standards without investing large amounts of money.

- ✓ This manuscript proposed an easily scalable and reproducible process for removal of polyaromatic hydrocarbons and even emerging contaminants such as carbamazepine from contaminated water (continuous fixed beds using enzyme-loaded aerogels for water decontamination.

Overall, the originality of the proposed research is “Devising in-situ remediation tools using local and natural mimics for unconventional oil contaminated sediments”

PART 7- THESIS LAYOUT

This dissertation consists of five chapters, hypotheses and objectives as described below.

Table.1. List of thesis chapters and corresponding objectives, and hypotheses

Chapters	Title for a major goal	Hypotheses	Objectives
1	Introduction and research objectives	-	-
2	Literature Review	-	-
3	Treatment of unconventional oil contaminated water using modified dolomite	Hypothesis I and II	Objective 1and 2
4	*In-situ* application of cocktail enzymes for contaminated soil	Hypothesis III	Objective 3
5	*In-situ* application of cocktail enzymes for surface water cleanup	Hypothesis IV	Objective 4
5	*In-situ* application of cocktail enzymes for water treatment	Hypothesis V	Objective 5
7	Conclusions and Recommendations	-	-

CHAPTER TWO: LITERATURE REVIEW

Abstract

It is a general understanding that *unconventional oil* is petroleum-extracted and processed into petroleum products using unconventional means. The recent growth in the United States (US) shale oil production and the lack of refineries in Canada built for heavy crude processes have resulted in a significant increase in U.S imports of unconventional oil since 2018. This has increased the risk of incidents and catastrophic emergencies during the transportation of unconventional oils using transmission pipelines and train rails. A great deal of effort has been made to address the remediation of contaminated soil/sediment following the traditional oil spills. However, spill response and clean-up techniques (e.g., oil recuperation, soil-sediment-water treatments) showed slow and inefficient performance, when it came to unconventional oil, bringing larger associated environmental impacts in need of investigation. Remediation techniques for this contaminant, can be chemical, physical, and biological treatment. However biological and bioremediation has attracted more attention because it is cost effective and environmentally friendly technology. To the best of our knowledge, there is no coherent review available on the biodegradability of unconventional oil, including Dilbit and Bakken oil. Hence, in view of the insufficient information and contrasting results obtained on the remediation of petroleum, this review is an attempt to fill the gap by presenting the collective understanding and critical analysis of the literature on bioremediation of products from the oil sand and shale (e.g., Dilbit and Bakken oil). This can help evaluate the different aspects of hydrocarbon biodegradation and identify the knowledge gaps in the literature.

2.1. Introduction

Unconventional oils are generally defined as hydrocarbons obtained by unconventional means and they are classified into the following groups: heavy oil, extra-heavy oil, oil sand (bitumen) and oil shale (Kerogen) (Speight, 2016). In Canada, oil sands is found in the form of bitumen in three main geological zones, named Canada's oil sands region (COSR), including the Athabasca, Peace River and Cold Lake which make up the third-largest proven oil reserves in the world, after Venezuela and Saudi Arabia (Gordon, 2012; Transportation Safety Board of Canada Pipeline Investigation Report. 2007; Turner, 2017). The technology of unconventional oil extraction from the rock, the costs of production and management of wastes and residues together with the oil transportation from sources are generally more complex and expensive than traditional petroleum e.g., North Africa and Persian Gulf. Despite these difficulties, the production of unconventional oil has increased with the rising price of crude oil after the economic recession in the US since the beginning of 2009. It is the case in the US with light oil that has largely come from tight resource formations in regions of the Bakken Permian Basin with a prevision of 2 M barrels per day (bbl/day) in 2025 or in Canada with bituminous sands (as Dilbit from Athabasca) with previsions exceeding the 3M bbl/day in 2024 (EIA, 2015; Radović et al., 2018).

Multiple factors including aging infrastructure, ground failures, such as densifications, pipeline incidents and increased rail transport that use unsafe tanker cars have increased the risk of unconventional oil spill incidents during the transportation of these hydrocarbons. With this rapid development of new supply sources, the other environmental problems associated with unconventional oils that have raised concerns over oil spills include waste generation and leakage from the streamer, underground tanks, and abandoned bitumen refinery sites. The aftermath of recent high impact oil spill incidents (e.g., spill of Bakken oil in Lac Megantic and Dilbit from Alberta's oil in Kalamazoo) highlights the lack of preparedness of governments to deal with unconventional oil emergencies (Saint-Laurent et al., 2018). The inability to timely control the hazards; to constrain the spread of oil and to efficiently protect polluted zones has been attributed to the differences between unconventional oil and traditional petroleum characteristics and their behavior in the environment. In order to address these issues, novel Dilbit/Bakken spill response techniques classified as chemical and physical/chemical have been recently applied to decrease the remediation time by: (1) promoting biodegradation and limiting the movement of surface oil

slicks using high-temperature oil booms,(Prendergast and Gschwend, 2014) (2) reducing the water/oil interfacial tension using dispersants, (Hua et al., 2018) (3) uptake of unconventional oil using superhydrophobic sorbents and magnetic particles applied in novel absorbent techniques, (Prendergast and Gschwend, 2014) and (4) separating oil and water *in-situ* without additional energy input using hydrophobic meshes (Khosravi and Azizian, 2017). Moreover, microbial metabolism of unconventional oil has also been considered as a cost-effective process in both microbially-enhanced recovery and upgrading of bitumen and bioremediation.(Ridley, 2018) However, it was generally thought that hydrocarbon-degrading microorganisms isolated from hydrocarbon polluted sites can only grow on the lighter components of bitumen/Bakken, not on the recalcitrant asphaltene, resin fractions and high molecular weight (HMW) alkylated polynuclear aromatic hydrocarbon (PAH) (Deshpande, 2016). There has been a great need to gain in-depth knowledge on the following aspects: a) fate of dangerous compounds during environmental emergencies, b) innovative attenuation measures and the recuperation of oil, c) integrated methods for evaluating residual toxicity, d) methods for understanding biological degradation while treating soils, and e) the specific mechanism by which microorganisms degrade hydrocarbons, biodegradation patterns, chemistry of transformation products and their residual toxicity.

In this review, the current state of knowledge about the biodegradability of unconventional oil in aquatic and terrestrial environments was presented. It is necessary to apply multidisciplinary strategic research to address technical and economic challenges regarding the biodegradability of Dilbit and Bakken petroleum. This review, thus, discusses the significance of microbes in unconventional oil biodegradation and risk-based assessment through responses of environment receptors (eco-toxicity and ecological impact) coupled with chemical analyses to study the bioremediation efficacy.

2.2. Problems of Unconventional Oil

2.2.1. The High Risk of Unconventional Oil spill Incidents

As mentioned previously, technological advancement in hydraulic fracturing and horizontal drilling caused a spike in unconventional oil well development in 2009 for oil-producing states of the US (Patterson et al., 2017). Subsequently, it raised concerns over oil spills at unconventional oil wells. For example, A. Patterson *et al.* analyzed databases of spills related to 31,481 unconventional oil wells located in the US and reported a spike in annual spill rates (14 and 16 %

increase in spill rates in Pennsylvania and North Dakota). Given the present situation, the transport of these hydrocarbons will also increase, raising the risk levels of spills or releases of chemicals and wastes (Gan, 2017; Huang et al., 2018). Table 1.1 shows spills attributed to unconventional oils that occurred in very close proximity to streams.

Table 1.1. North America's Major Unconventional Oil Spills

Events	Location	Oil	Year	Amount (Liters)	Reference
1. A Rupture in the Trans Mountain Pipeline	Westridge, Canada	Dilsynbit	2007	0.2 Million	(Crosby et al., 2013)
2. Rupture in the Enbridge Energy Pipeline	Kalamazoo River, US	Diluted Bitumen	2010	3.2 Million	(de Santiago-Martín et al., 2015; USEPA Dredging Begins on Kalamazoo River)
3. A Rupture in the Pegasus Pipeline	Arkansas, US	Diluted Bitumen	2013	-	(Deshpande et al., 2017)
4. Railway disaster	Quebec, Canada	Bakken	2013	5.7 Million	(Saint-Laurent et al., 2018)
5. Rupture in Tesoro Logistics Pipeline	North Dakota, US	Bakken	2013	0.9 Million	(McMurray et al., 2018)

2.2.2 Oil Spill Location

2.2.2.1 Soil

The condition of the spill location might adversely affect the bioremediation of unconventional oil spills. For example, the predominant soil types in COSR are chernozems and organic-rich lucidols. (Radović et al., 2018). For weathered or crude unconventional oil, the adsorption of higher molecular weight compounds to these organic fractions of soils increased retention of oil in soils. Even though the retained oils could be easily removed by reclamation measures or bioremediation, the microbial degradation of adsorbed compounds largely decreased. The region where the hydraulic conductivity is very high might also cause ground-water contamination even if the unconventional oil spill is low. Price *et al.* studied landscape restoration in dry Western Boreal Plains near Fort McMurray, Alberta. They reported the areas underlying a sloping layer of fine-grained materials with low hydraulic conductivity maintained a concentrated plume of crude unconventional oil in a sand layer with the conductivity of 10^{-5} m/s. This retained concentrated plume is very concerning because it can act as a long-term source of pollution (Gordon et al., 2018; Radović et al., 2018).

2.2.2.2 Ecosystem

Cleanup and recovery from an oil spill is difficult and depends on the ecosystem involved. For example, wetland areas that cover approximately 21 percent of Alberta are ecologically sensitive to the oil spill, owing to slow anaerobic biodegradation of substrates, such as PAHs and polar hydrocarbons (Radović et al., 2018). Anaerobic environments limit the number of microbial species and slow down the natural attenuation by preventing oxygen from acting as the most favorable electron acceptor. Further, the presence of the water might decrease the permeability of the subsurface so that the retained oil can act as a long-term source of pollution in the subsurface (McGenity, 2014; Price et al., 2010).

2.2.2.3 Climate

Exploration and production facilities, as well as transportation activities including pipelines, are often located in cold regions where Dilbit spills from ruptured pipelines cause more serious environmentally damaging pollution problems. For many cold region sites, natural attenuation is probably not a satisfactory option in these circumstances and petroleum contaminants rapidly

migrate off-site. On the other hand, the environmental consequences of bulk extraction and the cost of excavation varies with a wide range of factors and the removal of contaminated soil and media for off-site treatment as well as disposal might cause more damage to the fragile wetland than the oil itself (Atlas; Manzetti, 2014) .

2.2.2.4 Behavior of Unconventional oil in the Environment

The pattern of ecotoxicity and biodegradation might be different from traditional petroleum in aquatic and terrestrial environments due to the physicochemical differences between conventional and unconventional oils properties and characteristics as presented in Table 1.2 (Hodson, 2017).

Table 1.2. Comparison of selected properties for conventional Dilbit and Bakken crudes

Oil	Composition			Toxicity	API Gravity (°)	Kinetic Viscosity (cST)	Acidity (TAN)	Adhesion (g/m2)			Implication
After Initial Weathering / After additional weathering				Total EPA PAHs (ug/g)				Before Release	After Initial Weathering	After additional weathering	
Dilbit	Bitumen (Asphaltic)	Diluent	BTEX	176	20-22	199-230 at 15° C	0.85-4.3	98	146	1580	According to GC-MS data, Dilb characterized by a hump represe hydrocarbons more resistant cor to biodegradation (cyclic and br hydrocarbons)
	50-70% (10-17%)	30-50%*	0.56-1.96%								
Bakken	Heavy Hyd (Asphaltic)	Light Hyd	BTEX	139	38-40	1.9-3.9	0.1-0.2	0	2	9	Bakken oil as a tight formation o characterized by straight-chain ar saturated hydrocarbons (a signifi molecular weight distribution of wax content) and low asphaltene
	60% (0.04%)	40%	1-3%								
Conventional Oil (Brent)	Asphaltic	Paraffins/Naphthene	Aromatics	514	38	5	0-0.3	12	17	33	Unlike unconventional oils that t compositions are not publicly av compounds present in traditional regulated by quality criteria.
	6%	30%-49%	15%								

With regard to Dilbit, the US NAS reported that in comparison to other transported crudes, the properties relevant to environmental impacts of the bitumen component such as exceptionally high density, viscosity, acidity and adhesion differ from traditional crudes when the oil is subjected to weathering.(National Academies of Sciences and Medicine, 2016) Moreover, there is no good understanding of the fate of toxic and recalcitrant fractions in an environment following oil spills. Saint *et al.* demonstrated that the most toxic components in Bakken oil (e.g., the trace metals and alkylated PAHs) were very low in the river sediments due to the river currents that prevented the accumulation of contaminated sediments during spring floods (Saint-Laurent et al., 2018). But, Hossain *et.al* reported that gravel sediments with large pore spaces can trap oil for a longer period of time and are considered as a source of contamination (Hossain et al., 2017). Figure 1.1 shows the ultimate fate of the plumes for fresh (A) and weathered (B) diluted bitumen, influenced by the density of the fluid and the hydraulic conductivity of the subsurface, which might change the environmental engineering option for remediation of these contaminants. In the case of the weathered Dilbit spills on land regarded as dense nonaqueous phase liquids (DNAPL), the plume of oil will sink and when it interacts with the water table, less concentrated plumes move into the water table, but the main plume continues to sink into very deep subsurface. From an environmental health perspective this plume acts as a long-term source of pollution for the aquifer (Figure.1.1 B). When the plume reaches the bedrock surface, it might flow in a direction opposite to the flow of ground water. As a result, it can spread in unexpected directions from the leaking zone (Fetter et al., 1999).

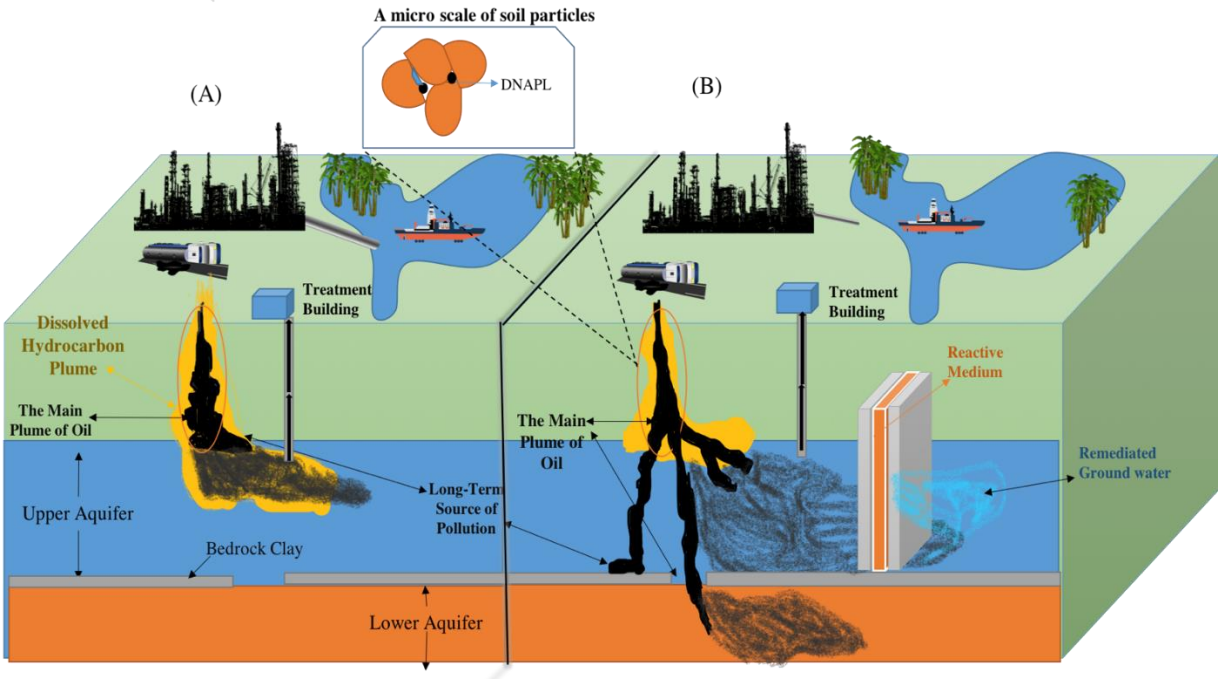

Figure 2.1 Subsurface contamination and transport of: (A) light non-aqueous phase liquid, such as traditional petroleum, gasoline and Dilbit; (B) dense non-aqueous phase liquid, such as weathered Dilbit,

2.3 Potential Solutions

The presence of complex mixtures of petroleum hydrocarbons, trace metals, volatile compounds have been reported in polluted sites after spills of unconventional oils, all of which presented high risks to the ecosystems and human health (de Santiago-Martín et al., 2015). A great deal of effort has been made to investigate the feasibility of applying new technologies of tar sand recovery (mass transfer practices such as vapor extraction, solvent extraction) to the remediation of soils contaminated with bitumen and other heavy oils (Prendergast and Gschwend, 2014). An environment agency survey conducted in 2009 indicated that about 90 % of the remediation techniques used on highly contaminated soils, particularly with heavy oils, were civil engineering methods and biological treatments were not considered as a treatment option in most cases.(Brassington, 2008) Still no single remediation practice is considered the best option for removal of two main classes of the major constituents of unconventional oils including polar nonhydrocarbons (heavy non-volatile compounds) and PAH from the environment (Dollhopf and Durno, 2011; Lacoursière et al., 2015). Figure 1.2 shows a three-component research project that

will be required to make a decision concerning the technologies to remediate the unconventional oil-contaminated site. In fact, a multiple lines of evidence approach is needed to study: a) advanced physical and chemical characterization of unconventional oil (i.e. Dilbit and Bakken oils)(Saint-Laurent et al., 2018) ; b) development of innovative efficient oxidants and non-chemical oil adsorbents; (Korfiatis and Christodoulatos, 1993) and finally, c) evaluation of *in-situ* toxicity (eco-toxicity bioassay); natural degradation and improvement of assisted oil-biodegradation. The assessment of the contamination characterization, ecotoxicity and the impact of unconventional oil on the indigenous microbial community is required to determine whether unconventional oil spill could be the worst-case scenario of all oil spills.(Grant, 2014) For example, following the Kalamazoo River incident, local officials did not discover that pipeline was carrying bitumen and not conventional oil. The submerged oil surprised them and the cost of the oil spill cleanup ($700 million) exceeded the company's $ 650 million insurance policy that it had for the pipeline in the event of a rupture (Dollhopf and Durno, 2011). Multidisciplinary research, thus, could deliver innovative assessment tools (genomics), eco-engineering sustainable cleaning processes and the ecological impact on the microbial community (analysis of 16s rRNA gene sequence or stable carbon isotope fractionation) as given in Figure 1.2. (Logeshwaran et al., 2018).

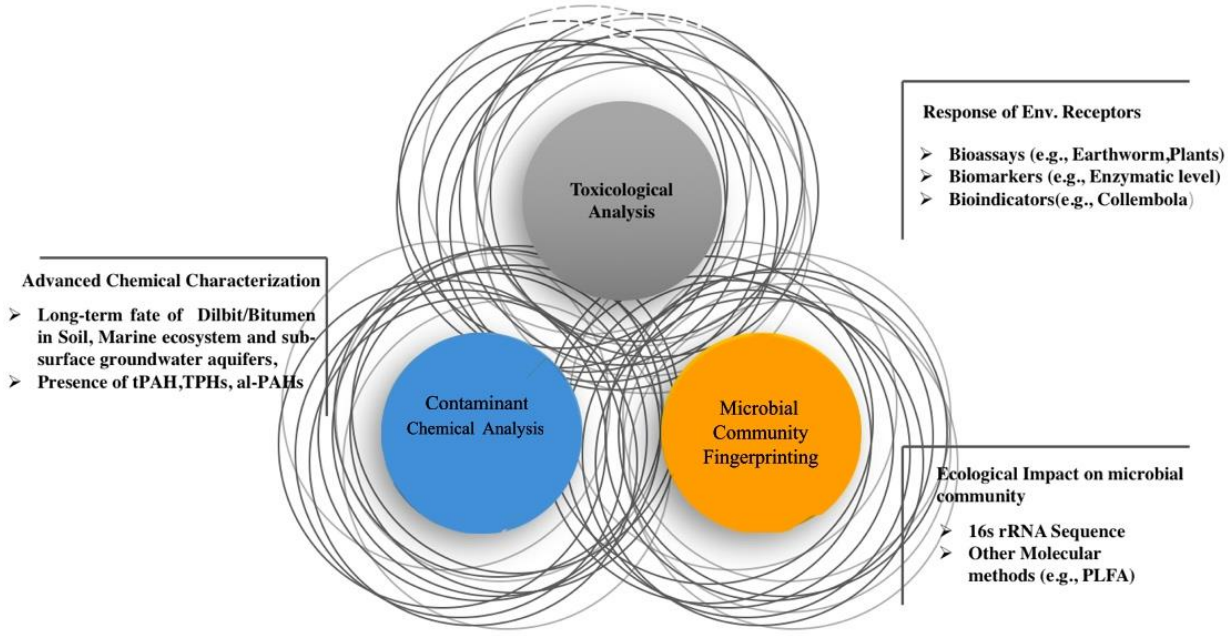

Figure 2.2. Illustration of a multidisciplinary strategic and structuring research approach to address unconventional oil contaminants.

2.3.1. Physical and Chemical Treatment

To enhance the efficiency of remediation, a series of physicochemical techniques, such as chemical oxidation, extraction, washing, and microbial biosorption has been developed for soil and water remediation (Das and Dash, 2017; Gisi, 2017). As seen in Figure 1.3, some of the physical treatment methods designed to remove unconventional oils do not remediate or detoxify toxic components.

2.3.1.1 Aquatic Ecosystem

Recently, the application of functionalized meshes, membranes or granular adsorbents has been studied to improve existing oil/water separation systems for oil recovery following a marine oil spill (Coene et al., 2018). The other treatment method to remediate an unconventional oil spill on the water is the use of a hybrid oil sorbent/boom. Warner *et al* recommended magnetizing oil spill which could then be magnetically manipulated and captured.(Warner) They implemented the simple principle, the addition of naturally-occurring magnetic minerals might form some sort of a bond with the oil, into an electromagnetic boom. This technique, unlike traditional boom and skimmers, target the unconventional oil below the water surface.(Schreiber et al., 2019) For weathered or crude oils that are unable to flow rapidly into a sorbent material, the available external surface area will determine the performance of adsorbents. Thus, loose strands of sorbent such as treated peat moss with a greater surface area than a boom might be expected to be more effective with these hydrocarbons (Wang et al., 2019b).

In order to remediate groundwater pollution, hydraulic control of unconventional oil movement and oil removal using discharge and recharge wells is the first option. The second option is to treat the pumped groundwater using *ex-situ* treatment, such as treatment columns. The pump-and-treat method was very common until 2000, but as the understanding of bioremediation increased, this method is less favored today. It might be difficult to pump out oil-contaminated water at a higher depth. Moreover, the entrapped oil between soil particles is never removed and this entrapped unconventional oil can disperse a low level of contamination for a long time (Figure 1.1) (Mercer).

2.3.1.2 Soil System

Even though physicochemical methods (e.g., dispersants, in-situ burning, and mechanical recovery) are the fastest treatments, they have not been considered eco-friendly and sustainable approached compared to bioremediation of oil spills. Recently, a great deal of effort has been invested in making these methods more environmentally friendly by applying pyrolysis techniques

(ShiungLam and Chase, 2015). A. Dominguez *et.al* studied the application of microwave irradiation method for drying, pyrolyzing and gasification of valuable sources (e.g. sewage sludge and used adsorbents that are abundant in the volatile matter) to produce useful products, such as gas, oil or char (Bandura et al., 2017; Domínguez). Thus, the sorbed oil might be used and recover as a source of energy and input for the production of lightweight compounds (Bandura et al., 2017). Figure 1.4 shows oil adsorbent applications as an environmentally friendly technique and methods that allow the recovery of oil, sorbents, and energy. As can be seen in Figure 1.4, modification of surface properties is needed to enhance the sorption capacity of oil adsorbents so that it can be further channelized to a small-scale pyrolysis plant for making fuel. Sustainable, reusable and recyclable oil adsorbents are recommended for the removal of land-based and marine oil spills that might be applicable to the treatment of spilled unconventional oil (Yu et al., 2018a). To the best of our knowledge, the feasibility of applying oil adsorbents to remove unconventional oils from contaminated soils and using them as valuable sources to produce gas, oil or char is not yet explored

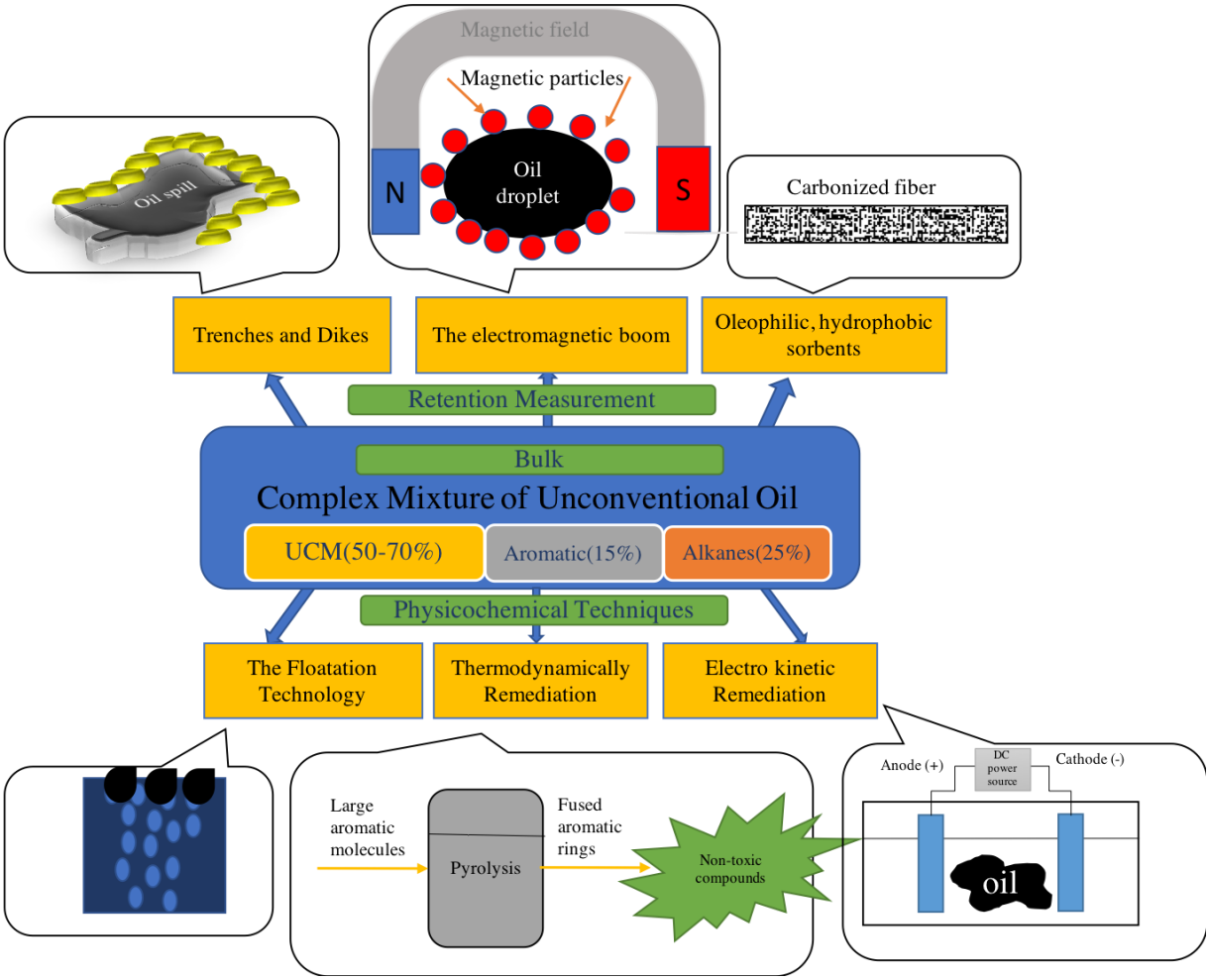

UCM: Unresolved Complex Mixture.

Figure 2.3. Measurements to reduce remediation time following an unconventional oil spill

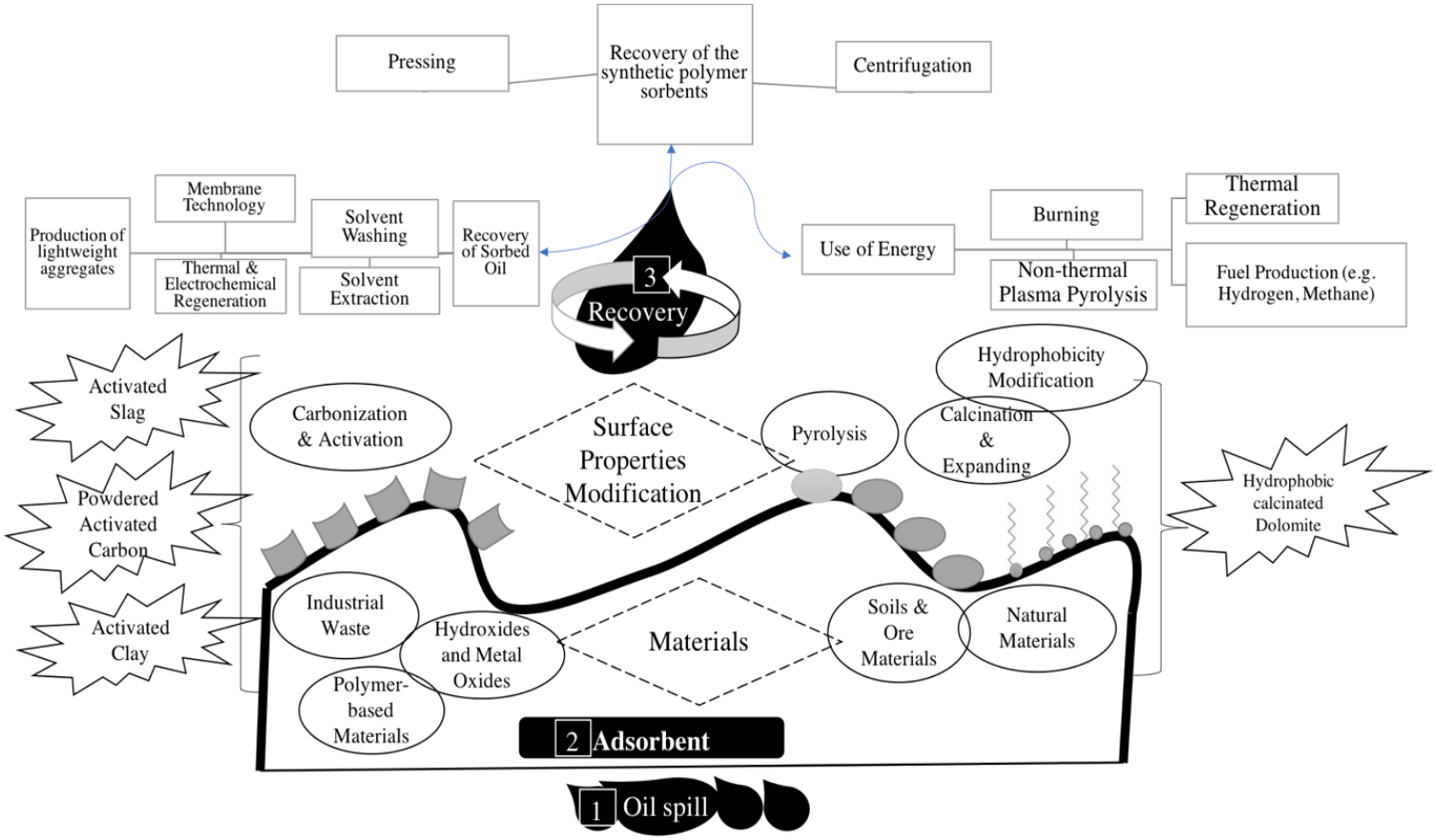

Figure 2.4. Schematic illustration of oil adsorbent applications as an environmentally friendly technique

2.3.2 Biological Remediation Approach

The organic nature of petroleum hydrocarbons including unconventional oil and traditional petroleum makes these contaminants suitable for biological degradation. One important requirement for the biological process is the presence of micro or microorganisms with the appropriate metabolic capabilities for contaminant removal. Biodegradation of hydrocarbons can be performed by ensuring adequate concentrations of oxygen and nutrients and optimal pH (Das and Chandran, 2011). In addition to indigenous microorganisms that might have the capability to degrade petroleum hydrocarbons, there are situations where the use of an exogenous microbial inoculum may enhance petroleum hydrocarbon biodegradation. This method can introduce a new degradation pathway for enhancing pollutant removal. However, using exogenous microorganisms can increase the competition between endogenous (native) and exogenous microbial populations. It can also result in the risk of introducing pathogenic microorganisms and the possibility of survival of exogenous microorganisms in the new environment; making it a very skeptical approach (Thornton et al., 2016; Wu).

2.4 Biological Degradation of Unconventional oils

Unconventional oils bioremediation can be problematic due to the presence of recalcitrance compounds and their toxicity.

2.4.1 Unresolved Issues

To date, traditional soil remediation, such as organic amendments using activated sludge, dead plant biomass, and other lignocellulosic substrates have been applied to enhance the biodegradation of residual fraction of TPH and highly recalcitrant PAHs fractions (Agamuthu et al., 2013; Radović et al., 2018; Shahsavari et al., 2013). However, these conventional means (e.g., bio-sludge) are not considered a viable stand-alone response option for the recovery of discharged oil and unconventional oil biodegradation. For example, with regard to spill of Dilbit into the Kalamazoo River near Marshall, the analytical methods described in the United States Environment Protection Agency (USEPA) report showed that even under optimum biodegradation conditions, approximately 25% of the viscous sample was degraded in the measured TPH concentration (USEPA Dredging Begins on Kalamazoo River).

Less disruptive strategies, such as natural attenuation and phytoremediation, that reduce the contaminants by naturally occurring processes, are crucial when managing unconventional oil-

contaminated soils. However, region-specific research is required to determine the capacity of natural degradation to reach cleanup goals. These processes are considered as a management strategy for low-level soil contamination. The assessment of degradation at high concentrations failed to meet strict regulatory standards for reuse of legacy brownfield sites with residual heavy hydrocarbon contaminants. Schreiber *et al.* evaluated the natural attenuation potential of Dilbit by microbial communities from Douglas Channel waters to mitigate the impacts of a potential unconventional oil spill (Schreiber et al., 2019). They reported that microbial communities were effective at removing alkanes, while no significant changes were observed for the overall concentration of aromatic fractions as biodegradation progressed.

2.4.2 Toxicity of Unconventional oils

The study of the actions undertaken after the Lac-Meganctic's Bakken oil spill revealed other issues regarding the unconventional oil degradation including some disadvantages and limitations on the effectiveness of unconventional oil bioremediation. The potential formation of intermediate compounds which are more toxic than the parent compounds, as well as the presence of other toxic contaminants, such as heavy metals are some examples of these limitations. (Ware) Moreover, bioremediation is not applicable in sites where a high concentration of inorganic salts, and organic compounds hinder microbial growth and Bakken oil spill. Thus, bioremediation should be applied with a thorough understanding of the metabolic, pathways and the microbial processes involved to prevent the production of more toxic substances (Saint-Laurent et al., 2018). Santiago *et al.* mentioned unresolved issues and requirements that may lead to higher initial costs for site characterization and feasibility evaluation for bioremediation (de Santiago-Martín et al., 2015). They suggested that the chemical monitoring associated with chemical/physical remediation, as well as microbiological assays are required during the implementation of bioremediation. Saint *et. al* studied the behavior of toxic and recalcitrant fractions of Bakken oil to address the above-mentioned issues. They carried out a full characterization of riverbed sediments and river-bank soils in the Chaudière River to measure the concentration of petroleum hydrocarbons (C_{10}-C_{50}), PAHs, and trace metals (Cd, Cu, Ni, Pb,

and Zn) (Saint-Laurent et al., 2018). They mentioned new issues regarding the Bakken oil remediation monitoring including the threshold of certain pollutants (i.e. some derivatives of PAH). Even though they measured the concentration of around 60 PAH and alkylated PAH, some of these compounds did not have classification criteria. In other words, they were not considered in the criteria for the protection of the environment due to their lower water-solubility and a little was known about the bioaccumulation and the adverse effects of higher mass PAHs on marine living organisms (Table 3).

Table 1.3. Analytical studies in soil/sediment/marine environment

	TPHs (C10-C50) analysis		Trace Metal Concentration MS Method				Aromatic analysis GC-MS / HPLC			
Regulation (soils contaminated) (mgkg-1)	Capillary GC with flame-ionization detection	Headspace GC–MS techniques	Cd	Cu	Ni	Pb	Polycyclic Aromatic			Heterocyclic Aromatic
							Group 1*	Group2	Group3	No toxicity data for heterocyclic aromatics
Criterion A	300		1.5	40	50	50	0.1	0.1	10	
Criterion B	700		5	100	100	500	1	5	50	
Criterion C	3500		20	500	500	1500	0.1	10	100	

*According to Criteria threshold PAH are classified to three groups:

Ø Group 1: 1,3-Dimethylnaphtalene/1-Methylnaphtalene/ 2,3,5-Trimethylnaphtalene/2-Methylnaphtalene/ 3-Methylcholanthrene/Benzo(ghi)perylene/Dibenzo(a, l) pyrene etc.

Ø Group2: Phenanthrene/ Naphthalene

Ø Group3: Acenaphtene/Anthracene/Acenaphtylene/Pyrene/Fluorene/Fluoranthene etc.

TPH: Total Petroleum Hydrocarbons;

Most of the previously mentioned literature was restricted to test the feasibility of attenuation and fertilization for biodegradation using chemical analysis such as gas chromatography, microbial respiration (physiological and biogeochemical approaches) and community analysis (e.g., genomics analysis). Thus, the fate and toxicity of both parent compounds and metabolites, in a mixture or alone has not been studied much (Saint-Laurent et al., 2018). Recent reports have considered ecotoxicological analyses and bioassay to study the effect of hydrocarbon transformation. For example, Logeshwaran *et.al* studied constructed microcosm and mesocosm to investigate the effect of treated sediments on biological receptors and provided more information on the pattern of toxicity during the biodegradation process (Logeshwaran et al., 2018). The bioassays applied during the biodegradation have been reported to estimate the effect of mixed contaminants and intermediate metabolites during the clean-up of contaminated sites. Likewise, Yu *et.al* measured acute toxicity to study the effect of UltraZyme-amended treatments (Yu). However, analytical technologies used in this study could not track the detailed changes in the composition of organic compounds in water residual bitumen and they were unable to explain the reduction of toxicity when DOC including naphthenic acid reduction did not occur (Yu et al., 2018b). The effectiveness of soil/sediment remediation can also be determined using toxicity evaluation (e.g., phytotoxicity) as well as other bioindicators such as microbial community composition. hydrocarbonoclastic bacteria such as *A.borkumensis*, showed their capacity to degrade a large number of alkanes, branched aliphatic, as well as isoprenoid hydrocarbons, and alkyl cycloalkanes (Deshpande; Ortmann; Schneiker). Inconsistent information and contrasting results regarding biodegradability of unconventional oil have been attributed to the lack of treatability results throughout all these studies (Saint-Laurent et al., 2018; Ware). It might also be associated with the difference in the experimental setup, and varied nutrition concentrations which have been reported to be important to reach maximum biodegradation rates. Yu *et al.* reported that inconsistent information could be attributed to the different types of inoculum source, the composition of microbial enrichment and surfactants applied that could affect the enrichment of microbial communities (Yu et al., 2018b). As can be seen in Table 1.4, some literature has reported the biodegradation of bitumen and Bakken oil as not being consistent with others suggesting limited degradation

Table 1.4. Constant rate results of bitumen biodegradation

		25		1.53/99.89%	0.24/98.47%	-	
Dilbit (AWB)	Non-Amended seawater	22	13	0.0014	0.0011	ND	
Dilbit (CLB)	Non-Amended seawater	22	13	0.0011	0.0005	ND	
Dilbit (AWB)	Seawater/ BH/Dispersant (AWB chemically dispersed)	22	42	0.14/99%	0.002/20%	ND	
	Seawater/BH (AWB naturally dispersed)	22	42	0.11/99%	0.0011/10%	ND	(Deshpande)
Dilbit (CLB)	Seawater/ BH/Dispersant	22	42	0.099/ND	0.004/ND	ND	
	Seawater/BH (CLB naturally dispersed)	22	42	0.099/ND	0.005/ND	ND	
Dilbit (AWB)	Costal microbes/Ammonium/Phosphate	4	5	0.023	ND	ND	(Deshpande)
Dilbit (AWB)	Coastal microbes/Nirate/Phosphate	4	5	0.0235	ND	ND	

2.5 Bio-Stimulation

One of the bioremediation approaches to address the above-mentioned issues regarding the removal of two main classes of the major constituents of unconventional oils including polar hydrocarbons and PAH from the environment is bio-stimulation. The bio-stimulation is a method to adjust environmental conditions (optimization of C-N-P relationships) so that the transformation of contaminants can be increased by indigenous microbes (Nwaogu). Unlike the food industry where extensive sterilization is required to minimize the level of microbial contamination before inoculating them with appropriate bacteria, the bioremediation is usually carried out by applying physiologically adapted native microorganisms present in the affected areas to remove petroleum products by adding nutrients, dispersants, surfactants, and fertilizers.

2.5.1 Oxygen Accessibility and Nutrient Content

Bioventing is an example of *in-situ* biodegradation for bio-stimulation of indigenous aquifer microorganisms by drawing oxygen through the soil. This technology is primarily designed to treat soil contamination by non-halogenated volatile organic compounds, pesticides, and herbicides. However, following the Bakken oil spill in Lac-Megantic (Canada), bioventing along with, nutrient addition and inoculation with oil-degrading bacterium was used to clean up Bakken oil in unsaturated soil in several platforms due to low concentration of heavy metals, and inorganic salts in the sites (de Santiago-Martín et al., 2015). This study also indicated that while physicochemical factors (e.g. metals, nutrition, and temperature) are important in the activity of microbial groups, the rate and extent of unconventional oil degradation strongly depends on previous exposure of the consortia to hydrocarbon contaminants. Agarry *et.al* studied the effect of inorganic NPK fertilizer and oxygen release compound (hydrogen peroxide) and their combination on the kinetics and the extent of bitumen biodegradation using autochthonous microorganisms in the soil resulting in 55 % TPH removal (Agarry). The introduction of pure oxygen to soil and injection of hydrogen peroxide has been suggested to address the issues regarding the inefficient air permeability of contaminated soil which provided sufficient oxygen for aerobic biodegradation. In this study, they assumed that the remediation of soil contaminated with bitumen can be expressed in terms of reduction in TPHs rather than risk reduction (Lee). However, the ecotoxicological assessment revealed that a reduction in TPH load could not be linked to a reduction in residual toxicity. They also applied gravimetric analysis to estimate the extent of utilization of the TPH in the bitumen.

Nevertheless, the gravimetric analysis cannot be accurate due to the fact that it does not indicate whether compounds of aromatic, asphaltene, alkanes have been degraded or not.

The effect of temperature on the efficiency of the bio-stimulation method for biodegradation of Bakken oil was studied on affected urban soils in Lac-Megantic. Diaz Sanz *et al.* reported that the bio-stimulation method enhanced the extent of Bakken oil degradation, especially for mesophilic microorganisms.(Díaz Sanz) However, they did not compare the effectiveness of other commercial fertilizers and other common methods, such as bioventing. Recently, Cobanli *et al.* compared the biodegradation rate of Dilbit using microbes enriched from seawater and freshwater and studied the effect of inorganic nutrient concentrations on coastal microbial community response to Dilbit following an oil spill (Table 5) (Cobanli). They reported that the coastal microbial community enriched by marine ecosystems degraded Dilbit (20% PAH removal) less effectively than freshwater microbial communities which were exposed to Dilbit following a pipeline spill in 2010 (up to 98 % PAH removal) (Table 5). Yu *et al.* evaluated the impact of labile organic substrates that are considered to stimulate hydrocarbon degradation (Yu et al., 2018b). They studied the microbial activity and the change in dissolved inorganic carbon, as well as insoluble hydrocarbons to demonstrate the effect of the addition of acetate on the degradation of heavy and light compounds. (Yu et al., 2018a) It had been reported that acetate accumulation and competition for electron acceptors resulted in a delay in biodegradation. However, Yu *et.al* did not observed that the inhibitory effect of acetate on recalcitrant degradation due to the difference in redox level or several metabolic pathways of various hydrocarbons in bitumen (Nopcharoenkul; Yu et al., 2018a). Table 5 summarizes the results from various recent research studies that have investigated the effect of nutrient addition on the extent and rate of unconventional oil degradation.

Table 1.5. The efficiency of bio-stimulation treatment on bioremediation of unconventional petreoleum

Nature of Pollutant	Effect on biodegradation	Nutrients Addition	Removal Efficiency	Reference
Extracted Bitumen	Removal of toxic hydrocarbons originated from bitumen	Nitrogen addition (ammonium nitrate)	53% toxicity	(Li)
Residual Bitumen	Simulation of bitumen/hydrocarbon-degrader growth	Sodium acetate	34% heavy fraction > C_{50}	(Das)
Nigerian bitumen	Significantly enhancement of kinetics and extent of bitumen degradation compared to being used singly	NPK fertilizer + Hydrogen Peroxide	61% TPH	(Clegg)
Bakken petroleum shale oil	Fertilization could manage polluted urban soils when the temperature dropped below 10 ^{O}C due to a limitation of macronutrients N and P	NH_4NO_3 + K_2HPO_4	20 %TPH @ 10^{O}C 12%TPH @ 20 ^{O}C	(Tamas)
Asphalt in bitumen mixture	The addition of glucose, malt extract, and polypeptide did not induce enzyme production significantly.	Mn^{2+} + H_2O_2	81% Asphalt in liquid medium 24% Asphalt in Soil	(Shi)
Dilbit	Freshly collected surface seawater used to set-up microcosm reduced any possible effects of changes in nutrients	Inorganic micronutrients in seawater	96% Alkane	(Kolenc)

2.5.2 Surfactants (Chemical and Biological) and Dispersant

The addition of dispersant might stimulate the growth of hydrocarbon degraders by increasing the bioavailability of hydrocarbon compounds. For example, Bookstaver *et.al* reported that non-ionic surfactants can enhance the growth of *A.borkumensis* on crude oil (Bookstaver et al., 2015). Moreover, the main ingredients of dispersants (e.g. glycols, dioctyl sulfosuccinate, and light petroleum distillates) might serve as a substrate for microbial growth. Interestingly, Schreiber *et al.* reported that the dispersant appeared to stimulate the enrichment of genera associated with Dilbit degradation. (Schreiber et al., 2019) As mentioned earlier, the biodegradation using microbial communities might not target toxicity that is due to methylated or more than three-ring PAHs fractions of oils. Thus, future studies are necessary to study the evolution of Bakken oil and Dilbit toxicity during the course of incubation in the presence of dispersants. Experiments were also recently carried out to characterize the optimal conditions for biosurfactant production by microorganisms growing on heteroatomic polyaromatic compounds to enhance aromatic component degradation. For example, Eric *et al.* reported favorable growth conditions for the production of surface-active compounds for a soil *Pseudomonas* strain requiring an elevated C-to-N ratio and limiting iron concentration (Deziel).

2.6 Bioaugmentation

This strategy may be used in different situations, for instance in areas requiring longer acclimation period e.g. cold regions (Miri et al., 2018) where the number of specific petroleum hydrocarbon degraders is low, and in the presence of recalcitrant compounds. In the case of unconventional oil, the commonly used methods for bioaugmentation are the addition of: (1) recalcitrant degrader strains; (2) consortium of different macro and micro-organisms; (3) genetically modified microorganism; and (4) emulsifier-producing strains. The effectiveness of this method is variable due to the fact that the survival ability of introduced microbial communities, enzyme activity and stability depend on environmental conditions (Hosokawa et al., 2009).

2.6.1. Unconventional Oil-Degrading Microorganisms

Microorganisms (e.g., fungi, yeast and bacteria) may have different preferences during biodegradation. It was reported that the bacterial communities were responsible for the degradation of saturated and partially aromatic hydrocarbons (Deshpande, 2016; Deshpande et al., 2017). As

for the fungal community, it was reported to transform HMW PAHs (six or more aromatic rings) as well as the asphaltenes (Hernández-López et al., 2016).

2.6.1.1 Bacterial Strains

Most of the literature on Dilbit/Bakken oil degradability has mainly focused on the growth of hydrocarbon-degrading microbes in the lighter components of bitumen/Bakken oil (not on the recalcitrant asphaltene fraction resins (Schreiber et al., 2019). Thus, the assumption is that the polar oil compounds were not biodegradable and recalcitrant fractions in bitumen did not support bacterial growth. For example, Wyndham demonstrated bacterial colonization of bitumen surfaces but microbial activity and degradation of bitumen have not been experimentally observed as reflected in a number of microorganisms (Wyndham and Costerton, 1981). A potential cost-effective solution that is greatly needed to increase the detoxification of unconventional oils might be to detect and isolate bacterial from oil reservoirs for degradation of fractions with structural complexity and high viscosity.(Schreiber et al., 2019; Wang et al., 2019b) Some of these bacteria, such as *A.borkumensis* SK2 might be enriched to Dilbit and Bakken oils under natural and assisted conditions to analyze the TPHs in the enrichment cultures. Most recently, Gao *et al.* and Zhou *et al.* demonstrated the ability of *P. aeruginosa* and thermophilic *Geobacullus Stearothermiphilus* strains to degrade HMW fractions including resins, asphaltenes and alkyl derivatives PAHs that are considered as subfraction of unconventional oils. These microorganisms can break the chemical bonds between monomers, such as naphthenic or aromatic rings in fused-ring compounds or by secreting enzymes producing surfactant and bio-emulsifier. Earlier literature has proven the biodegradability of asphaltenes and resin using bacterial strain (*Bacillus* sp., *Corynebacterium* sp., *Bacillus* sp., *Revibacillus* sp., *and Staphylococcus* sp.). However, the efficiency of asphaltenes biodegradation (e.g., the percent removal of asphaltene and biodegradation kinetics) was low compared with that of light fractions of the crude oil (Gao; Zhou). *Gao et.al* reported that the dominant groups of bacteria with a significant application in microbially-enhanced oil recovery, that belong to the genera *Pseudomonas, Clostridium, Bacillus,* and *Acinetobacter,* might emulsify and degrade heavy oil fractions more efficiently (59-73% of crude oil asphaltenes). They reported that some of these bacteria could be cultured under aerobic conditions on individual growth substrates (i.e. BTEX and PAHs) (Baquiran; Gao).

2.6.1.2 Fungal Community

The fungal community can remove recalcitrant polar hydrocarbons, such as asphaltene and resins by applying enzymatic and/or non-enzymatic reactions.(Peixoto) Hernandez-Lopez *et al* for the first time investigated the fungal transformation of asphaltene and various PAHs with six aromatic rings including benzo (g, h, i) perylene, indeno (1,2,3-cd) pyrene, and coronene by *Neosartorya fischeri*. They showed the role of cytochrome P450 system (CYP) as a monooxygenase in the oxidation of the recalcitrant compound.(Hernández-López) According to the assessment of PAHs contamination in the Riverbanks of the Chaudière River three years after the Lac-Megantic Railway disaster, the concentration of these PAHs exceeded the acceptance criterion B level (not the criterion C limit which is considered a high level of contamination) (Hernández-López; MDDELCC; Saint-Laurent et al., 2018). Thus, this fungus might be applied in biodegradation of heavy oil containing HMW PAHs. Hernandez *et al.* also reported the involvement of intracellular CYP enzymatic system in the transport mechanism of *Neosartorya fischeri*.(Hernández-López) Most recently, it has been reported that newly formed potential microbes (i.e. white-rot ligninolytic fungi) might be more efficient than those applied conventionally for unconventional oil biodegradation due to their strong capabilities for the initial transformation of heavy PAHs and other complex structures, such as hetero-polyaromatic hydrocarbons and alkyl chains. For example, Li *et.al* reported 45% biodegradation of phenanthrene and 90% of benz[a] anthracene under *in vivo* conditions by white-rot fungi non-selective peroxide enzymes. This is probably due to its mechanism of lignin-degrading, via unique extracellular, and nonspecific oxidative lignin-modifying enzymes (i.e. lignin peroxidase, manganese peroxidase, versatile peroxidase, and laccase). (Li)

It is reasonable to make the hypotheses that unconventional oils might select different microorganisms than conventional oil. Biodegradative gene analysis might help us to gain an overview of the restriction of oil-degrading bacteria in geographic distribution.

2.6.1.3 Biodegradative Gene Analysis

The recent improvement in the science of gene expression of microbes (i.e. metagenome, metatranscriptomics, microarray gene expression data, and real-time PCR) shows that metabolically versatile and pluripotent bacteria genera (e.g., *Alcanivorax*, *Rhodococcus, Pseudomonas, Corynebacterium,* and *Bacillus*) can be considered as unconventional oil-degrading

microorganisms (Brakstad). Most recent studies have applied metatranscriptomics to provide evidence suggesting the capacity of indigenous bacteria in the tailings to degrade bitumen aerobically. The gene sequence of hydrocarbon-degrading bacteria might yield unprecedented insights into the bacterial capacity for unconventional oil degradation. Susanne et.al showed that *A.borkumensis* SK2 has a streamlined genome with a plethora of genes accounting for its efficient oil-degradation capabilities (Schneiker et al., 2006). Table 6. summarizes microorganisms and microbial genes involved in unconventional oil sub-fractions degradation

Table 1.6. Degradative gene(s), enzymes and detective methods involved in the degradation of unconventional oil sub-fractions

Microorganisms	Genes	Enzyme /Protein	Nature of pollution	Isolation location	Detection Method	Reference
N. *fischeri*	• CYP1A1 gene	• Cytochrome P450 monooxygenases, • Flavin binding monooxygenase	HMW-PAHs/ Asphaltenes	Maya, Mexico	cMicroarray	(Hernández-López)
Microbial community *(*i.e. *Acidovorax, Rhodoferax, Pseudomonas and Pseudoxanthomonas spp.)*	• *alkB,* • *Nah*	• Alkane monooxygenase, • Naphthalene dioxygenase	Bitumen	Syncrude Canada Ltd	qPCR	(Yu)

ND: No Data

2.6.1.4 Microbial Consortium of Different Micro and Macro-Organisms

The literature presents strong evidence that the introduction of a large number of exogenous microorganisms into a bio-treatment system will promote the biodegradation of high molecular weight hydrocarbons (Boonchan et al., 2000; Wong et al., 2015; Zhou et al., 2018). Soil and water community analysis using shotgun metagenomic and metatranscriptomic data provides the required knowledge and pertinent information about the composition of microorganisms present in the environment. For example, Wong *et.al* studied microbial community compositions in outcrop bitumen-saturated sandstone from outcrop cliffs (i.e., an ecosystem that contains comparable highly diverse HMW hydrocarbons) by pyrosequencing of 16S/18S rRNA genes. The role of fungi to attack PAHs with soluble extracellular enzymes including lignin peroxidase, laccase, and manganese peroxidase together with cytochrome p450 mono-oxygenase was confirmed using metagenomic data (Wong). They showed that fungal-bacterial cocultures can degrade HMW PAHs faster than pure cultures of *Stenotrophomonas, Burkholderia, Rhodococcus,* and *Sphingomonas*. Application of different bacterial consortia, fungi and plant roots for the biodegradation of high-molecular-weight PAHs and heavy polar hydrocarbons in liquid media and soil has been investigated by Boonchan, Tamas, Garcia-Sanchez (Boonchan et al., 2000; García-Sánchez et al., 2018; Tamas et al., 2014). They investigated the hypotheses that non-ligninolytic (i.e. *Penicillium janthinellumm* and *Cunninghamella elegans)* and ligninolytic fungi might promote the degradation of heavy PAHs by their non-selective and extracellular peroxide enzymes and plant root would stimulate new microbes that have the potential to mineralize the residual metabolic intermediates of the degradation. Table 7. summarizes the results from various recent research studies that have investigated profitable approaches for cleaning up unconventional oil-contaminated soils and liquid media using the synergistic effect of different macro- and microorganisms. As seen in Table 7, only few studies focused on mycoremediation, fungal contaminant removal, as a new branch of bioremediation that uses the similarity between recalcitrant aromatic hydrocarbons (asphaltenes, 4-,5-and 6-ring and their alkyl derivatives PAHs that represented more than 50% of Dilbit/Bakken petroleum) and the components of the lignin macromolecules to imply fungal mycelia and their enzymes in the presence of rhizosphere microbiome. Moreover, to the best of our knowledge, there is no sufficient literature available on

bioremediation of unconventional oil-contaminated soil and liquid media using white-rot fungi and rhizosphere microbiome (Gao).

Table 1.7. Contribution of different micro and macroorganisms in the degradation of unconventional oil-contaminated soil or water media

Nature of pollutant	Organisms	Isolated Location	Removal Efficiency (% degradation)	Comment	Reference
WCS/PBC *	Bactérie Consortium (*Pseudomonas* + *Rhodococcus*+ *Xanthomonadaceae*+ *Parvibaculum*+ etc.,)	Kalamazoo River (Cryo culture)	99.9 / 99.9 % Alkane 98 / 98 % PAHs	On phylum level, no significant difference was observed in KMZ meson ad cryo cultures.	(Deshpande)
WCS / PBC	Bacteria Consortium (*Rhodococcus* + *Hydrogenphaga*+ *Pseudomonas* + *Polaromonas*+ etc.,)	Kalamazoo River (Cryo culture)	99.9 / 99.9 % Alkane 98 / 98 % PAHs	The cryo culture metabolized most of the alkanes, naphthalenes but residual HMW PAH was observed.	(Deshpande)
4,5-6 rings PAH**	The maize-*C. laeve* association	The Olza River	58% PAHs	The combination of inoculation of *Curriculum laeve* and root exudates provided for favorable conditions for hydrocarbon degraders	(García-Sánchez)
Crude bitumen	Fungi+ bacteria (anaerobic *Firmicutes*, thermophilic methanogens) + thermophilic Archaea + Eukarya	75.0 % Alkane 75/85% PAHs	ND	Analysis of carbon isotope fraction has been applied to identify the presence of active microorganisms in soils	(Wong)
Crude bitumen	Heterotrophs + *Medicago sativa* + *Phragmites australis*	Halle, Saxony-Anhalt, Germany	75% TPH	The type of plant significantly affected the physiological structure of the microbial community under bitumen contamination	(Muratova)

4,5-6 rings PAH	The non-ligninolytic fungus (*Penicillium janthinellum*) + bacteria (*Stenotrophomonas maltophilia*) Consortium	Sydney, Australia`		Fungal–bacterial co-cultures degraded benzo(a)pyrene, benzo(a)anthracene, chrysene, dibenzo(a,h)anthracene. low amounts of the PAHs were degraded when incubated with either the bacteria or the fungus.	(Boonchan)
Crude bitumen and PAH pollution	Heterotrophs + *Medicago Sativa* + *Phragmites Australis*	Halle, Saxony-Anhalt, Germany	ND	The efficacy of plants was particularly pronounced in the case of PAH	(Muratova)
Weathered bitumen hydrocarbon	Six different prairie plants + n-hexadecane, F2 diesel fuel, and PAH degraders	South-eastern Saskatchewan	50% TPH	Final population of degrader increased in planted amended soil using mixed plant species. Some species appeared to be dominant and selective influence by alfalfa in degrader population that doesn't favor overall degradation	(Phillips)
WCS / PBC	Bacteria Consortium (*Acinetobacter*+ *Hydrogenphaga*+ *Sphingobium*+ *Dokdonella*+ *Pseudoxanthomonas*+ ect,)	Ohio River (Meso culture)	99.9/99.9% Alkane 60/80% PAHs	The rate, as well as the degree of removal for two Dilbits (i.e., WCS and CLB ***), were comparable. So, WCS was used for further investigation	(Deshpande et al., 2017)
WCS / PBC		Ohio River (Cryo culture)	98/98% Alkane 50/78% PAHs	The rate of Dilbit degradation (WCS) and PBC were much alike, but PBC degraded to a greater extent,	

*WCS: Western Cadandia Select; PBC: Prudhoe Bay Crude

**6-ringed PAHs 6-ringed benzo(ghi) perylene are considered as the main bitumen subfractions

*** CLB: Cold Lake Blend (Dilbit)

ND: No Data

Recently, literature utilized multiple remedial approaches including physical, such as excavation, and an array of biological processes associated with phytoremediation, such as nutrient exchange through root exudates to bio stimulate hydrocarbon-degrading microorganisms in the rhizosphere or stimulate the expression of oxygenase genes to degrade heavy hydrocarbons to less toxic compounds. This approach is especially suggested for bioremediation of soil co-contaminated with heavy metal and bitumen. To the best of our knowledge, the application of phyto-treatment to stimulate degradation of the contaminants and its transformation products present in Dilbit or Bakken oil-contaminated soils has not been investigated.

2.6.1.5 The Use of Genetically Engineered Microorganisms (GEMs)

The components of unconventional oil are structurally diverse causing each compound to be present at low concentration, which compromises biodegradation of high molecular weight components. Thus, the addition of external microbial consortia and nutrients may not necessarily increase the efficiency of pollutant removal due to the fact that specific enzymes (e.g. oxidative enzymes) synthesis is endergonic and requires energy (Schreiber et al., 2019). This energy might be recouped only when a sufficient concentration of pollutant molecules is present in the complex mixture of oils. Shi *et.al* suggested the use of random oxidation such as chemical ozonation to generate less diverse substrates for subsequent biodegradation (Saint-Laurent et al., 2018; Shi; Wong). Recently, the application of the state-of-the-art tools to modify the expression of different sets of genes has been recommended as a promising method for increasing bioremediation yield and bringing together desirable biological oxidants (i.e. enzymes), biodegradation pathways and perform specific reactions. Genetic engineering also might enhance:(1) detoxification of toxic metals using construction of plasmids with combination of different metal resistant genes such as NiCoT , merA.(Schneiker) (2) expression of multiple genes such bacterial laccase (CotA), endoxylanase (Xyl) and pectate lyase (Pel) in a single host,(Kolenc) and (3) overexpression of hydrocarbon degrading enzymes such as laccase from *Thermus thermophilus* that might yield high laccase activity for oxidization of PAHs, asphaltene and resins.(Liu) There is not enough literature available on biodegradation of unconventional oil using this method that might be attributed to the fact that the ecological and environmental risks of genetically engineered microorganisms need to be considered to make this method successful. For instance, bioaugmentation with non-indigenous or GEM is banned in Iceland, Sweden, Antarctica and Norway. (Filler; Gaur)

2.6.1.5 Biosurfactant and Degradative Enzymes Mediated Unconventional Oil Degradation

The mass transfer problem of recalcitrant chemicals with large, tightly packed molecule structures, including resins and asphaltenes in the unconventional oil matrix as well as the bioavailability of soil-bound PAHs, can probably be overcome through surface-active compounds. Production of biosurfactants by bacteria, fungi, and yeasts is considered an important strategy that influences the bioavailability of hydrophobic chemicals, as well as releasing the trapped hydrocarbons from the porous medium in contaminated soils (Bezza; Hentati). Recently, the capability of different types of biosurfactants has been reported to enhance the metabolism of aged PAH, asphalt and heavy vacuum gas oil. *In-situ,* biosurfactant production through nutrient-only bio-stimulated treatment can serve as a biological tool to overcome problems in limited bioavailability of unconventional oil sub-functions, especially in soil. The bacteria isolated from bitumen contaminated soil contained efficient PAH and asphalt degrading, biosurfactant producing species like P.*aeruginosa*, *Ochrobac-trumps,* Bacilli–i.e., Bacil-*lusstratosphericus*, *Bacillus subtilis*, and *B. megateriumi* demonstrated good reduction in the surface tension (under 40 nM/m) and emulsification index values (55 %) (Bezza; Hoang). The slow rate of bioremediation for unconventional crude oil might be addressed by using enzymes instead of the whole microorganism. Enzymatic technologies for remediation unconventional oils can be especially suitable for conditions where rapid bioremediation is needed to mitigate the adverse effects of indigenous microbes. A great deal of effort has been made to address issues regarding the application of enzymes for soil and water remediation (Kadri et al., 2018d). However, the production of purified target enzymes is a costly process; thus, recombinant strains are usually constructed to overproduce the specific enzymes. The synergy between specific enzymes is more important than simply pursuing a higher enzyme activity due to the structural complexity and high viscosity of unconventional oil composition. Beilen *et.al* studied other practical issues and challenges in the application of enzyme remediation methods such as co-factor regeneration rates, oxygen mass transfer, overoxidation and substrate uptake. Moreover, Redox enzymes including oxygenases (e.g. monooxygenase and dioxygenase) require expensive co-factors, such as NAD(P)H and improved cofactor regeneration that increase the specific oxygenase activity of whole-cell oxygenase biocatalysts.(Sun et al., 2016; van Beilen) A combination of extracellular enzymes with enzymes that are more stable such as chloroperoxidase seems promising to result in faster degradation. Abolafia *et.al* determined an

optimal mixture of enzymes that would reduce asphaltene aggregation in bitumen. (Abolafia; Bezza) The application of enzyme cocktail containing specific enzymes, such as laccases, lipase, alkane hydroxylase, monooxygenase, and esterase might be explored in the future.

2.6.1.6 Immobilization Technique

The immobilization method has been proposed to overcome challenges for enzyme-based processes applicable to the oil industry including the processing and upgrading of unconventional oil and heavy hydrocarbons.(Ayala et al., 2007) Most recently, with the advent of nanotechnology, nanostructured materials (e.g. nanofibrous materials) with high porosity, well-designed selective wettability, and large specific surface area have been developed for highly efficient oil-water separation.(Qiao et al., 2019) These findings inspired researchers to combine the electrospinning methods and enzyme immobilization. For example, fabrication of electrospun fibrous membranes might be applied for adsorption and degradation of remaining heterocyclic compounds in soils and groundwater after applying non-biological treatment methods. Dai *et.al* demonstrated that the synergistic effect of the membrane adsorption and laccase immobilization increased PAH degradation.(Dai) Further work is necessary in this field to investigate potential application of portable oil spill cleaning mop with enzyme-immobilized nanofibers that mimic the octopus' long sticky tentacles grab food particles to adsorb contaminant and remediate contaminated water.

In the case of immobilized microbial cells, permeable reactive bio-barriers (PRB) have been suggested to remove pollutants from groundwater in full-scale projects with promising results (Figure 1.1). A wide range of reactive medium such as activated carbon and several materials as support to biofilm formation can be used in PRB (Cobas et al., 2013). Cobas *et.al* studied the performance of a permeable reactive bio-barrier filled with immobilized fungus as a potential useful method to adsorb and degrade PAH (Cobas et al., 2013). However, they did not provide details about the mechanism that cells attached to the supports and did not suggest the approach to immobilize microorganism on hard surface instead of porous support (Cobas et al., 2013). Surface engineering of cell walls of hydrocarbon-degrading bacteria might be applied to magnetically modify biofilm formation of hydrocarbon-degrading microorganisms on hard surface such as stainless steel and concentrate the cells using magnetic field (Cobas et al., 2013; Konnova et al., 2016). Further work is necessary in this field to investigate the combination of electromagnetic-based approach used for oil spill remediation and magnet-responsive oil-degrading bacteria to gather contaminant and degraders in a common location (Warner et al., 2018b).

2.7 Future Research Needs

Bioremediation of unconventional oil-contaminated soil, sediment, seawater, and groundwater are confronted with special challenges that include:

- Biodegradation of unconventional oil petroleum by means of microorganisms in seawater with high salinity is slower compared to other locations due to the harsh environmental conditions. The use of a material carrier to immobilize hydrocarbon-degrading bacteria consortium culture to improve extra heavy petroleum and unconventional oil in seawater might be an effective approach. Nevertheless, case studies on immobilized-microbial cells and enzymes for cleaning up unconventional oil-contaminated sites are still limited.
- Limited bioavailability of heavy hydrocarbons inspired researchers to study the use of surfactants (chemical and biological) to improve the dispersion of asphaltene transport in a liquid medium and release the trapped hydrocarbons from the porous medium in contaminated soils. Thus, *in-situ* biosurfactant production through nutrient-only bio-stimulated treatment can serve as a biological tool to overcome issues regarding increased viscosity of unconventional oil sub-fractions.
- The presence of structurally diverse high molecular weight components at ultra-low concentrations that act as competitive inhibitors has been reported to avoid the action of specific enzymes, compromising unconventional oil biodegradation. The ultra-low concentration of very toxic compounds, for example, NAs in a bitumen mixture might act as competitive inhibitors and adversely affect the activity of specific enzymes. Therefore, the co-remediation of unconventional oil sub-fraction using enzymes, such as laccase and locally isolated potential microbes, such as white-rot fungi might result in a higher rate of degradation due to their synergistic effect on laccase activity.

2.8 Conclusion

Due to the increased use of unconventional oil, its transportation by pipelines and subsequently the potential for leaks and spills is growing. This review has highlighted the fact that non-biotechnological (e.g., pump and treat method) might remove contamination from subsurface or surface of ecosystems, but biotechnological tools should be applied to remediate and detoxify unconventional oil (e.g., Dilbit and Bakken oil) under moderate temperature conditions and even

cold climate sites. Even though biodegradation of these hydrocarbons has been extensively improved using bioaugmentation and bio-stimulation (such as organic/active sludge amendments), integrated methods and mechanisms including bioaugmentation, bio-stimulation and phytoremediation are necessary to be applied to improve the performance of bioremediation of high concentrations of weathered hydrocarbons and bitumen. Other biotechnological approaches (such as genetically engineering bacteria, immobilization method, and enzyme remediation technology) and newly found potential microbes might also promote the degradation of recalcitrant components. To date, only a few scattered studies of these mentioned approaches have been carried out to effectively clean-up these hydrocarbons. Moreover, there are only a few studies on the hypothesis that unconventional oils would select different microorganisms than traditional petroleum due to the presence of metal, oxidizing compounds, asphaltene, resin fractions and high molecular weight alkylated PAH. Thus, further research is required to demonstrate the applicability of the above-mentioned methods in the mixture of unconventional oil. Nevertheless, it becomes all the more important to mention that unconventional oils remediation entails hybrid versus single methods.

CHAPTER THREE: Treatment of unconventional oil contaminated water by adsorption onto hydrophobically modified dolomite

PART 1

Hydrophobic dolomite sorbent for oil spill clean-ups: Kinetic modeling and isotherm study

Seyyed Mohammadreza Davoodi[1], Satinder Kaur Brar[1,2*], Rosa Galvez-Cloutier[3], Richard Martel[1]

[1]INRS-ETE, Université du Québec, 490, Rue de la Couronne, Québec, Canada G1K 9A9

[2] Department of Civil Engineering, Lassonde School of Engineering, York University, North York, Toronto, Ontario Canada M3J 1P3.

[3] Département de Genie Civil, Université Laval, Québec G1K 7P4, Canada

(*Phone: 1 418 654 3116; Fax: 1 418 654 2600; E-mail: *satinder.brar@lassonde.yorku.ca; satinder.brar@ete.inrs.ca;*)

***Fuel, 285,* 119191; DOI: 10.1016/j.fuel.2020.119191**

Abstract

A low-cost chemical hydrophobic sorbent was synthesized by the dip-coating method. The sorbent was characterized using different methods, including TGA, FTIR, XRD, SEM, and Zeta potential. The removal of unconventional oil from water by palmitic acid-modified dolomite was investigated by batch adsorption after varying pHs (1–9), contact times (5–80 min), adsorbent dosage (0.1–0.7 g mL^{-1}), initial oil concentration (3000–7000 mg L-1), salinity (0–0.1 g mL^{-1}) and different temperatures (299 and 309 K). TGA analysis revealed the increase in maximum oil sorption capacity of sorbent from about 64 to 498 mg g^{-1} (Dilbit) and 98 to 530 mg g^{-1} (Bakken oil) in the oil-water mixture. The kinetic studies showed that pseudo-second kinetic (PSO) model described unconventional oil sorption on hydrophobic sorbents in a much better manner than other models in term of R^2 values indicating that the overall rate of the oil sorption process might be controlled by a strong chemical reaction between oil molecules and active sites on the surface of sorbent. However, the obtained values of free energy estimated from Dubinin-Radushkevich (D-R) isotherm model were 7.57 and 7.833 KJ mol^{-1} for the sorption of Dilbit and Bakken oil, respectively, which indicated strong physical nature of unconventional oil sorption on the studied sorbent. PSO model is not the only rate-limiting step and other mechanisms may control the rate of sorption, as all of them may be operating simultaneously. The external mass transport of sorbate and external film diffusion in this sorption system was very fast in comparison with the intraparticle diffusion and adsorption. For both tested oils, the isotherm studies revealed that the experimental data agreed with Sips, Toth, Temkin, and Freundlich models due to the highly heterogeneous systems.

Keywords: Low- cost hydrophobic sorbent, Unconventional oils, Kinetics, Isotherm, Oil spill

3.1.1. Introduction

It is general understanding that unconventional oil is petroleum that requires extracted using techniques other than the traditional oil-well method to guarantee the viability of the oil recovery from tight and shale reservoirs and subsequent transportation to storage facilities, terminals and refineries (National Academies of Sciences and Medicine, 2016; Santos et al., 2014). Considering the devasting environmental impacts of the past pipeline spill incidents, the issue of pipeline oil transport is highly contentious and the remediation technologies for soil contaminated with unconventional oil have been under study. A series of different cleanup techniques including mechanical methods, in situ burning, dispersion method, extraction, thermal desorption and chemical oxidation have been suggested for soil and water remediation (Li et al., 2018a). Adsorption techniques involving natural organic sorbents, synthetic organic/polymers and mineral sorbents are also considered as the most popular solutions applied to prevent further migration of petroleum hydrocarbons on the land and water surface. In this field of research, two areas of study has been considered: enhancing the efficiency of petroleum removal technology and modeling the mechanism of oil removal to obtain a better understanding of the adsorption process (Khan et al., 1996; Naghdi et al., 2017).

Depending on the type of oil, spill scale and the location of accident, suitable adsorbent should be chosen (Abarghani et al., 2018). Numerous literature has investigated the use of mineral adsorbents in oil spills cleanup (Hosseinpour et al., 2013; Ukotije-Ikwut et al., 2016). Mineral materials used for petroleum spills cleanup in a form of granules/or powders (e.g., zeolites, Clay minerals, silica adsorbents) have a number of properties that make them appropriate adsorbents for cleaning up spilled oil effectively. With regard to the salts (other type of mineral materials such as calcitic and dolomite lime), even though crude unconventional oil that possess asphaltene and resins (polar functionalities) are particularly adsorptive to this type of minerals, they have not been considered as adsorbents of petroleum substance that contain petroleum fractions such as nonpolar alkanes. Thus, some literature recommended wettability alternation and the fabrication of superhydrophobic sorbents to achieve high absorption capacities for different types of contaminants (Gomari and Hamouda, 2006; Kelesoglu et al., 2012; Okhrimenko et al., 2013). For instance, Patowary et al. (2015) showed that conventional natural particle sorbents, including

mineral products, natural biomass can be modified with organic molecules by different method such as dip-coating method to improve their hydrophobicity (Patowary et al., 2015). Other approaches have been developed involving solution-immersion process, chemical etching, ultrasounds irradiation and others (Banerjee et al., 2006; Younis et al., 2017); however, the functionalization of mineral materials with palmitic acid through dip-coating method have been considered less expensive approach to obtain low-cost chemical, durable and efficient superhydrophobic adsorbent in clean-up of the oil in water.

In the present study, the rock limestone as a local available material is modified to develop an inexpensive sorbent for unconventional oil spill remediation. Esterification reaction was used for hydrophobic functionalization of dolomite via a simple and economic one-step synthetic approach to enhance sorbent selectivity and effectiveness in the removal of spilled unconventional oil from water surfaces. The synthesized superhydrophobic adsorbent was characterized using zeta potential, Fourier-transform infrared spectroscopy (FT-IR), X-ray powder diffraction (XRD), scanning electron microscope (SEM) techniques. Furthermore, the extend of sorption and the influences of several controlling variables such as the chemistry of unconventional oil, temperature, contact time, concentration of adsorbent, the composition of the aqueous liquid (particularly its pH and salinity) on the sorption capacity of hydrophobic dolomite were investigated. Pseudo-first-order, pseudo second-order, Elovich, film and intra-particle diffusion models were investigated to show that which one can well describe the kinetic behavior of Dilbit and Bakken oil sorption by hydrophobic dolomite. Different theoretical isotherm models were used to elucidate the mechanism involved in the Dilbit and Bakken oil sorption.

3.1.2. Materials & Methods

Sourcing, preparation and characterization of Modified Dolomite

Dolomite is a locally available material used for the batch adsorption experiments obtained from the Career Union Ltd., Quebec City. The surface modification of dolomite sorbent powder was carried out using a dip-coating method. In brief, to obtain the maximum oil adsorption capacity by palmitic acid-coated dolomite, different amounts of fatty acid (0 - 4 g) were incorporated into 5 g of natural dolomite. In order to prepare hydrophobic sorbent using dip-coating, Gomari et.al (2006) suggested that the pH of the water phase is responsible for palmitic acid dissociation that promoted

the reaction between dolomite ions and the dissociated fatty acid (Gomari and Hamouda, 2006). Thus, the dolomite was mixed with distilled water at a pH value of 7. Quast et.al reported the estimated pKa for palmitic acid (4.7) indicating that it will exist entirely in the anion form at pH values of 5-9 and therefore these anions absorb strongly to dolomite (Quast, 2016). Wang et.al also reported that the surface properties of mineral sorbents including dolomite are influenced by temperature and the interaction of fatty acid and mineral materials increases with increasing temperature (Wang et al., 2002; Wang et al., 2019a; Wang et al., 2005).

The modified sorbents were used for Dilbit and Bakken oil removal while other operating parameters were kept constant. Based on the percent removal, powder of palmitic acid presented the best performance; however, in order to study the application of dolomite to make low cost superhydrophobic dolomite-palmitic acid absorbents for up-taking spilled and dissolved unconventional oil from wastewater and stream water, 3 g of fatty acid was employed for loading onto 5 g of natural dolomite. Finally, the mixture was stirred at 80 ±1ºC for 2 h; thereafter, the aqueous solution was evaporated at 65±1ºC in a convection oven and sieved through 9.5 mm sieve. The crystalline structure and purity of modified dolomite were determined from XRD analysis**.** XRD patterns of sorbents were collected from 2 to 90°, two theta angular range in 0.05° steps, using graphite monochromatic CuKα radiation on a Bruker AXS Diffractometer D8 Powder XRD. (FT-IR analyses were recorded in the range of 400–4000 cm^{-1} using a Nicole IS50 FT-IR Spectrometer (Thermo Scientific, USA) in attenuated total reflectance (ATR) mode with 8 cm^{-1} resolution as reported elsewhere. Before applying FTIR, the samples were washed with Milli-Q water to remove unabsorbed acids. The morphology of the samples was examined by SEM analyses using EVO® 50 scanning electron microscope (Zeiss, Germany) at an acceleration voltage of 10.70 kV. Finally, the change of zeta potential on dolomite surface was studied using zetasizer nano ZS (Malvern Instrument Inc., UK) at different pHs. To measure the zeta potential of hydrophobic materials, it has been suggested to apply 2-propanol as the matrix. In this study, a mixture of water and 2-propanol (90:10) were prepared to disperse fatty acid and modified sorbent for zeta potential test.

In order to determine the maximum unconventional oil sorption capacity of sorbents and sorption selectivity between water and oils, standard test method developed for adsorption performance of sorbents based on ASTMF726-99 standard (ASTM) has been suggested in some literature. However, in the case of powder sorbents, where filtration could be difficult due to the small size

of the grain and loss of some number of powders, instrumental methods have been recommended to determine the amount of oil and water in the sorbents. To study the oil sorption in the pure oil medium, 20 mg of the sorbents powders was added to 25 mL of the oil samples (Dilbit and Bakken oil) and shaken for 30 min at 1000 rpm for complete sorption of oil by the sorbent. The mixture was filtered by vacuum filtration using Whatman 52 filter paper. The scraped sample was placed in a vial and stored in the refrigerator to reduce the chance of evaporation and was analyzed by thermos gravimetric analysis (TGA). The amount of water adsorbed by natural and treated dolomite were similarly determined for water sorption test, by following the same procedure. A known mass of sorbents was placed into a 25ml Erlenmeyer flask filled with 20 mL of Milli-Q water and shaken for 30 min at 1000 rpm, followed by vacuum filtration. To determine the amount of oil adsorbed by dolomite in water-oil system sorption test, the sorbent powders were added to the oil-water mixture and placed into the Erlenmeyer flask. After reaching a steady state condition, the saturated sorbent was removed by vacuum filtration. TGA analysis was performed in flowing compressed air with a heating rate of 20^{o}C min^{-1} to 500 ^{o}C min^{-1}.

Characterization of Unconventional Oil

The value of total acid number of Dilbit and Bakken oil were determined according to the GB/T 7304-2014 method that has been reported elsewhere (Li et al., 2018b). The I.R spectra of the tested Dilbit and Bakken oil were reordered in the region 4000-200 cm^{-1} on a Nicole IS50 FT-IR Spectrometer (Thermo Scientific, USA). The zeta potential of oil components in water suspensions were carried out by dispersing Dilbit and Bakken oil in water as small oil droplets were prepared by the probe and batch sonication and their zeta potential were examined using ZetaSizer.

Batch Sorption Studies

Batch adsorption experiments were performed by conventional method. The powder sorbents were put in a 40mL tube containing about 10 mL of oil mixtures. The reduction of surface tension between water and oil was done using ultrasonic technique. Moreover, in order to study the oil adsorption performance of sorbents, the initial concentrations of contaminants in water has been recommended to be low (Fard et al., 2016; Patowary et al., 2015). In other words, the appropriate adsorbent should meet the criteria including high sorption capacity toward oils when the oil

concentration of mixture is low. The variables that were investigated for possible effects on adsorption capacity and removal efficiency were types of oils (Bakken oil and Dilbit), contact time (1-80 min), initial oil concentration of mixture (700 – 7,000 mg L-1), temperature (26 to 36 ^{O}C), salinity (0 to 0.1 g mL^{-1}) and pH (3-11).Before the addition of adsorbent, initial pH of mixture was adjusted to required value (3,6, or 11) either by 1 N HCl or NaOH. Calcium chloride at 0.01 M was applied to study the effect of salinity on the removal efficiency and the adsorption capacity. The tubes were shacked at desired temperature to reach the equilibrium and the samples had to be destroyed in order to obtain capacity adsorption measurements. At the end of the adsorption period, the samples were centrifuged, and the solution were filtered through stainless steel mesh to avoid any sorbents in the aqueous phase. Then, oil-water sample was collected following each experimental run, transferred to liquid funnel containing n-hexane extracting solvent and acidified to pH 3 to facilitate extraction (Younis et al., 2017). Residual concentration of unconventional oil in n-hexane were measured via UV-visible spectroscopy for the batch adsorption experiments at a wavelength of 198 nm. For batch experiment, the difference of final and initial concentrations was calculated and considered as the amount of oil adsorbed. Sorption capacity and adsorption uptake were determined according to the Eq. (1):

$$q_t = \frac{(C_o - C_f)V}{W_g} \quad (1)$$

The oil removal percentage from aqueous solution is calculated using the Eg.2.:

$$R\% = \frac{(C_o - C_f)}{C_f} \quad (2)$$

After determining the optimum conditions for modified sorbent, the effect of initial oil concentrations was studied.

Error functions

To determine the coefficients of two/three-parameter isotherms and kinetic models, two methods are available. Ordinary least square method (OLS) that is frequently employed to estimate the unknown parameters in a linear regression model using transformed isotherm/kinetic variables. Solving the linear form of equations by measuring the difference between theoretical and experimental data in linear plots might violate the error equality of variance and fail to measure the errors in their non-linear forms. Thus, the non-linear regression method has currently been applied to select the optimum kinetic and isotherm for experimental data. Non-linear regression method involves the step of minimizing the error distribution between the predicted

kinetic/isotherm and the experimental data by maximizing or minimizing the error functions based on the error function definition. In this study, for isotherm and kinetic reaction models, seven sets of error functions were employed for optimization procedure to measure the goodness of fit based on the smaller error function values indicating a better-fitting curve (Table 3.1.1) (Ayawei et al., 2017; Crini and Badot, 2010; Mowla et al., 2013; Raji and Pakizeh, 2014). The optimum isotherm/kinetic was recognized as the models with the smallest sum of normalized error (SNE). The calculation method for SNE consists of five steps: (1) determination of model parameters by minimizing the applied error function (If the coefficient of determination is the applied error function, the solver add-in must be adjusted on maximizing); (2) determination of the value of other error functions based on the parameters obtained from step (1); (3) performing the above steps for other error functions; (4) selection of the maximum output of each error function from all sets. The value of other sets should be divided into the maximum value; (5) calculation of the summation of all of these SNE for each parameter (Crini and Badot, 2010; Sidik et al., 2012). The non-linear method is mathematically complex compared to linear regression. Thus, the trial-and-error procedure was developed to estimate the isotherm and kinetic parameters using an optimization routine to minimize the sum of the square of the errors (ERRSQ) between the experimental data and isotherm/kinetic model. For diffusion kinetic models, the parameters were calculated using linear and non-linear regression methods to determine the R^2 values and find the best-fitting paraments.

Table 3.1.1. Isotherm and Kinetic Models

Model	Type of Function	Nonlnear Form	Reference
Langmuir	Rational	$q_e = \frac{q_{max} K_L C_e}{1 + C_e K_L}$	(Wang et al., 2015)
Freundlich	Power	$q_e = K_F {C_e}^{1/n}$	(Sidik et al., 2012)
Redlich-Peterson	Rational	$q_e = \frac{A C_e}{1 + B {C_e}^{m}}$	(Wang et al., 2015)
PFO	Exponential	$q_t = q_e(1 - \exp(-tk_1))$ $h_1 = k_1 q_e$	(Rahman and Sathasivam, 2015)
PSO	Rational	$q_t = \frac{{q_e}^2 K_2 t}{1 + q_e K_2}$ $h_2 = k_2 {q_e}^2$	(Raji and Pakizeh, 2014)
Elovich	–	–	(Sidik et al., 2012)
Weber-Marris	–	–	(Raji et al., 2015)
D-R	Exponential	$q_e = q_s \exp(-K_{DR} \boldsymbol{\varepsilon}^2)$ $\boldsymbol{\varepsilon} = RTln(1 + \frac{1}{C_e})$ $E = \frac{1}{\sqrt{-2K_{DR}}}$	(Raji and Pakizeh, 2014)

3.1.3. Results and discussion

Characterization of oils and sorbents

Surface Morphology

SEM images of the raw dolomite and palmitic acid-modified dolomite are shown in Figure 3.1.1. Treatment of raw dolomite by palmitic acid resulted in the increase in the diameter of particles due to chemical changes on the surface layer that introduce the long chains in the surface of sorbent. The excellent sorption capacity of hydrophobic dolomite compared with raw sorbent might be ascribed to the rough surface of modified sorbents due to the presence of calcium and magnesium palmitate on their surface after the treatment with a fatty acid. Patowary et.al (2015) also reported rough surface of hydrophobically modified sorbents, whereas the smooth surface of precipitated calcium carbonate sorbent powder (PCC), that might be attributed to the presence of insoluble calcium palmitic on the surface of sorbents (Patowary et al., 2015). However, Sidik.et al (2012) stated that the surface area and rough surface gave less contribution to the crude oil adsorption compared to the hydrophobicity (Sidik et al., 2012).

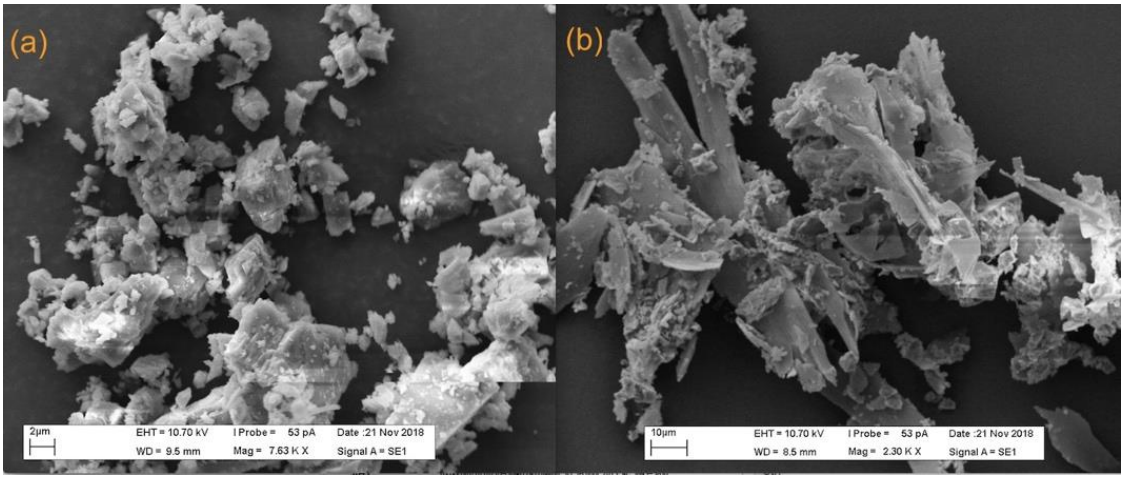

Fig. 3.1.1. SEM images of (a) raw dolomite; (b) hydrophobic dolomite.

Fourier transform infrared spectroscopy (FTIR)

The relationship between oil composition and IR peaks is somehow blurred due to overlapping absorption peaks, yet the spectra could provide us with a quick visual inspection by revealing some

trends in different regions. For example, the spectra give information on the abundance of asphaltenes and resins in the samples and evidence of biodegradation. For example, the larger area of the C=O peak at about 1600 cm^{-1} and the aromatic ring peaks between 720-850 cm^{-1} for Dilbit indicated the severe photooxidation/degradation and a higher percentage of aromatic molecules including resins and asphaltene in Dilbit. So, the degree of biodegradation and the absence of the C=C peak at about 1500-1600 cm^{-1} for Dilbit and smaller bands between 700 and 850 cm^{-1} for Dilbit. These results indicated the lower resin/asphaltene content of Bakken oil. Moreover, the peaks present at 2985 and 2930 cm^{-1} represent single bonded alkanes and revealed that two types of oils have paraffinic nature, and in this case, treating water with oil spills necessitated the use of hydrophobic sorbents. The presence of an aromatic amine (1381 cm^{-1}) that is protonated at low pH also explained the positive charge of oil surface at acidic condition (Abdulkadir et al., 2016; Banerjee et al., 2017). (See Fig 3.1.2)

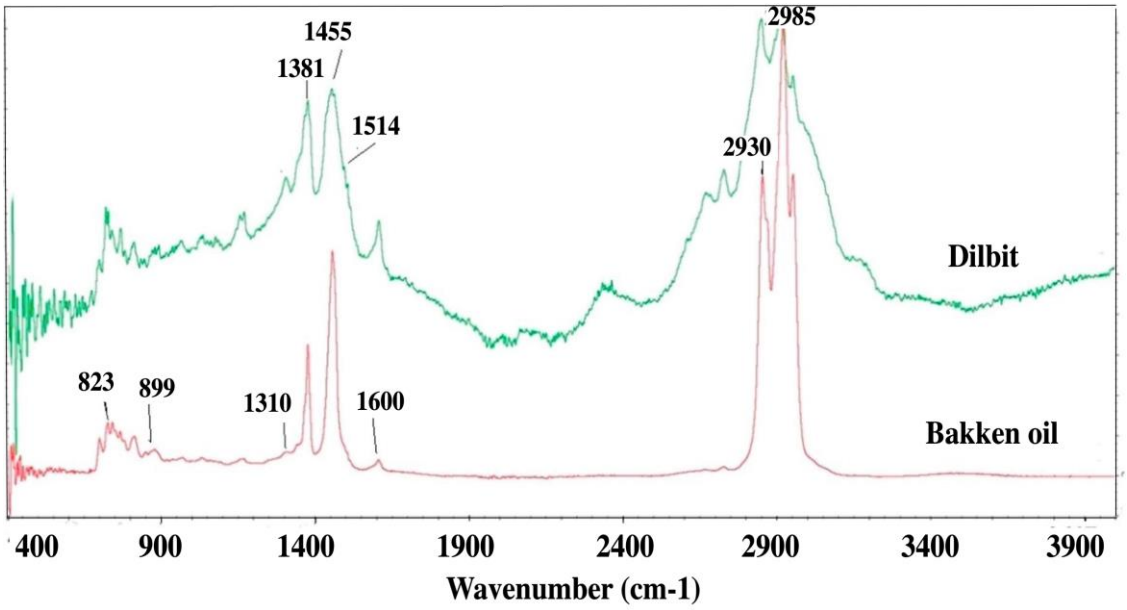

Fig. 3.1.2. IR spectra of the tested unconventional oils

The FTIR spectra of hydrophobic dolomite reveals characteristic bands for the symmetrical stretching vibration of -CH_2 group at 2,850 cm^{-1}. It can be clearly seen that the peak at 1,690cm^{-1} that signifies the C=O stretching vibration in palmitic acid s almost disappearance that might be attributed to the influence of fatty acid coating and esterification mechanism (Younis et al., 2017). As shown in Figure 3.1.3., dolomite FTIR analysis shows characteristic absorption bands of

dolomite at 1450. 880 and 730 cm^{-1} (due to O-H bending, HCO_3^{-1} group, and carbonates) that are in good agreement with the absorption frequencies reported by previous literature (Albadarin et al., 2012). By comparing the FTIR spectra of natural and hydrophobic samples, it can be seen that the increase in the peak intensity at 1000-1250 cm^{-1} (C-O) and 1735-1705 cm^{-1} (C=O) could be attributed to stretching ester linkage between cationic surface group of dolomite and the carboxyl group of palmitic acid which confirmed that the sorbent had been esterified (Albadarin et al., 2012; Asadpour et al., 2014). Moreover, intense peaks at 3000-2700 cm^{-1}, characteristic of methyl and methylene groups of palmitic acid, are related to the replacement of palmitic acid on the surface of dolomite.

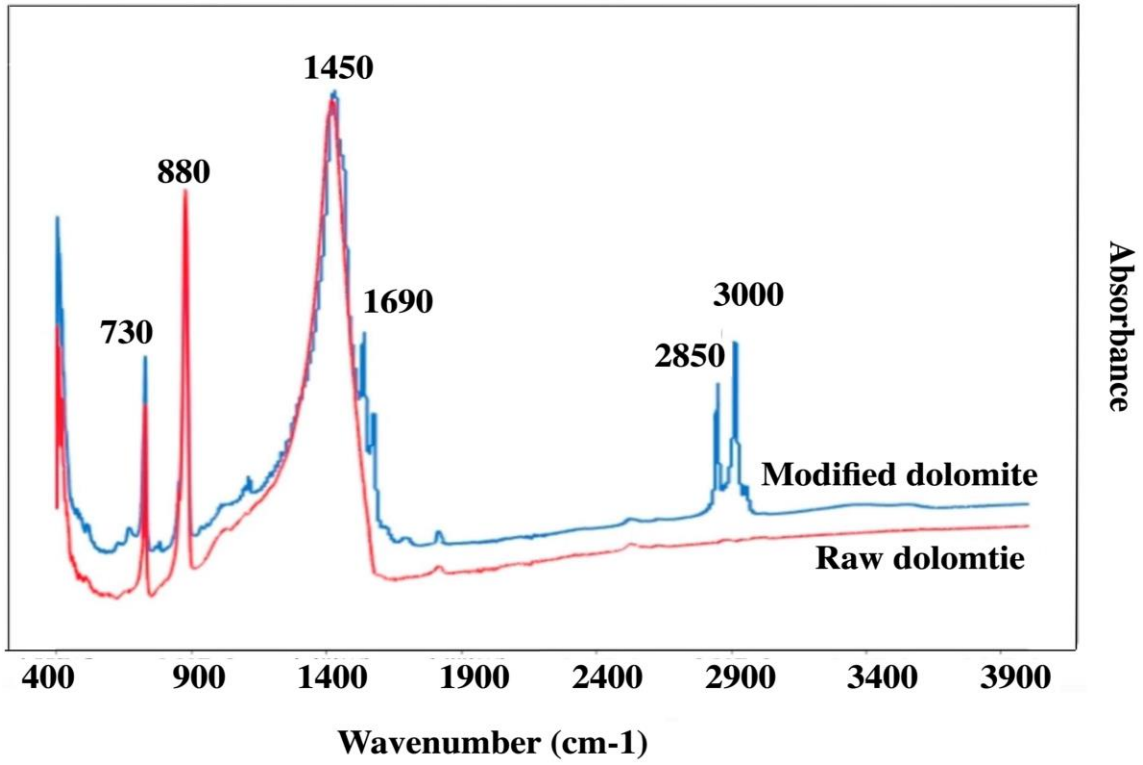

Fig. 3.1.3. FTIR spectra of natural and hydrophobic dolomite before oil adsorption

Total Acid Number

To study oil-solid interaction, the total acid number of oil can give us good insight into oil compositions. Xingang Li et.al measured total acid number of crude bitumen, and different fractions of unconventional oil including resins, asphaltenes, saturates and aromatics and reported the high content of polar groups in the heavy fractions that might cause strong interaction between

the oil component and mineral sorbent with hydrophilic surface such as dolomite. In the case of Dilbit and Bakken oil, the total acid number values were less than 0.7 and 0.3 mg KOH/g for Dilbit and Bakken oil, respectively, indicating that they mainly contain saturated nonpolar hydrocarbons. It has been reported that Dilbit mainly contains branched and cyclic hydrocarbons and Bakken oil is dominated by straight-chain, saturate hydrocarbons (National Academies of Sciences and Medicine, 2016). Thus, in the case of tested oils, the more hydrophobic surface is the more prone to oil adsorption it is (Cremaldi et al., 2015).

Zeta Potential

In order to confirm experimental results regarding the effect of pH on selective and efficient sorption of oil, the values of zero potential charge (pHzpc) for natural dolomite and hydrophobic sorbent were measured. Considering the fact that the composition of the surface of the particles is important in determining the zeta potential, the surface modification caused changes in the zeta potential of materials. In the case of raw dolomite, the charge of surface is the result of the formation of the ionic species to the liquid-solid surface which depends on the pH (Marouf et al., 2009). As can be seen in Figure 3.1.4, the zeta potential of modified dolomite versus pH curve differ markedly from the bulk composition (dolomite). Even though for strongly hydrophobic materials the net surface charge is close to zero (hydrocarbon chains are hydrogens and carbons bonded together that are similar in electronegativity), carboxylic group as the source of negative charge was dissociated around 3.5 and above. Thus, the negatively charged polar head of fatty acid brought up negative zeta potential. The zeta potential of fatty acid in 2-porpanol solvent is positive (6.7 mV at pH=7) due to the fact that carboxylic group are undissociated form and electrostatic forces are negligible as interfacial functional groups are neutrally charged in the absence of an aqueous phase. In the case of modified dolomite, the net surface charge is around zero at pH value of 7 and pHzpc around 5.5 were observed. For the zeta potential to change on the particle charge surface, they must have chemical groups that can be protonated or deprotonated and the chemical groups that usually render the surface of hydrophobic particles are of a non-polar nature and it means that pH has little effect on surface charge.

As mentioned previously, chemistry of crude oils is one of most important factors affecting the extent of petroleum hydrocarbon sorption onto adsorbents. Dilbit and Bakken oils are a complex mixture of hydrocarbons with a wide range of structures and molecular weights that are difficult

to characterize completely (Daughney, 2000). Thus, a great deal of effort has been made to explain the extend of petroleum hydrocarbon sorption using parameters that are related to oil chemistry. The oil-water interfacial tension, the zeta potential of oil droplets in aqueous solution, and the oil-water contact angle (Daughney, 2000) have been considered parameters that are more easily measured and describe the effect of the Dilbit and Bakken oil composition on sorption. The zeta potential of Bakken oil and Dilbit droplets in water are illustrated in Figure 3.1.4. In the case of Dilbit, the negative charge at higher pH can be attributed to the dissociation of acid-type species (Dai and Chung, 1995) and the positive charge on the Dilbit droplet surface at pH < 2 is due to the dissociation of amine-type groups in Dilbit. The lower amount of Dilbit PHzpc compared to the Bakken oil confirmed the higher content of acidic compounds in Dilbit than in Bakken oil. The point of zero charge (pzc) of Dilbit might also change by changing the naphtha-bitumen ratio. In the case of Bakken oil, the (Wahi et al., 2013) less effect of pH on charge of surface conformed the absence of ionizable and hydrophilic groups suggesting that Bakken oil containing mainly alkanes .

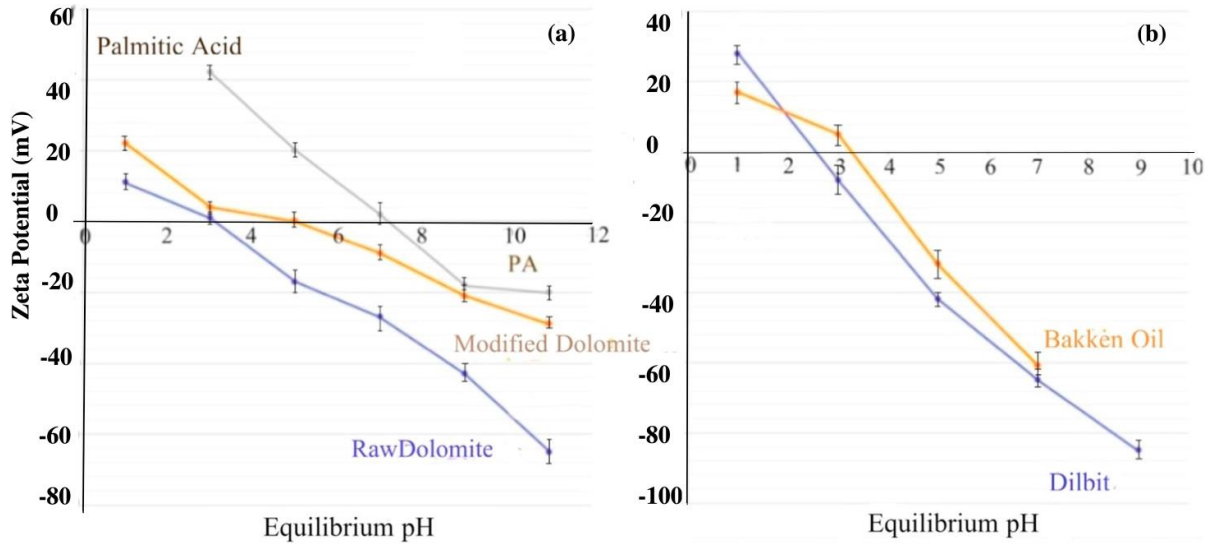

Fig. 3.1.4. The variation of the zeta potential with pH of a) raw dolomite/water suspension (RD), fatty acid/water-2-propanol suspension (PA), hydrophobic dolomite/water-2-propanol suspensions (MD); b) Dilbit and bitumen

XRD Characterization

X-ray diffraction (XRD) analyses (Figure 3.1.5) revealed that the purity of raw dolomite sample was very high (ASTM Committee D-2 on Petroleum Products and Lubricants, 2011). The diffraction peaks observed at 2theta values of 31, 33, 35, 37, 41, 45, 51, 52 and 60 ^{o} can be signed to the dolomite (CaMg $(Co_3)_2$) that have the preferred orientations in the direction of (104) with higher intensity and sharp peak and 2theta values of 21 ^{o} showed the small amount of quartz (SiO_2) in raw sorbent. The XRD pattern for modified dolomite was similar to that of raw dolomite without any peaks attributing to the palmitic acid molecules indicating the proper coating of dolomite with palmitic acid (Gruszecka-Kosowska et al., 2015).In other words, the coating process has no influence on the crystallinity of dolomite.

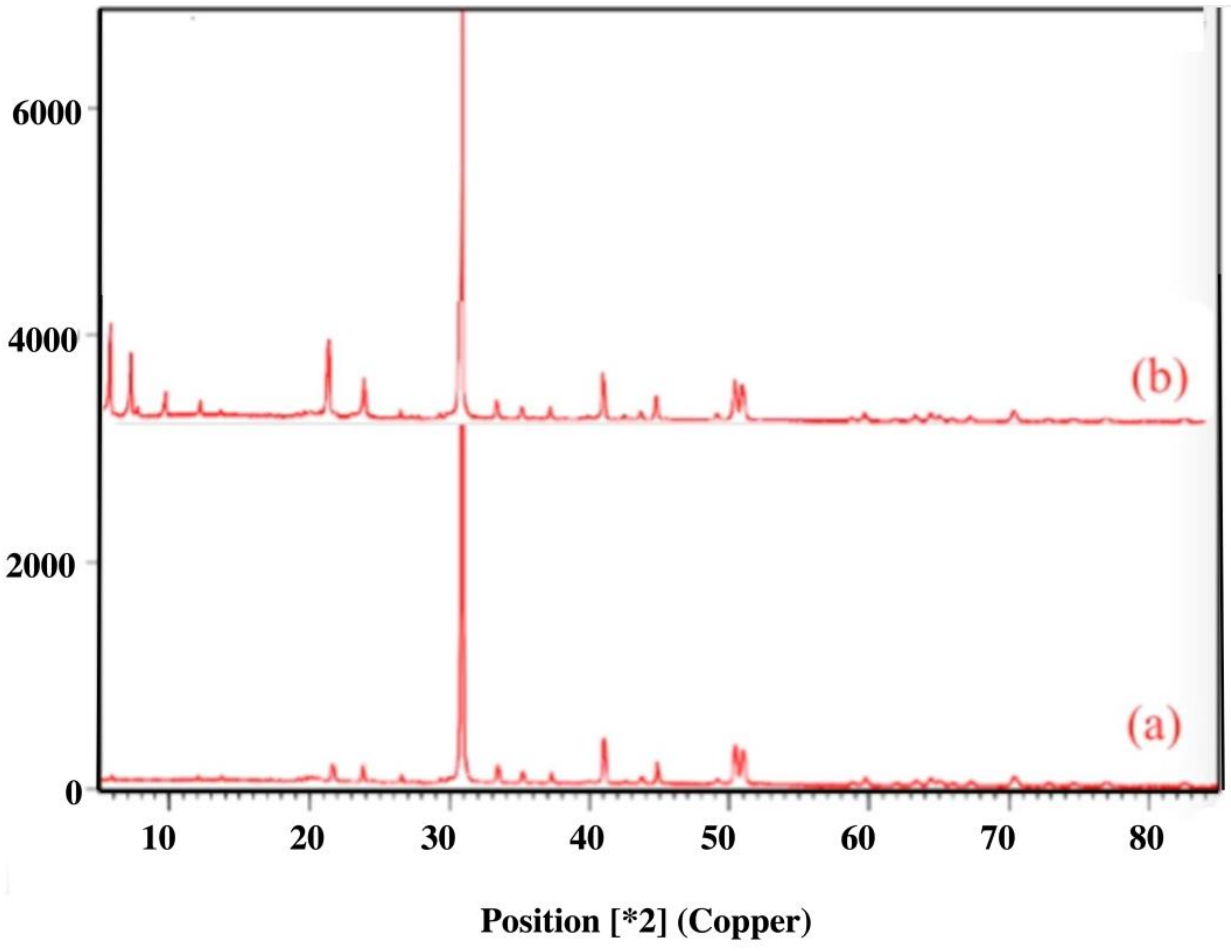

Fig. 3.1.5. XRD pattern of raw dolomite (a) and hydrophobic dolomite (b)

Oils Sorption Capacity and Sorption Rate

Figures 3.1.6 and 3.1.7 show the TGA analysis curves of nature and modified dolomite before and after sorption experiment, respectively. The difference in percent weight loss by the samples between room temperature-100 ^{o}C and 100-500 ^{o} C were attributed to the water and oil removal from the sorbents. As can be seen in Fig.6 (TGA data), for raw dolomite, the higher adsorption capacity for Bakken oil is higher than Dilbit in the presence of water that might be attributed to the fact that raw dolomite released cations (i.e., calcium and magnesium) in the presence of water and increased the pH of media up to 11.

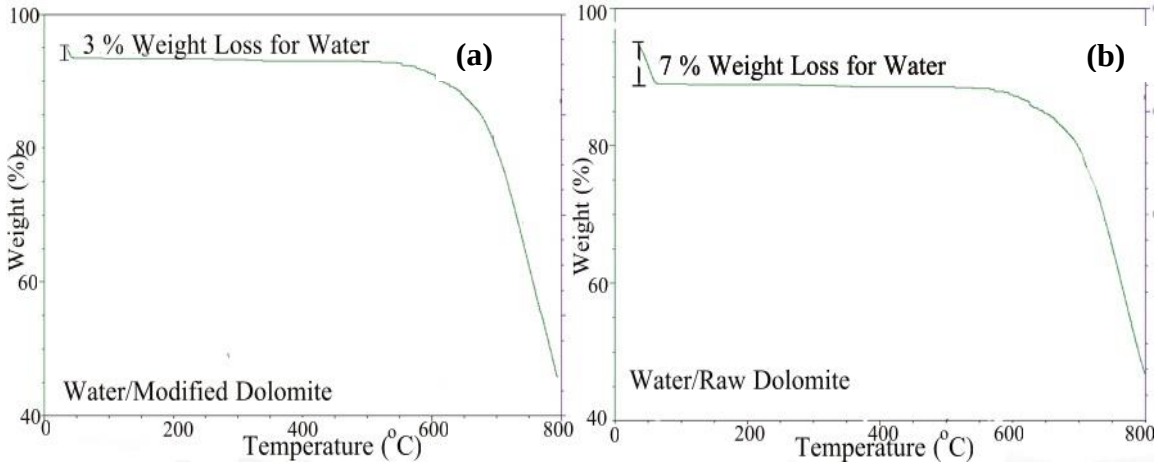

Fig. 3.1.6. TGA analysis cure of (a) modified and (b) raw dolomite before adsorption process. The difference in percent weight loss by the samples between RT-100^{o}C was attributed to the water removal from the sorbents.

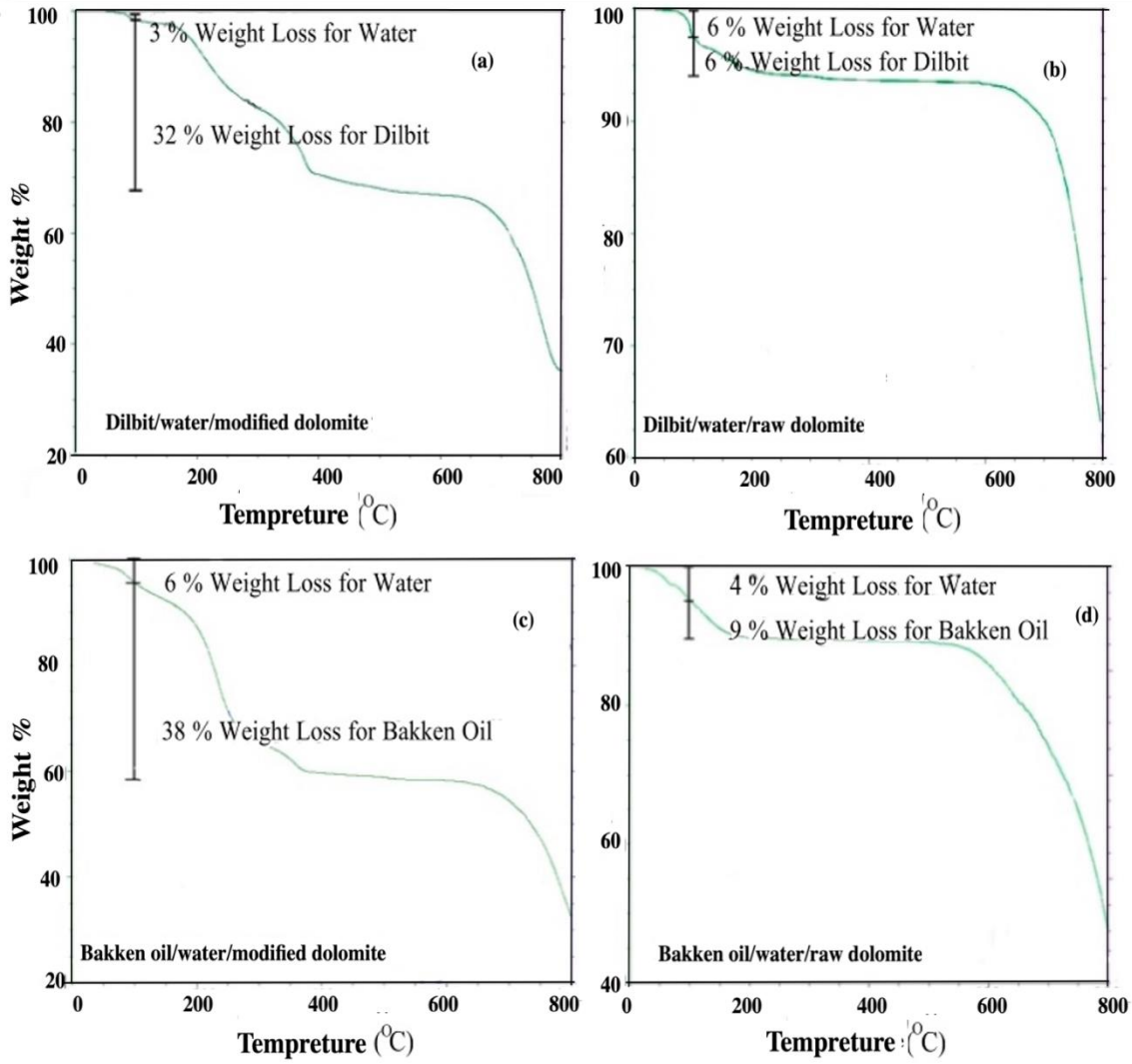
3 % Weight Loss for Water
(a)
32 % Weight Loss for Dilbit
Dilbit/water/modified dolomite
Weight %
Tempreture (°C)
6 % Weight Loss for Water
6 % Weight Loss for Dilbit
(b)
Dilbit/water/raw dolomite
Tempreture (°C)
6 % Weight Loss for Water
(c)
38 % Weight Loss for Bakken Oil
Bakken oil/water/modified dolomite
Weight %
Tempreture (°C)
4 % Weight Loss for Water
9 % Weight Loss for Bakken Oil
(d)
Bakken oil/water/raw dolomite
Tempreture (°C)

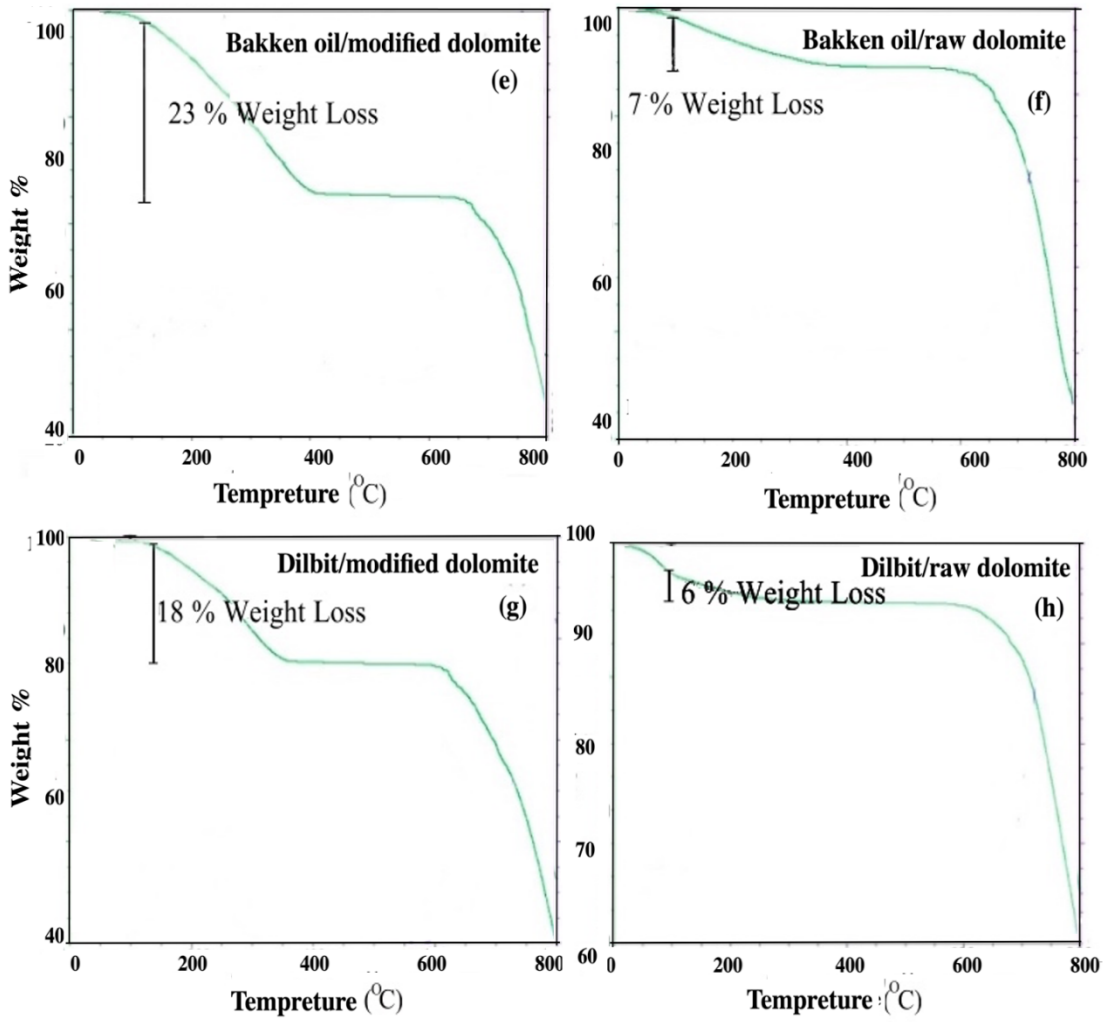

Fig. 3.1.7. TGA analysis curve of raw and modified dolomite for Bakken oil and Dilbit sorption calculation (a)-(d) oil-water micture and (e)-(h) pure oil

According to the Figure 3.1.8, the surface charge of raw dolomite has a net negative charge at this pH and Dilbit that contains a higher amount of acid-type species shows more negatively charged surface at pH 11 that increased the repulsion between raw dolomite and Dilbit. Thus, dolomite seems to adsorb it less effectively than Bakken oil (Dai and Chung, 1995; Emam, 2013). Moreover, the competitive sorption of water adversely affected the adsorption of Dilbit on natural dolomite, unlike the hydrophobic sorbents that do not interact with water molecules. In the land-based experiments, Dilbit that possessed richer acidic groups (negatively charged components of the crude oil) showed higher maximum sorption capacity on the positive charged raw dolomite surfaces compared to Bakken oil. It also might be attributed to a higher density of Dilbit compared to Bakken oil.

For modified dolomite, lower adsorption capacity for Dilbit from aqueous solution might be attributed to the steric hindrance that carbon branches present in Dilbit produce. In other words, it would be harder for non-polar molecules of Dilbit (branched and cyclic hydrocarbons) to have very close interactions with active sites of adsorbent; thus, modified dolomite has a stronger capacity to sorb Bakken oil molecules that are dominated by straight chain saturated hydrocarbon through hydrophobic bonding between alkyl chain of calcium and magnesium palmitate and oil molecules (Estell et al., 1986; National Academies of Sciences and Medicine, 2016).

As expected, modified dolomite powder showed superior water/oil selectivity and performance in adsorbing Dilbit and Bakken oil compared to natural sorbents. The higher removal of the emulsified oil and excellent oil-water selectivity on modified sorbent could be attributed to the hydrophobic character of modified powder which enabled it to repel the water molecules that is an essential parameter for oil sorbents used to remove spills from water surface (Elanchezhiyan et al., 2018).

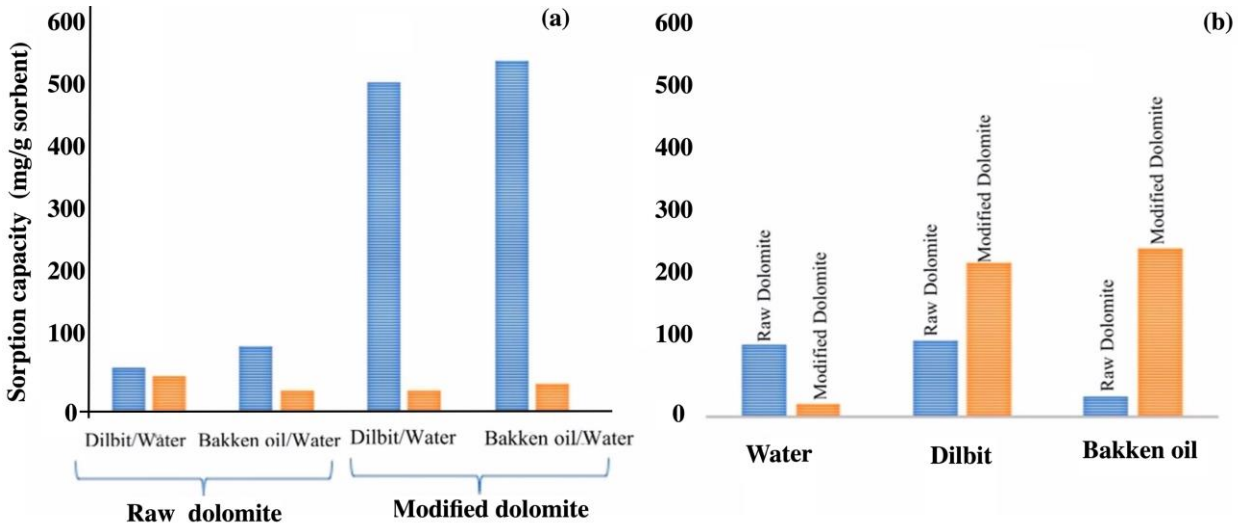

Fig. 3.1.8. Oil and water sorption capacities of RD and MD performed on oil-water mixtures; (b) pure oil mediums and pure water

Figure 3.1.9 shows the proposed mechanism of palmitic adsorption onto the sorbent surface. It also showed natural and modified dolomite powder positions onto the water phase of a water-oil mixture. As can be seen in Fig.S3, the natural dolomite settled down into the bottom-water phase, whereas modified dolomite that adsorbed unconventional oils, floated on the surface of the water

and attached to the surface of the glassy hydrophobic container. The highest adsorption capacity of modified dolomite, especially for oil-water samples provided justification in using modified dolomite as an adsorbent for the subsequent experiments. Non-polar molecules of oils with asymmetric distribution of charge did not show electric dipole moment and did not interact favorably with water. Due to this, so when oil was added to water, the water molecules formed a cage around the oil molecules that was not favorable because it limited the interaction of water molecules amongst each other. As mentioned previously, the oil adsorption process occurred after reducing the surface tension between water and oil to study the effectiveness of adsorbent to remove oil from water. The other explanation has been given to account for the adsorption of Bakken oil and Dilbit in natural dolomite. π- π interactions acted between aromatic rings present in oils and the ionic surface of dolomite and, the physical interactions (i.e., electrostatic forces, hydrogen bonding and van der Waals) involved between mineral sorbent and oils (Li et al., 2018b).

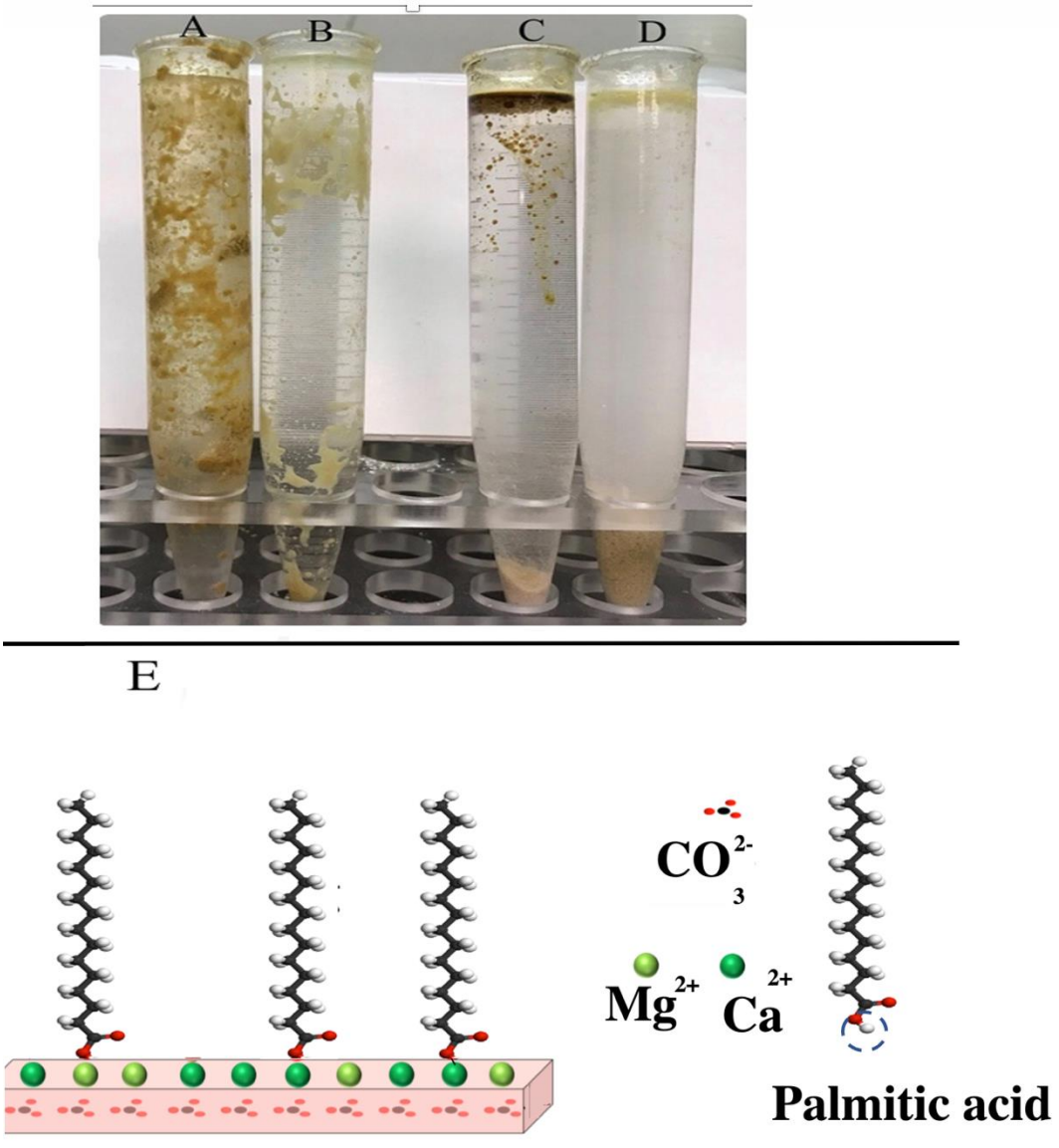

Fig. 3.1.9. Hydrophobic dolomite into the oil-water mixture (A) Bakken oil; (B) Dilbit. Raw dolomite into the oil-water mixture (C) Bakken oil (D) Dilbit. And Schemicatic representation for the proposed mechanism palmitic acid adsorption on raw dolomite surfaces

Adsorption of Bakken oil and Dilbit

Palmitic Acid Loading

As can be seen in Fig.3.1.10, the Dilbit and Bakken oil removal of natural dolomite were only about 14 and 11 %, respectively, while the hydrophobic sorbent could remove almost 84 and 91% of the oils from water. In this part, removal efficiency was provided to determine the appropriate loading due to the fact that the high removal efficiency matters during the economic comparison. Not only did the C_{16} hydrophobic tails improve adsorption affinity of hydrophobic dolomite to non-polar fractions, but also two oxygen and carbon atoms with sp^2 hybridization (unshared pairs of electrons on oxygen atoms) might facilitate the affinity of sorbent to a polar fraction of oils (Younis et al., 2017). The subsequent decrease in Bakken oil removal with sorbent loading might be attributed to the fact that oil molecules have a finite size, needing a finite space from every direction. Thus, some of the active centers cannot be accessed by oil molecules when neighboring active sites have been occupied (Liu).

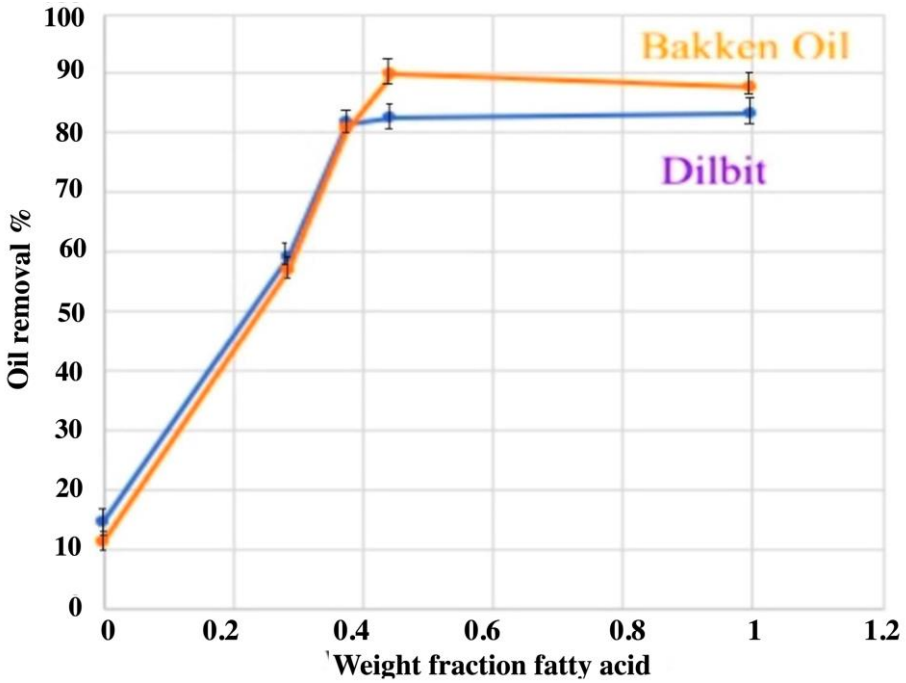

Fig. 3.1.10. Bakken oil and Dilbit removal efficiency of oils as a function of fatty acid loading (Co= 7000 mg L^{-1}; T=$26^{O}C$, pH=6.5, 1000 rpm)

Effect of Adsorbent Dosage

To estimate the standard adsorbent dosage for this study, batch adsorption experiments were conducted for a range of hydrophobic dolomite between 0.1 and 0.7 g in 10 mL solution. The adsorbent was subject to a constant concentration of oils (low enough, 2000 mg L^{-1}), and all the experimental parameters were also kept constant at 60 min and 299 ±1 K (Figure 3.1.11).

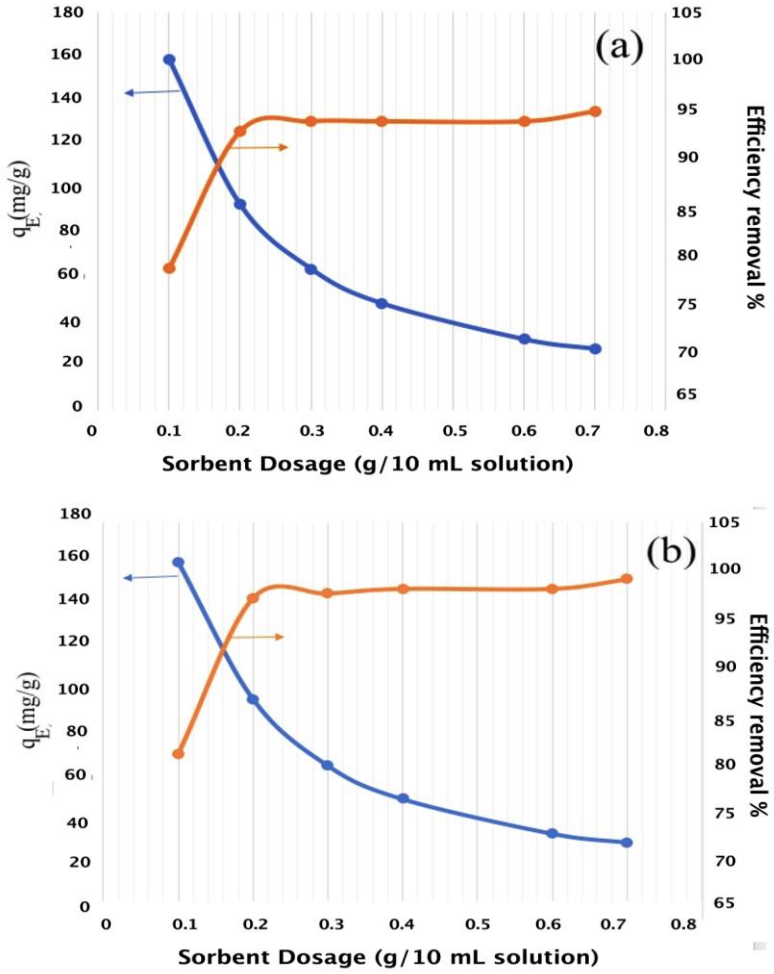

Fig. 3.1.11. Effect of adsorbent dosage on efficiency removal and sorption capacity (a) Dilbit;(b) Bakken oil. (Co= 2000 mg L^{-1}; T=$26^{O}C$, pH=6.5, 1000 rpm

The percentage of the oil sorption increased from 79 to 95.5 and 80 to 98 for Dilbit and Bakken oil as the sorbent dosage was increased from 0.1 to 0.7 g (0.07 gmL^{-1}) mixture. The increase in removal of oils can be attributed to the increase in active sites and higher interaction between oils particles and adsorbents, and the decrease in oil uptakes per unit of adsorbent is due to higher unsaturated adsorption sites during the adsorption process as adsorbent dosage increases (Sidik et al., 2012). In the case of Bakken oil, the removal efficiency reached almost 100% and for both cases, the adsorbent dosage of 0.2 g in 10 mL solution was considered as the standard adsorbent dosage, because percentage removal remains constant for higher dosages.

Dynamic adsorption of oil

Figure 3.1.12 depicts the dynamic Bakken and Dilbit adsorption as a function of contact time at different oil concentrations. As can be seen in Fig.8, the equilibrium time and capacity are dependent on sorbents, and initial oil concentrations. Briefly, the lowest sorption capacity and shortest equilibrium time were observed for the lowest initial concentration. The equilibrium stage (slower stage) that is observed especially in the case of higher initial concentration might be attributed to the adsorbed oil molecules that serve as a base layer upon which further non-polar molecules could adsorb. It has been expected that Dilbit (API gravity (^{o})= 20-22) that possessed higher viscosity adhered strongly with sorbents resulting in highest sorption capacity. However, considering TGA analysis and batch sorption experiments, the sorption capacity of Bakken oil (API gravity (^{o})= 38-40) was almost the same as the Dilbit due to the fact that Dilbit contained branched and cyclic hydrocarbons that might reduce the hydrophobic interactions and sorption capacity compared to Bakken oil with straight chain saturated hydrocarbon. It might be because of steric hindrance that carbon branches produce, and it would be harder for non-polar molecules of oil to have very close interactions with active sites of sorbents. However, the effects of steric hindrance in oil adsorption have not been discussed yet due to the fact that it is difficult to isolate the steric hindrance effects from other factors (Fini et al., 2019; Kiso et al., 2001). Some literature studied molecular width parameter to evaluate steric hindrance effects on diffusion of molecule species into sorbent pores (Fini et al., 2019). Batch experimental results indicated that, in the case of hydrophobic sorbent, initial high rate of oil uptake might be attributed to a large number of active adsorption sites as more than 85 and 95% of Dilbit and Bakken oil removal was achieved in less than 20 min (initial concentration: 7000 mg L^{-1}). The very rapid process of oil adsorption

(rapid stage), especially for Bakken oil, might be attributed to the non-covalent interaction between active functional groups of the sorbents having a long tail of sixteen carbons and non-polar hydrocarbon molecules of oils, that do not show electric dipole moment and do not interact favorably with water. In the case of Dilbit, equilibrium stage (slower stage) might be attributed to the diffusion of oil molecules from the boundary layer film onto the exterior surface contacting vacant π-orbital that participated in the oil adsorption through π-π bonding mechanism, leading to diffusion into the interior adsorbent surface and porous structure (Younis et al., 2017).

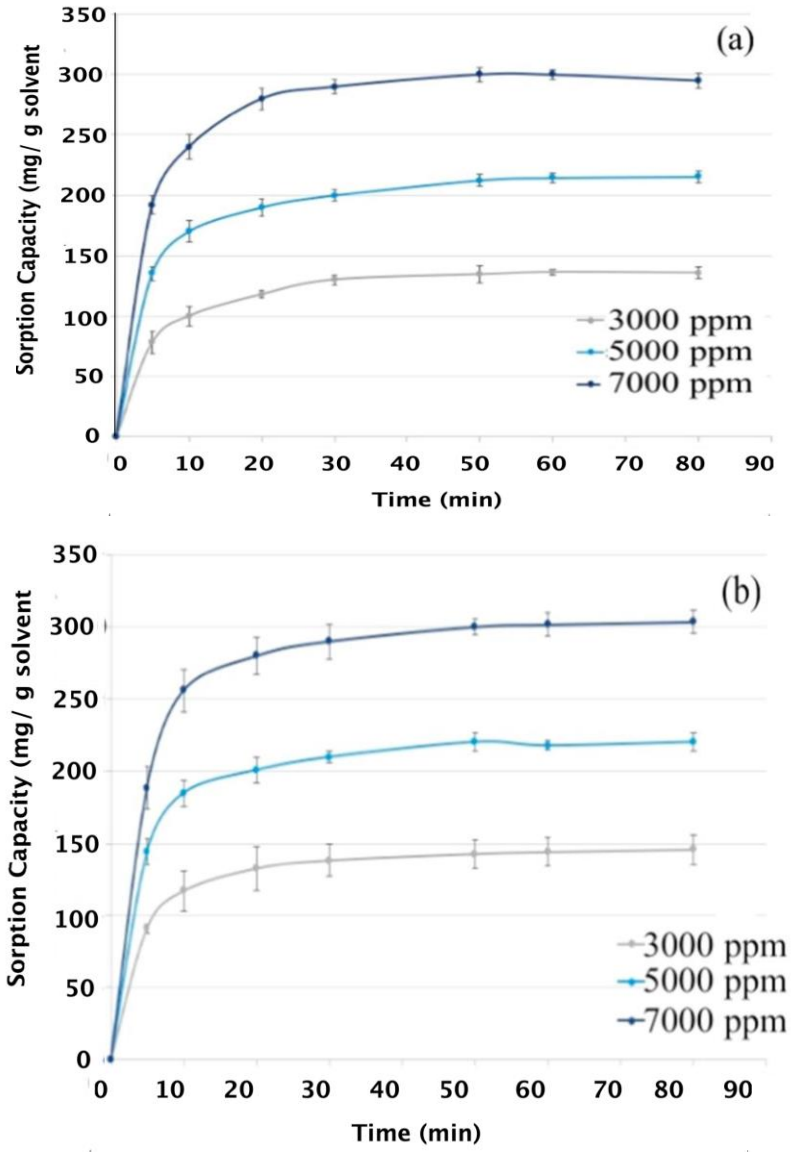

Fig. 3.1.12. Effect of contact time and initial concentration of oil on the adsorption (a) Dilbit; (b) Bakken oil onto hydrophobic dolomite. (T=26^{O}C, pH=6.5, Sorbent dosage = 0.02 g/mL, 1000 rpm)

Effect of pH

The initial pH of the oil-water mixture is one of the most important parameters in oil spill treatment studies using adsorbent as it significantly affects sorption capacity and mechanism at the solid-solution interface. The effect of pH on Dilbit and Bakken oil sorption by hydrophobic sorbent is shown in Figure 3.1.13. As mentioned previously, pH has little effect on the surface charge of

hydrophobic dolomite. The results indicated that an increase in pH led to increasing in oil uptake at pH value of 9-12 that was inconsistent with the literature that employed NaOH as a surfactant to facilitate the desorption of oil components (Li et al., 2018b). Some studies reported the highest adsorption uptake at high pH that did not correspond to the oil removal efficiency (Lim et al., 2017; Sadeghi et al., 1992). The increase in oil removal when the pH was increased, might be attributed to the fact that the addition of aqueous base (e.g., NaOH) for alkaline pH adjustment resulted in alkaline hydrolysis of oils compounds and surfactant production (carboxylate salt) via NaOH reaction with long-chain acidic compounds of crude oil. Thus, in order to avoid the saponification process, the oil-water sample was collected following each experimental run, transferred to liquid funnel containing n-hexane extracting solvent and acidified to pH 3 to facilitate extraction. As mentioned previously, the pH has little effect on non-polar groups on the modified dolomite surface; however, at a pH near the point zero charges (pzc) of oils, the oil droplet surface has 0 net charges, resulting in predominantly hydrophobic interaction with modified dolomite (Xia et al., 2005). Moreover, Acidic condition could increase oil removal by promoting destabilization of Dilbit and Bakken oil droplets thus resulting in the formation of larger oil droplets. At strong acidic condition, hydrophobic interactions decreased especially in the case of Dilbit at pH <pzc (Figure 3.1.13) that contained higher amounts of polar and acidic fractions, having more basic amine-type species properties at acidic pH (more positive charge on the surface) and a more positive charge on the oil droplet surface (Wahi et al., 2013). Because dolomite is soluble at pH=1, the pH value above 3 can be considered to determine the optimum sorption capacity and removal efficiency.

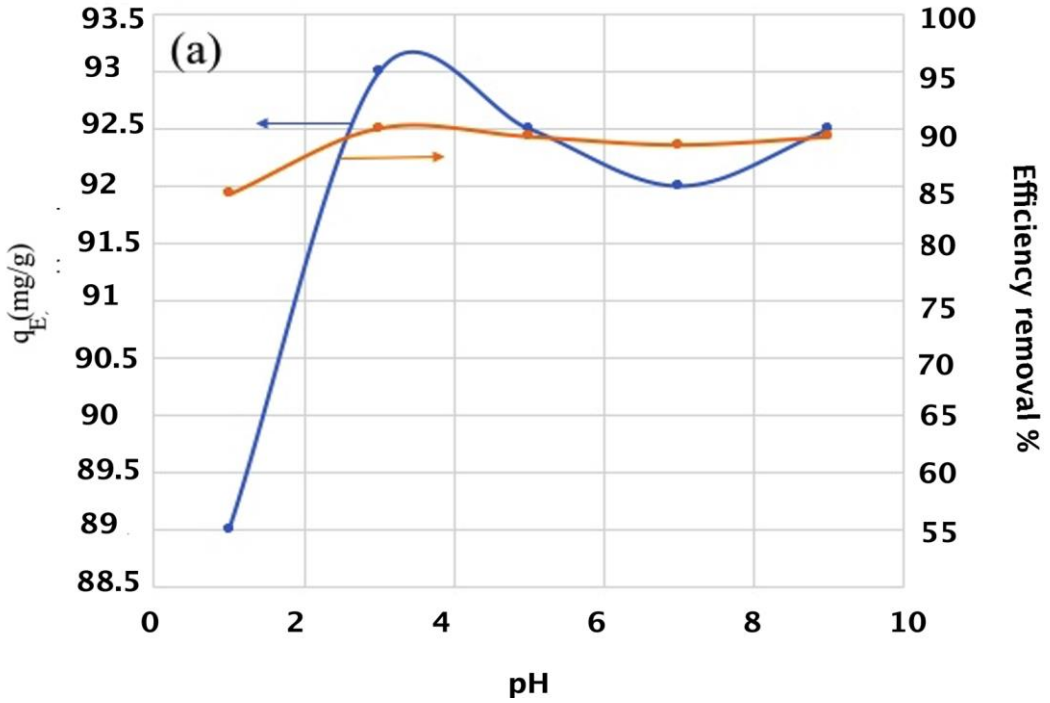

Fig. 3.1.13. Effect of pH on efficiency removal and sorption capacity (a) Dilbit (T=26^{O}C, pH=6.5, Sorbent dosage = 0.02g/mL, 1000 rpm)

Effect of Salinity

Figure 3.1.14 depicts the effect of salinity (NaCl from 0 to 2000 mg L-1) on Bakken and Dilbit adsorption and the removal efficiency. It has been reported that higher water phase salinity deters migration of oil molecules into the water phase due to the fact that salt is more soluble in water than oil phase due to the high polarity of water. In other words, when no salt is present in the solution, there are plenty of water molecules present that can interact with the polar/acidic compounds of oils, especially Dilbit. When the salt was added the charged ions interacted with water and this means that there are less H_2O molecules to interact with oil molecules (Mohamed et al., 2018; Mohamed et al., 2017).

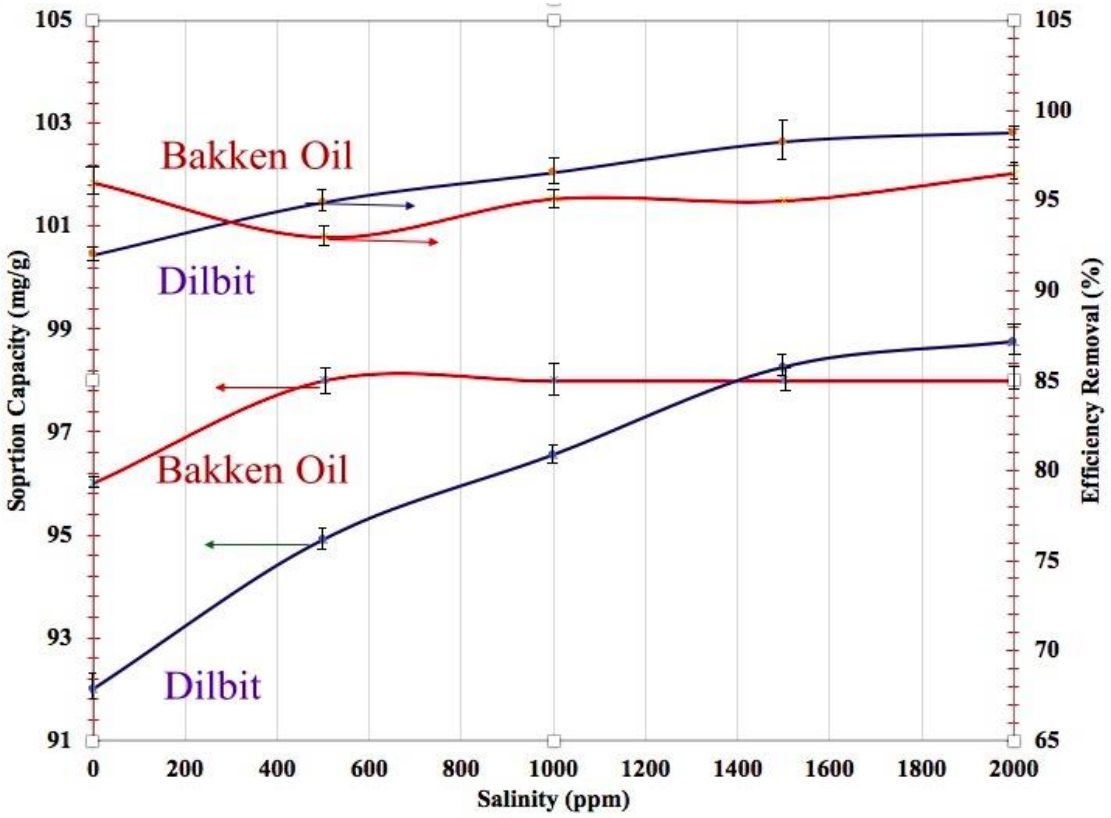

Fig. 3.1.14. Effect of salinity of mixture on the adsorption (a) Dilbit; (b) Bakken oil onto hydrophobic dolomite. (T=$26^{O}C$, pH=6.5, Sorbent dosage = 0.02 g/mL, 1000 rpm)

It is important for practical applications, such as oil spill cleanup to understand the kinetics of the oil adsorption. Moreover, the oil uptake rate can be determined to evaluate the performance of

fixed-bed or any other continues and residence time required for completion of adsorption. Thus, the sorption rate is an important factor for the selection of sorbents. To describe adsorption data and find the possible rate-controlling steps involved in the adsorption of Bakken oil and Dilbit, mathematic models can be classified as adsorption reaction and diffusion models that are different in nature (Qiu et al., 2009). Adsorption process consists of three steps: 1) film diffusion, i.e. diffusion from the bulk liquid phase through a film surrounding the particle; 2) intraparticle diffusion, i.e. diffusion within the pore fluid of the particle; 3) mass action (the oil molecules reacts with an active site on the surface of sorbent). Adsorption transfer (diffusion) models have been used to describe the adsorption kinetic results according to the first three steps and reaction models focus on the last one. In the present study, one film transfer model, two intra-particle diffusion models, and three adsorption reaction models were investigated to ascertain the kinetic behavior of Dilbit and Bakken oil sorption by hydrophobic dolomite.

Adsorption Reaction Models

In adsorption reaction models, it is assumed that the sorbent removed oil from aqueous solution by complexation mechanism. The kinetics of oil removal can be represented as Eq. (3):

$$A + O \underset{K_{-1}}{\overset{K_1}{\rightleftarrows}} AO \qquad (3)$$

Where O is the concentration of free oil in solution, A is the number of active functional groups of the sorbents having a long tail of sixteen carbons and AO is the concentration of oil bound to the sorbent. K_1 and K_{-1} are the adsorption and desorption constant rate, respectively(Raji and Pakizeh, 2014). Table 3.1.1 shows the equations associated with three adsorption reaction models (Rahman and Sathasivam, 2015). All kinetic parameters and error functions data obtained using the non-linear method (using Excel Add-in Solver) are listed in Table 3.1.1. Model parameters are obtained by minimizing the error functions with smallest SNE. According to the SNE values, Chi, SRE, and ARE were the optimum sets of error functions for PFO, PSO and Elovich. The values of error functions data and Kinetic parameters obtained using the non-linear method for PFO, PSO and Elovich models based on the optimum sets of error functions are shown in Table 3.1.2

Table 3.1.2. Equations of the error function used in this study

Error Function	Equation and Number	Reference
Correlation Coefficient	$r^2 = \frac{\sum(q_{exp}-\bar{q}_{calc})^2}{\sum(q_{exp}-\bar{q}_{calc})^2+\sum(q_{exp}-q_{calc})^2}$ (1)	(Ayawei et al., 2017)
Chi square Statistic	$\chi^2 = \sum_{i=1}^{n} \frac{\sum(q_{exp}-q_{calc})^2}{q_{meas}}$ (2)	(Rahman and Sathasivam, 2015)
Root means square error	$RMSE = \sqrt{\frac{1}{N-2}\sum_{i=0}^{N}\sum(q_{exp}-q_{calc})^2}$ (3)	(Raji and Pakizeh, 2014)
Average relative error	$ARE = \frac{100}{N}\sum_{i=0}^{N}\left\|\frac{q_{exp}-q_{calc}}{q_{meas}}\right\|$ (4)	(Ayawei et al., 2017)
Standard deviation of relative errors	$S_{RE} = \sqrt{\frac{1}{N-2}\sum_{i=0}^{N}\left[\frac{(q_{exp}-q_{calc})-ARE}{q_{exp}}\right]^2}$ (5)	(Raji et al., 2015)
Marquard's percent standattd deviation	$MPDS = 100\sqrt{\frac{1}{N-F}\sum_{i=1}^{N}\left[\frac{q_{exp}-q_{calc}}{q_{exp}}\right]^2}$ (6)	(Vijayaraghavan et al., 2006)
Sum squares errors	$ERRSQ = \sum_{i=0}^{N}\left[q_{exp}-q_{calc}\right]^2$ (7)	(Vijayaraghavan et al., 2006)

Pseudo-First-Order Kinetic Studies As can be seen in Table 3.1.3., regression coefficient values (R^2) of PFO model were reasonably high, especially in the linear regression method. However, the calculated equilibrium sorption capacity values obtained through this model were not consistent with the experimental data. It can imply that the unconventional oil (e.g., Bakken oil and Dilbit)

adsorption process onto hydrophobic sorbent does not follow this kinetic model. The increase of the initial rate of sorption (h_1) by increasing the oil concentration might be due to higher

Table 3.1.3. Parameters of the kinetic models for Dilbit and Bakken oil adsorption onto modified sorbents

		Dilbit								Bakken oil					
		Linear Regression			Non-Linear Regression					Linear Regression			Non-Linear Regression		
Kinetc Model	Model Parmeters	3000	5000	7000	3000	5000	7000	Kinetc Model	Model Parmeters	3000	5000	7000	3000	5000	7000
PFO	q_e,exp (mg/g)	136.3	215.5	295.5	136.3	215.5	295.5	PFO	q_e,exp (mg/g)	145.7	220.35	303.3	145.7	220.35	303.3
	q_e,predic(mg/g)	49.12	82.54	214.36	132.90	210.54	294.48		q_e,predic(mg/g)	56.82	114.97	121.94	141.29	215.60	297.30
	K_1(1/min)	0.064	0.061	0.054	0.215	0.199	0.159		K_1(1/min)	0.062	0.06	0.057	0.192	0.190	0.191
	h_1	3.15	5.10	11.64	28.66	42.06	47.25		h_1	3.55	6.89	6.95	27.25	40.96	56.78
	R^2	0.977	0.979	0.998	0.961	0.917	0.994		R^2	0.965	0.980	0.974	0.960	0.954	0.987
PSO	q_e,exp (mg/g)	136.3	215.5	295.5	136.3	215.5	295.5	PSO	q_e,exp (mg/g)	145.7	220.3	303.3	145.7	220.3	303.3
	q_e,predic(mg/g)	144.92	217.39	303.03	135.77	215.31	297.07		q_e,predic(mg/g)	151.5	232.5	322.6	146.4	221.1	305.8
	K_2(g/mg.min)	0.00024	0.00015	0.00021	0.00032	0.0002	0.0002		K_2(g/mg.min)	0.0003	0.00014	0.0001	0.00044	0.00024	0.0002
	h_2	5.133	7.231	19.602	5.898	8.904	18.796		h_2	6.291	7.398	10.951	13.724	12.9634	18.702
	R^2	0.999	0.999	0.999	0.999	0.983	0.974		R^2	0.999	0.998	0.999	0.999	0.996	0.977
Elovich	α (mg/g min)	5.9257	7.10586	19.5033	10.9466	19.627	48.422	Elovich	α (mg/g min)	6.2785	7.01775	10.599	9.50339	15.34	56.4491
	β (g/ mg)	0.049	0.028	0.018	0.075	0.038	0.0225		β (g/ mg)	0.0411	0.0282	0.02	0.075	0.038	0.026
	t_0 (min)	11.39	7.51	4.63	0.01	0.01	0.06		t_0 (min)	6.27	7.79	6.97	0.0013	0.01	0.02
	R^2	0.873	0.716	0.756	0.997	0.992	0.987		R^2	0.854	0.701	0.721	0.990	0.975	0.988

concentration gradient (i.e., driving force) at the higher initial concentration of oils. For this kinetic model, the calculated equilibrium sorption values obtained from non-linear regression differed from the results obtained from linear regression. This difference might be attributed to the fact that the transformation of non-linear to linear PFO model implicitly altered error structure and might violate the normality assumption of standard least squares (Raji and Pakizeh, 2014).

Pseudo-Second-Order Kinetic Studies: The values of the regression coefficient of the linearized and non-linear PSO model shown in Table 3.1.3, were the highest among the other studied models, especially for Bakken oil. Moreover, the experimental sorption capacity matched well with the calculated values. Figure 3.1.12 shows that as the initial concentration of oil increased the initial rate of sorption (h_2) values increased due to greater driving force at higher initial oil concentration. Moreover, with increasing the initial concentration of oils the time required for reaching a specific fractional uptake increased and subsequently the K_2 rate constants decreased.

Elovich Model: Elovich equation has been applied to describe the adsorption process of pollutants from aqueous solution (Xie et al., 2017). The integrated and non-linear Forms of the Elovich equation are presented in Table 3.1.1. The Elovich equation constants (α and β) can be calculated using the q_t versus log ($t+t_0$) plot. But t_0 value should be adjusted using trial and error. After guessing the t_0 value, the amount of intercept/slope ratio should be equal to the assumed value; otherwise, a new guess should be again applied to repeat the process. The non-linear regression was also applied to analyze the kinetic sorption data ability of Elovich model. The Elovich equation constants (αand β) determined in the linear regression method have been applied as an initial guess to determine the coefficient of determination by minimizing Root means square error. For both types of unconventional oils, the results obtained from nonlinear regression for Elovich equation shows relatively high R^2 compared to PFO model and it might be attributed to the heterogeneous adsorption sites on the sorbent's surface as this model has been recommended for highly heterogeneous systems. This model is suitable for a highly heterogeneous system that adsorption rises rapidly with a shorter time and could describe activated chemical adsorption. The high affinity of unconventional oil molecules to active sites due to hydrophobic nature of sorbent surface, as well as low solubility of oil in water, resulted in the very rapid process and trapping of oil molecules with strong physical bond (Itodo and Itodo, 2010; Wu et al., 2009)

According to the obtained results of the above kinetic models, it was clear that the PSO gave a reasonable amount of sorption capacity values for both oilsands, especially Bakken oil and in a low concentration of oil. This model assumed that chemisorption is the rate-limiting step in the adsorption of unconventional oil. Cheu at.al (2016) also attributed it to the fact that the rate of occupation of active sites with adsorbed oil molecules is proportional to the square number of the unoccupied binding sites on the sorbent surface when the kinetic process follows the pseudo-second-order model (Cheu et al., 2016). However, the adsorption process is very complex phenomena and theoretical models, such as PFO and PSO might fail to determine whether the adsorption is a chemical or physical process. Some spectroscopy tests at the soil-liquid interface, such as sum frequency generation spectroscopy (SFG), X-ray photoelectron spectroscopy (XPS) have been suggested to study the adsorption of liquid on solid (Wang, 2011). In this study, the equilibrium data have been analyzed using the Dubinin-Radushkevitch isotherm model to study the adsorption mechanism further. Figure 3.1.15 and 3.1.16 show a comparison of different kinetic models for Dilbit and Bakken oils onto hydrophobic dolomite at three different initial concentrations.

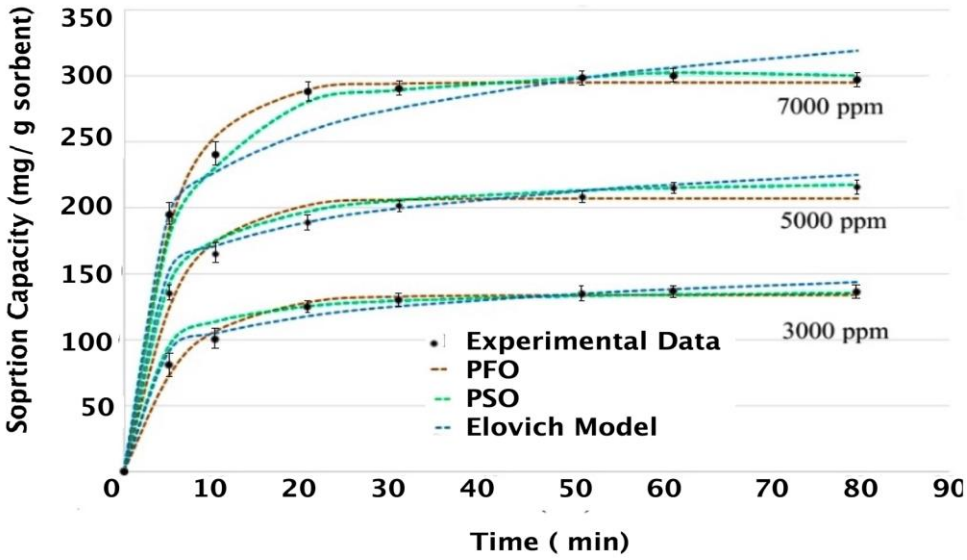

Fig. 3.1.15. Comparison of different adsorption reaction models for Dilbit adsorption onto hydrophobic dolomite at three different concentration (a) 3000 mg L^{-1}, (b) 5000 mg L^{-1}, and (c) 7000 mg L^{-1} (T = 299 K, pH = 6.5, Sorbent dosage = 0.2 g/10 mL, 1000 rpm)

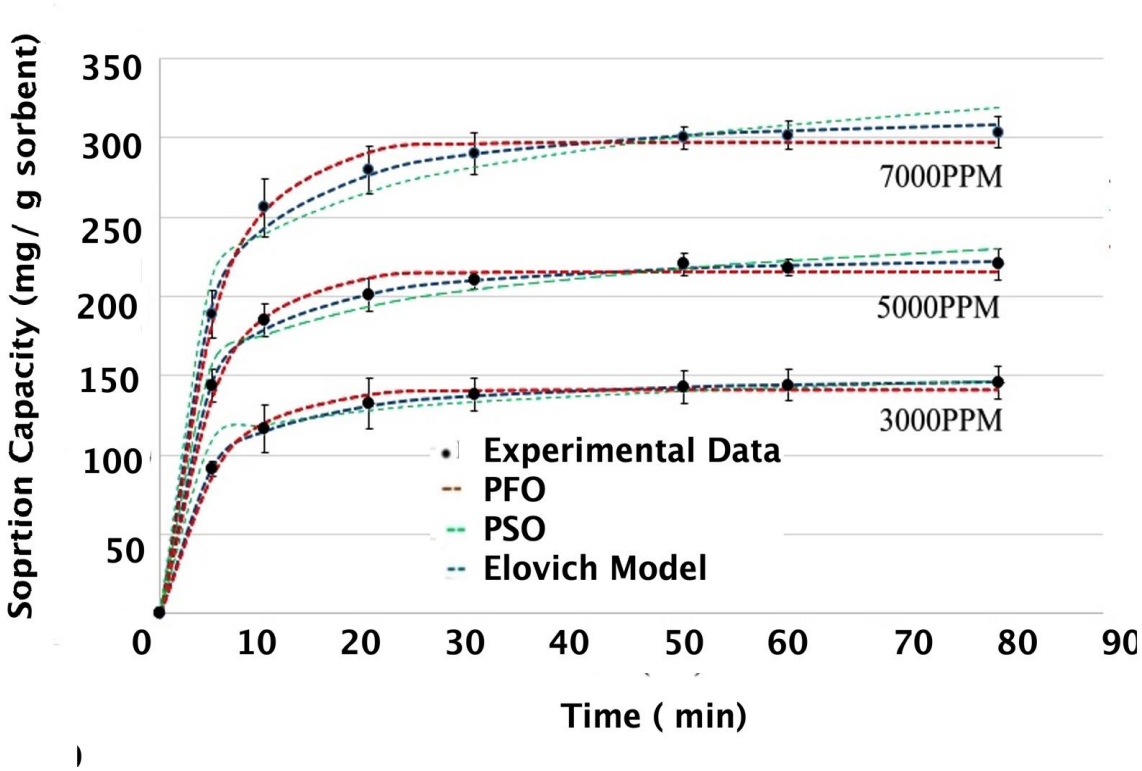

Fig. 3.1.16. Comparison of different adsorption reaction models for Bakken oil adsorption onto hydrophobic dolomite at three different concentration (a) 3000 mg L^{-1}, (b) 5000 mg L^{-1}, and 7000 mg L-1 (T = 299 K, pH = 6.5, Sorbent dosage = 0.2 g/10 mL, 1000 rpm)

Adsorption Diffusion Models

As mentioned previously, adsorption transfer (diffusion) models have been used to describe the adsorption kinetic results. Sorption of oil molecules onto hydrophobic sorbent is composed of three main steps. Due to the strong agitation of the particles during the adsorption process, mass transfer from the bulk solution to the external surface is so rapid that it never constitutes the rate-limiting step (well-mixed system). Among three remaining mass transport processes (external film, pore and surface diffusion), pore diffusion and surface diffusion act in parallel in the interior of the particles and the proposed models considered only one single internal transport mechanism additionally to the external film diffusion. In this study, linear film-diffusion (LFD) model for a spherical-particle geometry and intraparticle diffusion model (Weber-Morris and the homogenous surface diffusion models) have been used to determine which kind of adsorption diffusion was a rate-limiting step. For diffusion kinetic models, the method of non-linear regression was applied to maximize error function (correlation coefficient) and calculate the R^2 values.

Linear Film Transfer Model

Linear film transfer model (initial slope model) was applied to calculate the mass-transfer coefficient for surface diffusion proposed by Mathews and Weber (Raji and Pakizeh, 2014). This model assumed equilibrium between the average adsorbent loading (solid phase concentration) and the concentration of the oil at the interface between the bulk liquid and the particle surface (Cs). The amount of oil transfer across the liquid film is equal to the rate of adsorbate accumulation in the solid phase and is given by following mass balance over the solution on the basis of spherical-particle geometry as depicted in Eq. (4).

$$\frac{dC_b}{dt} = - K_f \beta (C_b - C_s) \quad (4)$$

Where

$$\beta = \frac{3m}{V r_p \rho_p} \quad (5)$$

According to Eq.5., β depends on some parameters (i.e. the mass of sorbent, volume of batch reactor, radius of the particles and the bulk density of the dry sorbents) that have been kept constant during the present experiments.

In our experiment, it is also assumed that C_s is negligible at small values of time compared with C_b (Linear Film-Transfer Model) so Eq.4. can express as follows:

$$\lim_{t \to 0} \left(\frac{\partial(\frac{C_t}{C_o})}{\partial t}\right) = - K_f \beta \quad (6)$$

The linear film-transfer model can describe the concentration of oil at the particle surface over the initial portion of the kinetic curve when the oil concentration of the intraparticle solid phase is still small enough and the intraparticle diffusion is not relevant. The value of film transfer coefficients ($K_f \beta$) were determined using the C_t/C_o versus time plot (Figure 3.1.17).

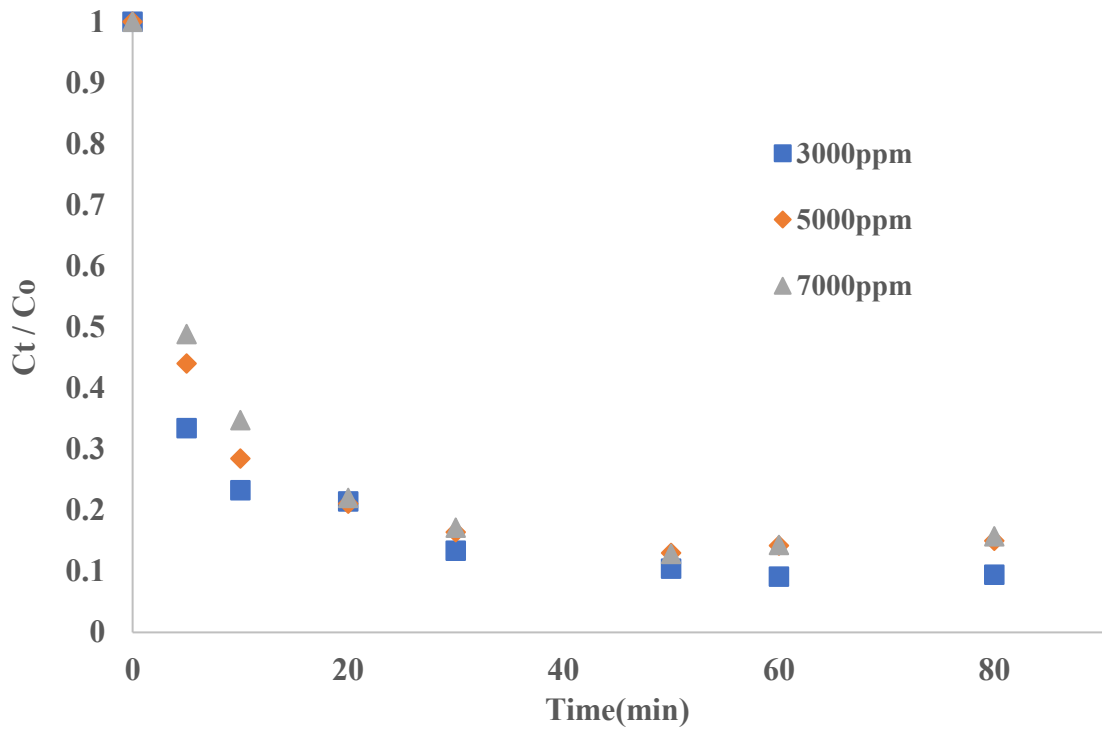

Fig. 3.1.17. Sorption of Dilbit onto hydrophobic sorbent using linear film transfer model

The initial rapid uptake represented an initial rapid surface adsorption and external surface loading; thus, the assumption of negligible intraparticle diffusion might be valid (Raji and Pakizeh, 2014). As can be seen in Table 3.1.4, the R2 values of linear Film-transfer model were not high compared with the kinetic reaction models and the inadequacy of the model means that the intraparticle diffusion became relevant by proceeding the process, but the system is controlled by film transfer model when the curve is linear in the early stages of oil adsorption experiments and with the lapse of time due to the effect of intraparticle diffusion, the model curve deviated from experimental data. The initial concentration of oil, especially for Dilbit, might have affected the mechanism of adsorption as the R^2 values increased by increasing C_o.

Table 3.1.4. Error functions data and Kinetic parameters obtained using the non-linear method for PFO, PSO and Elovich models (conditions: sorbent dosage = 0.2 g in 10 ml solution; stirring speed = 1000 rpm; T = 26℃; pH 6.5).

Model	Parameters	Initial oil Concentration (mg/L)					
		Dilbit			Bakken Oil		
		3000	5000	7000	3000	5000	7000
PFO	R^2	0.961	0.971	0.970	0.960	0.959	0.987
	Chi	7.569	9.376	3.802	8.700	7.467	6.713
	RMSE	11.304	11.969	10.960	16.203	7.879	7.750
	ARE	5.020	10.907	9.117	8.456	7.345	19.129
	SRE	15.232	16.764	18.672	1316.386	15.232	18.564
	MPSD	2.348	1.336	0.225	0.071	1.1830	2.294
	ERRSQ	1465.248	1697.4629	1808.572	1312.697	2001.983	2125.415
	SNE	6.0331	7.236	8.458	7.018	6.921	7.323
PSO	R^2	0.999	0.983	0.974	0.999	0.996	0.977
	Chi	0.888	0.665	0.655	1.222	1.198	1.322
	RMSE	5.731	7.163	8.274	7.468	6.233	6.109
	ARE	0.128	-2.876	-5.098	4.153	4.276	6.259
	SRE	202.572	204.907	203.685	270.494	269.371	264.248
	MPSD	0.014	0.012	1.123	0.138	0.124	4.012
	ERRSQ	20.083	21.416	33.638	14.119	15.242	13.900
	SNE	3.803	3.9258	3.814	3.402	3.698	3.598
Elovich	R^2	0.997	0.992	0.987	0.990	0.975	0.988
	Chi	5.142	7.598	6.364	4.6774	3.553	2.4327
	RMSE	1.738	4.193	2.960	11.378	12.502	11.381
	ARE	12.344	14.794	13.562	5.944	4.709	5.821
	SRE	2.773	5.229	3.995	651.050	653.394	653.271
	MPSD	0.091	2.548	4.313	0.041	0.028	5.012
	ERRSQ	290.816	293.273	292.0390	645.402	633.169	621.047
	SNE	4.481	6.9377	5.7033	5.523	5.982	5.779

Intra-particle transfer Model

The intraparticle diffusion model was applied to determine whether particle-diffusion (diffusion through the sorbent pores) control mechanism or not. In this study, two different intraparticle diffusion models were applied as expressed in Table 3.1.1. This model assumes that external mass transfer and film diffusion are negligible and the intraparticle diffusion is the controlling step

Weber-Morris Model

Intra-particle diffusion model based on the theory proposed by Weber-Morris has been considered as the simplest intra-particle transfer model that estimates the boundary layer thickness C (mg g^{-1}) and intra-particle transfer constant rate (K_{WM} (mg g^{-1} $min^{-1/2}$)) (Table 3.1.1) (Raji and Pakizeh, 2014). The K_{WM} values were calculated from the slope of the curve at a different initial concentration of oil and reported at Table 3.1.5. The intercept of the plot between q_t versus $t^{1/2}$ presented the external resistance, and the observed multiple steps might be attributed to the fact that the gradually decreasing oil concentration in bulk might prevent further diffusion (Wang et al., 2002). Moreover, Weber and Morris's model stated that intraparticle diffusivity (K_{WM}) is constant and the linear plots of q_t versus square time pass through the origin if intraparticle diffusion is the rate controlling factor. For Weber-Morris model, the obtained R^2 values showed that the diffusion through the sorbent pores are not the only rate-limiting step, especially in the initial and final stages of adsorption when the intraparticle diffusion is relatively small and another mechanism might contribute to oil adsorption.

Table 3.1.5. The file transfer model parameters for sorption of oil

Oil	C_o (mg L^{-1})	$K_f\beta$ (min^{-1})	R^2
Bakken Oil	3000	0.0780	0.905
	5000	0.0745	0.937
	7000	0.0731	0.930
Dilbit	3000	0.0767	0.847
	5000	0.0655	0.877
	7000	0.0640	0.903

Homogenous Solid Diffusion Model (HSDM)

HSDM is a typical intra-particle model that describes mass transfer in a homogeneous and amorphous sphere (Qiu et al., 2009). The HSDM equation is written as follows by Eq. (8):

$$\frac{\partial q}{\partial t} = \frac{D_s}{r^2}\frac{\partial}{\partial r}\left(r^2\frac{\partial q}{\partial r}\right). \quad (8)$$

Crank's solution of this model is presented as follows by Eq. (8)(Crank, 1979)

$$\frac{q_t}{q_e} = \sum_{x=1}^{x=n} f_{ax}\left[6\left(\frac{D_{app}t}{{a_x}^2}\right)^{.5}\left\{\pi^{-0.5} + \sum_{n=1}^{\infty}(-1)^n ierf\frac{n\,a_x}{\sqrt{t\,D_{app}}}\right\} - 3\,\frac{t\,D_{app}}{{a_x}^2}\right] \quad (9)$$

A simpler form (Eq.9.) for Crank's solution has been proposed that besides the preceding assumptions (constant surface concentration for HSDM), it is assumed that the highest amount of uptake of oil obtained shortly after the beginning of the process, and the individual particles that have the same size principally contributed to the oil adsorption process

$$\lim_{t\to 0}\left(\frac{\partial\left(\frac{q_t}{q_e}\right)}{\partial(\sqrt{t})}\right) = 6\sqrt{\frac{D_{app}}{\pi a^2}} \quad (10)$$

Figure.3.1.18 shows the fractional attainment of equilibrium, q_t/q_e versus the square of the time, $\sqrt{t}$, for intra-particle transport of oil molecules by modified sorbents at 3000 mg L-1 initial oil concentrations. As can be seen in Fig.13., the slope of curve decreased with the lapse of time that might be attributed to the restriction of oil molecule movement into the pore volume. The value of D_{app} from long-time data can be determined by the slope of "q_t/q_e versus $\sqrt{t}$" plot by considering the particle sizes of the isolated sorbent particles. Figure 3.1.18 depicted a reduced diffusion coefficient by plotting the variation of diffusion coefficient calculated at time t=0 versus time. The diffusion coefficient of Dilbit that contained branched and cyclic hydrocarbons decreased more significantly compared to Bakken oil dominated by straight-chain, saturated hydrocarbons.

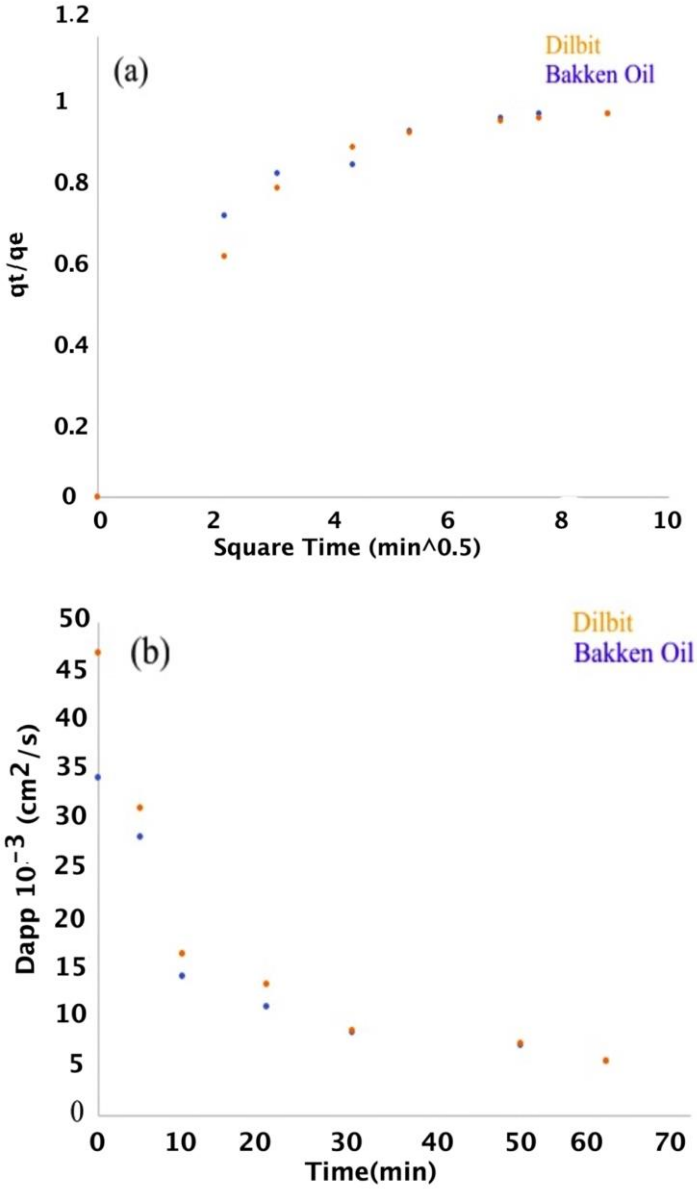

Fig. 3.1.18. (a) and (b) Variation of Dilbit/Bakken oil fraction adsorbed with time, (c) and (d) Variation of Dilbit/Bakken oil diffusion coefficient into the sorbent pores as a function of time

Finally, according to all the above-mentioned models, PSO model described unconventional oil sorption on hydrophobic sorbents in a much better manner than other models in term of R^2 values indicating that the overall rate of the oil sorption process might be controlled by the oil molecules reaction with active sites on the surface of sorbent. However, PSO model is not the only rate-limiting step and other mechanisms may control the rate of sorption, as all of them may be operating simultaneously (Figure 3.1.19).

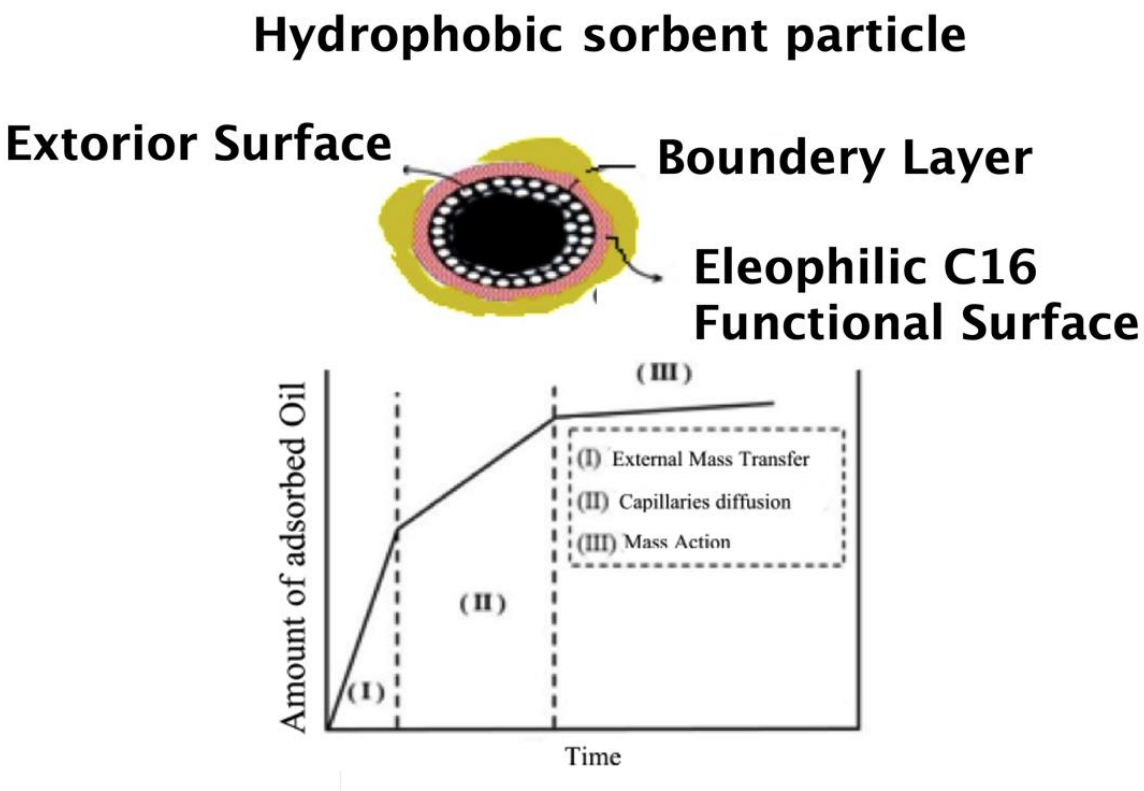

Fig. 3.1.19. (a) and (b) Variation of Dilbit/Bakken oil fraction adsorbed with time, (c) and (d) Variation of Dilbit/Bakken oil diffusion coefficient into the sorbent pores as a function of time

The contribution of diffusion in this process is time and concentration dependent. As mentioned previously, the adsorption existed in three stage mechanisms. The external mass transport of sorbate and external film diffusion in this sorption system may be very fast in comparison with the intraparticle diffusion and adsorption. In this step, as the initial concentration of oil increased, the thickness of the boundary layer and resistance to the film diffusion increased. Then oil species diffuse through the sorbent pores to access the active sites by intraparticle diffusion. In this step, as the initial oil concentration increased, the intraparticle diffusion rate constant increased. With the lapse of time, the oil molecules are transported into the interior of sorbent due to capillary action; however, according to obtained R^2 values for diffusion models, diffusion steps are not rate-limiting. It might be concluded that large pores size of the adsorbent decreased the contribution of diffusion in oil adsorption. Even though the adsorption diffusion models can not represent the real course of adsorption for hydrophobic modified sorbents, they can determine mass transfer and intraparticle diffusion coefficient that are useful for the design of fixed-bed systems. Sidik et.al

applied the model of Boyd and Reichenberg to study the dynamic of crude oil adsorption with modified oil palm leaves (Sidik et al., 2012). They showed that the film-diffusion was the major mode of adsorption. Finally, the oil molecules were adsorbed physically by the active site of sorbent and non-polar molecules of oils served as a base layer upon which further non-polar hydrocarbons could adsorb and it might lead to an equilibrium time of 80 min to achieve higher removal efficiency/

Adsorption Isotherm

The experimental data on the sorption capacity of hydrophobic sorbents to unconventional oils (e.g., Bakken oil and Dilbit) were correlated with six isotherm equilibriums namely Langmuir, Freundlich, Temkin, Redlich-Peterson (P-R), Khan and Sips models (Table 3.1.1). Isotherm and equilibrium information of unconventional oil adsorption on adsorbent is critical for the effective design of adsorption system and the overall improvement of the adsorption mechanism pathway (Ayawei et al., 2017). Sidik et.al reported that the adsorption of crude oil onto adsorbents modified by oil palm leaves takes place through multilayer adsorption process due to the heterogeneous adsorption sites on the sorbent surface (Li et al., 2018a). They simply employed the least square method and Marquardt's percent standard deviation to determine the regression coefficient, error values and model parameters. In our experiment, according to the nature of the surface and coating materials, it seems that the sorption of oils followed almost all adsorption models. Thus, in this study, seven different error functions were examined and the isotherm parameters were determined by minimizing each set of error function across the concentration range studied using the *solver* add-in with Microsoft's spreadsheet (Crini and Badot, 2010). All of the coefficient and error deviation data for the adsorption of oils onto hydrophobic sorbent obtained by non-linear and linear regression method are presented in Table 3.1.5 and 6.

Table 3.1.6. Weber and Morris intraparticle diffusion model parameters for the isotherm

Type of Oil	C_0 (mg L^{-1})	K_{MW} (mg g^{-1} $min^{-1/2}$)	C (mg g^{-1})	R^2
Dilbit	3000	12.49	47.64	0.9723
	5000	20.51	20.51	0.9254
	7000	29.88	97.55	0.8731
Bakken oil	3000	14.03	45.33	0.9530
	5000	20.94	72.40	0.9091
	7000	29.13	87.46	0.8328

Linear Regression

In this study, the correlation of isotherm data at C_o of 2000-7000 mg L-1 using six linear regression isotherm equations, namely the Langmuir, Freundlich, Redlich-Peterson, Temkin, Toth, and Sips models were tested to fit the adsorption of unconventional oil by the hydrophobic sorbents (Table 3.1.7). Based on the R^2 values, it is not surprising that the adsorption behavior deviates from the adsorption isotherm of Langmuir for two reasons. Firstly, the surface heterogeneity of dolomite that is common in nature might arise from the association with other mineral particles as well as energetic heterogeneity of Ca and Mg sites of dolomite surface (Pokrovsky et al., 1999). Thus, the chemical heterogeneity of dolomite surface indicates the heterogeneous distribution of surface hydrophobicity due to the non-uniform adsorption of fatty acid during the coating process. Secondly, it is reasonable to expect that adsorbate molecules on the surface of sorbent would interact with each other. For Dilbit, the R^2 value of Langmuir isotherm decreased as the concentration increased (not presented here) and this indicated that the idealization of non-interaction between oil molecules is not a valid assumption because of steric interaction between

branched and cyclic hydrocarbons (Silva et al., 2013). The higher value of R^2 for the Freundlich isotherm, especially for Dilbit, indicated that stronger active binding sites on sorbent surface have been occupied first and the binding strength decreased by proceeding the process. Considering that the Langmuir model was relatively better to describe Bakken adsorption, it can be inferred that heterogeneity might also be due to Dilbit compounds. In fact, the presence of non-polar and polar organic chains caused different properties depending on the oil/naphtha ratio. The calculated maximum sorption capacity values obtained from Toth model give reasonable values compared with the maximum sorption capacity obtained using TGA analysis. Table 3.1.7 indicated that the adsorption of Bakken oil and Dilbit decreased with a temperature that might be contributed by the effect of temperature on physical properties of oil, water, and interfacial films. Higher temperature reduces the viscosity of the bulk phase which increases the coalescence rate. Thus, even though all factors, such as the effect of temperature on the degree of hydration of the organic chains and other outcomes must be considered, it seemed that the oil viscosity was the most important factor during the adsorption process (Datta et al., 2017).

Table 3.1.7. Isotherm constants for Dilbit and Bakken oil adsorption onto hydrophobic dolomite at 26 and 36 ℃

Isotherm	Parameters	Dilbit		Bakken oil	
		299	309	299	309
Langmuir	q_{max} (mg g^{-1})	476	485	320.9	315
	K_a (mg g^{-1})	0.0022	0.0006	0.009	0.0054
	R^2	0.8301	0.9529	0.9631	0.9810
Freundlich	K_f (L mg^{-1})	5.35	1.64	27.33	20.69
	1/n	0.55	0.6	0.66	0.7
	R^2	0.9986	0.99	0.9964	0.99
Redlich-Peterson	A (L g^{-1})	91	96	224	208
	B (Lg^{-1})	32.6	31.8	8.07	9.6
	m	0.3	0.39	0.69	0.64
	R^2	0.97	0.91	0.97	0.97
Temkin	K_T	0.0156	0.0068	0.097	0.06
	B	18.8	22.8	39	64
	R^2	0.99	0.979	0.94	0.98
Sips	q_{max} (mg g^{-1})	373	479	7311	12456
	Ks (Lg^{-1})	1.4	0.0005	0.0036	0.0016
	n	1.3	0.97	1.37	2.7
	R^2	0.9	0.98	0.94	0.99
Toth	q_{max} (mg g^{-1})	479	289	498	471
	Kto (mg g^{-1})	10^11	10^18	10^11	10^6
	n	0.24	0.36	0.192	0.37
	R^2	0.99	0.99	0.92	0.94

Non-Linear Regression

In order to determine isotherm parameters and evaluate the suitability of the Freundlich, Langmuir, Redlich-Peterson, Sips, Temkin and Toth isotherm equations to the experimental data, error functions are the best optimization procedure. These data are presented in Table 3.1.8 and 3.1.9. For Dilbit, the coefficient of determination (R^2) set was obtained as the optimum sets of error function for Freundlich, R-P, Toth, and Sips models and, Chi set indicated the best set of error function for Langmuir and Temkin models. However, the optimum sets of isotherm models do not have higher R^2 values than the other sets. thus, it is appropriate to use the R^2 value for comparing the best fitting isotherm. The obtained maximum sorption capacity values obtained from these error functions gave reasonable values compared with other sets. Figure 3.1.20 showed adsorption isotherm plots for Dilbit and Bakken oil onto hydrophobic dolomite using the best sets of error functions for corresponding isotherm models.

Table 3.1.8. Isotherm parameters and error functions data obtained using the non-linear method for R-P, Langmuir, Freundlich, Sips and Toth models for Dilbit adsorption (Conditions: Sorbent Dosage: 0.2 g in 10 mL solution, T=26 ℃; pH = 6.5)

Dilbit adsorption onto hydrophobic dolomite

Redlich-Peterson (Three-parameter Isotherm)

	R2	Chi	RSME	ARE	S RE	MPSD	ERRSQ
A	0.5	0.48	0.5	1.89	0.55	0.48	0.5
B	0.00E+00	0.00E+00	0.00E+00	0.28	0	0.00E+00	0.00E+00
m	2.08	2.35	2.06	0.41	1.15	1.53	2.06
R2	0.99	0.99	0.99	0.95	0.94	0.95	0.99
Chi	1.78	1.61	1.78	7.78	8.87	6.47	1.78
RSME	9.45	7.58	9.45	20.99	25.84	21.75	9.45
ARE	4.14	0.2	4.15	7.64	8.88	99.95	4.15
SRE	12.33	287.01	270.49	21.66	16.53	12.33	270.49
MPSD	8.61	0.01	0.01	17.25	14.76	12.57	0.01
ERRSQ	268.2	287.3	268.2	1322.9	2004.9	1419.5	268.2
SNE	4.42	4.86	4.57	6.63	5.72	5.91	4.82

Langmuir (Two-parameter Isotherm)

	R2	Chi	RSME	ARE	S RE	MPSD	ERRSQ
q_m	590.62	653.68	590.64	605.41	569.36	608.55	590.68
Ka	0.001	0.0009	0.001	0.001	0.0009	0.0009	0.001
R2	0.97	0.97	0.97	0.97	0.92	0.94	0.97
Chi	4.68	4.1	4.67	4.45	10.88	8.59	4.67
RSME	14.69	12.06	11.37	14.74	28.58	24.94	11.37
ARE	5.94	0.29	5.94	5.67	9.35	8.22	5.94
SRE	12.33	730.95	651.05	21.66	16.53	12.33	651.05
MPSD	14.31	0.02	0.04	13.69	16.05	14.55	0.04
ERRSQ	647.4	728.17	647.4	652.11	2453.41	1866.3	647.4
SNE	5.65	4.96	5.52	5.56	7.75	6.96	5.52

Temkin (Two-parameter Isotherm)							
	R2	*Chi*	*RSME*	*ARE*	*S RE*	*MPSD*	*ERRSQ*
KT	*0*	*0*	*0*	*0*	*0*	*0.01*	*0*
N_t *B*	*18.38*	*18.06*	*18.38*	*18.11*	*20*	*19.99*	*18.38*
R2	*0.99*	*0.99*	*0.99*	*0.99*	*0.94*	*0.96*	*0.99*
Chi	*0.96*	*0.88*	*0.96*	*1.11*	*7.28*	*4.89*	*0.96*
RSME	*8*	*5.73*	*6.19*	*9.01*	*23.81*	*19.7*	*6.19*
ARE	*2.6*	*0.12*	*2.6*	*2.09*	*7.51*	*5.64*	*2.6*
SRE	*12.33*	*202.57*	*192.2*	*7.08*	*16.44*	*12.46*	*192.2*
MPSD	*5.24*	*0*	*0*	*5.09*	*12.85*	*10.32*	*0*
ERRSQ	*192.03*	*202.08*	*192.03*	*243.82*	*1700.96*	*1165.44*	*192.03*
SNE	*4.28*	*3.4*	*3.72*	*3.29*	*7.04*	*5.77*	*3.72*
Sips (Three-parameter Isotherm)							
	R2	*Chi*	*RSME*	*ARE*	*S RE*	*MPSD*	*ERRSQ*
qm	*342.57*	*336.72*	*342.59*	*480.1*	*408.56*	*369.63*	*342.59*
Ks	*2.56E-05*	*1.86E-05*	*2.55E-05*	*0.000618*	*0.0002925*	*0.0001637*	*2.55E-05*
n	*0.55*	*0.53*	*0.55*	*0.87*	*0.77*	*0.69*	*0.55*
R2	*0.99*	*0.99*	*0.96*	*0.98*	*0.94*	*0.96*	*0.96*
Chi	*0.33*	*0.88*	*0.33*	*3.28*	*8.34*	*5.01*	*0.33*
RSME	*5.14*	*5.73*	*3.98*	*12.4*	*25.06*	*19.72*	*3.98*
ARE	*1.73*	*0.12*	*1.73*	*4.69*	*7.55*	*6.17*	*1.73*
SRE	*12.33*	*202.57*	*79.77*	*26.93*	*23.55*	*12.08*	*79.77*
MPSD	*2.77*	*0*	*0*	*11.89*	*13.99*	*10.69*	*0*
ERRSQ	*0.09*	*202.08*	*79.32*	*0.52*	*1884.96*	*1167.77*	*79.32*

Table 3.1.9. Isotherm parameters and error functions data obtained using the non-linear method for R-P, Langmuir, Freundlich, Sips and Toth models for Bakken oil adsorption (Conditions: Sorbent Dosage: 0.2 g in 10 mL solution, T=26C; pH = 6.5)

Redlich-Peterson (three-parameter Isotherm)							
	R2	Chi	RSME	ARE	S RE	MPSD	ERRSQ
A	318.4	6.81	0.51	4.54	3178.51	4.49	0.51
	11.33	0.13	0.01	0.05	103.1	0.06	0.01
B							
m	0.67	0.76	2.07	0.83	0.68	0.83	2.07
R2	0.96	0.95	1	0.95	0.95	0.95	1
Chi	7.18	7.29	124.62	7.76	8.02	7.76	124.62
RSME	20.9	17.34	72.84	23.79	23.04	23.95	72.84
ARE	8.29	0.4	31.32	7.89	9.11	99.96	31.32
SRE	12.34	1498.93	15829	21.99	19.89	12.34	15829
MPSD	14.99	0.05	1.03	14.13	15.69	13.96	1.03
ERRSQ	1309.69	1501.83	15914.36	1696.57	1592.27	1720.44	15914.36
SNE	6.96	6.86	7.96	7.83	7.86	6.74	6.38

Freundlich (Two-parameter Isotherm)							
	R2	Chi	RSME	ARE	S RE	MPSD	ERRSQ
Kf	26.98	22.29	22.63	17.39	19.82	21.41	22.63
1/N	0.34	0.37	0.37	0.41	0.38	0.37	0.37
R2	0.95	0.97	0.97	0.96	0.96	0.97	0.97
Chi	7.13	5.06	5.09	6.7	6.15	5.12	5.09
RSME	20.85	12.33	12.87	18.66	18.84	16.79	12.87
ARE	8.18	5	7.18	5.94	6.87	6.83	7.18
SRE	12.33	1009.14	829.18	236.93	235.97	12.33	829.18
MPSD	14.41	0.03	0.03	15.08	14.07	13.22	0.03
ERRSQ	1304.35	832.81	829.04	1045.01	1065.57	846.55	829.04
SNE	7.78	6.79	5.57	6.59	6.53	5.82	5.57

Temkin (Two-parameter Isotherm)							
	R2	Chi	RSME	ARE	S RE	MPSD	ERRSQ
KT	0.09	0.07	0.07	0.07	0.07	0.07	0.07
B	39.37	37.71	37.45	36.65	37.45	37.68	37.45
R2	0.944	0.977	0.963	0.962	0.957	0.964	0.963
Chi	7.65	5.18	5.22	5.6	6.23	5.21	5.22
RSME	23.69	11.94	15.16	20.07	21.37	19.73	15.16
ARE	7.69	0.31	6.46	5.76	6.64	6.27	6.46
SRE	12.33	1159.17	1150.41	17.07	17.13	17.66	1150.41
MPSD	12.79	0.02	0.02	11.97	12.65	11.4	0.02
ERRSQ	1679.25	1157.11	1150.23	1208.7	1371.26	1168.97	1150.23
SNE	7.97	6.97	7.97	5.52	6.34	5.88	5.78

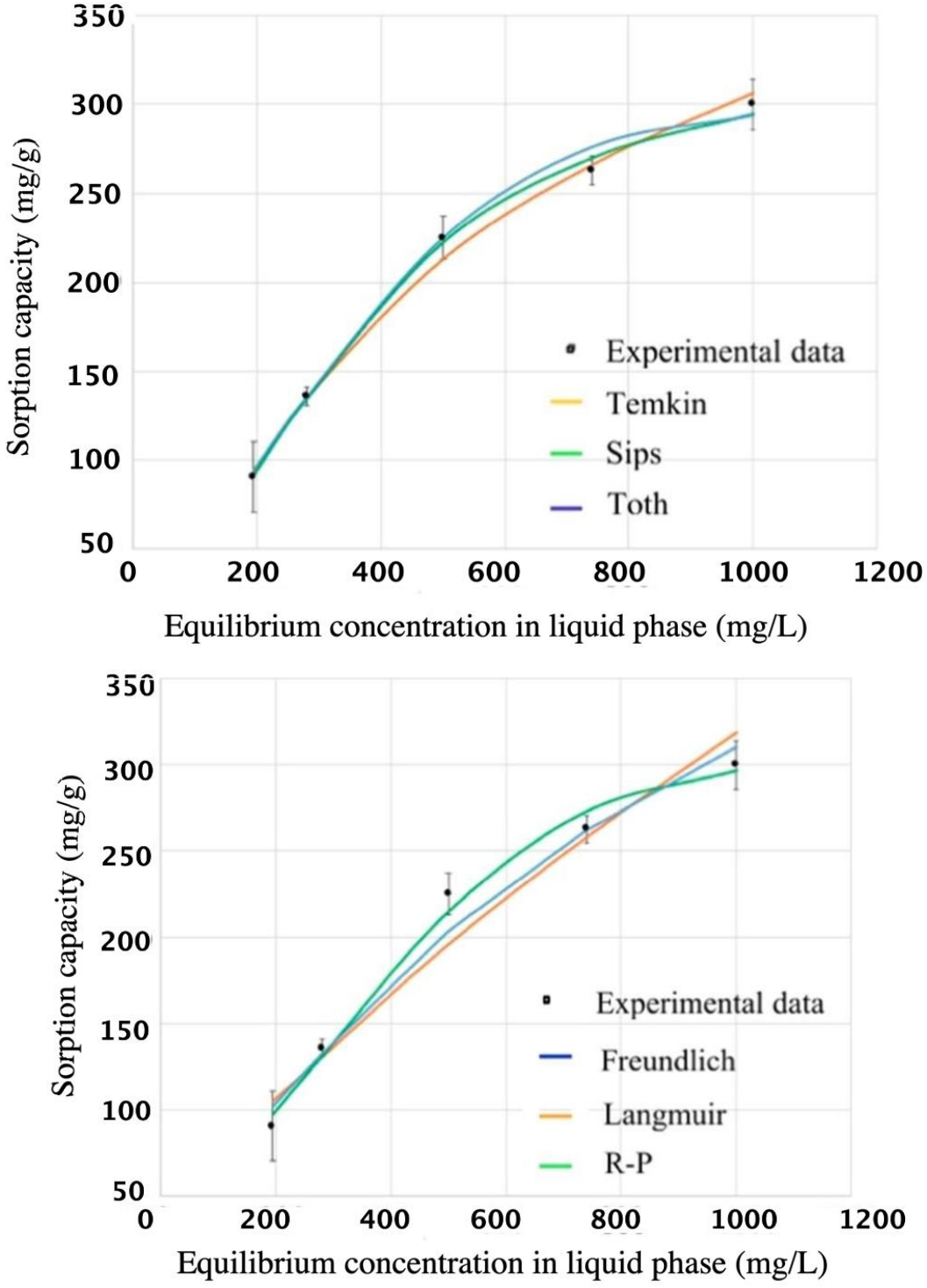

Fig. 3.1.20. Adsorption isotherm plot for (a)and (b) Dilbit; (c)and (d) Bakken oil at 26^{O}C

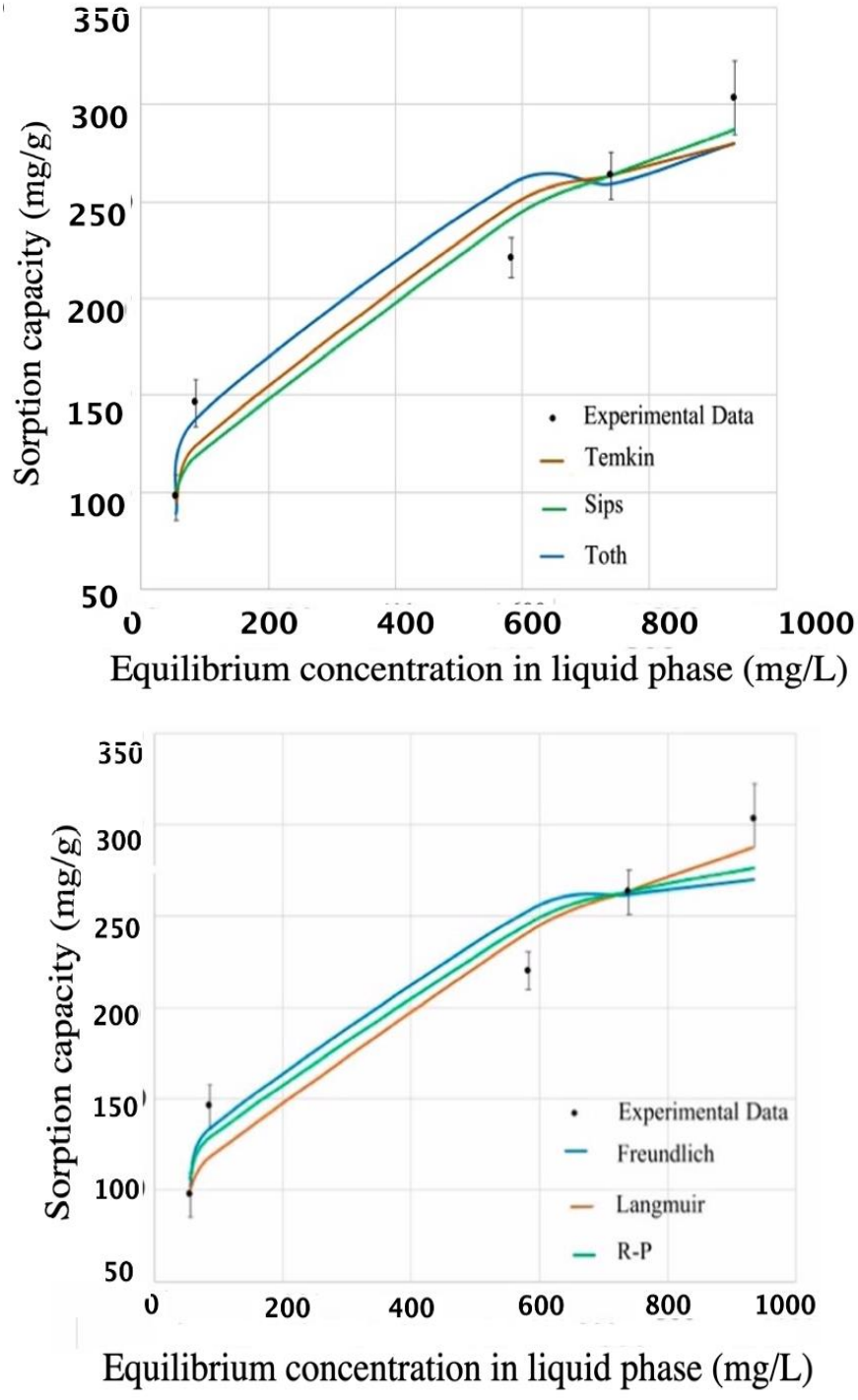

Fig. 3.1.21. Plot of sorption capacity versus equilibrium concentration of Bakken Oil in the aqueous phase for the determination of the thermodynamic parameter. (T= 299 K, pH=6.5, Sorbent dosage = 0.02g/mL, 1000 rpm)

Sorption Nature

As mentioned previously, theoretical models such as PFO and PSO might fail to describe whether the adsorption process is chemical or physical; thus, the Dubinin-Radushkevitch (D-R) isotherm model were studied to take into account the adsorption energy, as well as distinguish between the physisorption and chemisorption with Gaussian energy distribution onto a heterogenous surface. As can be seen in Figure 3.1.22, D-R fitted to the experimental data provided details about process that include maximum adsorption capacity (q_m), K_{DR} the activity coefficient related to sorption mean free energy ($mol^2\ j^{-2}$), and the Polanyi potential ($\boldsymbol{\varepsilon}$= RT ln (1 + 1/C_e)) and E the mean free energy ($E = \frac{1}{\sqrt{-2K_{DR}}}$; Kj mol^{-1}). The E value presents information about the mechanism of the adsorption process, describing whether adsorption is occurring chemically or physically.

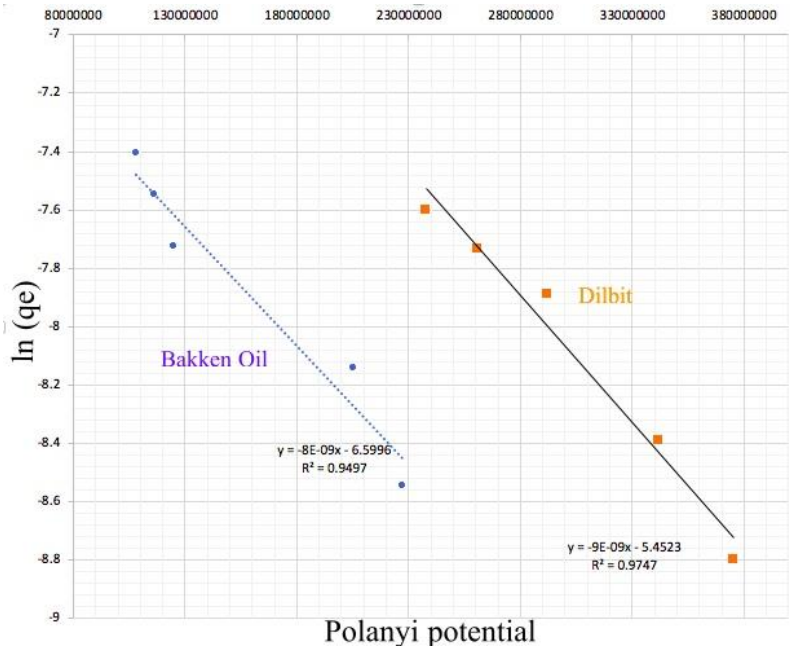

Fig. 3.1.22. The D-R isotherm linear plot for adsorption of Dilbit and Bakken oil. (T = 299 K, pH=6.5, Sorbent Dosage = 0.2 g in 10 mL solution)

The mean sorption energy were determined as 7.57 and 7.833 Kj mol^{-1} for the sorption of Dilbit and Bakken oil; thus, these results suggest that the sorption process of Dilbit and Bakken oil onto hydrophobic sorbents might be carried out by a physical mechanism.

Adsorption Capacity

Along with reusability and sorbent cost, adsorption capacity is one of the main factors to compare the sorption capability of sorbent. The adsorption capacity, q_e, is strongly dependent on the m, V and $C_{o;}$ thus, comparison of adsorbents' capability to adsorb unconventional oils or traditional petroleum-based on q_e must be calculated under similar conditions. To get maximum efficiency, literature optimizes the conditions and reported different initial concentration and V/m; thus, the comparison of sorbents based on the adsorption capacity or maximum capacity can be considered if all the accessible sites of adsorbents are occupied by oil molecules. The ratio of the volume of the solution over the mass of the dry sorbent (V/m ratio) can be applied to determine the volume of water/oil solution that can be treated using 1 gram of sorbents. (see Tabl2 3.1.10)

Table 3.1.10. Unconventional oil and traditional petroleum adsorption capacities of various sorbents

Adsorbent	Contaminant	C_0 range (mg L^{-1})	V/m (L g-1)	qm (mg g^{-1})	qe (mg g^{-1})
Hydrophobic Dolomite	Dilbit	2000-7000	0.05	498	295
Hydrophobic Dolomite	Bakken oil	2000-7000	0.05	530	303
Hydrophobic oil palm leaves	Crude oil	6400	0.1	1160	645.73
Graphene Oxide	Diesel	25-200	40	1335	570
rGO-Fe2O3	Diesel	25-200	40	1213.2	337
Egg-shells	Crude oil	195	150	109	108
Hydrophobic Wood Sawdust waste	Gasoline	1000	250	225.94	123.46

A greater V/m ratio and initial concentration enhance the mass transfer driving force and lead to greater q_e. Choosing low initial oil concentration and high V/m ratio result in better comparison.

3.1.4. Conclusion

The natural dolomite and other types of mineral salts are generally adsorbed polar components due to their ionic nature and possess poor sorption capacity for non-polar and highly insoluble contaminants. But the palmitic acid-modified dolomite (MD) was a low-cost chemical and efficient hydrophobic adsorbent for the removal of spilled unconventional oil (i.e., Dilbit and Bakken oil) from water surfaces. Hydrophobic modification of dolomite results in a high affinity of the surface for aliphatic compounds, especially in the presence of hydrogen bonds between water molecules that repel oil droplets. Following the surface modification, the SEM images showed the rough surface of modified sorbents due to the presence of magnesium and calcium palmitate on the surface of sorbents. The FTIR spectra of modified sorbent revealed the influence of fatty acid coating and esterification mechanism. In the case of complex mixtures of unconventional oil, the extent of petroleum hydrocarbon sorption was studied using a parameter that is easily measured, such as zeta potential. The lower amount of Dilbit pHzpc compared to the Bakken oil confirmed the higher content of acidic compounds in Dilbit than in Bakken oil. TGA analysis demonstrated that the adsorption process was a function of palmitic acid loading, temperature, adsorbent dose, and initial oil concentration. Even though the removal of unconventional oil by hydrophobic sorbent is very rapid, as more than 85 and 95% of Dilbit and Bakken oil removal are achieved in less than 20 min, the adsorbed non-polar molecules of oils served as a base layer upon which further non-polar hydrocarbons could adsorb and it might lead to an equilibrium time of 80 min to achieve higher removal efficiency. Equilibrium was achieved in 80 min; the Freundlich, Langmuir, Redlich-Peterson, Sips, Temkin, and Toth isotherms were fitted to the equilibrium sorption data by linear and non-linear regression methods in the following order (Dilbit and Bakken oil), according to the SNE values: Sips (2.13) > Toth (2.81) > Temkin (3.40) > Freundlich (3,49) > R-P (4.42) > Langmuir (4.96). And Toth (4.04) > Sips (4.5) > Temkin (5.52) > Freundlich (5.57) > R-P (6.3) > Langmuir (7.1). For both tested oils, kinetic adsorption behaved as a pseudo-second kinetic model. The Dubinin-Radushkevitch (D-R) isotherm model was studied to take into account the adsorption energy, as well as distinguish between the physisorption and chemisorption with Gaussian energy distribution onto a heterogeneous surface.

The mean sorption energy was determined as 7.57 and 7.833 KJ mol $^{-1}$ for the sorption of Dilbit and Bakken oil. The sorption process of Dilbit and Bakken oil onto hydrophobic sorbents was carried out by a physical mechanism.

BRIDGE-1

After preparation and characterization of low-cost hydrophobic sorbent, the extend of sorption and the influence of controlling variables on the sorption capacity of modified dolomite were investigated. Next phase of study focused on the practical application of prepared sorbent in large scale water treatment. The potential of both packed and fluidized bed treatment columns of modified dolomite for removing unconventional oil as well as the modelling of these processes were investigated

From here on, "Bridge" means: Link between the previous study and the next study.

PART 2

3.2 Performance of packed and fluidized bed columns for the removal of unconventional oil using modified dolomite

Seyyed Mohammadreza Davoodi[1,2], Satinder Kaur Brar[1,2*], Rosa Galvez-Cloutier[3] , Richard Martel[1]

1. Department of Civil Engineering, Lassonde School of Engineering, York University, North York, Toronto, Ontario M3J 1P3, Canada

2. INRS-ETE, Université du Québec, 490, Rue de la Couronne, Québec G1K 9A9, Canada

[*] Corresponding author, Email address: satinder.brar@lassonde.yorku.ca, P: 416-736-5228; 416 736 5228; 416-736-2100 ext. 55228 · F: 416-736-5360

***Fuel*, *285*, 119191; DOI: 10.1016/j.fuel.2020.119191**

Abstract

In our previous work, it was reported that modified dolomite exhibited higher oil sorption capacity and oil/water selectivity than raw dolomite. In this study, the performance of modified dolomite for removing oil from laboratory synthetic oil-in-water (o/w) emulsions in packed bed (PB) and fluidized bed (FB) modes was investigated. The breakthrough experiments were accomplished, and several aspects such as process operating conditions, mass transfer characteristics, and hydraulic characteristics of the columns were determined. The conditions (i.e., surfactant concentration, mixing stirring rate, and zeta potential) at which the emulsion stability was found to be maximum was studied to increase the resistance of the dispersed oil droplets against coalescence. For the most stable emulsions, a series of experiments were performed to investigate the effect of parameters, such as influent oil concentration (400-650 mg L^{-1}), flow rate (10-20 ml/min), and particle radii (0.08- 0.15 cm) on the oil removal efficiency of the modified dolomite in a fixed bed treatment column. Optimal operating conditions: 15 ml/min flow velocity, 450 mg L^{-1} influent concentration of oil in the o/w emulsion and 0.08 cm of particle radii resulted in the adsorption capacity of 0.41 $_{\text{mg oil/g dolomite}}$ of the bed. As the adsorption isotherm was favorable, we assumed the same breakpoint criteria and for large size column, oil concentration in the outlet was determined by experiments can be done to verify the results. To circumvent the occurrence of coalescence and flow rate limits for fixed-bed column, a fluidized bed of hydrophobic dolomite was applied. A model was also developed to predict the fixed and fluidized bed experimental results based on kinetic and equilibrium batch measurements of the modified dolomite and the stabilized o/w emulsion. The results showed that the breakthrough curves in fluidized bed adsorbent are different than those obtained from fixed bed adsorbent due to axial mixing occurring in the solid and liquid phase.

Keywords: oil adsorption column, hydrophobic dolomite, unconventional oil, Packed bed columns, Fluidized bed columns

3.2.1. Introduction

Unconventional oil is petroleum that requires extraction using techniques other than the traditional oil-well method to guarantee the viability of the oil recovery from tight and shale reservoirs and subsequent transportation to storage facilities, terminals and refineries. The share of unconventional fuel sources in the oil market is growing in terms of usage. For the past 50 years, the United States has been importing products of unconventional oils from oil sand deposits concentrated in the northeastern part in Athabasca, Cold Lake, and Peace River regions. The demand for the commercial level of oil sand implies a much higher transport demand and as a result higher risk for the occurrence of pipeline accidents. Therefore, the removal of spilled oil from water resources is still a very topical environmental and economic issue for Canadians (Davoodi et al., 2020; Davoodi et al., 2019; Mowla et al., 2013).

A great deal of effort has been made for treatment of pollution caused by unconventional oil spill as well as produced oil-water emulsion that has been linked to industrial sources, such as the general food, textile, transportation, and petroleum industries (Huang and Lim, 2006). For example, the development of innovative efficient oil adsorbents has been studies recently as processes for oil recuperation and attenuation measures to efficiently and timely contain the spread of oil and control the hazards (spills) (Ivshina et al., 2015). As for industrial oily wastewaters and immiscible oil/water mixture, they have to be separated to meet stringent emission limits before disposal. At present, various methods have been used to decontaminate the water of petroleum and oil products. The best available technologies for oil removal include chemical treatment, gravity separation, parallel plate coalescers, gas flotation, air flotation, jet flotation, electro-flotation, cyclone separation, granular media filtration, cartridge filtration, biological aerated filtration and adsorption. (Pintor et al., 2016) American Petroleum Institute (API) separators and Dissolved Air Flotation (DAF) devices are used to remove free oil and dispersed oil from wastewater, respectively (Bennett and Peters, 1988; Refining, 1969). They can achieve an efficiency of 98% of oil removal. However, for API separators, the oil droplets need to be relatively large to coalesce, and DAF separators require the injection of air and addition of pH regulators and coagulants which contribute to the operating cost.

The use of dispersants which makes water resources more toxic than oil has changed the scenario for spilled oil clean up. Therefore, the removal of spilled oil from water resources is still a very topical issue. (Doshi et al., 2018) Coalescers for oil/water separation are not appropriate for dispersions that contain surfactants and electrolytes. So, among physicochemical methods, adsorption has attracted much attention in recent years. Manufacture and use of modular equiplemt for control and recovery of oil spills by engineered adsorption systems using granular acticated carbon ad orgaoclay is one example for this physicochemical method. (Mowla et al., 2013) Due to the low initial cost and low maintenance costs, packed bed systems are commonly used to perform separation processes in the industrial processes, such as absorption, stripping, and distillation, and to carry out chemical reactions involving sold particulates either as a reactant or a catalyst. For environmental water treatment, many studies using packed beds for the adsorption of oil and VOCs from an aqueous phase are also well documented in the literature. (Wang, 2011) Removal of emulsified oils can be achieved by using activated carbon adsorption or membrane filtration. (Ayotamuno et al., 2006; Cambiella et al., 2006; Mathavan and Viraraghavan, 1992) Using organoclay or other adsorbents such as sawdust, peat moss, organoclay, and nylon fibers in packed bed filters have also been studied to enhance carbon filtration performance as a pre-treatment for activated carbo adsorption system. As the aqueous solution passes through the packed bed column containing low-cost adsorbents, the organic contaminant is adsorbed by the sorbent and the quality of the effluent is improved. A packed bed operation has some disadvantages, including channeling, dead zones, and a high-pressure drop across the column (Pintor et al., 2016). Wang *et al*. have studied the benefits of using inverse fluidization (i.e., excellent mixing between the solid particles and the liquid) as compared to a more simple packed bed of particles (Wang, 2011).

The objective of the present study was to investigate the potential of both packed and fluidized bed treatment columns of hydrophobic dolomite granules for removing unconventional oil from laboratory synthetic oil-in-water emulsions, and the modeling of these processes. First of all, the effect of several process variables on the stability of o/w emulsion was studied by measuring the relative volume of the emulsion after 24 h of the preparation of the emulsion. Subsequently, removal of the synthetic unconventional oil in water emulsion stabilized with Tween 80 was studied using packed and fluidized bed treatment columns. Finally, the effects of various parameters such as oil concentration, flow rate and particle radii on the oil separation coefficient have been studied.

3.2.2. Experimental Section

Experimental Setup

Hydrophobicity of synthesized particles

Contact angle measurements were conducted using a FTA 200 Dynamic Contact Angle Analyzer (First Ten Angstroms, Inc., Portsmouth, Virginia). To obtain the contact angle associated with the hydrophobic dolomite, the contact between water drops and a chip of modified dolomite pressed from the powder (baseline) was defined manually and the water outline was determined automatically. The contact angle was automatically calculated by the FTA 200 software at the right and left side of the water drop profile. The water drop was symmetrical that shows the smoothness of the surface (Lapointe et al., 2016).

Packed Bed Columns

The test columns consisted of a 5 mm thick Teflon tube (141 mm long by 51 mm inside diameter). Each column end acts as a reservoir to distribute uniformly the water inflow and outflow. Four stainless steel plates and threaded rods with nuts keep both ends and the Teflon tube tight together. Before the experiment, the modified dolomite was placed into the columns in successive layers of 10 mm thick and then compacted by dropping a 365 g weight. Nylon meshes were placed between the adsorbent and the end of caps on both extremities to prevent dolomite particle losses. The columns were weighted to establish the quantity of adsorbent inside (full column minus empty column). Figure 3.2.1. shows the experimental setup of the fixed-bed column.

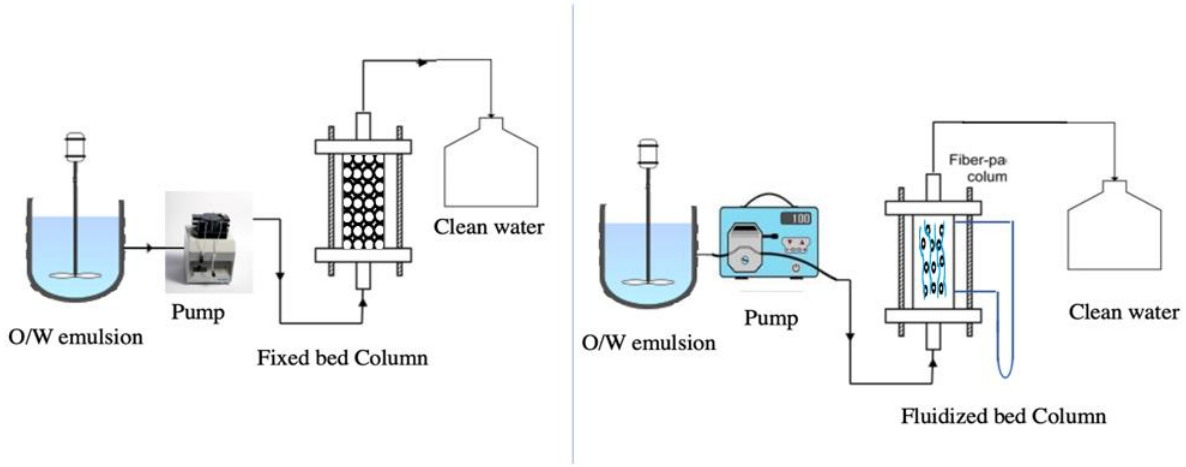

Figure.3.2.1. Experimental setup of fixed and fluidized bed columns

The columns were filled with water, following the circulation of CO_2 at a pressure of 4 psi to ensure complete water saturation by removing entrapped air. CO2 is soluble in water and gas bubbles were assumed to be dissolved in water. The columns were then saturated with deaerated water at a flow rate of 5 ml/min for about 24 hours from bottom to top to eliminate CO_2. The saturated columns were weighed and the volume of pores in each column was measured using the following Eq. (1)

Pore Volume = m_1 - $m_2 - m_3$ (1)

Where m_1 , m_1 and m_1 are the saturated column mass, the mass of water in both ends reservoir and the mass of dry column. The porosity was determined by converting this mass of water into volume at ambient temperature.

Packed Bed Column Characterization

For laminar flow through the saturated column, the permeability coefficient K of each column was obtained using Darcy's law (Eq. (2)) and performing the permeability test in duplicates for the three hydraulic gradients imposed at 5, 10 and 15 cm.

$$K = \frac{Q}{A \times i} \quad (2)$$

The permeability coefficient of the clean column and the used one was determined and compared to confirm the assumption of the constant column porosity during the experiments (Figure 3.2.2).

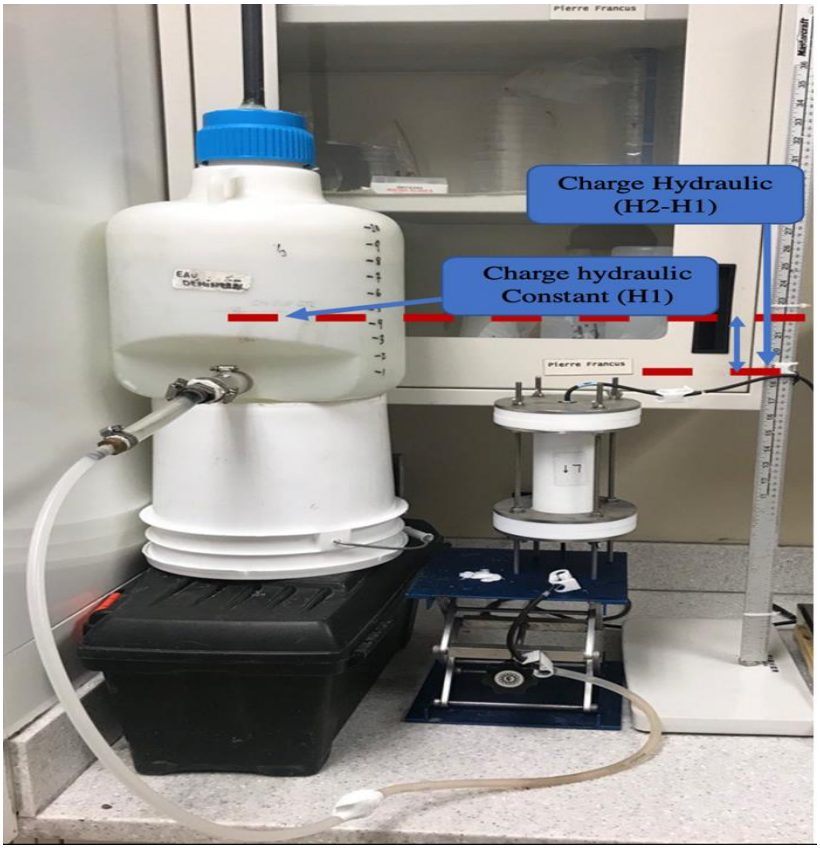

Fig.3.2.2. Hydraulic conductivity measurement set up

Permeability of fresh and saturated columns was measured using Darcy's law that describes the flow of a fluid through a porous medium. Permeability was measured in the laboratory by flowing fluid of known viscosity and setting the fluid to flow at a set hydraulic gradient and measuring the flow rate produced. The porosity and pore volume (the media's own internal porosity) of each column was measured by subtracting the weight of a fully saturated column and the total weight of dry-packed columns.

To describe the dynamic behavior in the fixed-bed column, the axial dispersion coefficient (D_L) was measured to verify the assumption of dispersed plug flow. Potassium bromide was used as a conservative tracer for column study and its concentrations in the effluent were measured through time using a bromide ion-selective electrode detector. Ogata-Banks solution was applied to the 1-D advection-dispersion equation for a continual source of bromide released from the column at an initial concentration C_o of 1000 μg/L. Dispersity was obtained by trial and error with dimensionless form by using the one-dimensional dispersion Eq. (3) as given below:

$$\frac{C}{C_o} = \frac{1}{2}\left[erfc\left(\frac{x-vt}{\sqrt{4D_{ax}t}}\right)\right] \quad (3)$$

To measure the oil removal capacity and efficiency, a high- concentration stable oil-in-water emulsion was stirred by a magnetic stirrer and was injected into the piping system by the peristaltic pump upstream of the static mixer and the fixed-bed column. Samples of water of about 10 ml, upstream and downstream of the fixed bed were taken at regular intervals for silica gel column fractionation.

Fluidized Bed Columns

Liquid-solid fluidization systems have been applied in industry for chemical, petrochemical and biochemical processing, including leaching and washing, adsorption and ion exchange with inert and electrically conduction fluidized particles. (Pintor et al., 2016) In this study, the oil-contaminated water flowed upward through a distributor and the bed of particles as shown in Figure 3.2.1 The test columns consisted of a transparent PVC tube (150 mm long by 51 mm inside diameter). The oil droplets entering the fluidized bed were smaller than 20 μm (emulsified oil). The experimental set-up used for the fluidization of modified dolomite that consisted of a fluidization column, valves and piping, pressure gauge and a barometer. Only clean deionized water was used in the hydrodynamics experiments. To run a typical experimental test, the pressure drop across the empty fluidized bed column was measured to determine the correlation between the pressure drop and fluidized bed with flow rate. The particles were loaded into the fluidization column, and it was filled with water from the bottom and air was completely removed by a vent. Next, the water flow was fed at the bottom of the column through a distributor to prevent challenging and clogging. The particles were fluidized by increasing the flow until the pressure drop is greater than the weight-of-bed pressure drop. Pressure drop and bed height were measured at each flow rate by gradually decreasing the flow of water until the bed height had expanded by at least a factor of two. In the fluidized bed experiments, the oil removal efficiency and capacity were measured at a constant water superficial velocity above the minimum fluidization velocity and a constant static pressure before the column to ensure consistent reading. As mentioned in the fixed-bed column section, samples of water of about 10 ml were taken at regular intervals for silica gel column fractionation until the expanded bed reached the bottom of the column. No control valve was used in the inlet line to prevent possible coalescence of the dispersion. A filter cloth was used as the distributor at the bottom and top to prevent the backflow of the bed materials for the fluidization process and the entrainment of fine particles. To avoid the problem of air entrainment

during the stirring, a stainless-steel sheet was attached to the baffles and the liquid surface was adjusted to leave no gap between the sheet and the liquid surface. The hydrodynamic characterization of liquid phase fluidization was done to determine fluidized-bed column voidage (Richard-Zaki Equation), and solid-phase axial dispersion coefficient (E_s = 0.04 $u^{1.8}$ m^2/s).

Preparation of O/W emulsion

The o/w emulsion was prepared synthetically by mixing Bakken oil in tap water, and sodium lauryl suphate (SLS) at 1300 rpm. Since SLS is more soluble in water (the continuous phase) than the oil, with a very high hydrophile–lipophile balance (HLB) has been applied to stabilize the emulsion. The stability of o/w emulsion was characterized by measuring the relative volume of emulsion defined as the ratio of o/w emulsion volume after 24 h of its preparation to the total volume of oil, surfactant and water used to prepare the samples.

Silica gel column fractionation

According to ASTM D4124, de-asphaltened unconventional oils were separated using column chromatography into saturates using n-hexane, aromatics using DCM followed by a blend with n-hexane, resins using a blend of methanol with DCM and other polar hydrocarbons using methanol. (Rudyk, 2018) To determine different fractions of crude oil, about 100 mg of unconventional oil was loaded on the top of a silica gel column and eluted with 40 ml non-polar hexane solvent. After collecting 40 ml hexane containing alkane fractions, the column was loaded using hexane/DCM (50:50) to separate aromatic fractions from the column. Finally, resin and other polar fractions were collected using 40 ml of methanol/DCM (4:96) and methanol, respectively. Table 3.2.1. shows the composition for unconventional oil used in this experiment.

Table 3.2.1. Composition of unconventional oil (Bakken oil)

Sample	Typical Composition Range (wt.%)			
	Aliphatic	Aromatic	Resin and other polar compounds	Volatile Components
Bakken oil	40.27	23.03	0.61	36.07

Figure 3.2.3 shows schematic of the process of components fractionation. As mentioned previously, samples of water of about 10 ml were taken at regular intervals and the hexane was used to extract the crude oil from samples (using 10 mL Hexane). After 10 minutes of mechanical extraction, a water bath evaporator using a nitrogen sample concentrator was applied to recover the oil from oil/hexane mixtures and prepare the sample for analysis. As mentioned previously, alkane concentration in samples was applied for modeling the behavior of contaminant adsorption in treatment columns with modified dolomite and total petroleum hydrocarbon (TPH) was determined to study the adsorption performance.

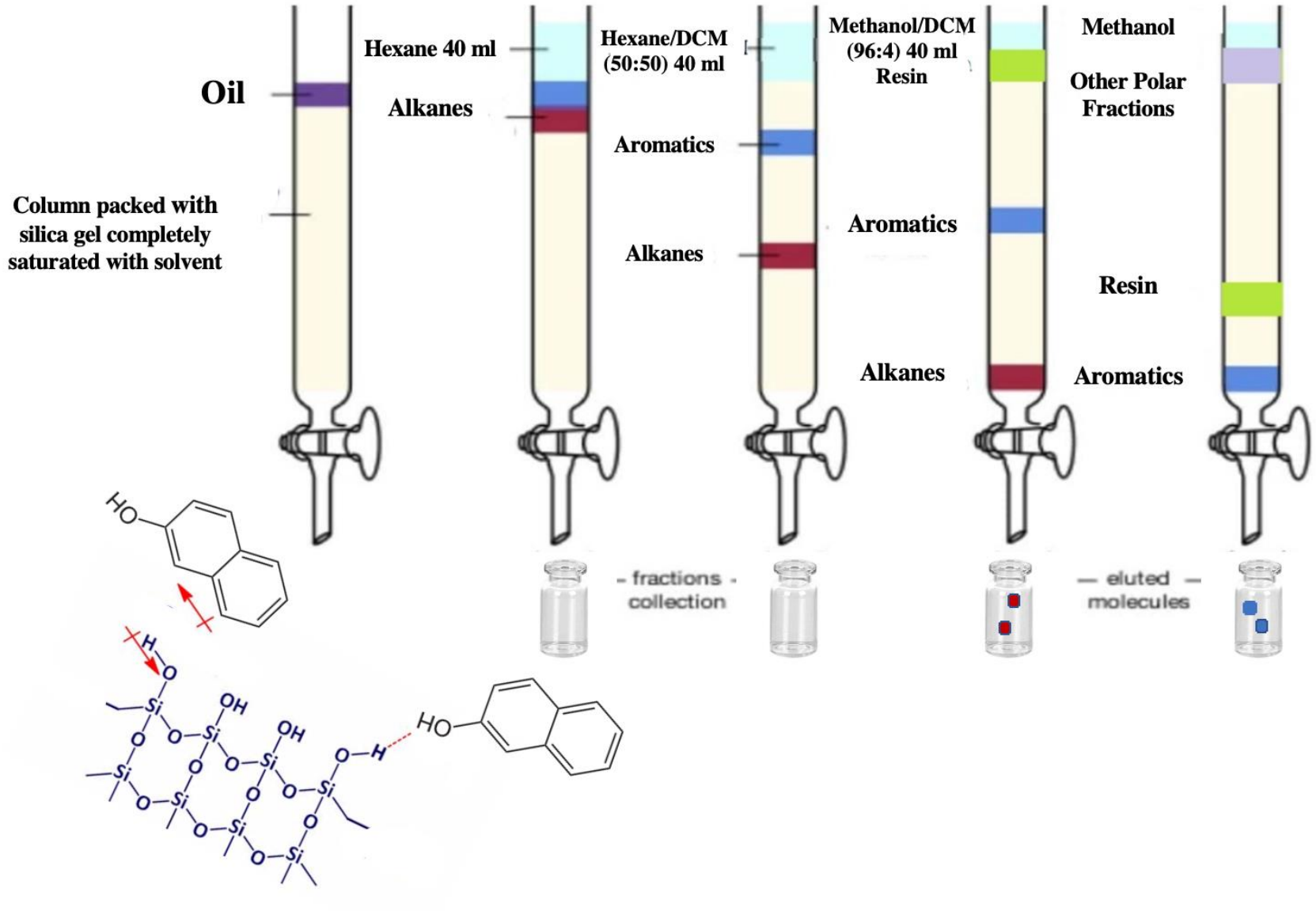

Fig.3.2.3. Silica Gel Diagram

Theoretical Model

The performance of a column is described through the concept of the dynamic breakthrough behavior of oil adsorption with the adsorbent. The shape of the breakthrough curves and the time for the appearance of the contaminant in the effluent are important characteristics to describe the emulsified oil adsorption in the treatment column. The effect of mass transfer in the breakthrough curve is complex, mainly if the isotherm is expressed by non-linear mathematical equations. (Barros et al., 2013) The breakthrough curves in fluidized column are different than the fixed bed adsorbent due to the axial mixing occurring in the solid and liquid phases, especially when the bed height is relatively short.

As discussed elsewhere, the adsorption exhibited in four-stage mechanisms (Davoodi et al., 2019; Zhang et al., 2016):

a. The external mass transfer of sorbate $\frac{\partial C}{\partial x}$
b. External film diffusion i.e., k_{film} $[c - c_{p_{|r=r_p}}]$
c. The intraparticle diffusion and adsorption i.e., $\frac{\partial c_p}{\partial r}$
d. In the final stage, the oil molecules were adsorbed physically i.e. $q_e = k_{fr}\, c_e^{\frac{1}{n}}$

For the fixed-bed column, the governing equations of the model were derived based on the assumptions listed below:

1. A dispersed plug flow model with an axial dispersion coefficient.
2. The radial concentration gradients are negligible in both the solid and liquid phases of the adsorbent.
3. The adsorption is sufficiently rapid so that a local equilibrium is established at the particle surface between the oil concentration in the solution and the adsorbed phase.
4. Uniform flow rate, porosity, and no chemical reactions.
5. The mass transfer coefficient is lumped by external fluid film resistance and diffusion.
6. The linear velocity of the liquid phase varies along the column.
7. The macro-porous adsorbent particles are spherical and homogenous in density and size.
8. The external-film mass transfer coefficient $k_{film,}$ is used to characterize the mass transfer across the boundary layer surrounding the solid particles
9. The solid-phase solute concentration (amount of solute adsorbed onto the adsorbent) is assumed to be in equilibrium with the liquid-phase concentration at the adsorbent surface ($c_{p_{|r=r_p}}$).

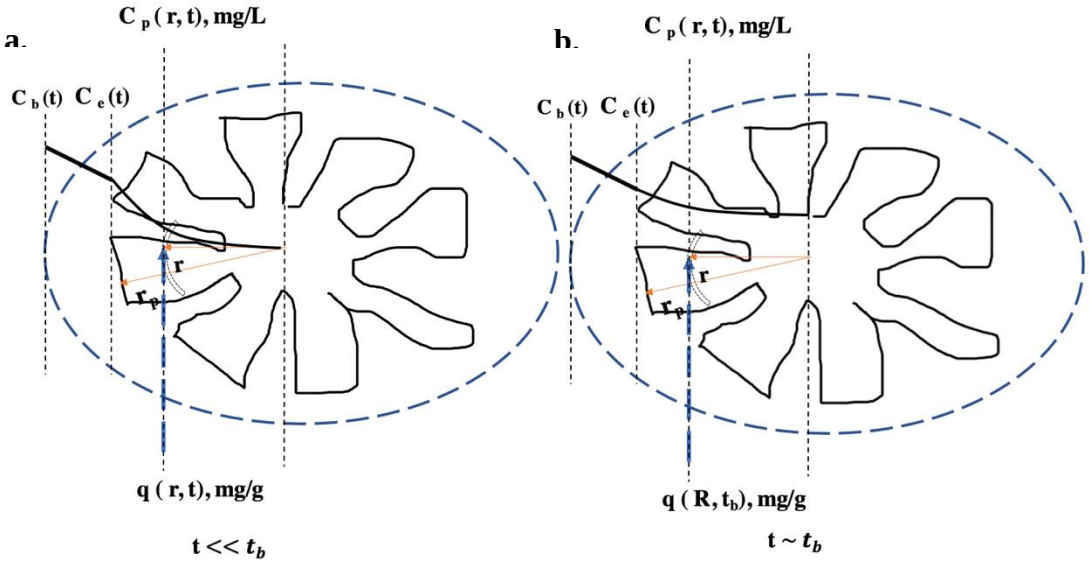

Fig.3.2.4. Concentration profile in a dolomite particle. a) at $t << t_b$, b) at t ~ t_b

Figure 3.2.4 shows a schematic drawing of concentration distribution of the oil under a combined resistance such as the external diffusion and pore diffusion control. In a fixed bed, the continuity equation around a segment of the solid phase during the time dt and between the height of x and x+ dx is

$$\frac{\partial C}{\partial t} = D_{ax}\ \frac{\partial^2 C}{\partial x^2} - C\ \frac{\partial v}{\partial x} - v\frac{\partial C}{\partial x} - \frac{1-\varepsilon_l}{\varepsilon_l}\frac{\partial(\bar{\bar{q}})}{\partial t} \qquad (4)$$

Where bed porosity (ε_l) and superficial liquid velocity (v) may be expressed by Eq. (5) and (6)

$$v = \frac{Q_f}{A_c \varepsilon_l} \qquad (5)$$

$$\varepsilon_l = \frac{V_m}{V} = \frac{Weigh\ of\ fully\ saturated\ column - Weight\ of\ dry\ dearated\ column}{Weigh\ of\ fully\ saturated\ column} \qquad (6)$$

$\bar{\bar{q}}$ denotes average concentration of sorbate in adsorbent particle, which forms a link between the fluid and solid-phase mass balance equations. As can be seen in Eq. (4) the concentration of the sorbate varies with the time and position; thus. the phenomenological model is represented by partial differential equations that are difficult to be solved analytically. (Barros et al., 2013) The relevant initial and boundary conditions are described as follows in breakthrough curves:

Initial Condition:

t = 0, 0 < x < L_{Column}; c = 0

Boundary Condition:

x = 0, t > 0; $D_{ax}\frac{\partial C}{\partial x} = -v\,(c_o - c_{|x=0})$

x = L_{Column}, t > 0; $\frac{\partial C}{\partial x}_{|x=L_{Column}} = 0$

The initial condition mathematically represents the fact that initially there is no oil concentration in the column. Boundary condition 1 relates the effects of the axial dispersion to the feed concentration of oil. Boundary condition 2 implies that at the top of the column where there are no more adsorbent particles, there is no change in oil concentration. The superficial velocity is fixed-bed adsorption is not constant because of oil adsorption. For liquid adsorption, the total mass balance is given by Eq. (7) by assuming the liquid density to be constant to determine the variation of velocity of the bulk fluid along the axial direction of the bed.

$$\rho_l \frac{\partial V}{\partial z} = -(1-\varepsilon_l)\rho_s \frac{\partial \bar{\bar{q}}}{\partial t} \qquad (7)$$

The term $\frac{\partial \bar{\bar{q}}}{\partial t}$ represents the overall rate of mass transfer averaged over a particle. The velocity boundary conditions are

V = V_O , Z = 0, t > 0

$\frac{\partial V}{\partial t}$ = 0, Z = L, t > 0

When instant equilibrium is reached (equilibrium theory) in the bed between the bulk flow and the adsorbed phase, i.e., no mass resistance, the $\bar{\bar{q}} = q = k_{fr}\ c_{p_{|r=r_p}}^{\frac{1}{n}}$ and $\frac{\partial \bar{\bar{q}}}{\partial t} = \frac{\partial q}{\partial c}\frac{\partial c}{\partial t}$. But non-equilibrium theory has been applied in this study due to the mass transfer resistances. The mass balance for an adsorbent particle yields the following expression

$\frac{\partial \bar{\bar{q}}}{\partial t}$ = f (c_i, q_i)

The above-mentioned mass transfer rate expression has been written as a single equation, but it commonly consists of a set of equations comprising one or more diffusion equations.

By assuming steady-state conditions at the fluid-solid interface, the mass transfer rate acrros the external film is supposed to be equal to the diffusive flux at the particle surface. Thus, In the solid phase, there is no convective flow, and the solute uptake is controlled by the diffusion rates hence

[accumulation rate of the oil concentration in the dolomite particles] =

[gain by adsorption]

i.e., it gives Eq. (8), mass-transfer rate across the external film,

$$\rho_s \frac{\partial \bar{q}}{\partial t} = \frac{3 K_{film}\left(c - c_{p|r=r_p}\right)}{a_p} \quad (8)$$

Where C and $c_{p|r=r_p}$ represent the adsorbate concentration in the fuid phase and the average free concentration inside the particle. Eq. (8) can be applied to determine the las term in the Eq. (4). As can be seen in Figure 3.2.4, It is supposed that the mass transfer resistance between the bulk phase and the macro-porous liquid phase is localized to an external film around the adsorbent particles. (Ahmad and Hameed, 2010; Salim et al., 2019; Shafeeyan et al., 2014) In order to determine the overall rate of mass transfer averaged over a particle ($\frac{\partial \bar{q}}{\partial t}$), $c_{p|r=r_p}$ should be determined using macropore diffusional resistance that is applicable for diffusion in sufficiently large pores is often referred to as macrospore diffusion. In macropore diffusion, transport occurs within fluid-filled pores inside the particles. (Shafeeyan et al., 2014) In this stage, the macroscopic conservation equation for a spherical adsorbent taking into account pore diffusion of the adsorbate is given as Eq. (10).

Macropore balance:

$$\varepsilon_p \frac{\partial c_p}{\partial t} + \left(1 - \varepsilon_p\right)\rho_p \frac{\partial \bar{q}}{\partial t} = \frac{1}{r^2}\frac{\partial}{\partial r}\left[r^2\left(D_{app}\frac{\partial c_p}{\partial r}\right)\right]; \quad (10)$$

This differential mass balance equation is used to determine the concentration of contaminant penetrating macropore volume at each radial position. Initial Conditions:

$0 < r < r_p$, $t = 0$; $c_p = 0 \approx 5 \times 10^{-6}$ mg L^{-1}

Boundary Conditions:

$r = r_p$, $t > 0$; $\frac{\partial c_p}{\partial r}|_{r= r_p} = \frac{Kfilm}{\varepsilon_p D_{app}}\left(c - c_{p|r=r_p}\right)$; (The continuity condition on the external surface)

$r = 0$, $t > 0$; $\frac{\partial c_p}{\partial r}|_{r= 0} = 0$; (The symmetry condition at the center of the particle)

Eq. (10) represent a differential mass balance equation over a spherical adsorbent particle. In the above equation, $\bar{q}$ is the average adsorbed-phase concentration in the macropore, which is related to the adsorbate flux at the micropore mouth by using $\frac{\partial \bar{q}}{\partial t} = Kbi\ (q^{*}\text{-}\bar{q})$. Where $\bar{q}$ is the distributed adsorbate concentration in the micopore and Kbi is the barrier transport coefficient. In this study, the sorbed oil is assumed to be in equilibrium with free concentration at all points within the particle according to the equilibrium isotherm ($\bar{q} = q_p$). In this equation, the right side represent adsorbed-phase diffusion and approximate diffusive process in macropore resistance. (Shafeeyan et al., 2014) For particles that have no macropores, such as gel-type ion-exchange resins, or when the solute holdup in the pore fluid is small, ε_p may be zero. (LeVan et al., 1997) In this study it is assumed that the sorbed analyte is in equilibrium with the free concentration at all points within the particle according to the equilibrium isotherm. In some literature, $C_p = C_b$ @ r = R (Bulk concentration at the surface of particle) boundary condition has been applied instead of the continuity condition on the external surface due to the lack of information about mass transfer coefficient. Eq. (10) is solved using these stated initial and boundary conditions. The presence of internal diffusion resistance affects the shape of the breakthrough curve (S-shape). The initial condition describes the fact that the adsorbent particles initially contain no oil. There is symmetry at the center of the particle according to boundary condition 1. Physically, the second boundary condition describes the fact that the increase in the oil concentration might be attributed to the mass of oil that is transferred to a particle at its surface. The boundary conditions for pore diffusion relate the pore concentration changes to film mass transfer effects as a function of position in the column. Likewise, the second boundary condition describes that the diffusional flux at the surface equals the external flux. This boundary condition relates the changes in the pore concentration to surface phenomena such as solid dispersion (in fluidized bed) and film mass transfer as a function of axial position in the column.

Assuming instantaneous equilibrium, it gives Eq. (11),

$$\frac{\partial q_p}{\partial t} = \frac{\partial c_p}{\partial t}\,\frac{\partial q_p}{\partial c_p} \tag{11}$$

Then rearranging Eq. (9), it leads to Eq. (12),

$$\frac{\partial C_p}{\partial t} = \frac{D_{app}}{\varepsilon_p}\left(\frac{1}{1+(1-\varepsilon_p)\rho_p\frac{\partial q_p}{\partial c_p}}\right)\left(\frac{\partial^2 C_p}{\partial r^2} + \frac{2}{r}\frac{\partial C_p}{\partial r}\right) \tag{12}$$

Eq. (12) implies that the component accumulates on both pore and solid phases with the local equilibrium between them. As can be seen in the Figure 3.2.4, due to the external film resistance measured by the external mass transfer coefficient, k_{film}, the concentration of emulsified oil dropped from $c_{b\,(t)}$ at the bulk, to the equilibrium value $c_{e\,(t)=}\, c_{p_{|r=r_p}}$ on the particle surface. Later, the value of $c_{e\,(t)}$ dropped further to zero at point r in the particle interior due to the internal resistance measured by D_{app}. (Ko et al., 2001) Based on the preliminary result of the batch studies, transport model parameters of D_{ax}, and pore diffusion coefficient (D_{app}) were calculated using Darcy's law, and Homogenous Solid Diffusion Model ($\lim_{t \to 0}\left(\frac{\partial\left(\frac{q_t}{q_{e'}}\right)}{\partial t}\right) = 6\sqrt{\frac{\mathrm{Dapp}}{\pi a^2}}$), respectively. (1-109.) Mass transfer into the particles was determined using Linear Film-Transfer Model ($\lim_{t \to 0}\left(\frac{\partial(\frac{c_t}{c_0})}{\partial t}\right) = -k_{film}\,\beta$), and compared with obtained values using column study results (i.e., the average free concentration inside the particle $C_{P(ave)}$ ($c_{p_{|r=r_p}}$) (Eq.S12) and concentration gradient inside the particle near the surface). $\frac{\partial c_p}{\partial r}\,|r=\,r_p = \frac{Kfilm}{\varepsilon_p D_{app}}(\,\mathrm{c} - c_{p_{|r=r_p}})$

Freundlich model isotherm was applied to relate the equilibrium concentration of the oil in the solution and on dolomite particles. Because of the very fast mass action occurring on the oil adsorbent sites to uptake the oil, the solid-phase concentration and the pore solution are assumed to be in equilibrium, and denoted by Eq. (13):

$$q_p = k_{fr}\;\; c_{p_{|r=r_p}}{}^{\frac{1}{n}} \qquad (13)$$

The proposed model can be used for understanding the dynamics of the fixed-bed treatment column for the adsorption of organic compounds. This model that is composed by Eq. (4,8,12) is used to describe the aliphatic compound removal in a fixed bed column packed with hydrophobic dolomite and take into account the external and internal mass transfer resistance. Figure 3.2.5 shows the computational procedure for simulating the fixed bed adsorber performance.

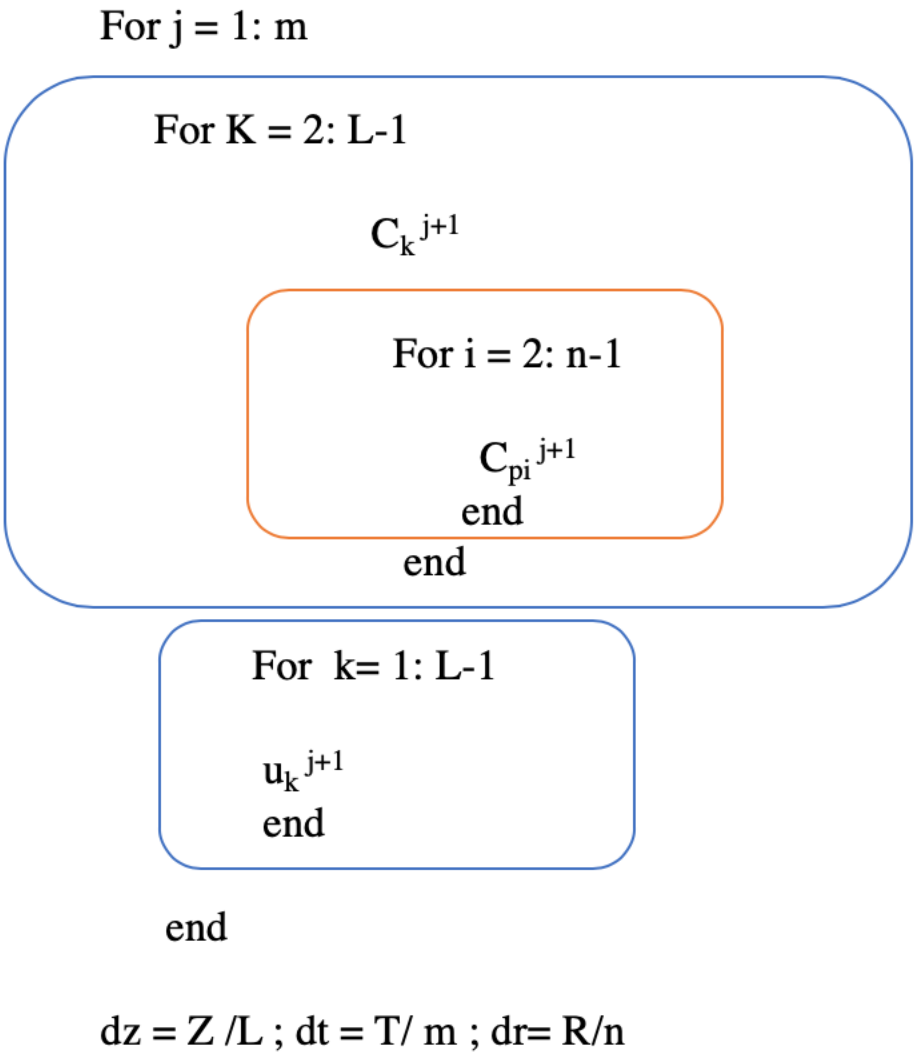

Figure.3.2.5. Schematic of computational procedure for simulating the fixed-bed adsorbent performance

n stages were considered, with the stage numbering starting on bottom of column (K=1) and continuing until top is reached (k = L). After calculating $C_{P(ave)}$ ($c_{p_{|r=r_p}}$) at stage K and time j+1, concentration of oil and velocity of bulk were obtained at stage K and time j+1.

For the fluidized bed column, the mass balance with respect to the adsorbate in the liquid phase and boundary conditions are the same as Eq. (14) in the packed model and the only difference is that the void fraction (ε_l) is applied

$$\varepsilon_l \frac{\partial C}{\partial t} = \varepsilon_l D_{ax} \frac{\partial^2 C}{\partial x^2} - \varepsilon_l C \frac{\partial v}{\partial x} - \varepsilon_l v \frac{\partial C}{\partial x} - (1 - \varepsilon_l) k_{film} [c - c_e] \quad (14)$$

The initial and boundary conditions are the same as in the packed bed model. The liquid void fraction in the expanded bed (ε_l) was calculated using Eq. (15).

$$\varepsilon = 1 - \frac{m_p}{AH\rho_p} \quad (15)$$

Liquid-phase axial dispersion coefficient (D_{ax}) has been calculated using the Ogata & Bank solution that is a famous analytical solution to the following form of advection-dispersion equation.

$$\frac{\partial C}{\partial t} = D_{ax} \frac{\partial^2 C}{\partial x^2} - v \frac{\partial C}{\partial x} \quad (16)$$

Some literature applied Eq. (17) in the solid phase that accounted for solid-phase axial dispersion in terms of the amount of oil adsorbed:

$$\varepsilon_s \frac{\partial(\bar{q})}{\partial t} = E_s \frac{\partial^2 \bar{q}}{\partial z^2} + \frac{3k_f \varepsilon_s (C - C_e)}{\rho_p R} \quad (17)$$

Since there are no experimental data available for solids mixing for the particles of interest in a fluidized bed, literature usually applied the correlation of Van Der Meer et.al. (1984) that used experimental values for the superficial velocity at each expansion:

Solid-phase axial dispersion coefficient (E_s) = 0.04 $u^{1.8}$ m^2/s (18)

Our results showed that the axial dispersion model might not be applicable for a solid phase and for each experiment solid-phase axial dispersion coefficient has changed due to agglomeration of particles. Some literature applied stirrer in fluidized bed reactors and columns where particles are smalls to provide large surface area and avoid particles from sticking to the walls and aggregating. (Sahoo and Sahoo, 2013) Without the use of stirrer that provides agitation, the following mass balance could be applied in solid phase instead of Eq. (19).

$$H \frac{\partial q}{\partial t} = \int_0^H \frac{k}{\rho_p} (C - C_e)\, dz \quad (19)$$

Where q is the average solid-phase concentration at a given height. The initial condition is

t = 0, q(z,0) = 0, $0 \leq z \leq H$

In the calculations, the error between experimental and predicted values was calculated using the absolute average deviation (AAD):

$$AAD = \sum_{I=1}^{n} \left(\frac{C_i^{exp}|z=l}{C_O} - \frac{C_i^{model}|z=l}{C_O}\right)^2 \quad (20)$$

Where n is the number of experimental data; $C_i^{exp}|z = l$ and $C_i^{model}|z = l$ are the aliphatic concentrations in the solution at the column outlet experimentally obtained and determined by the model (mg/L), respectively. AAD ≤ 0.05 shows that the predicted results could be highly consistent with the experimental data. Thus, the model may not provide a general agreement with the experimental data if AAD > 0.1. (Lin et al., 2017)

Removal of oil from water in a packed and a fluidized bed of modified dolomite

In this work, the oil removal efficiency and capacity of the adsorbent particles are studied by measuring both the inlet and exit concentrations of oil as a function of time and the breakthrough point ($C_{t,out}/C_0$ = 0.05) and saturated point ($C_{t,out}/C_0$ = 0.95) breakthrough time using numerical integration of the area above the breakthrough curve Eq.(21):

$$m_{removal} = \frac{Q_f c_f}{m_B} \int_0^t \left(1 - \frac{c_{t,out}}{c_f}\right) \mathrm{dt} \quad (21)$$

The breakthrough curve in each experimental run is obtained from the experiment concentration versus time data. Performance investigation on fixed bed treatment column applied the breakthrough curve, a plot of the duration of the test against the total petroleum hydrocarbon in the effluent stream of a mixture of oil and water. Aliphatic compound concentration in the effluent stream was applied for mathematical modeling and comparison of different mechanisms.

Statistical Analyses

Statistical analysis related to the analyzed parameters, such as student t-test, the p-value of all the data sets were performed in ORIGIN software (version 8.5; Origin Lab).

3.2.3. Results and Discussion

previous study. (Davoodi et al., 2019) In this study, the contact angle measurement confirmed the hydrophobic nature of modified dolomite which plays an important role in adsorption process. Figure 3.2.6 shows the contact angle between the droplet of water with the adsorbent surface. The water droplets on the chip surface flows easily and retain its special shape with contact angle more

than 90 degree. Thus, the introduction of fatty substituent with chain length greater than C6 in the dolomite that formed hydrophobic dolomite, enhanced the affinity of modified dolomite toward adsorbates. (Lavagna et al., 2019)

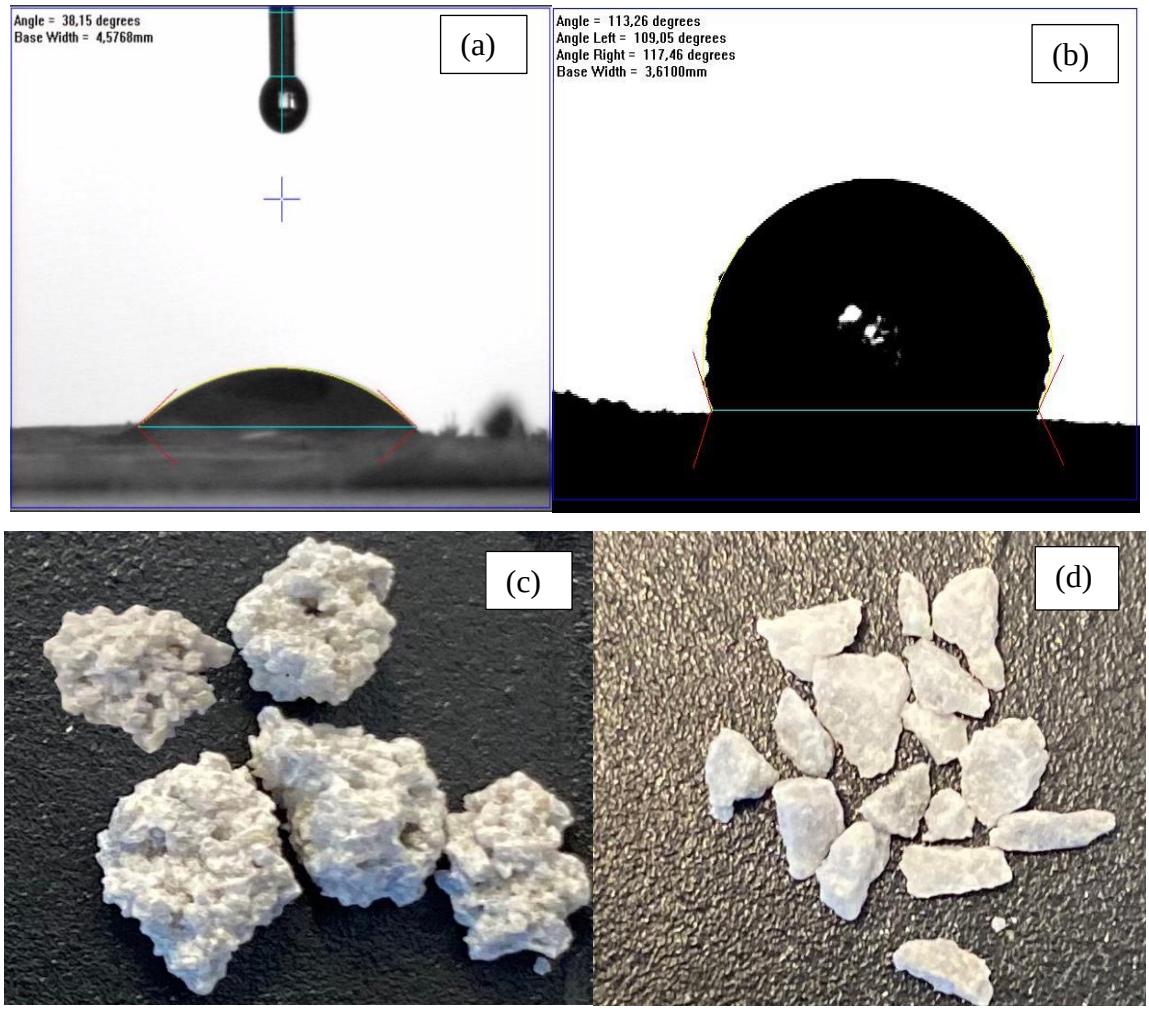

Figure.3.2.6. Water contact angle on (a) raw and (b) modified dolimite surface (c) Modified dolomite (d) raw dolomite

As mentioned previously, the value of the kinetic mass transfer parameter (k_f and D_{app}) and axial dispersion (D_{ax}) would be estimated from the fitting of the model to the experimental data of the breakthrough curves in this study. However, the performance of modified dolomite should have been investigated in a batch system for gaining a good initial guess. Our previous study also compared modified

dolomite adsorbent capacity for oil removal with other low-cost adsorbents and found it as a promising alternative for removal of emulsified oil from solutions. (Davoodi et al., 2019) The study of adsorption column is very difficult due to several mechanisms that occur simultaneously including sorption and coalesce. Preparing a stable emulsion was important to circumvent the coalescence; thus, the effects of various process variables on it were studied as described in the following sections.

Effect of surfactant concentration, agitation and the time of mixing on emulsion stability

Figure 3.2.7 (A, B, C) shows the effect of surfactant concentration, stirring intensity and mixing time on emulsion stability. It was observed that the stability of emulsion increases with an increase in the surfactant content up to a certain concentration that might be attributed to the formation of tough film at the interface that prevents the coalescence of oil droplets. The optimal surfactant concentration (0.9 %) showed 95 % stability of emulsion but as the concentration of surfactant increased further, the rapid coalescence of oil droplets resulted in the emulsion stability decrease. Similar results were reported by other authors as well. Tcholakova *et.al* showed that at low emulsifier concentration, the mean drop size rapidly decreases with the increase of emulsifier concentration, which might be attributed to the important contribution of the drop-drop coalescence. Higher intensity of agitation that resulted in higher turbulence and shearing action in a system also was applied to obtain smaller oil droplets and more stable emulsion. As can be seen in Figure 3.2.7, after 1500 rpm, the relative volume of the emulsion increase is very slow. The selection of suitable mixing time is one of the most important tasks in the preparation of o/w emulsion. As can be seen in Figure 3.2.7 (C), the o/w emulsion stability remains almost constant from 25 min to 40 min and thereafter slowly decreases with an increase in mixing time.

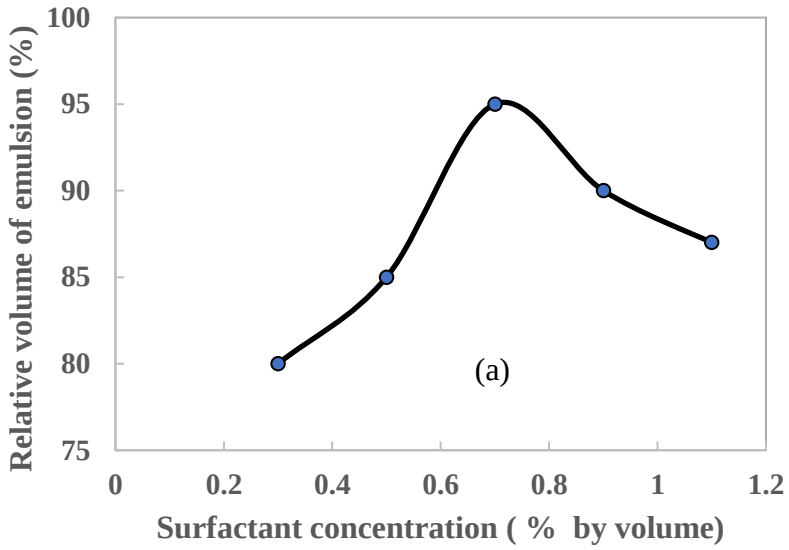
Relative volume of emulsion (%)
100
95
90
85
80
75
0
0.2
0.4
0.6
0.8
1
1.2
Surfactant concentration (% by volume)

(a)

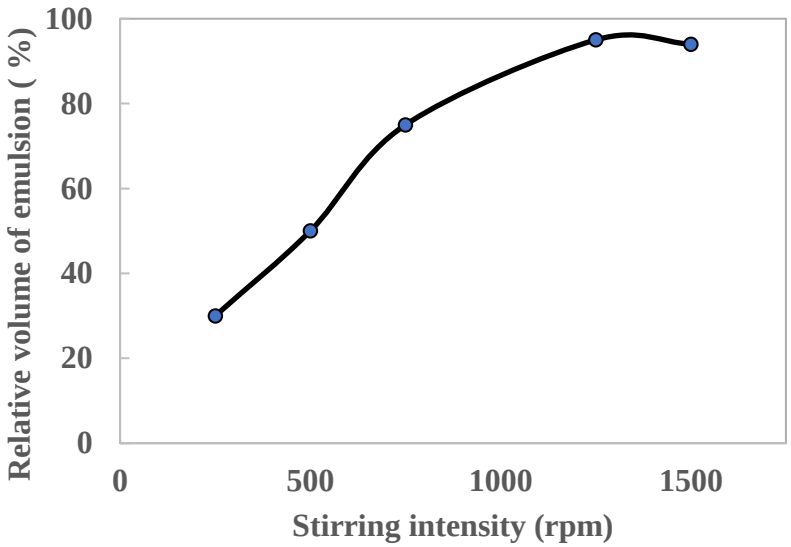
Relative volume of emulsion (%)
100
80
60
40
20
0
0
500
1000
1500
Stirring intensity (rpm)

(c)

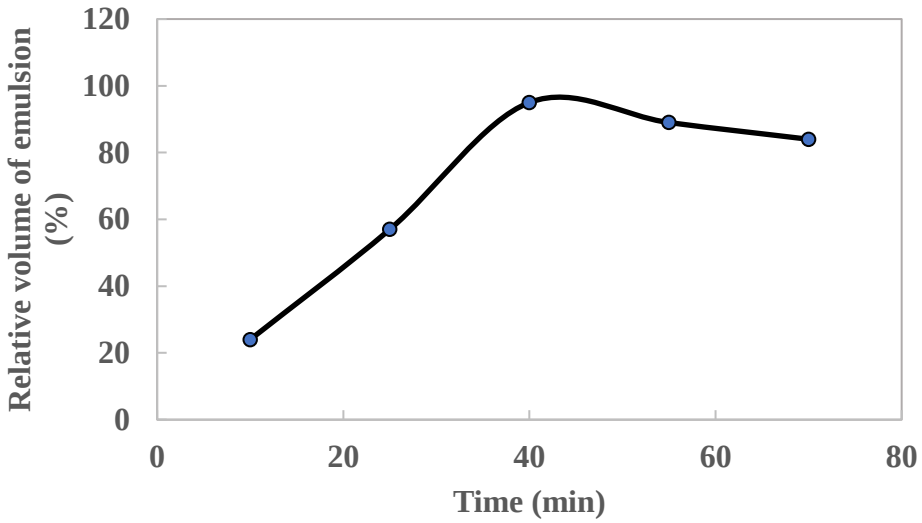

Figure.3.2.7. Effect of (a) surfactant concentration; (b) stirring intensity and; (c) mixing time on emulsion stability

Figure 3.2.8 shows the schematic presentation of the process of drop deformation to drop breakage, which could be enhanced using 1 % surfactant concentration, and finally to collision and coalescence due to the excessive mixing time.

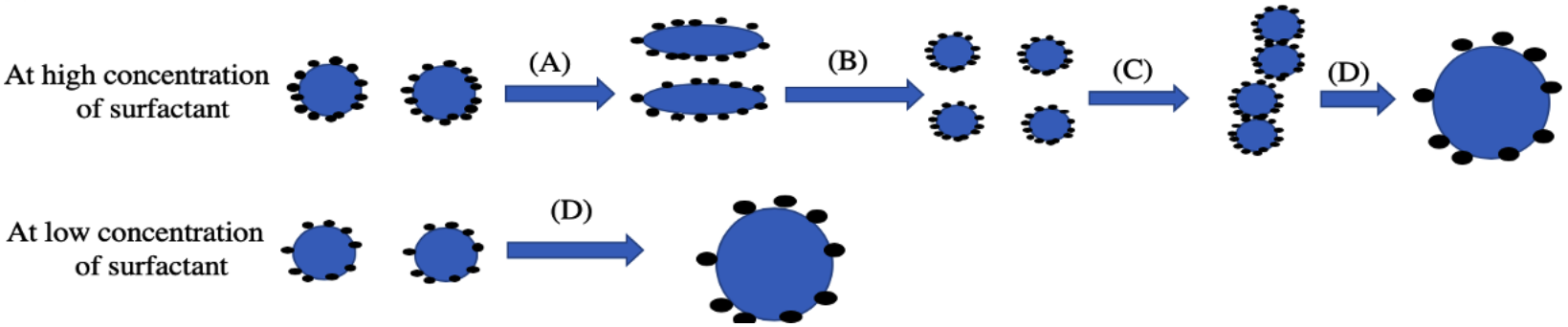

Figure.3.2.8. Schematic presentation of the process of (A) drop deformation to (B) drop breakage to (C) collision to (D) coalescence

.

Column Characterization

To predict the exact distribution of concentrations and get a more accurate indication of the arrival time, the dispersion was measured using bromide as a conservative tracer and is presented in Figure 3.2.9. Figure 3.2.9 shows that for fluidized bed color (D_{ax} = 15 cm^2/min) it is approaching a well-mixed system in terms of how concentrations respond as a function of step input (Q = 250 ml/min). The axial dispersion coefficient was determined using the excel solver to minimize the sum of the square of the errors by adjusting the value of the axial dispersion coefficient. For fixed bed columns, the low value of the axial dispersion coefficient (D_{ax} = 0.431 cm^2/min) might be assumed the characteristic of normal well-packed beds which can be neglected for liquid phase systems (Q = 20 ml/min). It physically represents the behavior of having a small number of fast pathways through the bed and the relative concentration is 0.5 at t = Advective velocity/ length of the column. For columns that have been packed unproperly and the dispersion is really large, bromide arrived earlier, and 50 % relative concentration appeared at the point earlier than one pore volume (PV= 98 ml). (Diffusion dominated flow)

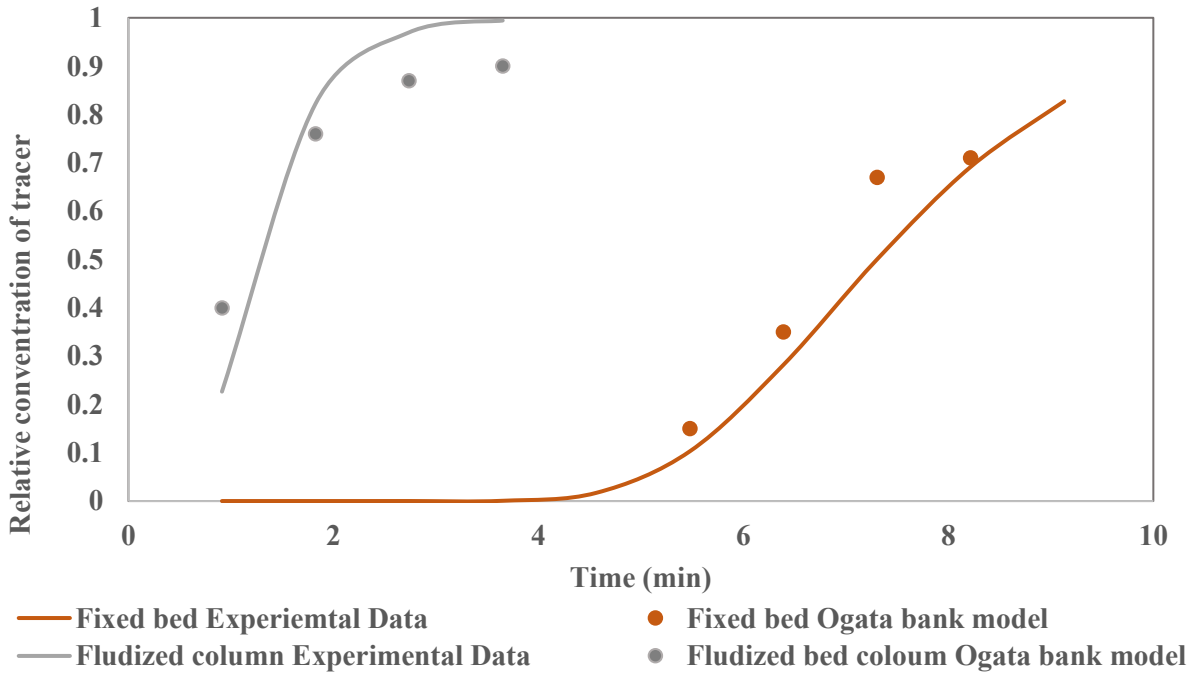

Figure.3.2.9. Breakthrough curve of conservative Bromide in treatment columns.

Adsorption isotherm for the most stable emulsion

For mathematical modeling of oil sorption, it is necessary to obtain the considerations of the system phase equilibrium and the dynamic isotherm of aliphatic compounds in modified dolomite at the optimal conditions (i.e., pH= 6, and surfactant concentration 0.9 %). Figure 3.2.10 presents the adsorption isotherm data of alkane compounds of crude oil onto palmitic acid-coated dolomite particles at 298 K along with the Freundlich isotherm model. The Freundlich isotherm parameters were adjusted by the data of equilibrium obtained from the experiment in the batch system. Batch sorption measurements of crude oil from water by the modified dolomite were performed in glass bottles as described in our previous study (Davoodi et al., 2019). As shown in Figure 3.2.4, the sorption of alkane compounds onto adsorbents could be well expressed by the Freundlich isotherm and the calculated parameters $^{1}/_{n}$ and K_f $(\mathrm{mg/g})/(\mathrm{g/l})^{\,1/n}$ are 0.66 and 0.8, respectively.

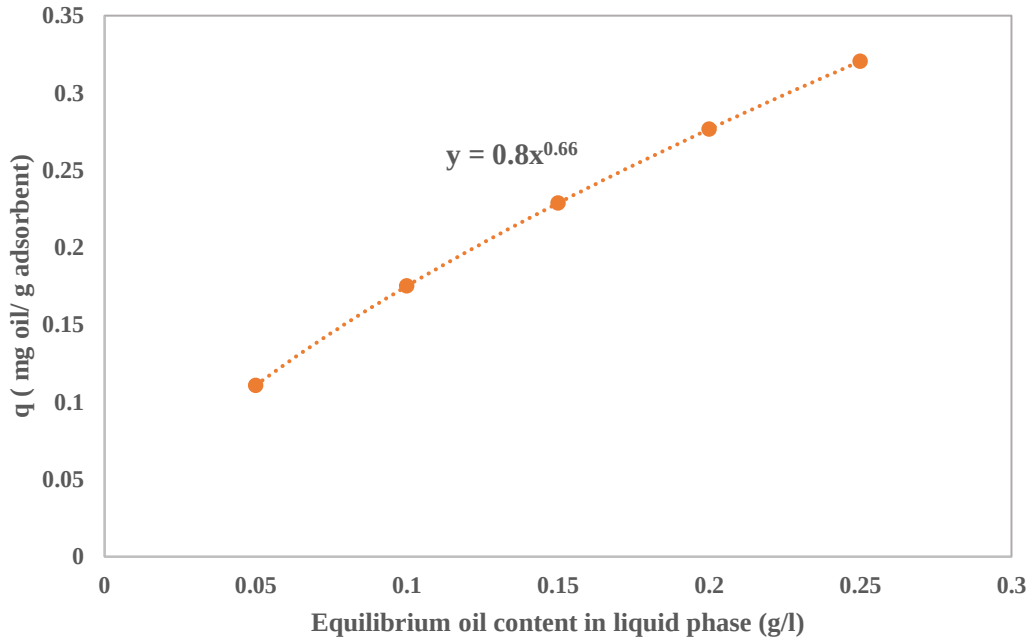

Figure.3.2.10. Adsorption isotherm of Alkane compounds of Bakken oil onto modified dolomite pH= 6, and surfactant concentration 0.9 %.

Removal of oil from water in fixed and fluidized beds of modified dolomite

The oil removal efficiency and capacity of the modified dolomite particles are studied by measuring both the inlet and exit concentration of oil (i.e., TPH) as a function of time and plotting a breakthrough curve. The inlet oil concentration should remain constant throughout the experiment but small changes in oil pump flow rate, the stability of the emulsion result in different

inlet concentrations with time; hence the amount of an average value was applied. Table 3.2.2 shows operating conditions for each experiment.

Table 3.2.2. Summary of experimental conditions (F: 18 combinations, FL: 4 combinations) and oil removal capacity from water using fixed and fluidized beds of modified dolomite.

Bed type	Initial oil concentration (mg/l)	Flow rate (ml/min)	Particle mass (g)	Particle Radii (cm)	Breakthrough time (min)	Removal capacity at t 0.5 (mg oil/ g adsorbent)
P	400	10	421	0.08	15.6	0.148
				0.15	13.2	0.125
P	400	15		0.08	10.1	0.143
				0.15	9.4	0.133
P	400	20		0.08	7.4	0.140
				0.15	6.8	0.129
P	450	10		0.08	13.1	0.140
				0.15	10.4	0.111
P	450	15		0.08	8.3	0.133
				0.15	7.9	0.126
P	450	20		0.08	6.4	0.136
				0.15	5	0.106

P	650	10		0.08	9.4	0.145
				0.15	7.6	0.117
P	650	15		0.08	7.1	0.164
				0.15	5.7	0.132
P	650	20		0.08	5.4	0.125
				0.15	4	0.123
F	650	250	50	0.2	4.1	0.162
F	650	250	100	0.2	5.3	0.151
F	650	500	50	0.2	3.5	0.143
F	650	500	100	0.2	4.6	0.140

F: Fixed bed column; FL: Fluidized bed column

The oil removal results from Table 3.2.2 show that: (1) as the flow rate increased the removal capacity decreased that is not consistent with the results obtained in Sec.3.4 . It might be attributed to the fact that hydrophilic and semi-polar compounds that exist in Bakken oil (i.e., resin and polar derivatives of PAHs such as oxygenated PAHs) bypass adsorbents and come out first from the column earlier and it resulted in a dramatic change in breakpoint time as the flow rate increased. The presence of long-chain fatty acid with a 16-carbon backbone on the surface of dolomite resulted in strong affinity for molecules with aliphatic or semi-aliphatic chains and rings but these physically adsorbed molecules might serve as a base layer upon which further hydrocarbon could adsorb but it might lead to an equilibrium time of more than 20 min to achieve higher removal efficiency. Maja et.al studied aromatic adsorbents for emerging pharmaceutical removal.(Sekulic et al., 2019) They showed that aromatic adsorbents with high electronic density could remove almost 80 % of all contaminants with π-electron donor groups include aromatic benzene rings that exist in PAHs. Thus, the absence of aromatic carbon content on the surface of adsorbent resulted in strong Van Der Waals interaction between a majority of aliphatic groups in adsorbent and sorbates which are much stronger than π-π interactions between sorbates and aromatic components in biofilms (Wang et al., 2019a). (2) The oil removal capacities are higher in the fixed bed than those in the fluidized bed. The comparison of columns permeability coefficient showed that as the flow rate and initial concentration of oil increased above the value of Q = 20 ml/min and C_0 = 650 mg L^{-1}, the assumption of constant porosity of the bed column might not be correct due to the occurrence of coalescence. Thus, fluidized bed columns were applied to study the application of bed systems for adsorption of oil compounds with modified dolomite when flow rate and initial concentration increased.

Predicting breakthrough curves and breakpoint times

Phenomenological mathematical modeling

Table 3.2.3 presents the value of the kinetic mass transfer parameter (k_f and D_{app}) and axial dispersion (D_{ax}) estimated from the fitting of the model to the experimental data of the breakthrough curves as well as the value of AAD and objective function.

Table 3.2.3. Characteristic parameter of the aliphatic compound breakthrough curve under various operating conditions

Initial Concentration (mg L^{-1})	Flow rate (ml/min)	Particle Radii 0.08 cm						
		Kf (cm/min)	Dapp (cm2/min)	Dax	AAD	LUB*	Biot Number	Removal capacity (mg/g adsorbent)
400	10	0.0013	0.000062	0.084	1.29E-02	3.80E+00	21	0.36
	15	0.0035	0.000025	0.431	0.041	3.55E+00	140	0.40
	20	0.0054	0.000071	0.94	0.75	4.70E+00	76	0.37
450	10	0.0004	0.000019	0.065	0.018	5.08E+00	21	0.38
	15	0.0015	0.000026	0.95	0.029	3.58E+00	58	0.41
	20	0.0014	0.000093	1.1	0.46	5.10E+00	15	0.38
650	10	4.50E-05	0.000017	0.081	0.025	5.08E+00	3	0.37

15	1.20E-04	0.000031	0.95	0.046	6.35E+00	3	0.39
20	5.90E-04	0.000043	1.4	0.74	5.30E+00	13	0.39

LUB: Length of unused bed (L (1 - $\frac{t^*}{t_b}$))

A comprehensive evaluation of the physical meaning of the estimated values of the kinetic and dynamic parameters allows us to analyze the robustness of the obtained results from the mathematic model. According to the values of AAD in the range of 0 – 1, the model-stimulated breakthrough profiles matched well with the experimental data at a low flow rate and initial concentration of oil. As can be seen from Table 3.2.3, the axial dispersion coefficient and external mass transfer decreased for various initial oil concentrations but increased with feed flow rate. It seems reasonable that a slight increase in the flow rate would increase the driving force and therefore the rate at which aliphatic molecules pass from the bulk solution to the particle surface across the boundary layer increased. (McKay et al., 1986) However, in the case of initial concentration, this is not the case. It is possible that increasing the concentration of aliphatic compounds, reduces its mobility to transfer rapidly across the boundary layer. Thus, the external mass transfer coefficients decreased as the initial concentration of oil increased which is inconsistent with batch adsorption study. (Davoodi et al., 2019) Low efficiency of the fixed bed column and higher axial dispersion coefficient at higher flow rate might be attributed to the fact that aliphatic molecules will not have sufficient time to diffuse in the pores of adsorbent and leave the bed before reaching the equilibrium. The time to reach equilibrium is slightly concentration dependent. It also depends on the particle size and flow rate. Moreover, the effective pore diffusion coefficient obtaining from the simulation of adsorption kinetics increased slightly as the flow rate increased, however, the Bi number that reflected the significance of the internal mass transfer versus external mass transfer resistance are more than 100 at various operating conditions that might be attributed to the fact that the pore diffusion resistance is not the dominant phenomenon. When the operational condition is experimentally and theoretically optimized, the film and intraparticle resistances of the sorption are minimized in the experimental range investigated. In other words, the film thickness is the thinnest one and there is no significant steric resistance in the particle pores. (Barros et al., 2013) In this study, the flow rate of 15 ml/min and the initial oil concentration of 450 mg L^{-1} resulted in the appropriate value for removal capacity.

Effect of flow rate

The flow rate of the emulsified oil-water stream is an important design parameter of an oil adsorption column. Fixed-bed column studies on oil adsorption were conducted at different values of flow rates that varied from 10 – 20 ml/min, while the inlet oil concentration and mass of

adsorbent were kept constant at 400 mg L^{-1} and 421 g, respectively at a pH of 8. Based on the successful implementation of velocity variation in the model, the proposed model shows more justifiable results with theoretical phenomena occurring in the adsorption system due to consideration of continuous decrease of velocity inside the bed concerning the bed length. However, the experimental results show that for low inlet concentration of emulsified oil and single-phase flow, the effect of velocity variation on the breakthrough curve was not significant (t-value = 2.75 and p-value ~ 0.02). Figure 3.2.11 shows the effect of flow rate on the breakthrough curve following the plug flow pulse arrival of contaminant and retardation of oil. As the flow rate decreased, two phenomena happened: 1) it was travelling less quickly, so it would be delayed and 2) and as the flow rate increased because it was becoming closer to plug flow, the dispersion and the steepness of the breakthrough curve decreased; however, the flow rate equal to 20 ml/min resulted in higher axial dispersion coefficient (Table 3.2.3). Retardation factor (*Rf*) is the most frequently used indicator to describe the transport of contaminants through fixed-bed columns. (Tsai et al., 2008) In this work, the *Rf* value (i.e., 3.28) was determined using the model fitting curve method at relative concentration 0.5. The variability of data and uncertainty in measured effluent concentration might stem from instantaneous changes of flowing path, fractions of immobile water in columns or the combination of caused stated previously along with something happened in micro-scale.

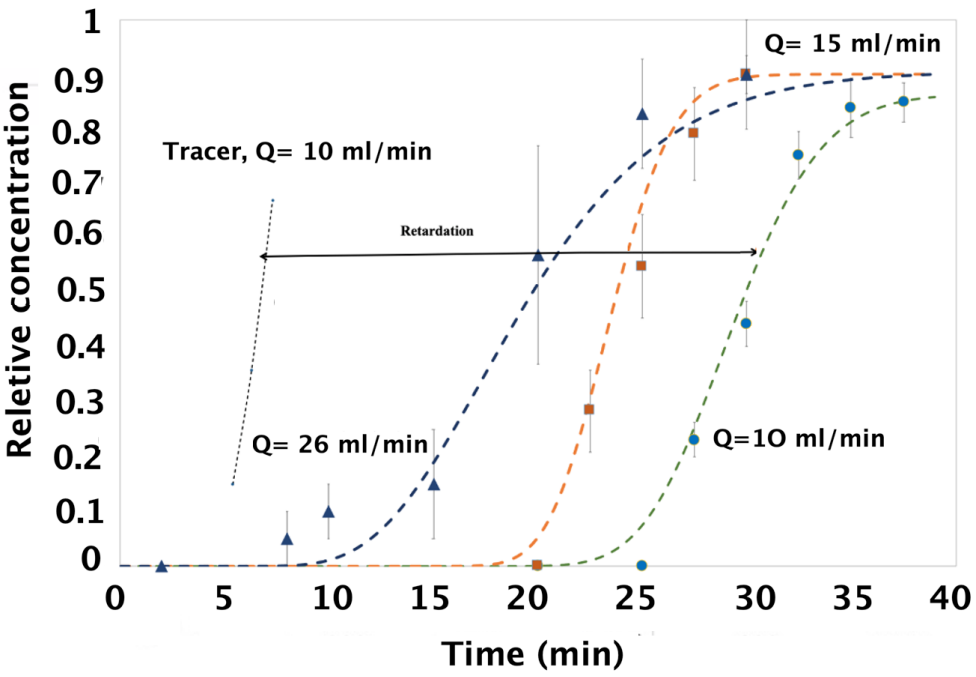

Fig.3.2.11. Effect of flow rate on the breakthrough curve for oil removal using modified dolomite (W = 421 g and C_f = 400 mg L^{-1})

The effect of the flow rate on the breakthrough curve is also shown in Table 3.2.3, assuming the constant velocity during the simulations. The literature reported a fixed saturation capacity of the bed based on the same driving force for adsorption. (Ahmad and Hameed, 2010) In other words, it has been assumed that unlike the hydraulic conditions that affects the adsorption kinetics, other conditions such as temperature of the bed, porous structure, surface area and surface properties of adsorbents might contribute to equilibrium isotherm and subsequently column adsorption capacity. Our results showed that as the feed flow rate increased from 10 to 15 ml/min, the break point time decreased from 1474 to 1193 sec and the adsorption capacity increased from 0.24 to 0.28 mg/g (16 % increase). Flow rate changes also affected the sorption kinetics (the shape of the breakthrough curve) by decreasing the external mass resistance that resulted in the increase in the slope of the breakthrough curve at Q = 15 ml/min (Table 3.2.3). Further increases in flow rate resulted in not long enough residence time of the solute in the column for adsorption equilibrium to be reached. In order to study this phenomena, Eq. (4) as well as mathematical models that describe the movement of fluids can be used for these cases. At high flow rate the Eq. (4) would be reduced to following equation

$$\frac{\partial C}{\partial t} = -v\frac{\partial C}{\partial x} - \frac{1-\varepsilon_l}{\varepsilon_l}\frac{\partial(\bar{q})}{\partial t}$$

At high flow rate, the thickness of adsorbed water layer around particles may be decrease due to the disruption of the structure of the water film. In other words, unlike laminar flow the fluid does not flow in parallel layers, the lateral mixing is high and there is a disruption between layers. Thus, the fluid at a point is undergoing changes in both direction and magnitude. Thus, the Eq. (4) Naiver-Stokes equation should be solved simultaneously to exhibit turbulent solution. Moreover, by assuming one element of fixed bed, the mass balance for the control volume for limiting situation $z \rightarrow 0$ net rate of depletion would be because of adsorption and mass transfer in the bulk phase and as the flow rate increases the moleculres in the bulk are transported via conversion (not axial convection and Fickian diffusion on the particle surface). Thus, at high flow rate mass transfer

zone and the difference between equilibrium and effective adsorption capacity of particles increased. To further study the effect of flow rate on adsorption behavior of oil on modified dolomite, mathematical modeling for adsorption ar the various length of the column was studied. Figure 3.2.12 displays the concentration profile predicted by the verified proposed model for emulsified oil in the liquid phase at all locations within the fixed-bed column (L_{column}= 15.1 cm, C_o = 400 mg L^{-1}) for flow rate of 15 and 26 ml/min.

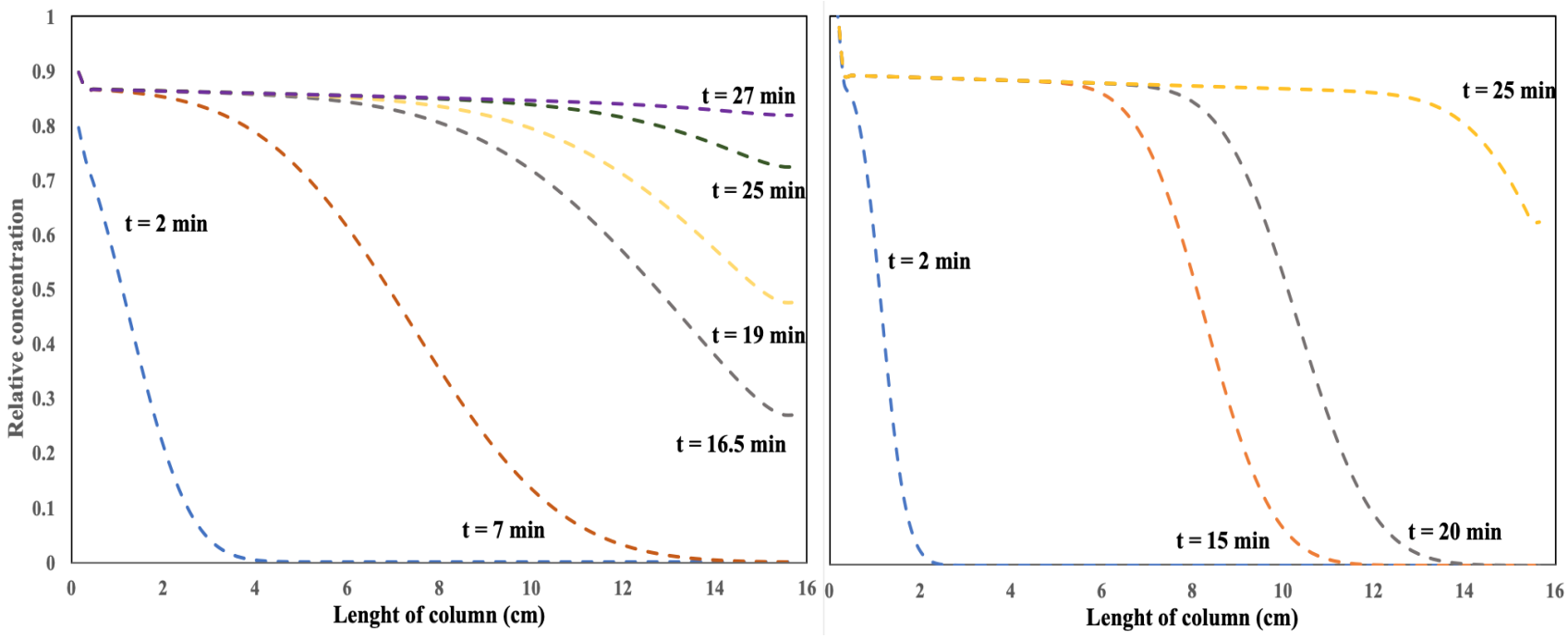

Fig.3.2.12. The concentration profile predicted by the verified proposed model for emulsified oil in the liquid phase at all locations

The effect of high flow rate can be observed while solving ODEs equations. In other words, after each irritation the initial concentration in each element would be determined and used for next time and at high flow rate as can be seen in Figure 3.2.12 the initial concentration calculated at each irritation was higher compared to lower flow rate. Figure 3.2.12 also showed one possible explanation for decrease in the steepness of the breakthrough curve. As can be seen in Figure 3.2.12 the break point time is less than 16.5 min however the column becomes saturated around 10 min after the break point time. Some literature attributed the expansion of mass transfer zone to turbulent mixing occurring due to back mixing around adsorbent particles, i.e. eddy currents (Patel, 2017).

Effect of inlet oil concentration

The effect of inlet concentration on the effluent oil content is presented for the flow rate of 15 ml/min, and particle radii of 0.08 cm in Figure 3.2.13. The considered initial oil concentrations are 400, 450 and 650 mg L-1. It was observed that similar to the flow rate, feed concentration, which can influent contact time, might affect the mass transfer flux from the bulk solution to the particle surface. After introducing the emulsified oil water solution, some molecules leave the bed to the breakthrough curve (i.e., term $-v\frac{\partial C}{\partial x}$) while some of them migrate to the surface of particles. The migration process of aliphatic molecules into an adsorbent particle includes convection and diffusion from the bulk to the outer layer of a stagnant film around the dolomite particles, external mass transfer from out layer to the surface of particles and finally diffusion to the surface of individual particles. The initial oil concentration just like flow rate did not affect the apparent diffusion coefficient that depends on structure of the particles. But, as mentioned previously, the Boundary Conditions r = r_p, t > 0; $\frac{\partial c_p}{\partial r}|_{r=r_p} = \frac{Kfilm}{\varepsilon_p D_{app}}(c - c_{p|r=r_p})$ that has been applied to determine concentration gradient inside the particle near the surface shows that initial concentration and

subsequently bulk concentration could affect concentration gradient inside the particle near the surface. To explain the effect of initial concentration on external and internal mass transfer in the process of aliphatic compounds removal by hydrophobic dolomite, the estimated $Kfilm$ from the fitting of the model to the experimental data were applied. As can be seen in Table 3.2.3, as the initial concentration increased the resistance to the film diffusion increased. Other literature explained the effect of initial concentration on external mass transfer coefficient by studying Sherwood/Schmitt ratio –initial concentration diagram. McKay et al explained how the driving force for mass transfer (based on the difference between the bulk liquid concentration and the particle surface liquid concertation), depends on time and will affect the way in which the external mass transfer coefficient varies with different pollutants (McKay et al., 1986) .

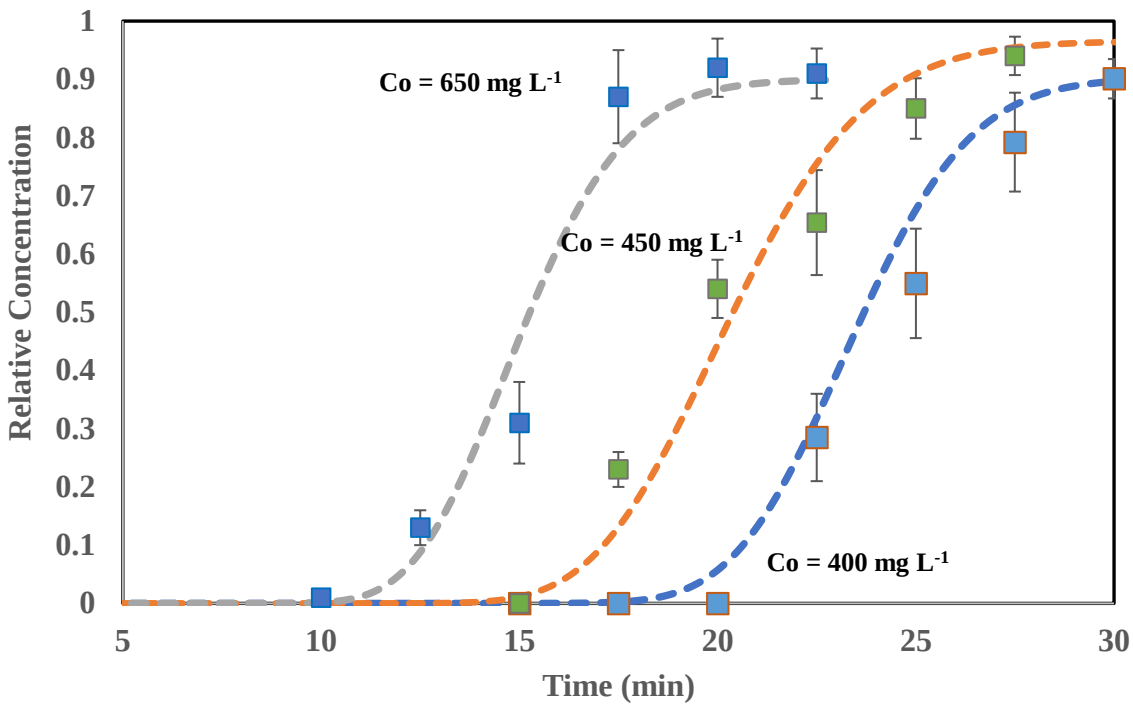

Fig.3.2.13. Effect of initial oil concentration on the breakthrough curve for oil removal using modified dolomite (Particle radii = 0.08 cm, Q = 15 ml/min

Figure 3.2.14 showed a closer look at the propagation of normalized free concentration profile of oil inside the particles located at the end of the column for different initial concentration of oil at their corresponding breakthrough time. Figure 3.2.14 was obtained using the solution for the resultant ordinary differential Eq. (10). The initial concentration on the one hand increased the driving force and the rate at which aliphatic compounds pass from the bulk solution to the particle surface across the boundary layer; on the other hand, higher concentration reduces molecules mobility to transfer rapidly across the boundary layer. The result of these effects would be decreased gradient concentration as the initial concentration increased (Fig.10.)

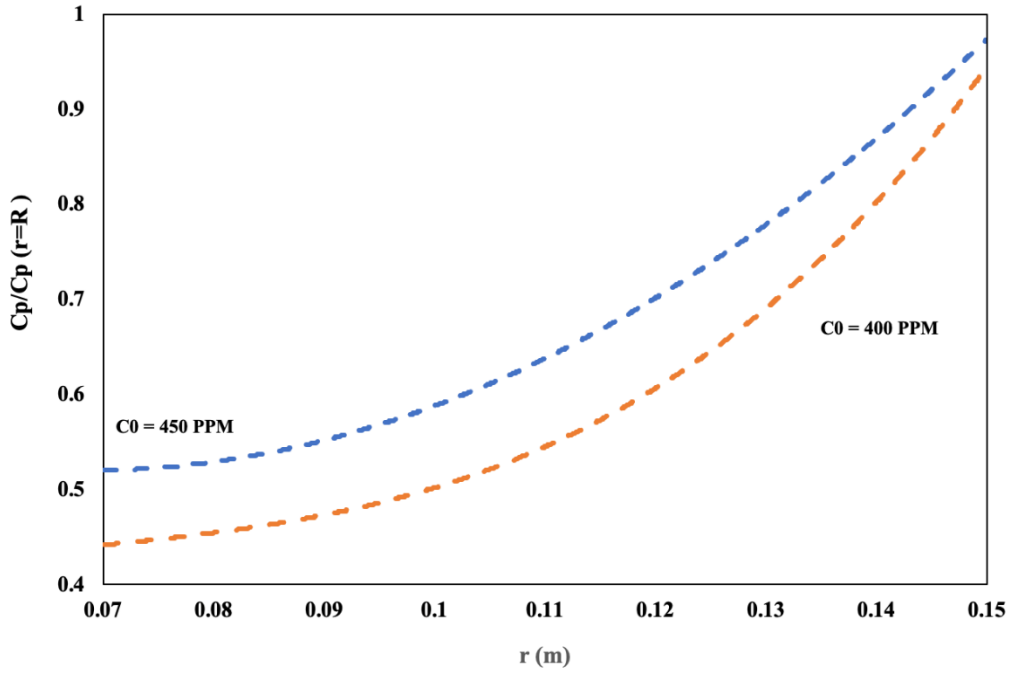

Fig.3.2.14. Propagation of the normalized free concentration profile inside the particles

Figure 3.2.14 shows that the increase in initial concentration the gradient of concentration inside the particles will tend to change in a direction that brings it closer to its equilibrium state. As can be seen in Figure 3.2.14, at the break point the adsorbent at the end of column is not saturated (in equilibrium); however, in this study, the common t_b at $0.01\ C_o < C < 0.05\ C_o$ was considered as stop loading time to avoid many contaminants in the outlet, but it also resulted in a lot of unused capacity.

Effect of particle radius

Figure 3.2.15 shows the effect of particle size on the distribution of oil concentration at effluent and arrival time for samples at constant initial oil concentration of 450 mg L-1 and a flow rate of 15 ml/min. The particle radii are considered 0.08, and 0.15 cm. Freundlich isotherm model has been applied to multilayer adsorption, and it assumed that the surface of the adsorbent is heterogeneous. Any change in particle size and shape might have a significant effect on multilayer adsorption for other contaminants. For example, “edge and corner” defect-like sites can exhibit lower adsorption enthalpies than high-coordination sites and as a result these sites can serve a portal for rapid adsorption compared to the rest of the surface. fAs for kinetic of sorption, Figure 3.2.15 showed that the breakthrough curve steepness decreased as the particle radius increased from 0.08 to 0.15 cm because smaller particle size adsorbent provided quicker adsorption kinetic.

Moreover, as the diameter of the particle decreased, the thickness of stagnant film around the particles decreased and the overall kinetics of the process increased under these conditions. Thus, the concentration of oil inside the particles (C_p) at the end of the column reached a constant value more quickly compared to larger particle sizes (Data not shown here).

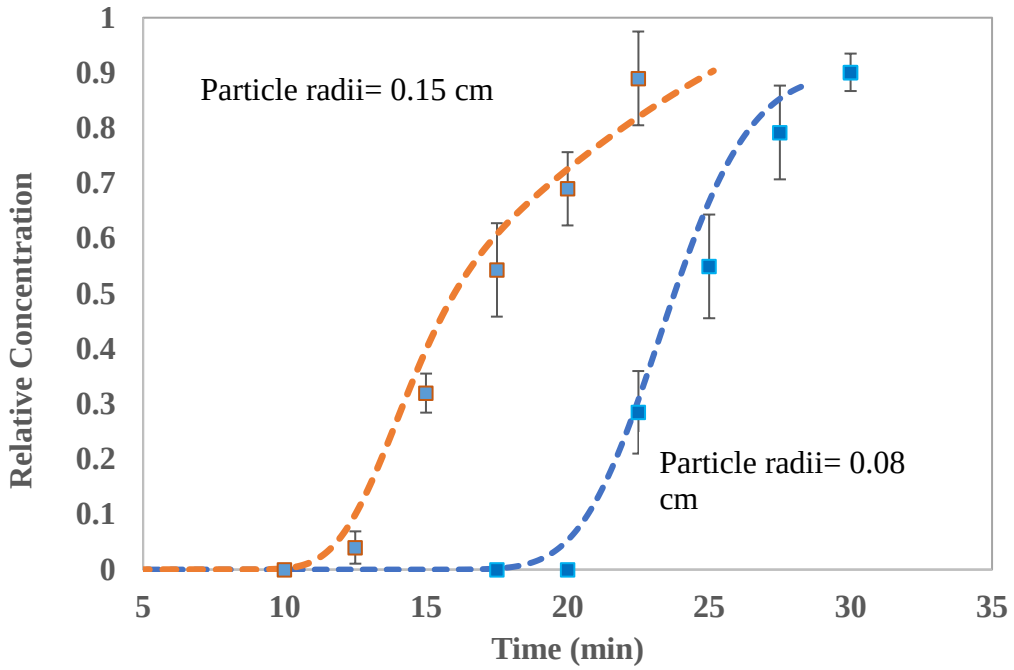

Fig.3.2.15. Effect of particle radii on breakthrough curve for oil removal using modified dolomite (Q = 15 ml/min, C_o =450 mg L-1)

As can be seen in Figure 3.2.15., the breakthrough curve is asymmetric for larger particles that might be due to mass transfer resistance in the column meaning that the adsorbate needs to diffuse through a stagnant layer for example inside the porous materials before being actually adsorbed.

Upscaling adsorption column

When the fixed-bed column adsorption reaction (flow rate = 10 ml/min, L_{column}= 15.1 cm, D_{column}= 5 cm, C_o = 400 mg L-1) was performed for 2, 15, 20, and 25 min, the emulsified oil was diffused to the fixed-bed column length of 0.5, 5.4, 7.1 14 cm, respectively.

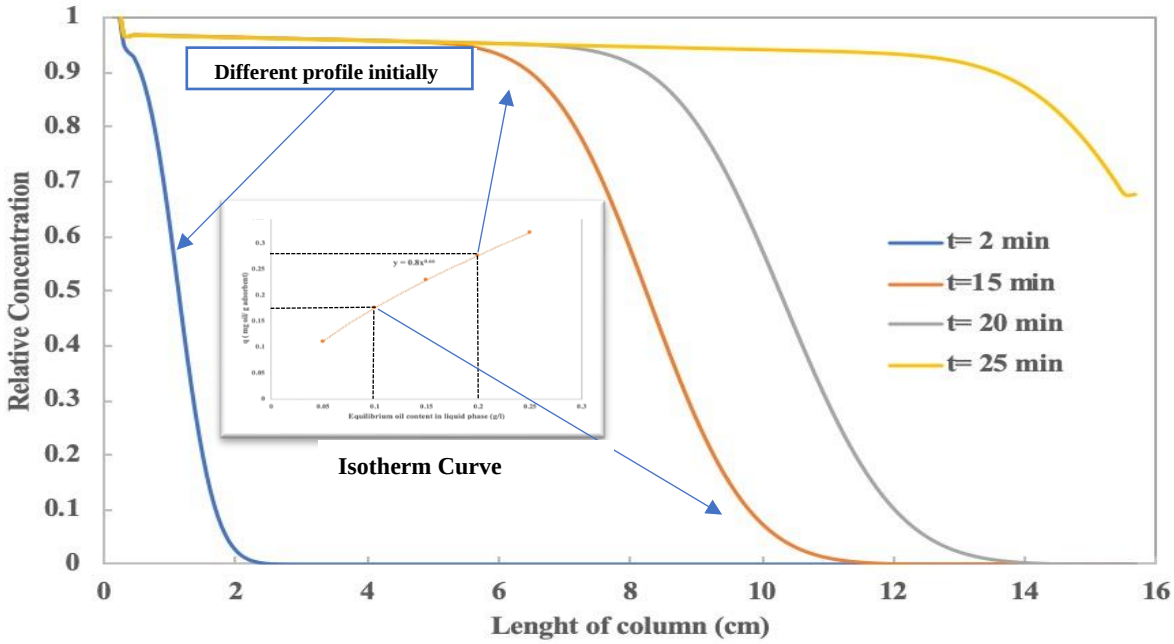

Fig.3.2.16. Concetration profile for emulsified oil in the solution at all locations within the fixed-bed column

Figure 3.2.16. shows that as the bed height increased, the breakpoint time increased. Moreover, smaller bed height corresponded to a smaller capacity for the bed to adsorb emulsified oil from the solution resulted in less time needed for saturation of the column. Thus, as the surface area increased, not only retardation but also the attachment of oil particles to adsorbent resulted in a lower concentration of oil in the effluent. When the adsorption isotherm is favorable, then the fraction adsorbed at low concentration is high; this eventually slows down the low concentration part of the front so much that it counteracts the broadening of the front.

Small scale experiment using 15 cm long column with a diameter of 5 cm is fed with an inflow with the concentration of 450 mg L^{-1} and the feed flow rate is 15 ml/min. After choosing the break

point and scaling up to 600 cm column with a diameter of 20 cm, the degree of utilization and the average concentration in the outlet of the large column have been calculated. The saturation time (t^*) for small and large columns is approximately 21 min. In this study, the common t_b at 0.01 C_o $< C <$ 0.05 C_o was considered as stop loading time to avoid many contaminants in the outlet but it also resulted in a lot of unused capacity. Table 3.2.4 shows the parameters calculated for small and large columns. As can be see in Table 3.2.4, with the same break point criteria a large increase in the degree of utilization and a large decrease in average concentration in the outlet have been observed.

Table 3.2.4. Obtained parameters for small and large columns

Parameters	Small column	Large column
Degree of utilization (%)	75.5	99.3
LUB (cm)	3.58	3.58
Cave (mg/L)	0.008	0
t_b (min)	16.3	854.8
t^* (min)	21.5	860
Flow rate (ml/min)	15	24,000

Fluidized bed modeling results and experimental measurements

Figure 3.2.17 shows model results for the breakthrough curve using 50 g dolomite particles and the experimentally observed concentration of oil.

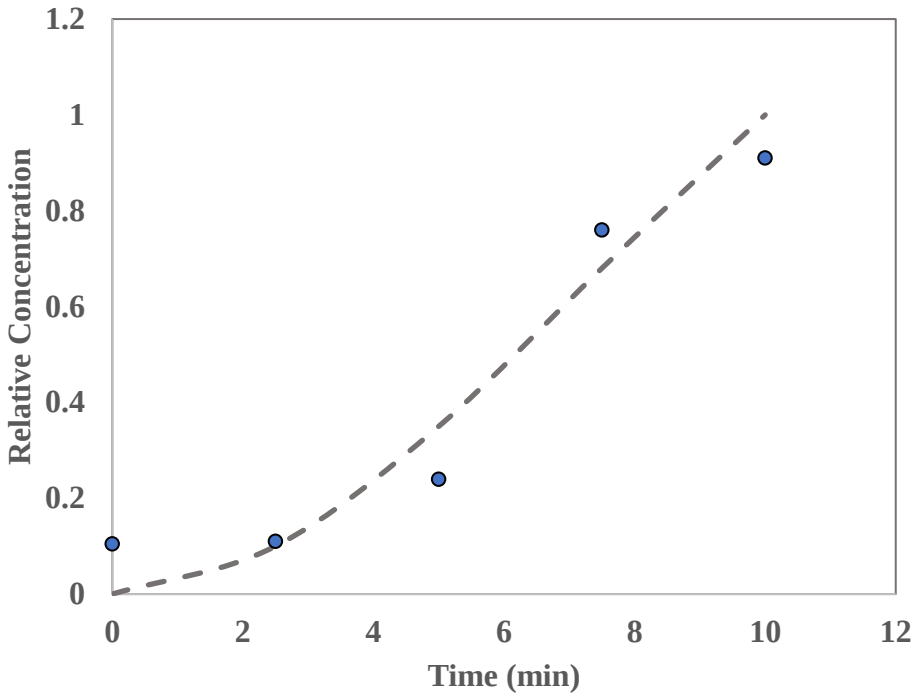

Fig.3.2.17. Model results for the breakthrough curve using 100 g dolomite

As mentioned previously, our results showed that the axial dispersion model might not be applicable to study the mass transfer between liquid and solid phases. In other words, for each experiment solid-phase axial dispersion coefficient has changed due to agglomeration of particles and the measurement of axial dispersion for solid-phase might not be repeatable and vary day to day. Some literature applied stirrer in fluidized bed reactors and columns where particles are smalls to provide large surface area and avoid particles from sticking to the walls and aggregating. (Sahoo and Sahoo, 2013) Without the use of stirrer that provides agitation, Eq. (17) was applied in solid-phase instead of Eq. (19). The rate constant K in Eq. (17) was obtained from batch experiments by using a linear driving force model defined as,

$$\frac{\rho_p V_l}{m} = - K (C - C_e) \quad (22)$$

$$\frac{\rho_p V_l}{m} = - \frac{dq}{dt} \quad (23)$$

q (t = 0) = 0 , C(0) = 420 mg L^{-1}

The benefit of using the above-mentioned equation is that batch experiments have been applied to solve mass balance equations for fluidized bed columns. To calculate the oil concentration in liquid

and solid phase during the time, Eq. (22) and (23) can be solved simultaneously using Runge-Katta 4th order and Eq. (13). Figure.3.2.18 and 19 show the aliphatic concentration as a function of time in a batch kinetic experiment, and the schematic of computational procedure for obtaining the rate constant as well as liquid phase concentration changes during the time, respectively. As can be seen in Figure 3.2.17, the results of the model and experiments are in good agreement however the initial concentration of Eq. (14) resulted in a negative value for q and imaginary numbers for outlet concentration. Thus, in this study following initial boundary condition was applied to obtain concentration profile.

t = 0, 0 < x < L_{Column}; C = positive small value larger than Ce

Zero initial concentration were avoided as it resulted in stiffness of the numerical integration.

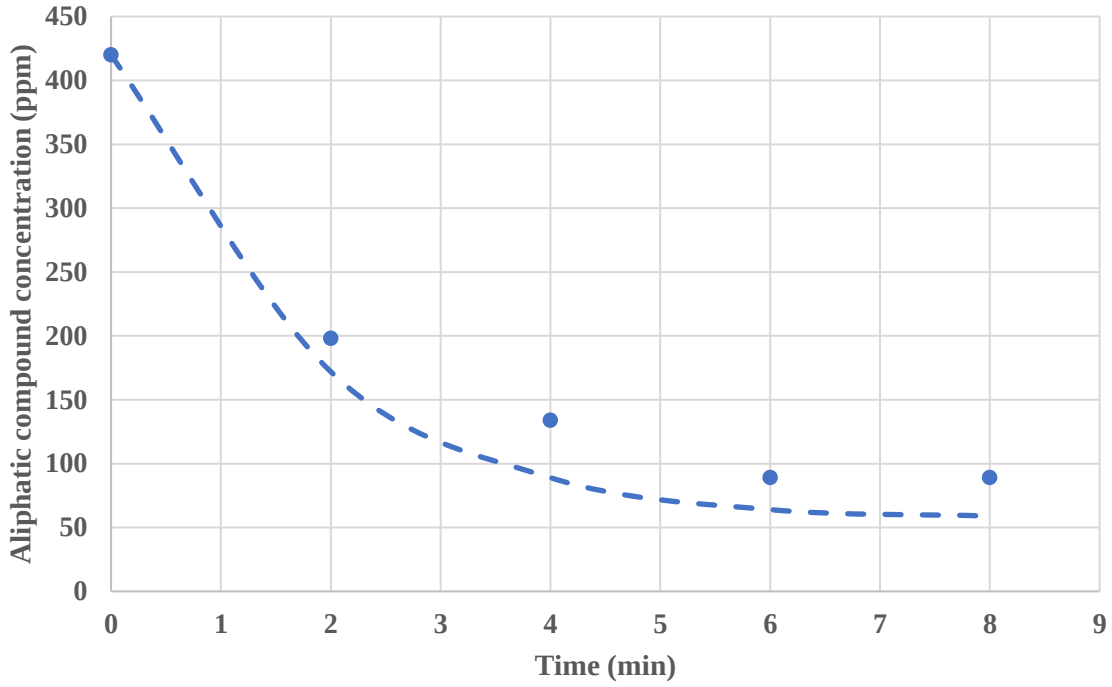

Figure.3.2.18. aliphatic concentration as a function of time in a batch kinetic experiment.

```
For   t =1: n

          % implementing Runge- kutta

        end

      % using Freundlich equation for computing Ce

       if abs(C_e_new - C_e) < 1e-6
            Break
      else

      end
end
```

Figure.3.2.19. Schematic of computational procedure for obtaining the rate constant and liquid phase concentration with time

3.2.4. Conclusion

The performance of modified dolomite for removing oil from laboratory synthetic oil-in-water (o/w) emulsions in packed bed (PB) and fluidized bed (FB) modes was investigated. In this study, Bakken oil that is dominated by straight-chain saturated hydrocarbons (~ 43 %) has been chosen as model oil. From the experimental data of oil removal from salty water, data analysis and fixed-bed column modeling, the following conclusions are drawn:

(1) For low value of inlet concentrations C_o = 450 mg L-1 of emulsified oil, the effect of velocity variation on the breakthrough curve was not significant (t-value = 2.57) and permeability test of the clean and saturated columns showed that the porosity of columns and hydraulic conductivity of beds did not change during the experiments.

(2) Unlike the aliphatic compounds removal capacity of fixed bed columns, as the flow rate increased crude oil removal capacity of fixed bed columns decreased. It might be attributed to the fact that hydrophilic and semi-polar compounds that exist in Bakken oil (i.e., resin and polar derivatives of PAHs such as oxygenated PAHs) bypass adsorbents and come out first from the column earlier and it resulted in a dramatic change in breakpoint time as the flow rate increased (15.6 min to 7.4 min).

(3) Unlike other operating conditions, particle radius might change isotherm, kinetic and even hydraulic parameters and radius of 0.08 cm were chosen as the most appropriate size.

(4) The benefit of using the fluidized bed as compared to a fixed bed of particles is an adjustable void of the fluidized bed by changing the fluid velocity, excellent mixing between the liquid and the solid particles, low pressure drops when operating above the minimum fluidization velocity.

CHAPTER FOUR: *In-situ* application of cocktail enzymes for contaminated soil

PART 1

4.1 Enzymatic biodegradation of polyaromatic hydrocarbons contaminated soil using cold-active enzymes: A soil column study

Seyyed Mohammadreza Davoodi[1], Saba Miri[1], Satinder Kaur Brar[1*], Richard Martel[3]

[1] Department of Civil Engineering, Lassonde School of Engineering, York University, North York, Toronto, Ontario Canada M3J 1P3.

[2] INRS-ETE, Université du Québec, 490, Rue de la Couronne, Québec, Canada G1K 9A9

(*Phone: 1 418 736 2100 ext. 55228; E-mail: satinder. brar@lassonde.yorku.ca)

Environmental Science & Technology (under review)

Abstract

Enzymatic biodegradation is a rapid method of removing environmental contaminants to address unresolved issues such as bioremediation inefficiency for highly contaminated sites. Most literature recently focused on peroxidase and laccase with strong oxidative ability however these enzymes are not able to attach un-fictionized aromatic compounds. In this study, oxygenase enzymes, the key enzymes involved in PAHs degradation with matching end products, were brought together from different arctic strains for biodegradation of highly contaminated soil. To increase the concentration of enzymes at produced cocktail, these enzymes were produced via multi-culture of psychrophilic *Pseudomonas*, *Rhodococcus* strains. As a result of biosurfactant production, the removal of pyrene was sufficiently prompted by *Alcanivorax borkumensis*. The key enzymes obtained via multi-culture were characterized by kinetic studies and tandem LC-MS/MS. Bioremediation of soil contaminated with pyrene was carried out in soil columns (140 mL) to mimic in-situ application of enzyme mixtures. Different enzyme cocktail mixtures obtained from most prompting synthetic consortia were used to treat pyrene-contaminated soil. Enzyme cocktail contained about 35.2 U/mg protein pyrene dioxygenase, 61.4 U/mg protein naphthalene dioxygenase, 56.5 U/mg protein catechol-2,3-dioxygenase, 6.1 U/mg protein 1-hydroxy-2-naphthoate hydroxylase, and 33.5 U/mg protein protocatechuic acid (P3,4D) 3,4-dioxygenase enzymes. The average values of pyrene removal after 8 weeks indicated that the enzyme cocktail can be an appropriate concentration for soil enzymatic bioremediation in the soil column system (80-85% pyrene degradation).

Keywords: biodegradation, cold-climate, p-xylene, monooxygenase, dioxygenase

Graphical Abstract

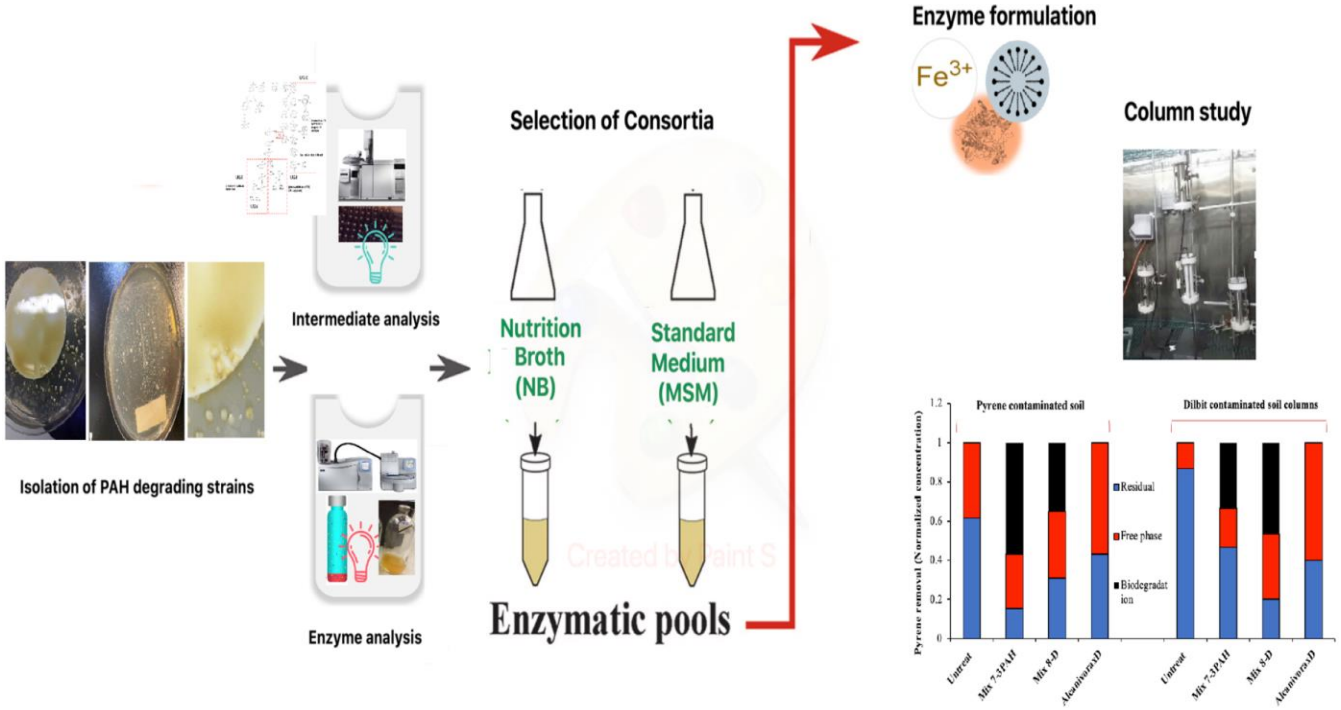

4.1.1. Introduction

There is a frequent threat of environmental contamination, including contamination of water bodies and soils by oil spills. This is particularly relevant for both the United States and Canada where the transportation of unconventional oils and traditional petroleum over long distances inland is accomplished by railways and pipelines. Depending on the contaminated site condition, level and type of contamination, various treatment approaches such as physical, thermal and chemical method for the remediation of PAHs in crude oil contaminated soils and water have been designed (Davoodi et al., 2020; Kwean et al., 2018) There are several disadvantages of these methods in cold climates, including energy consumption, cost and production of toxic intermediates.

As compared to the other methods, bioremediation is more effective and economically viable, while causing less undue damage to environments in cold climates. However, it is not possible to achieve the highest levels of biodegradation efficiency. (Kwean et al., 2018) For example, the main challenge mentioned in recent literature is to design bioremediation for highly contaminated sites located in cold climate regions. (Miri et al., 2022)

Accordingly, over the last few years, the use of degrading enzymes in comparison with whole-cell degrading microorganisms has gained increasing attention.(Alcalde et al., 2006) In comparison with whole-cell bioremediation, enzyme-based bioremediation has several potential advantages: (1) the enzymatic reactions do not produce harmful by-products (2) a safe technology to use for human beings and animals (3) shorter duration of treatment; and (4) high degree of specificity.(Miri et al., 2022) Despite such advantages, the high cost of enzyme production as well as its stability limit their application for environmental purposes.(Miri et al., 2021a) An approach to decrease enzyme production in this study is: 1) the use of biosurfactant/enzyme systems to assist the treatment of soil; 2) utilizing the multi-culture of two psychrophilic bacteria to improve the production of cold-active enzymes (Miri et al., 2022) and; 3) utilizing the activator to further enhance the activity of key enzymes.

Some researchers devised biodegradation utilizing the ligninolytic enzymes of white rot fungi, particularly for compounds that are not readily degraded by bacteria. As a result, extracellular enzymes such as peroxidases and laccases are produced, which demonstrate strong oxidative abilities and low specificity. However, fungal oxidases, such as laccase, are not able to efferently attack un-functionalized aromatic compounds (El Fantroussi and Agathos, 2005; Marques and

Hogland, 2003; Thompson et al., 2005). Thus, the application of other key enzymes involved in the degradation of petroleum aromatic hydrocarbons, hydroxylases and ring cleavage dioxygenases should be studied for *in-situ* application.

In comparison with their mesophilic counterparts, cold-active enzymes are ten-fold more active at low temperatures (below 20-30°C)(Feller and Gerday, 2003). Several studies have examined the role of enzymes in bioremediation of petroleum hydrocarbons using microorganisms adapted to cold temperatures. Only a few studies have been conducted on the application of cold-active enzymes to the degradation of petroleum contaminants (Davoodi et al., 2020; Miri et al., 2021a; Miri et al., 2022). Previously, cold-active xylene monooxygenase and catechol 2,3 dioxygenase were applied for the enzymatic degradation of p-xylene in groundwater at 15℃ (Miri et al., 2019). Several critical factors that contribute to the enzymatic biodegradation of the target contaminant should be confirmed in *ex-situ* tests e.g., soil columns and batch tests. The soil column test can be used to simulate the *in-situ* application of enzyme mixtures and predict the impact of bioremediation by modelling the essential characteristics of the environment. To the best of our knowledge, no studies have been conducted to characterize and apply soil column systems for enzymatic biodegradation of heavy molecular weight PAHs.

This work aims to: (1) develop an enzyme-based bioremediation approach to effectively degrade PAHs in cold contaminated sites and (2) investigate the application of psychrophilic enzymes for remediation of highly contaminated samples. Pyrene was examined as a model of a polycyclic-aromatic hydrocarbon because it has a structural similarity to several carcinogenic PAHs. The outcome of the study was the development of a biochemical remediation method for petroleum aromatic hydrocarbons using appropriate enzyme cocktails. For this purpose, the synergistic effect of mixed-culture bacteria, the use of growth media as well as the production of vital enzymes were studied. The enzyme cocktails were obtained from mixed bacteria cultures which led to PAH biodegradation relatively quickly with no accumulation of toxic metabolites. The unique formulation obtained during fermentation was characterized.

4.1.2 Materials and Methods

Bacterial strains and chemicals

The strains used for bioremediation of contaminated aquifer matrix material mixture are *Alcanivorax borkumensis* SK2 (DSM 11573), newly isolated *Pseudomonas* URS-5, URS-6, URS-

8 and *Rhodocucus* URS-10. The strain, *Alcanivorax borkumensis* was purchased from DSMZ (Braunschweig, Germany). The following analytical/microbiological grade chemicals were all purchased from Fisher Scientific (Ontario, Canada) for enzyme preparation: dichloromethane, tryptic soy broth/agar (TSB, TSA), KNO_3, NaCl, Ca_2CO_3, Na_2HPO_4, KH_2PO_4, NaOH, and HCl, yeast extract. For cultivation of PAH degrading bacteria, sea salt-defined media were prepared with 10% salinity as described by Zhao et.al (2009) (Zhao et al., 2009). It was composed of $MgSO_4 \cdot 7H_2O$ (10.45 g/L), $MgCl_2 \cdot {}_6H2O$ (6.9 g/L), NaCl (79.45 g/L), $NaHCO_3$ (0.1 g/L), $CaCl2 \cdot 7H_2O$ (0.75 g/L), KCl (2.1 g/L), and NaBr (0.25 g/L). This medium was supplemented with 1 ml of a trace element solution including $FeSO_4 \cdot 7H_2O$ (400 mg/L), $CuSO_4 \cdot 5H_2O$ (80 mg/L), $MnSO_4 \cdot 4H_2O$ (40 mg/L), $NaMO_4 \cdot 2H2O$ (8 mg/L), $Ca(NO_3)_2 \cdot 4H_2O$ (800 mg/L), $ZnSO_4 \cdot 7H2O$ (40 mg/L), and H_3BO_3(6 mg/L). Finally, the following compounds were added: $(NH_4)\ 2SO_4$ (1 g/L), K_2HPO_4(0.5 g/L). (Quesada et al., 1987; Zhao et al., 2009) Nutrient broth (NB) medium was purchased from Sigma-Aldrich Co. (USA). M3 medium described by Rowbotham *et.al* (1977) was prepared using 0.233 g KH_2PO_4, 0.336 g Na_2HPO_4, 0.01 g Ca_2CO_3, 0.145 g NaCl, 0.05 g KNO_3, 0.1 g sodium propionate and 9 g agar. (Rowbotham and Cross, 1977) Unconventional oil e.g., Dilbit for this study was derived from Syncrude coke-feed bitumen, which was extracted from the Athabasca oil sands (Wu, 2003).

Isolation and identification of PAH degrading bacteria obtained from contaminated sediments

To isolate PAHs degrading strains from coastal marine environment, 0.5 g of the impacted sediments was transferred in a crimp sealed 150 mL-serum bottle contained 25 mL of sea salt-defined media (SSM) with crude oil (200 mg/l) as the sole carbon source and incubated for a month at 4 ℃ as described in the supplementary information (Section A.1.1).

Inoculum preparation of aliphatic degrading bacteria

Alcanivoracx borkumensis was grown aerobically in a liquid medium by inoculating the flasks containing seawater media using lyophilized powder and then incubating the flasks in an orbital shaker at 27 ±1 ℃ for 4 days. Later, 150 μl of the medium was incubated in nutrition broth (NB)-agar plates at 27 ±1 ℃ and the plates were stored 27 ±1 ℃ for future use.(Kadri et al., 2018d)

Silicone O-Ring passive dosing format

It is very important to control the freely dissolved PAH concentration and keep it unchanged throughout the experiment by equilibrium partitioning from the silicone. Silicone O-rings (1 g each) were used as passive dosing format to provide constant concentrations of dissolved solutions and avoid spiking with cosolvents as described in elsewhere.(Butler et al., 2013) In brief, the rings were loaded by equilibrium partitioning i.e., pushing PAHs (log K_{OW}, 3.33−4.88) from a methanol suspension of naphthalene, anthracene, phenanthrene, pyrene into the polymer, followed by methanol removal with water. (Smith et al., 2010) More detailed information on using O-Ring passive dosing is provided in the supplementary information (Section A.1.2).

Preparation of synthetic consortia and microbial community study

Several combinations of the above pre-selected strains have been used to create the synthetic consortiums (Table A1). Inoculum from equal volumes of freshly grown bacteria was prepared whose cell concentrations had been adjusted to 2.5×10^{12} CFU/mL (approximate OD600: 0.6) at 20°C. Several co-cultures and mixed culture consortia were seeded NB supplemented with different inducers (e.g., crude oil, motor oil and 4 PAHs) for assessing the degradation potential of the synthetic consortia.

As part of the investigation to determine whether synergistic activity exists between the strains, 3 PAHs and dilbit were used as the carbon source in the culture medium. The suspension of mixed bacteria was added to a culture medium containing varying concentration of 3 PAHs (25-75 mg/L) or dilbit (150-500 mg/L) inoculated in 200 mL NB. Afterwards, next-generation sequencing was carried out to determine the proportion of the bacteria in multi-culture samples as described in our previous work (Section A.1.3). (Miri et al., 2022)

Pyrene solubilizing capacity in the aqueous phase

The solubilization was performed in 20 mM Tris-HCl (pH 7.0). Stock solutions of pyrene prepared in hexane were poured into glass test tubes (10 x 170 mm) to yield 60 mg of pyrene. To remove solvents, the tubes were left open in an operational fume hood for 30 minutes, and 3 ml of assay buffer and cell extracts were autoclaved at 121°C for 30 minutes. (Barkay et al., 1999) The experiments were conducted in triplicate. The tubes were closed with plastic and incubated overnight at 30°C with shaking (150 rpm). Glass microfiber filters Grade GF/C with a pore size of 1.2 mm were used for filtering samples, and 2 mL of the filtrate was transferred to a tube containing 2 mL of hexane. There was a centrifugation step needed (12,000 x g for ten minutes) in order to separate the phases of an aqueous and hexane emulsion that had formed in tubes.

Spectrophotometric measurements of PAH concentrations in hexane extracts were performed using calibration curves for PAH concentrations in hexane. As described above, extraction buffers containing cocktail at various concentrations, but no PAHs were extracted with hexane served as blanks.

Screening for biosurfactant-producing bacteria

All the bacterial isolates were prepared in nutrient broth (NB) as seed inoculum with the same optical density (OD_{600} = 1.0). The production of biosurfactants by the bacteria isolates was assessed through drop collapse tests and reduction in the surface tension of the culture medium provided in the supplementary information (Section A.1.4). The surface tension reduction by cell extracts by 12.5, 16 and 24.5 $mN.m^{-1}$ compared with distilled water for URS-6 ,10 and *Alcanivoracs* confirmed the ability of isolated to produce biosurfactants.

Identification and analysis of metabolites

The culture was constructed in accordance with Section 2.5 to examine the pathway followed by pyrene. Upon completion of the culture, 50 mL of ethyl acetate was added to the culture twice and vigorously mixed for the separation of phases. A rotary evaporator was used to dry the organic phase (R-100, BUCHI, Flawil, Switzerland). For GC-MS analysis, dried extracts were dissolved in 1 mL of methanol (HPLC grade). The metabolites were identified by Agilent model 6890-GC, 5973-MSD. With an ionization energy of 70 eV, the GC-MS was operated in positive mode. In the range of 35 to 1000 m/z, mass units were monitored. Injection volume was 0.7 µL. (Ausuri et al., 2021)

Enzyme identification, enzyme activity assay and kinetic analysis of enzymes

After incubation for enzyme production (Section A.1.5), naphthalene dioxygenase (ND), pyrene dioxygenase (PD), catechol 2,3- dioxygenase (CD), 1-hydroxy-2-naphthoate (HY), Protocatechuic acid (P3,4D) 3,4-dioxygenase activity was monitored by spectrophotometric assay as described in supplementary information (Section A.1.6). The proteins remained in the samples were identified by carrying out LC-MS/MS to confirm the presence of target enzyme in enzyme mixture obtained from multi-culture (Section A.1.7).

Principal component analysis (PCA)

A PCA was conducted separately for each of the inducers used under different incubation conditions using ORIGIN software (version 8.5; originLab) in order to assess similarities and relationships between variables such as enzyme activities and consortia (Kumar et al., 2020a). As

a threshold for component extraction, an Eigenvalue > 1 was chosen, and biplots with ordination were generated to project the transformed observations and original variables and onto the plane covered by the first two principal components (Sadalage et al., 2020)

Degradation kinetics of pyrene in the soil columns

A biodegradation kinetics study can be used following the determination of the pyrene mass distribution in the soil using the fitting curve of $C_t = C_0 + kt$ *(zero-order kinetics relation) or* $C_t = C_0 \cdot e^{-kt}$ *(first-order kinetics relation).* C_0 and C_t are the concentrations of pyrene at the beginning and end of the experiment, respectively, and k_{obst} is the kinetic constant when expressed in reciprocal time units.(Miri et al., 2022) A soil sample was divided into three parts: the top, middle, and bottom soil layers, which were labelled as top, middle, and bottom in the treated and untreated columns, respectively. The concentration of pyrene in soil and water was determined as described in supplementary information (Section A.1.8) (Li et al., 2021a)

Formulation for more operational stability in soil

The enzyme stability in soil batch test was studied as described in supplementary information (Section A.1.9). The reactivation of enzymes with Fe_3SO_4 were also studied to determine the minimum concentration (% w/v) required for optimal activity. Incubation of enzymes (50 μg) including NDH, PDH, and C2,3D that became inactive was carried out with varying concentrations of metal ion (30-300 μM FeSo4) in 50 mM sodium phosphate buffer, pH 6.2, for 30 minutes at 20 ºC and their activity was measured with their substrates.

Laboratory Experiments Approach for in-situ application: Application of enzyme mixture in soil

For soil application, key factors pertaining to enzymatic biodegradation should be verified in batch tests and soil column study. Key factors are enzyme stability, degradation kinetics, dispersion of enzymes, and availability of contaminants. The characterization of the soil and the set-up of the column is also crucial to carry out the in-situ application of enzymatic bioremediation. In our previous work, soil and column set-up preparation and characterization were described (Miri et al., 2022). In cold climate regions, soil properties vary considerably between the different ecological zones owing to the differences in soil-forming parent materials (minerals) and to prevailing environmental conditions (temperature, moisture, and biota). An analysis of soils from cold climate regions (Quebec and Laval, Canada) was conducted using XRD crystallography and sorption studies. (Miri et al., 2022) (Olu-Owolabi et al., 2014) According to ASTM D422-63

(ASTM, 2007), sieving analysis was performed. Supplementary Material (Section A.1.10) summarizes the grain size distribution and characteristics of the soil. There were approximately 55% of particles in the soil sample with a size range of 1-5 mm, 38% with a size range of 250 µm-500 µm, and 3% with a size range of 0.3 mm or smaller (less than 250 µm in size). In a soil/water suspension of 1:2.5, the pH was measured with a potentiometer. An externally heated acidic medium was used to oxidize organic material with potassium dichromate, which was then titrated with ferrous ammonium sulfate to determine the amount of organic carbon present.

Mass distribution of pyrene in soil: One of the factors that influence the biodegradation of pyrene is its concentration available for biodegradation. Therefore, a study of the distribution of pyrene in the solid, liquid, and gas phases was conducted in order to determine the possibility of biodegrading the pollutant and the effect of enzymatic bioremediation on the fate of this PAH as described in our previous work (Section A.1.11) (Miri et al., 2022).

Batch biodegradation tests in soil columns: The packed soil columns (pyrene/Dilbit contaminated soil) include eight treatments are shown in Table *A.1.*6. On day 20, the columns were passed with water (untreated soil column), cell extract obtained from *Alcanivorax* or cell extracts obtained from the most promising consortium. The effluent sample was collected, and pyrene concentration was measured as described in the supplementary information (*S*ection A.1.7). The pyrene removal was reported as percent (%) removal discriminated into two different sections viz. removal due to 1.) solubilization and water washing (physical removal); 2.) biodegradation (removal difference between free phase and physical adsorption) (Kumar et al., 2019). Total pyrene in liquid phase was measured directly by GCMS considered as solubilize + mobilize as free phase. The adsorbed pyrene was also the residual pyrene extracted from soil samples measured by GCMS. Solubility was determined for samples with/without enzyme, and free phase was calculated based on mass balance.

Statistical Analyses

It is used in this study to summarize the data as mean ± standard deviation (SD). The test groups were analyzed using one-way ANOVA followed by a Tukey's posthoc procedure to determine if there were any significant differences between the two groups at a significance level of $p < 0.05$.

4.1.3 Results and discussion

Identification of isolates for pyrene degradation

Figure 4.1.1 shows the percent depletion of PAHs in the silicone O-ring after 37 and 47 days of the biodegradation experiments. As can be seen in Fig 4.1.1, under a mixture substrate system, URS-5, URS-6, URS-8, and URS-10 could degrade 27, 39, 17 and 41 % of pyrene after 47 days. *Alcanivorax borkumensis* almost failed to degrade pyrene. Measurement of the PAH degradation rates showed that *Pseudomonas* URS-5, URS-6 and URS-8 showed less than 25 percent removal of pyrene in a mixture substrate system within 37 days at 15 °C. The initial concentrations were 18.31, 2.98, 1.01, and 0.095 mg/L of naphthalene, anthracene, phenanthrene, and pyrene in the medium, respectively. A comparison of the degradation of pyrene by strains under a single substrate system and a mixture substrate system was conducted in order to determine if the presence of another substrate would affect (either suppressing or enhancing) the degradation of the primary substrate (Fig 4.1.1 (a) and (b)). in Fig. (b), plots the normalized concentration of pyrene in the presence of pre-selected strains and synthetic multi-culture under single substrate system.

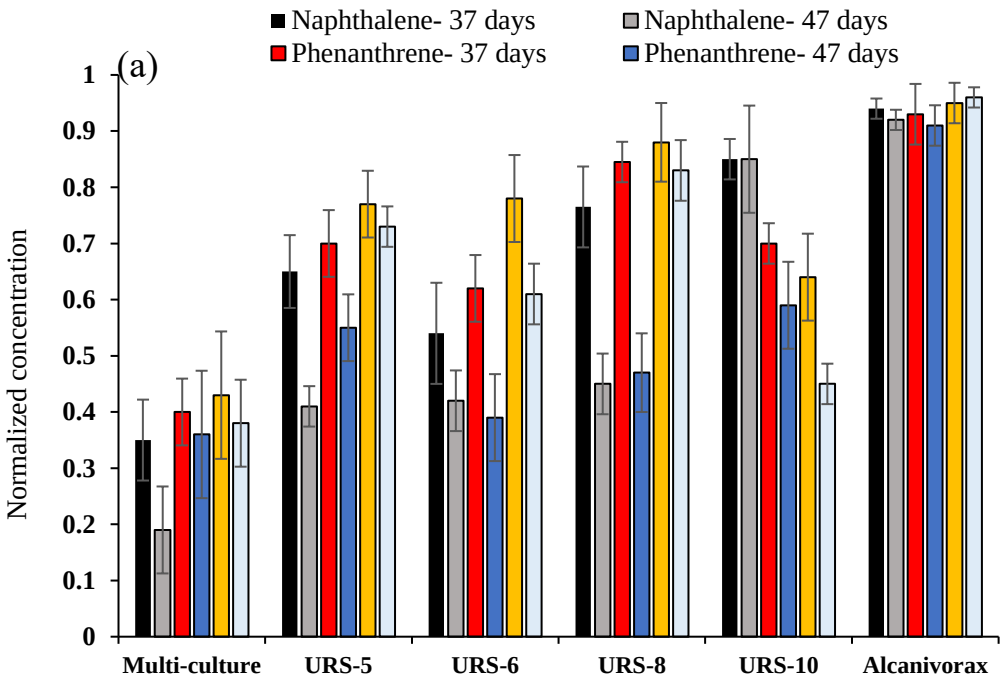
(a)
Naphthalene- 37 days
Naphthalene- 47 days
Phenanthrene- 37 days
Phenanthrene- 47 days
Normalized concentration
0
0.1
0.2
0.3
0.4
0.5
0.6
0.7
0.8
0.9
1
Multi-culture
URS-5
URS-6
URS-8
URS-10
Alcanivorax

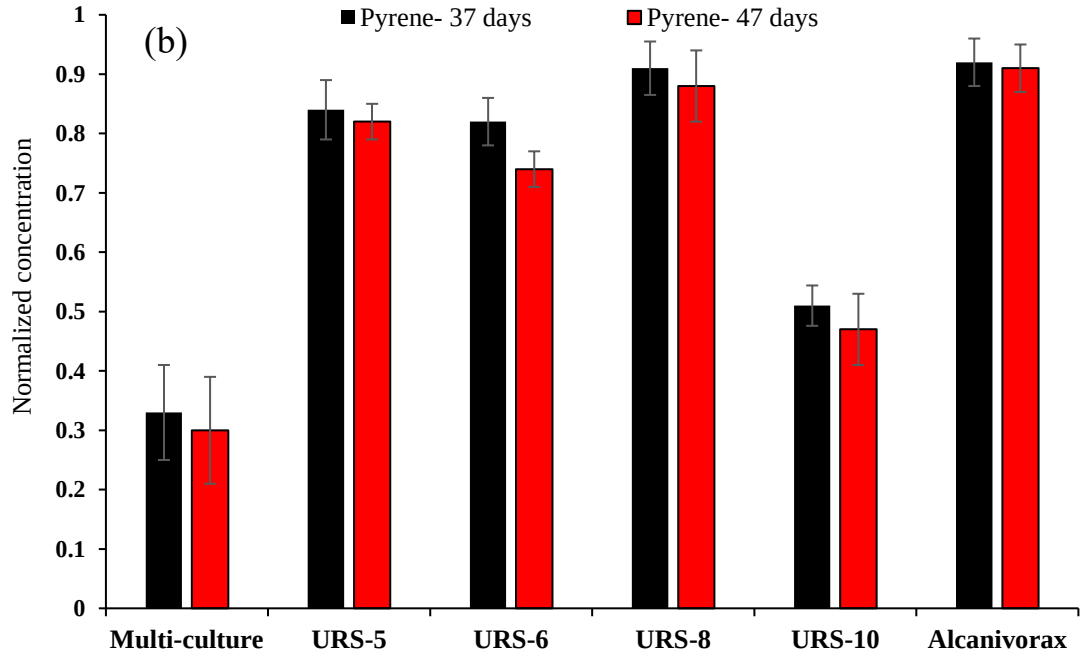
(b)
Pyrene- 37 days
Pyrene- 47 days
Normalized concentration
0
0.1
0.2
0.3
0.4
0.5
0.6
0.7
0.8
0.9
1
Multi-culture
URS-5
URS-6
URS-8
URS-10
Alcanivorax

Fig. 4.1.1. Normalized concentration of PAHs (initial concentration for each PAHs was assigned a value of 1 after 37 and 47 days of incubation on a rotary shaker at 15 °C. (a) mixture substrate and (b) pyrene

Pseudomonas URS-5, and URS-6 could grow in the range of temperature between 4 ± 1 °C and 25 ± 1 °C, but not as effective at 37 ± 1 °C as previously reported for *P. synxantha* and *P. mandelic* strains. (Miri et al., 2021a) The presence of these characteristics indicated that the strains do not pose any potential pathogenic risk to humans or animals. The partial 16S rRNA sequencing showed that URS-6 was close to the type of strain of *Pseudomonas putida* strain NR 043434.1^{T} with 99% identity. The sequence identity of URS-5 and URS-8 were 99% with a type of strain of *Pseudomonas mandelic* strain CIP 105273^{T} and *Pseudomonas syringae* ATCC 19310^{T} respectively. In the sequence analysis of URS-5, the sequence identity was 98% with a type strain of *Rhodococcus erythropolis* JCM 3201T.

The sequences for URS-5, URS-6, URS-8, and URS-10 have been deposited in the NCBI Genbank database and were assigned the accession of MZ144068.1, MZ144069.1, MZ144070.1 and MZ959374, respectively. Phylogenetic analysis also grouped URS-5, URS-6, URS-8 and URS-10 with the strain of *Pseudomonas putida, Pseudomonas mandelic* (*P. mandelii*), *Pseudomonas syringae*, an *Rhodococcus erythropolis* with 98% bootstrap support (not shown). *Pseudomonas spp.* and *Rhodococcus spp.* degraded various xenobiotics and were often isolated from hydrocarbon-contaminated sites. (Van Hamme and Ward, 2001) Wald *et.al* 2015 indicated that the *Pseudomonas syringae* group (namely *Pseudomonas cichorii* LMG 2162T) was one of the most dominant *Pseudomonads* in the sequestration and of carbon from naphthalene in the samples and potential degradation of other PAHs upon aeration of the sediment at 20 (7%) and 10°C. (Wald et al., 2015) Margesin et al., (2008) isolated cold-tolerant strains from contaminated soil that could degrade BTEX at 10 °C. (Margesin et al., 2008)

Determination of pyrene degradation rate by individual strain and multi-culture strains

Regarding the URS-5, a general sequential pattern of degradation was observed in which naphthalene was transformed first, followed by phenanthrene, and pyrene (Figure 4.1.1(a)). As a

result of this pattern of degradation, this is also in agreement with previous studies that have shown that degradation rates generally decrease with increasing molecular weight. Aqueous solubility is thought to be responsible for this phenomenon.(Bacosa and Inoue, 2015) Our results showed that partially purified dioxygenase converted three PAHs (section 3.). This was also previously observed for other dioxygenases from *Pseudomonas* sp. strain NCIB 9816-4 and *Sphingomonas* CHY-1strain that the enzymes in the upper part of the naphthalene pathway possess broad substrate specificities. (Jouanneau et al., 2006; Parales et al., 1998) The lack of accumulated intermediate for the degradation of PAHs in samples can be attributed to the fact that the rate-limiting step for the biodegradation might be the initial ring oxidation reaction. The other reason for simple degradation pathway might be the enzyme activities observed for the oxidation of Nicotinamide adenine dinucleotide (NADH) in the presence of salicylate and 1-hydroxy-2-naphthoate hydroxylase in the cultures grown on three PAHs .

For URS-8, the same pattern of degradation for pyrene was observed. This strain did not show extensive degradation of pyrene in the PAHs mixture; however, the lack of accumulated intermediate can be considered positive effect that might be attributed to the enzyme system present in the liquid medium. The lack of 1-hydroxy-2- naphthoate hydroxylase activity in cell-free lysate suggested a pathway for three PAHs that does not pass through salicylate. However, protocatechuic acid 3,4-dioxygenase enzyme assay suggested the pathway for the catabolism of phthalate to central metabolites via intradiol cleavage of protocatechuic acid (Krishnan et al., 2004; Mawad et al., 2020).

Compared to URS-5 and URS-8 strains, URS-6 showed a higher degradation rate that might be attributed to increasing the bioavailability of pyrene as well as the high activity of the naphthalene dioxygenase enzyme. This isolate was considered an efficient biosurfactant producer based on surface tension measurement. The surface tension reduction by cell extracts by 12.5 $mN.m^{-1}$ compared with distilled water for URS-6 confirmed the ability of isolated to produce biosurfactants.

For URS-10, different patterns of degradation were observed in which this strain degraded small amount of pyrene in the PAHs mixture, and degraded considerably more pyrene when it was present as the sole substrate. These results suggested the presence of pyrene degrading enzymes repressed in culture grow in the mixture of PAHs. The enzyme activity and catalytic efficiency of pyrene dioxygenase were calculated using the partially purified dioxygenase (Section A.1.10).

Naphthalene did not appear to be transformed by this dioxygenase and no particular reaction was observed when indole was added to the reaction. There is a possibility that a negative result for a given PAH can be attributed to undetermined factors other than substrate specificity (e.g., poor expression, and enzyme instability) (Singleton et al., 2012).

As shown in Figure 4.1.1, the degradation effect of mixed bacteria composed of pre-selected isolated bacteria and *Alcanivorax* borkumensis was better than pure cultures in the precence of 4 PAHs solution. Adding biosurfactant-producing bacteria i.e., *Alcanivorax* borkumensis and URS-6 increased the bioavailability of the pyrene and phenanthrene (Section.). In a more complicated system, the presence of other PAHs had no effect on the degradation of pyrene that might be attributed to the comprehensive PAH-degradation capability of URS-10.

Effect of culture conditions on enzyme activity

Produced biomass in NB was around 5-fold higher than minimum saltwater media (MSM), and enzymes were produced 10-fold higher in NB compared to MSM (not shown here). The extract cells from the cultured bacteria in the presence of 100, 250 and 500 mg L^{-1} of Dilbit (containing 7,15 and 20 mg/L pyrene, respectively) and 25, 50 and 75 mg L^{-1} solution of 3PAHs (naphthalene, phenanthrene, pyrene) showed a significant difference in activity of enzyme in order of 250> 100>500 mg/L ($p < 0.05$) for Dilbit and 50> 25>75 mg/L ($p < 0.05$). Thus, 50 and 250 mg l^{-1} of 3PAHs and Dilbit as the optimal concentration for enzyme production. (Miri et al., 2022) It is noticeable that our Dilbit contained less than 1 mg/L pyrene, this spiked pyrene is needed for effective induction of targeted enzymes. The activity of target enzymes was measured for different consortia incubated on mixture of 3PAHs and Dilbit to determine the optimum time for incubation and production of enzymes (Section A.1.11).

PCA of enzyme activities

As PCA facilitates the easy representation of multi-dimensional data sets by scaling them and aids in identifying any significant trends or patterns, it was applied to analyze the correlations and similarities among the tested synthetic consortiums about enzyme activities produced on the tested substrates. Figure 4.1.2 shows individual PCA biplots with the ordination of enzyme activities produced on PAHs mixture, Dilbit, and motor oil at 15 ˚C. The PCA biplot graph for the observation variables in the form of tested consortia and enzyme activity as the variables showed that there is strong correlation among the enzyme activity variables as they are on the right side of the biplot graph.

For 3 PAHs mixture, PC1 and PC2 accounted for 63 % and 25% of the total variation in data, respectively, for a total of 89% (Figure 4.1.2 (a)). Upper pathways enzymes are closely aligned with PC2 while other enzymes are closely aligned with PC1. This indicated a strong correlation (> 0.5) among the upper and lower pathway enzymes. The consortia Mix1-3PAHs, and Mix7-3PAHs were the most naphthalene dioxygenase, and catechol dioxygenase whereas, consortia Mix4-3PAHs was found pyrene dioxygenase and 1-hydroxy-2-naphthoate hydroxylase active. Mix5 and 8-3PAHs showed more correlation towards the lower pathways. Mix7-3PAHS is closely spaced between upper and lower pathways indicating a positive correlation with them and hence signifies better consortia resulting in a high activity of corresponding enzymes. The combined load score on (PC1+PC2) for Mix7-3PAHs was found to be 5.1. This further stated that these tested synthetic consortia worked better for enzyme production.

In the case of Dilbit, PCA biplot accounted for 66 % and 25% for PC1 and PC2, respectively, for a total of 91 % variation in data. Akin to the 3PAHs mixture case, upper pathway enzymes clustered together around PC2 (though less as compared to the 3 PAHs biplot) while lower pathway enzymes clustered around PC1. The poor performance of Mix1-D and Mix3-D was evident from the PCA biplot which shows their position in the far end 2^{nd} and 4^{th} quadrant, respectively and no proximity with eigenvectors of enzyme activity. Unlike the PCA biplot for 3 PAHs that the PD eigenvector showed a negative correlation with P3,4D and C2,3D, strong correlation among the targeted enzyme was observed in this biplot. This further illustrate all consortia with *Alcanovorax* were found near the studied enzyme vectors and they can be suitable for an effective production of these enzymes using Dilbit as an inducer in NB media.

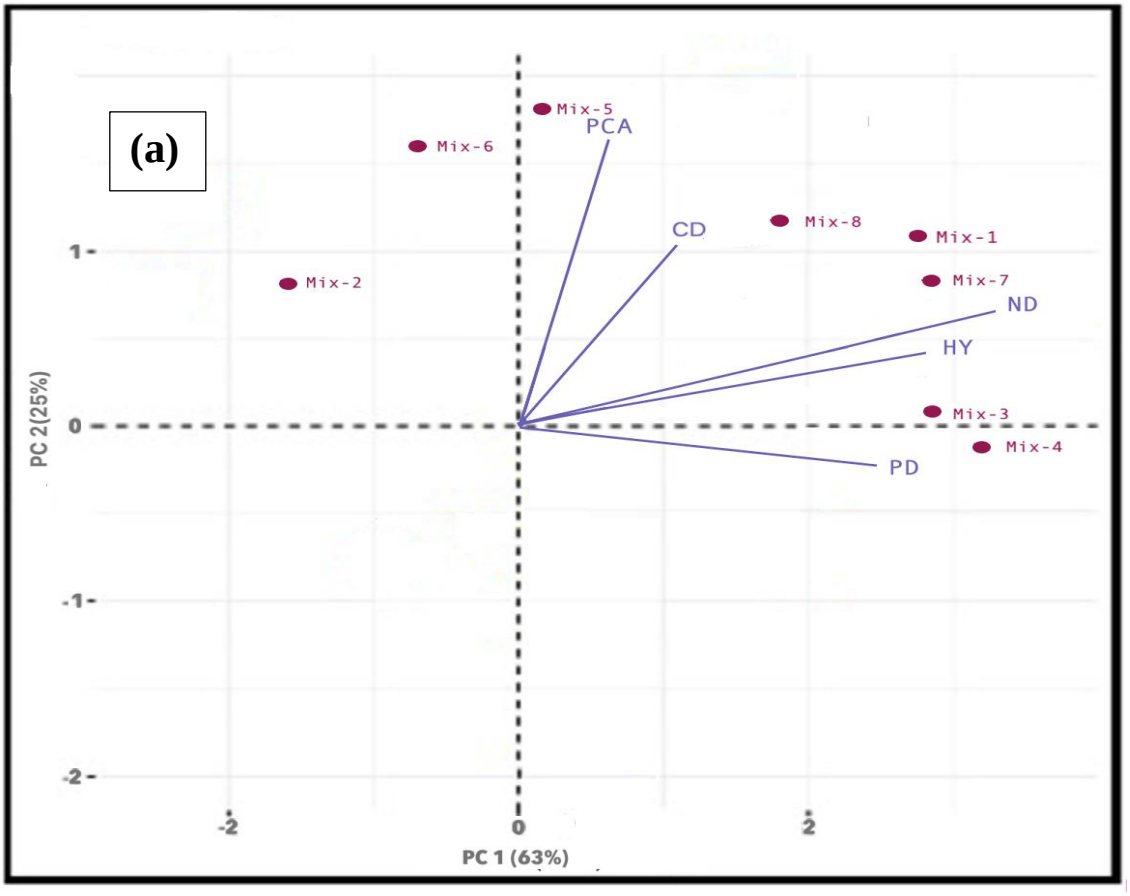
(a)
Mix-5
PCA
Mix-6
CD
Mix-8
Mix-1
Mix-2
Mix-7
ND
HY
Mix-3
Mix-4
PD
1
0
-1
-2
-2
0
2
PC 2 (25%)
PC 1 (63%)

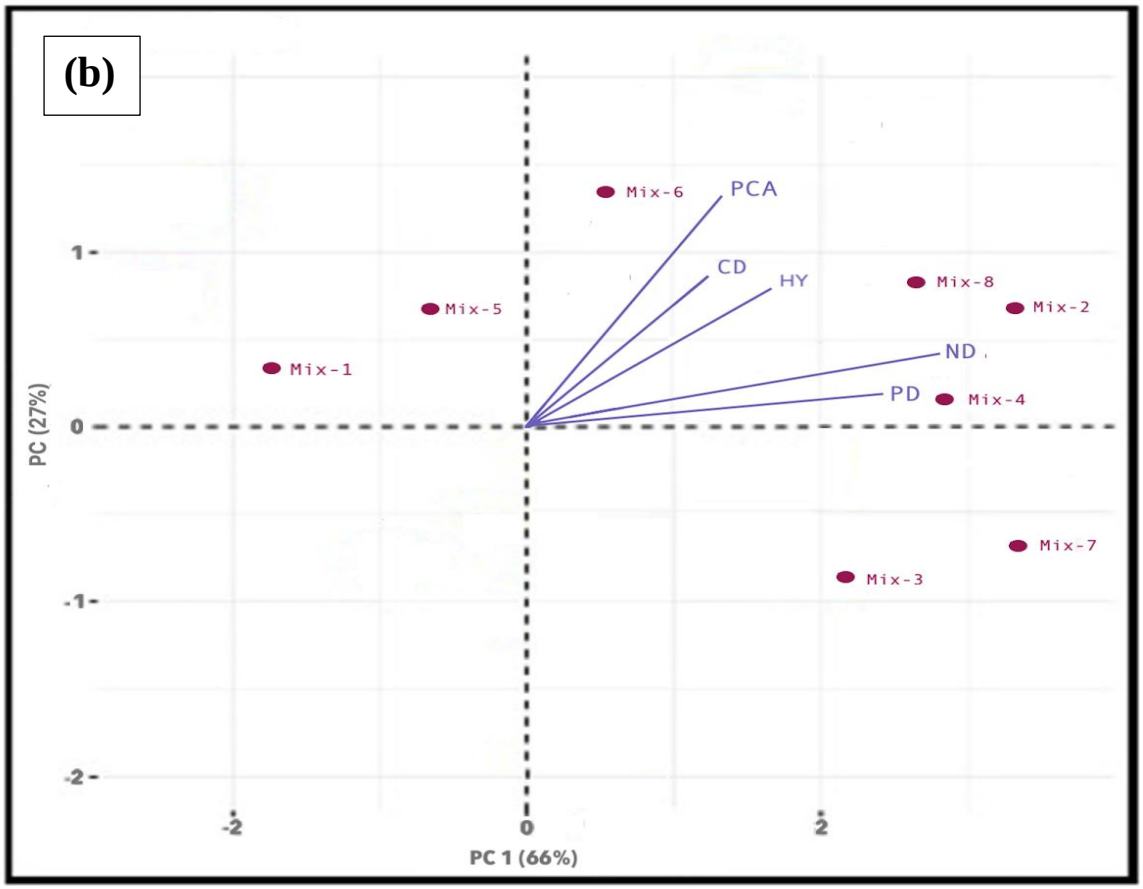

Fig. 4.1.2. Principle Component Analysis biplots of pyrene degrading enzyme activities produced by different consortia cultivated in NB supplemented with: (a) 3 PAHs mixture and (b) Dilbit

Microbial community analysis

To understand how different types of inducers affect the activities of target enzymes in tested consortia, it is necessary to analyze the composition of the microbial community by using the next-generation sequencing of 16s rRNA after 8, 12, 16 hours of enzyme production for the most promising consortium. Figure 4.1.3 illustrates the composition of microbial communities in optimum tested consortia including Mix1-3PAHs, Mix7-3PAHs, and Mix8-D. The results showed high relative abundance of genera URS-5 (31.4% % after 8 hours of incubation), URS-6 (44% after 8 hours of incubation)) and URS-8 (44.6% after 16 hours of incubation) in Mix1-3PAHs. The high activity of naphthalene dioxygenase, catechol dioxygenase, and 1-hydroxy-2-naphthoate hydroxylase can also be attributed to the high relative abundance of these bacteria. After 8 hours of incubation with Mix7- 3 PAHs, URS-10 (18%) was relatively inactive in terms of pyrene dioxygenase activity. A high relative abundance of genera URS-10 (25.1%) after 8 hours of incubation in Mix8-D compared to relative abundance of genera URS-10 (7 %) in Mix7-3PAHs showed that synergistic activity exists between URS-10 and *Alcanovorax* that resulted in superior ability to utilize a higher concentration of pyrene. The high concentration of pyrene dioxygenase in Mix8-D can be attributed to this synergistic effect.

(a)

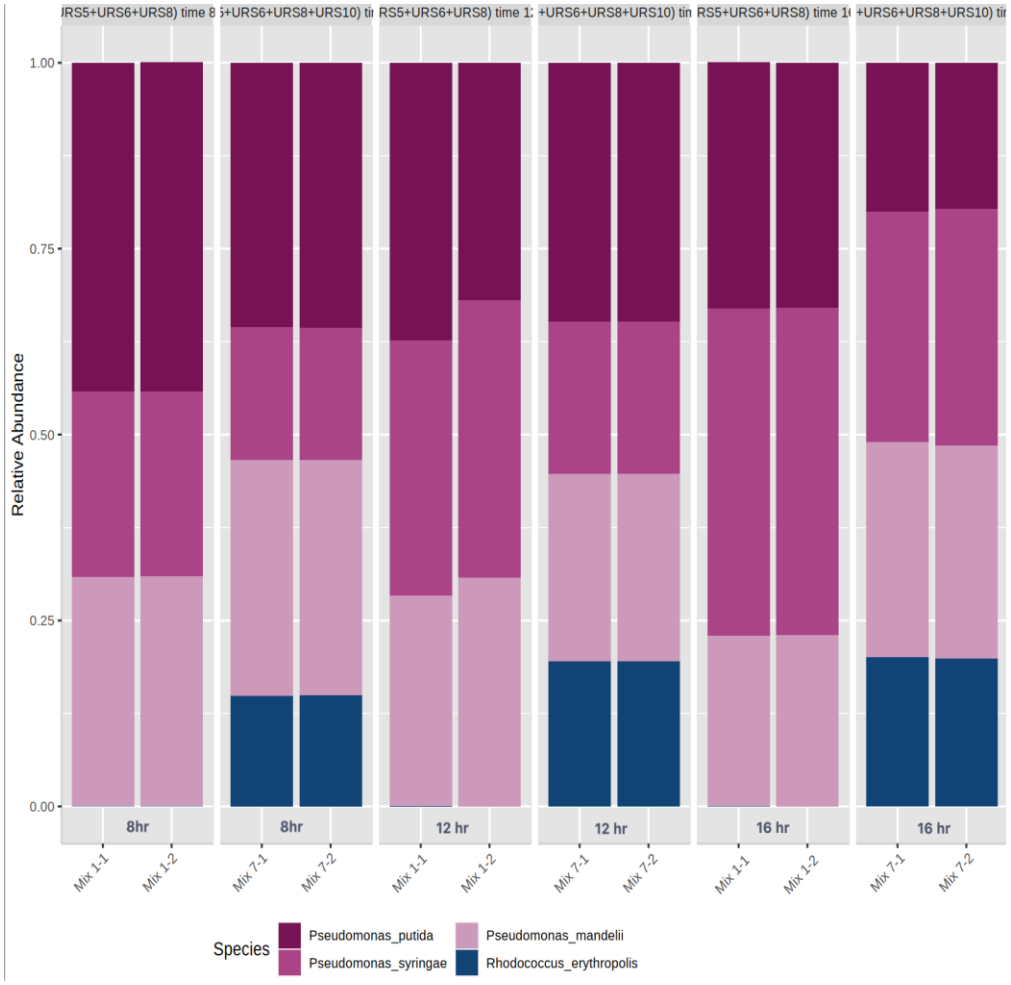
Relative Abundance
1.00
0.75
0.50
0.25
0.00
8hr
8hr
12 hr
12 hr
16 hr
16 hr
Mix 1-1
Mix 1-2
Mix 7-1
Mix 7-2
Species
Pseudomonas_putida
Pseudomonas_syringae
Pseudomonas_mandelii
Rhodococcus_erythropolis

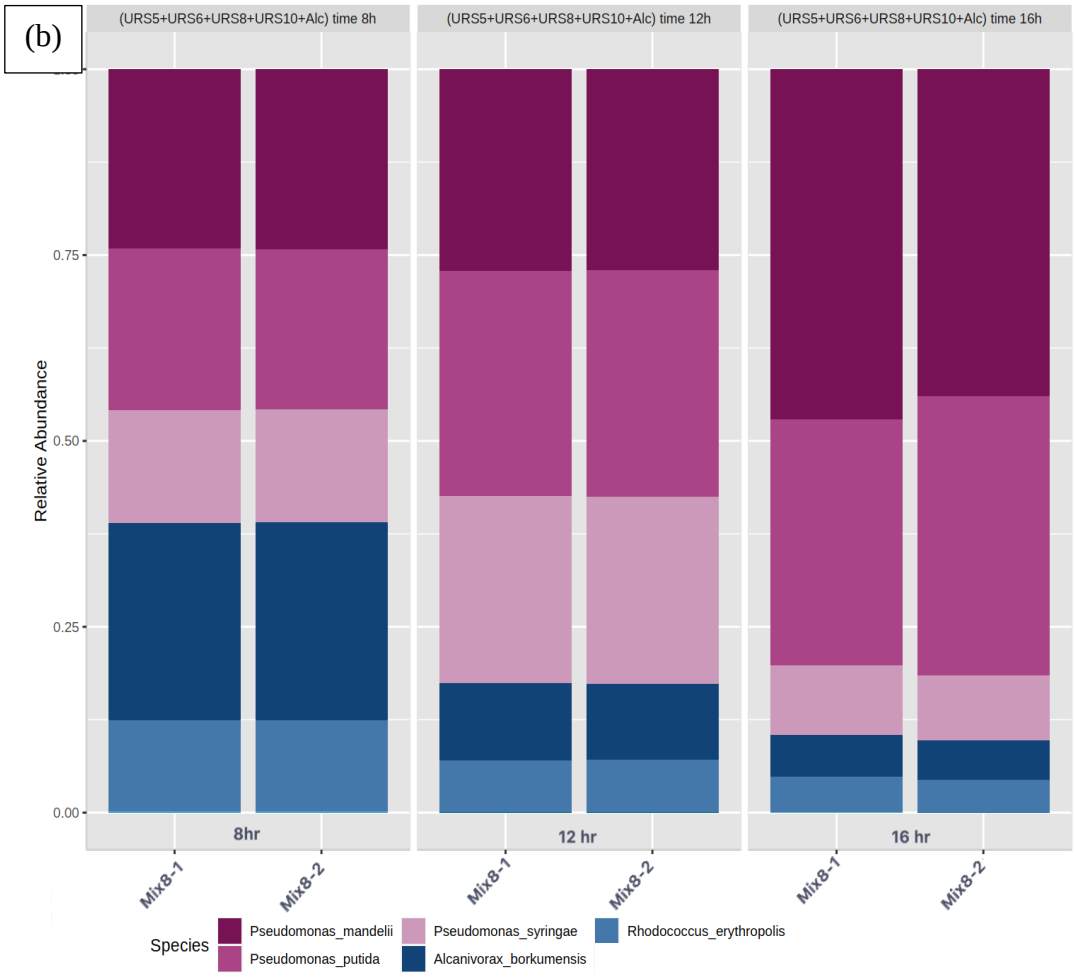

Fig. 4.1.3. Genus-level comparison of the microbial community (a) direct quantitative comparison of abundance in Mix1-3PAH and Mix7-3PAH, (b) Mix8-D

Identification of enzymes by LC-MS/MS

To confirm the presence of target enzymes in the crude cocktail obtained from consortia Mix8-D, the liquid chromatography-Tandem mass spectrometry (LC-MS/MS) was carried out. This method could provide substantially more information in the identification of enzymes in a mixture compared to conventional biochemical assays. (Jardine et al., 2018)

Based on other literature, the proteomic analysis indicates that 18 enzymes in the pathway are upregulated more than twofold, as indicated by the peptide sequences counting after the organism has been incubated with pyrene.(Peng et al., 2008) Established from proteomic data, 27 enzymes were identified that were necessary for the complete breakdown of pyrene. The identified proteins in our cocktail of enzymes with more than 1% false discovery rate (FDR) are listed in Table 4.1.1. Following PAH-degrading enzymes were identified: pyrene dioxygenase, naphthalene dioxygenase, naphthalene 1,2-dioxygenase, catechol-2,3-dioxygenase, 1-hydroxy-2-naphthoate hydroxylase, salicylaldehyde dehydrogenase, salicylate hydroxylase and PCA dioxygenase. The sequence of the crude cocktail showed the presence of other proteins (such as membrane proteins, stress-response proteins, ATP-binding proteins, etc.), however they did not show strict identity to the sequences of any proteins of PAH-degrading function in the mixture.

Several proteins that are associated with oxidative stress, which prevent unfolding of proteins were detected. High levels of reactive oxygen or chlorine species (ROS/RCS) leads to the protein unfolding and aggregation in the cytosol. To cope with this stress, bacterial cells employ ATP-independent chaperones such as the DnaK system and the GroEL system, which bind unfolded or aggregated proteins and maintain their solubility. (Voth and Jakob, 2017) It is clearly reported that the oxidation of PAH trans-dihydrodiols to catechol's generates reactive ROS. (Penning et al., 1999) Presence of chaperones in the crude cocktail obtained from multi-culture of PAH-degrading bacteria indicated that growth on these compounds induces a stress response. Similarly, Tomás-Gallardo et al., (2006) reported that Rhodococcus sp. strain TFB produced 60-kDa Chaperonins in the presence of phthalate. They identified phthalate-induced proteins using matrix-assisted laser desorption/ionization mass spectrometry (MALDI-MS/MS). (Tomás-Gallardo et al., 2006)

Table 4.1.1. Identification of partially purified enzymes by LC-MS/MS analysis and assignment to the corresponding UniProtKB entry

Protein/Enzyme	Molecular function	Gene	Mass[1] (kDa)	Mass[2] (kDa)	UniProt ID	Coverage (%)
Naphthalene dioxygenase	Component of the naphthalene dioxygenase	*doxB*	49.6	49.1	P0A111	85
Naphthalene 1,2-dioxygenase	Ferredoxin component of the naphthalene dioxygenase	*doxA*	11.4	11.8	P0A170	81
Dihydrodiol dehydrogenase	The oxidation of naphthalene dihydrodiol	*nahB*	27.5	27.4	P0A169	79
Catechol-2,3-dioxygenase	The meta cleavage of catechol to 2-hydroxymuconic semialdehyde	*catE*	31.5	31.2	P54721	61
salicylate hydroxylase	The decarboxylative hydroxylation of salicylate into catechol	nahG	101.3	102.1	6BZ5	60
F-ATPase subunit beta	ATP synthesis	*atpD*	51.9	51	C1A1X8	57
Salicylaldehyde dehydrogenase	Involves in pathway naphthalene degradation	*doxF*	51.9	52	P0A390	58
Pyrene dioxygenase	Catalyzes the first step in the oxidative degradation of aromatic hydrocarbons	phnA1a	215.7	125.4	2CKF	58
Alkyl hydroperoxide reductase	Protects the cell against DNA damage	*ahpF*	55.3	55.8	P0A155	56

Chaperone ClpB	Protein refolding & Stress response	*clpB*	92.3	93	I3UXE4	51
Bacterioferritin	Iron storage	*bfr*	18	18.4	A0A4V3X737	50
F-ATPase subunit alpha	ATP synthesis coupled proton transport	*atpA*	58.4	57.7	C1AW01	20
Citrate synthase	Involves in the pathway tricarboxylic acid cycle	*gltA*	39.69	39.2	F8QR44	20
50S ribosomal protein L3	Ribonucleoprotein	*bipA*	67	66.9	A0A1G5MQC5	5
ATPase subunit beta	Proton-transporting ATPase activity,	*atpD*	49.5	50	A0A024ED61	5
Glutamine synthetase	Glutamate-ammonia ligase activity	*glnA*	51.6	51.6	A0A5D3GGF0	5
Elongation factor Tu	Promotes the GTP-dependent binding of aminoacyl-tRNA	*tuf*	43.57	43.2	A0A1H2I8D2	5
Alkyl hydroperoxide reductase C	Plays a role in cell protection against oxidative stress by detoxifying peroxides	*OU5_0185*	20.4	20.8	A0A024E2Y4	5
Alkyl hydroperoxide	response to reactive oxygen species	*ahpF*	55.8	54.9	K9NK88	4

reductase subunit F						
60 kDa chaperonin	Prevents misfolding and promotes the re-folding and proper assembly of unfolded polypeptides produced under stress conditions	*groL*	56.6	56	B0KFQ2	3
Chaperone protein DnaK	Acts as a chaperone.	*dnaK*	65.73	65.7	A0A161TLX0	3
DNA-directed RNA polymerase subunit beta	Catalyzes the transcription of DNA into RNA	*rpoC*	154.9	154.5	A0A4S4IZF1	2
Polyribonucleotide nucleotidyltransferase	Involves in mRNA degradation	*pnp*	74.9	75.3	A0A0K8M9A6	2
Protein translocase subunit SecA	Has a central role in coupling the hydrolysis of ATP to the transfer of proteins into and across the cell membrane	*secA*	102.9	102.9	B0KFR8	1
Aconitate hydratase	Involves in tricarboxylic acid cycle	*acnA*	100.4	100.1	A0A1X0UMG3	1

[1]Molecular mass was calculated from the respective UniprotKB entry (Theoretical Mass).

[2] Molecular mass was obtained from LC-MS/MS (Experimental Mass)

Analysis of metabolites

In addition to the study of enzymes involved in pyrene biodegradation, analysis of metabolites in the multiculture bacteria would provide a better understanding of the enhanced biodegradation compared with each strain. URS-10 was cultivated in NB supplemented with 10 mg/L pyrene, and two characterized metabolites were presented including 5-hydroxy-5H-4-oxapyrene-5-carboxylic acid and phthalic acid. This study was similar to the result of *Rhodococcus* sp. UW1 strain as reported by Walter et.al.(Walter et al., 1991) The chief pathway of pyrene degradation was also reported in other literature that is started by the initial attack at the 4,5- position to produce cis- and trans- 4,5- pyrenedihydrodiol by pyrene dioxygenase. (Heitkamp et al., 1988; Krishnan et al., 2004) Peng et.al offered multiple pathways of pyrene degradation for other strains that can oxidize pyrene via initial deoxygenation at the 1,2-positions, however, in this case, the dead end product such as 4-hydroxy-perinaphthenone was not detected. (Peng et al., 2008) Thus, the principal pathway of pyrene degradation is deoxygenation at the position 4,5-positions to produce trans-4,5-pyrenedihydrodiol by dioxygenase (Figure 4.1.4). In this study, the results suggested that phthalic acid is a dead-end product of bacterial metabolism for URS-10 because the ratio of pyrene: phthalic acid was at high value. This is an important observation of the incomplete mineralization pyrene.

Regarding Mix7-3PAHs cultivated in NB, patterns of simultaneous degradation of PAH mixtures was complex. The observed pattern of utilization of PAHs might not be only the result of bioavailability but also of metabolic interactions related to competition and metabolism effects. (Bouchez et al., 1999) During the incubation, a number of acid metabolites carried out by consortium MIX7 accumulated in the medium. As a result of the utilization of growth substrates (naphthalene, phenanthrene, or pyrene), most of these metabolites were dicarboxylic aromatic acids by multibranched pathways including 1,2- dihydroxynaphthalene and phthalic acid pathways. However, no dead-end product was detected and this suggested that other species utilized the intermediate metabolites produced by one or two species.

it was hypothesized that by incorporating each of the above-mentioned isolated strains, benefits would be gained from enzymes produced by each strain and toxic intermediates produced during incomplete removal of pyrene would be eliminated. Miri et.al (2022) reported that the complete biodegradation of monoaromatic compounds such as p-xylene requires a mixture of different bacterial by two bacteria strains, *Pseudomonas synxantha* S2TR-26 and *Pseudomonas mandelii*

S2TR-08 (Miri et al., 2022). The result of this study showed that the multi-culture of strains and their enzymes could degrade pyrene to the inter final product. This study showed that a multi-culture of strains and their enzymes can degrade pyrene to final products (Figure 4.1.4).

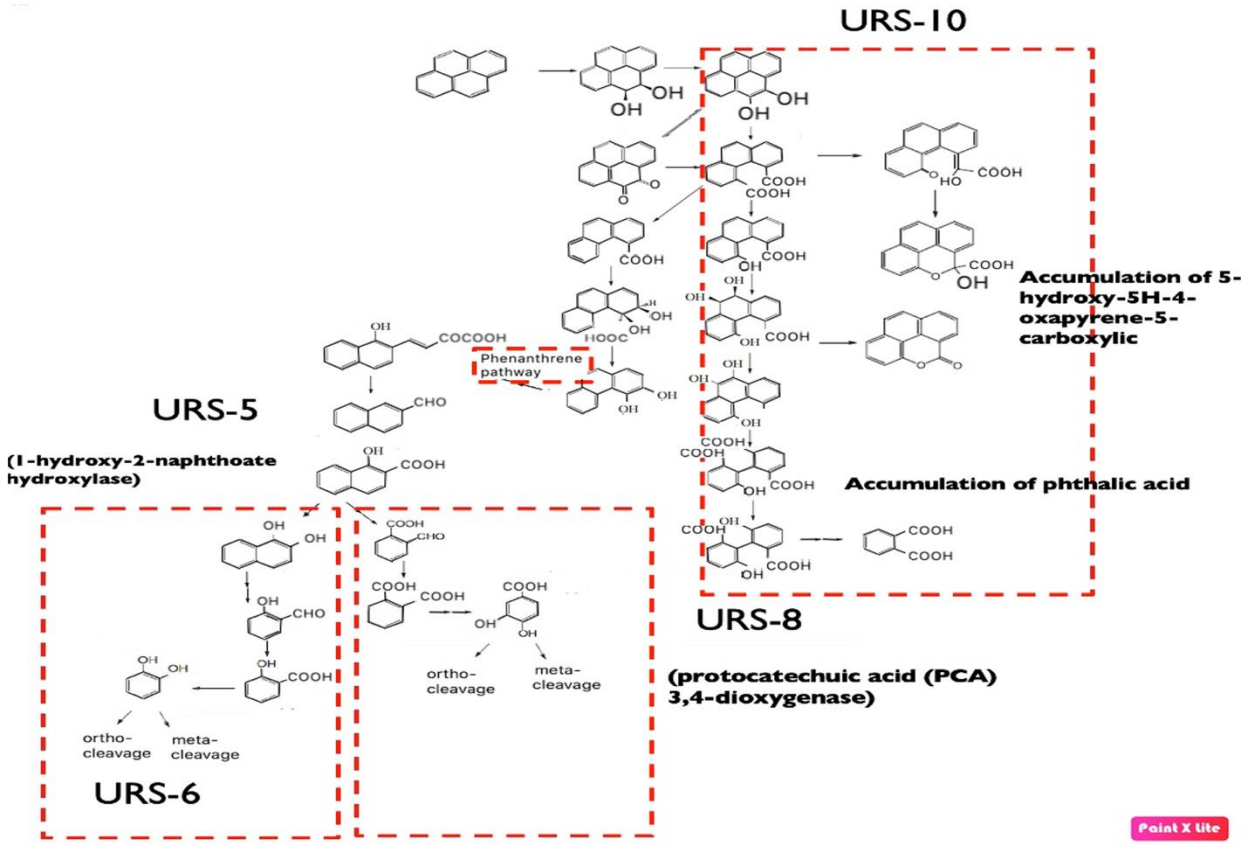

Fig. 4.1.4. Proposed catabolic pathway of pyrene for pre-selected strains

Enzyme stability in soil Formulation for more operational stability

The batch stability experiments for key enzymes involved in biodegradation of 3 PAHs including NDH, PDH, and C2,3D was conducted to determine the operational stability of enzymes in soil contexts, the necessary time to re-inject a fresh enzyme solution into a column experiment in order to maximize degradation efficiency. Figure 4.1.5 depicts the profile of relative activity of NDH, PDH, and C2,3D compared to the highest activity on the first day.

A remarkable restoration of activity has been observed after addition of Fe_3SO_4 to the extract cell. The minimum concentration of the Fe_3SO_4 required for optimal activation was found to be 1,1.5

and 2 % (w/v) Fe_3SO_4 for NDH, PDH, and C2,3D, respectively. As can be seen in Fig, 1.5 % (w/v) $FeSO_4$ increased the activity of NDH, PDH, and C2,3D up to 145, 134 and 170% of their original activity, respectively. For evaluation of the stability of enzyme activities during the soil column test, enzyme activities were determined at 15 C for 3 weeks at one-day intervals in the presence of soil. Results indicated that NDH, PDH, and C2,3D enzymes were active for 20,17 and 22 days in presence of soil, with half-lives of 6.1, 7.4 and 7.8 days, respectively. In the presence of soil, NDH, PDH, and C2,3D lost 81, 85% and 86% of their activity respectively after 14 days. In the column test, NDH, PDH and C2,3D maintained 1%, 0% and 3% of their catalytic activity after 3 weeks, which is the necessary period to re-inject a new enzyme solution.

There has been an increase in applications of various oxidoreductases in recent years, such as tyrosinases, laccases, dioxygenases, and peroxidases, however, these molecules are characterized by low operational stability. Xu et al. (2013) reported that pure laccase from *Trametes versicolor* lost about 90% of its initial activity after 10 days at room temperature. (Xu et al., 2013) The crude catechol 2,3 dioxygenase from *Stenotrophomonas maltophilia* KB2 did not exhibit any activity after 24 hours of incubation at 4 °C. (Wojcieszyńska et al., 2012) Miri et.al (2022) studied the production of xylene monooxygenases and catechol dioxygenases for degradation and detoxification of p-xylene through oxidation, and ring cleavage. They suggested the enzyme injections after 4 weeks for the columns because both XMO and C2,3D enzymes showed the presence of activity until 26 days in presence of soil.

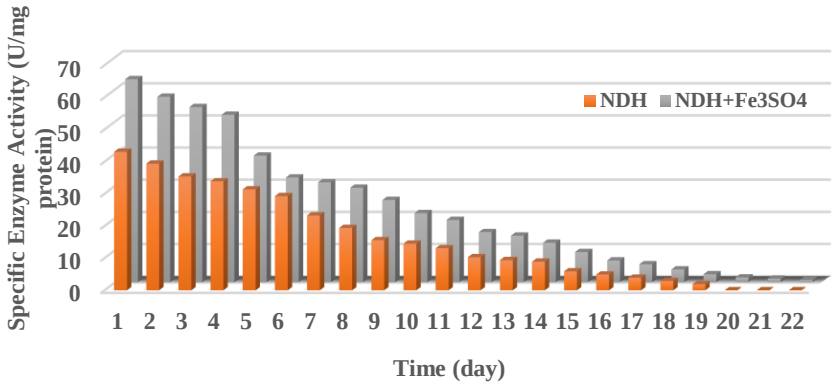
Specific Enzyme Activity (U/mg protein)
70
60
50
40
30
20
10
0
NDH
NDH+Fe3SO4
1 2 3 4 5 6 7 8 9 10 11 12 13 14 15 16 17 18 19 20 21 22
Time (day)

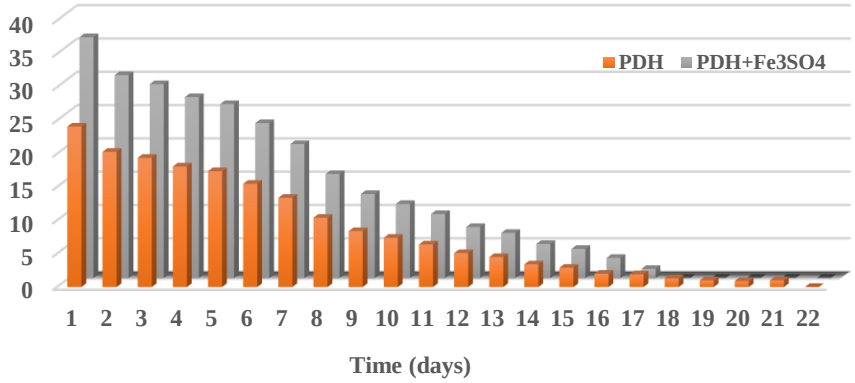
40
35
30
25
20
15
10
5
0
PDH
PDH+Fe3SO4
1 2 3 4 5 6 7 8 9 10 11 12 13 14 15 16 17 18 19 20 21 22
Time (days)

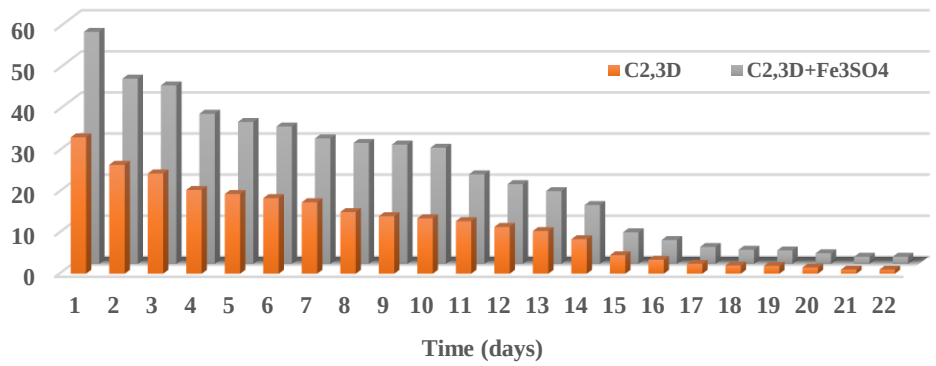

Fig. 4.1.5. Stability of Naphthalene dioxygenase (NDH), Pyrene dioxygenase (PDH) and Catechol 2,3 dioxygenase (C2,3D) enzymes in the batch test.

Soil and column characterization

Table A.4 and A.5 show the physicochemical characteristics of samples collected from cold climate zones. The pH values were mainly neutral, and soil organic matter values was high. XRD crystallography (Table A.5) determined that the major minerals in the soil are gibbsite, aragonite, calcite, dolomite, montmorillonite, and quartz. The most common mineral was Gibbsite (52%), and quartz was a close second (24%).

To determine the fate of contaminant in soil as well as the enzymatic degradation in the column, sorption of contaminant in soil was studied. In this regard, various sorption isotherm models were fitted to the equilibrium sorption data of pyrene on soils at 15 ℃ (Table A.5). The parameters of each isotherm model are presented in Table A.7. The Langmuir and Freundlich models were not found to be appropriate for explaining the sorption of pyrene on these soils. Microscopically, most natural soils are heterogeneous in composition and intrinsically heterogeneous. It is noteworthy that even though neither Langmuir nor Freundlich could adequately fit the sorption data, the low values of the Freundlich parameter of n (around 0.6) suggested that most of the isotherms involved in pyrene sorption tended to be nonlinear (Table A.7). In some cases, the n value may be viewed as an indicator of the energy distribution on the surface of the site (adsorption), (Weber Jr et al., 1992) where a small n value indicates sorption on predominantly heterogeneous surfaces.

Our findings are in consistent with other study that proposed the mechanisms governing pyrene as the sorption on these soils is sorption onto specific sorption sites, as well as partitioning into the pores of soil components, such as clay minerals, and weak hydrophobic interactions between soil sorption surfaces and pyrene molecules. (Diagboya et al., 2018; Olu-Owolabi et al., 2014) Table A.5 presents the results of the fitting of the equilibrium sorption data for pyrene at 15 ℃. Based on the correlation coefficients (r^2) of 0.979, the sorption of pyrene fitted the distributed reactivity model (DRM). In the DRM, it is assumed that the final soil isotherm consists of several linear and non-linear isotherms. As a result, these isotherms were regarded as composites of a particular sorption process's general linear and nonlinear isotherms.

The characteristics of the packed soil columns employed in treatment experiments are presented in Table A.8. It was important to mix different soil samples to obtain a uniform soil type for the experiments. The soil type was a mixture of course, medium, and fine particles (with grain sizes of 0.25-2.0 mm) corresponding to the site stratigraphy described in our previous work. (Miri et al.,

2022) In order to obtain a more accurate estimation of saturation time, the dispersion was measured by measuring the total protein concentration in the effluent samples by using Bradford's method. As shown in Figure 4.1.6, the relative concentrations of the conservative tracer (Br^-) and total protein were determined during enzyme injection of effluent samples.

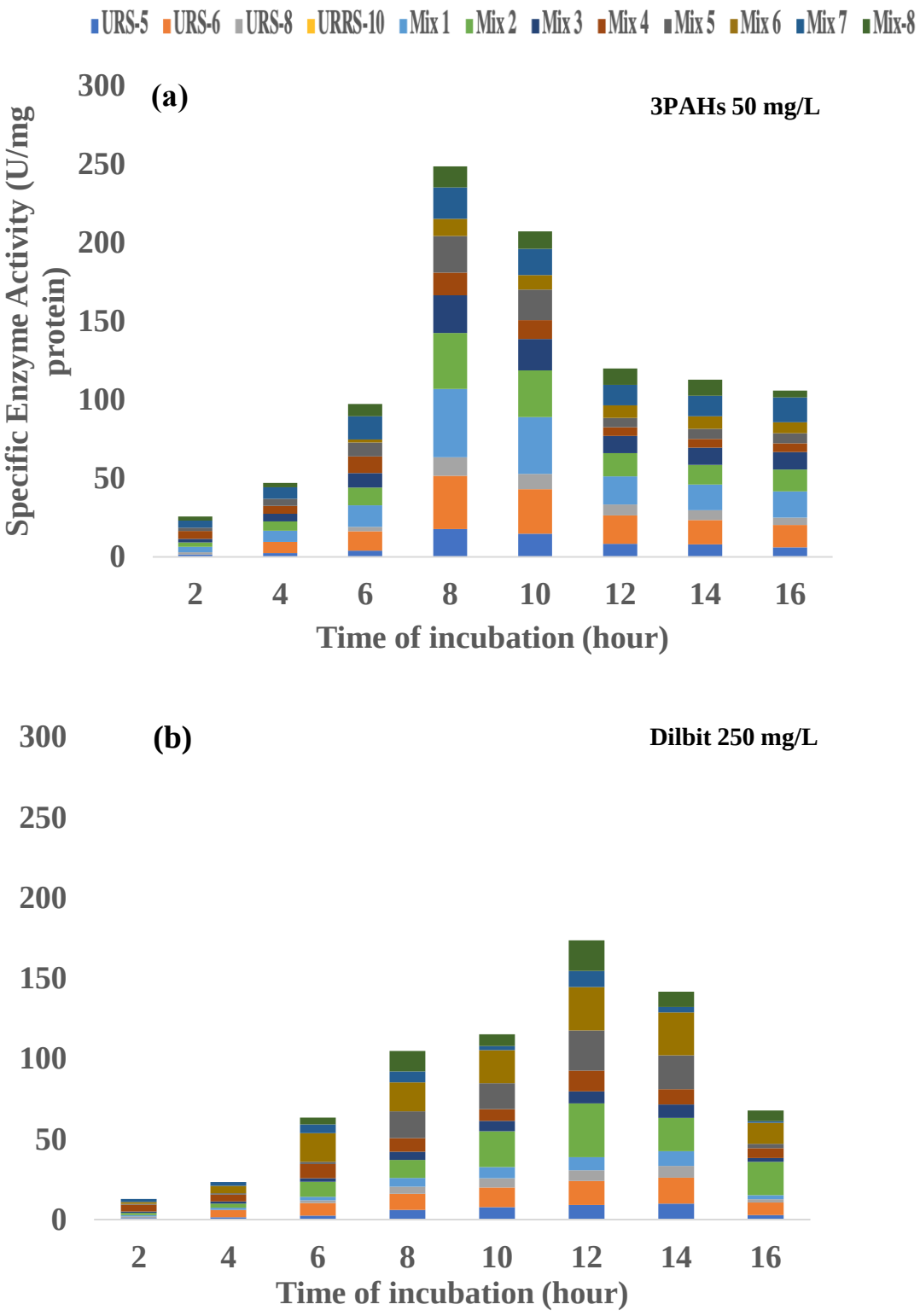
URS-5
URS-6
URS-8
URRS-10
Mix 1
Mix 2
Mix 3
Mix 4
Mix 5
Mix 6
Mix 7
Mix-8
(a)
3PAHs 50 mg/L
Specific Enzyme Activity (U/mg protein)
300
250
200
150
100
50
0
2
4
6
8
10
12
14
16
Time of incubation (hour)
(b)
Dilbit 250 mg/L
300
250
200
150
100
50
0
2
4
6
8
10
12
14
16
Time of incubation (hour)

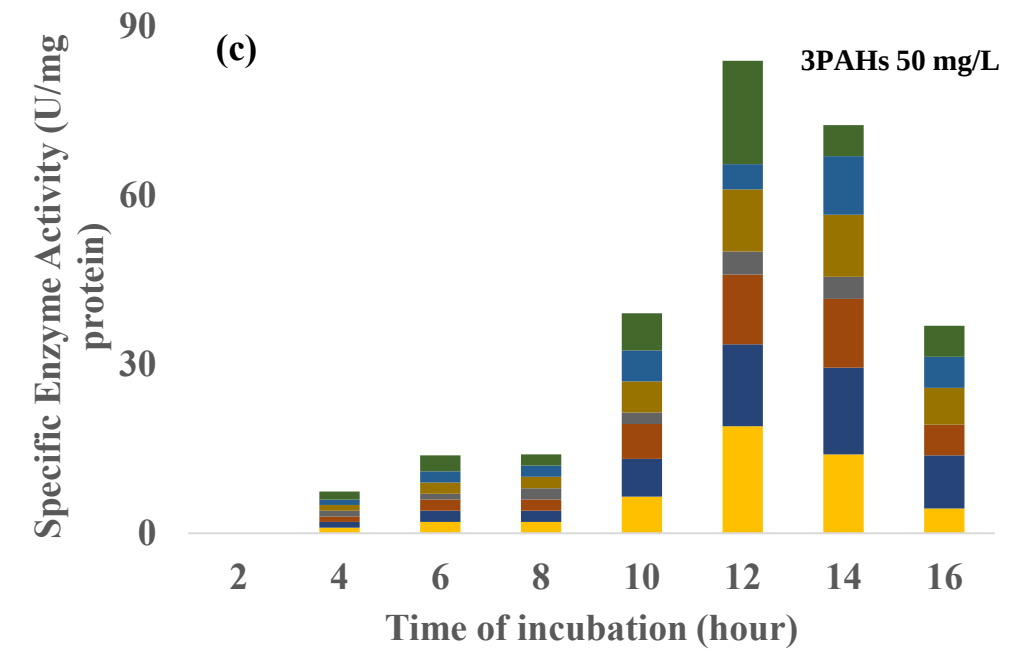
(c)
3PAHs 50 mg/L
Specific Enzyme Activity (U/mg protein)
90
60
30
0
2
4
6
8
10
12
14
16
Time of incubation (hour)

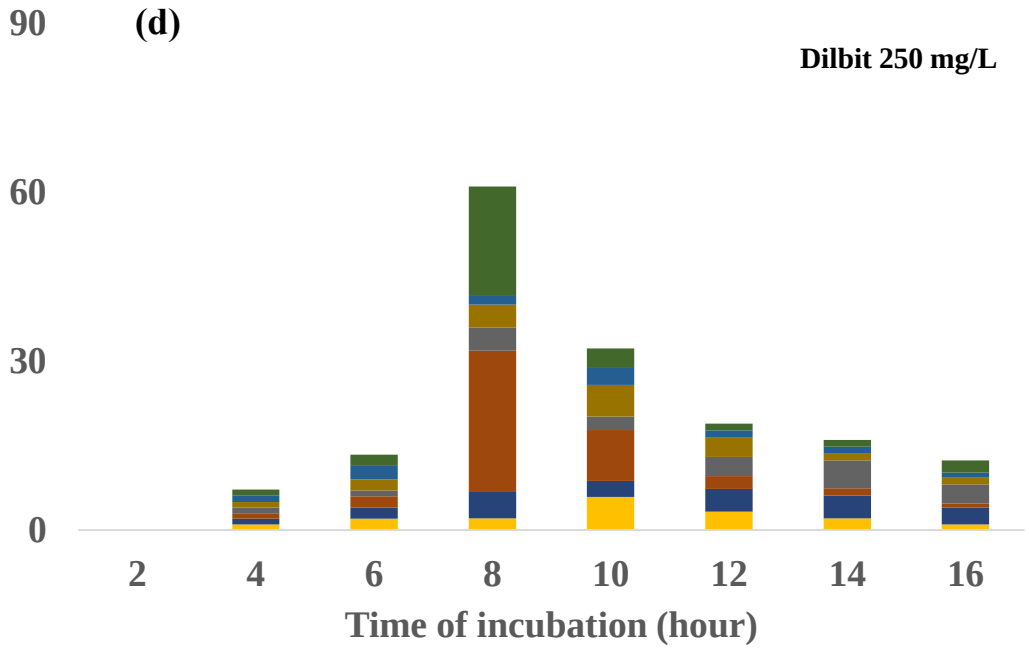
90
(d)
Dilbit 250 mg/L
60
30
0
2
4
6
8
10
12
14
16
Time of incubation (hour)

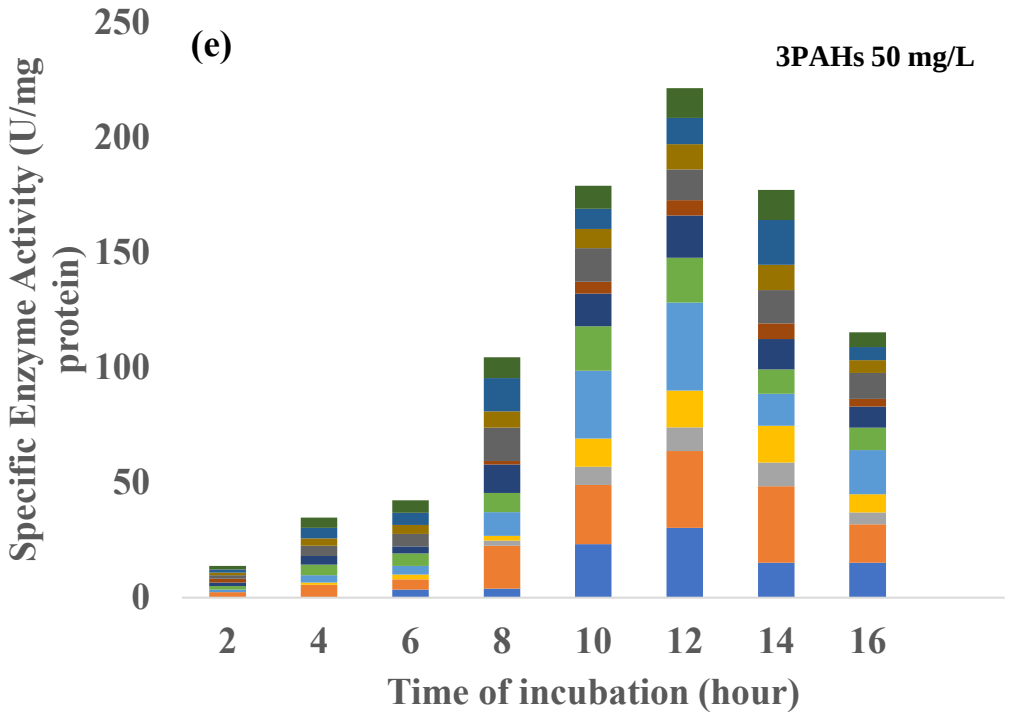
(e)
3PAHs 50 mg/L
Specific Enzyme Activity (U/mg protein)
250
200
150
100
50
0
2
4
6
8
10
12
14
16
Time of incubation (hour)

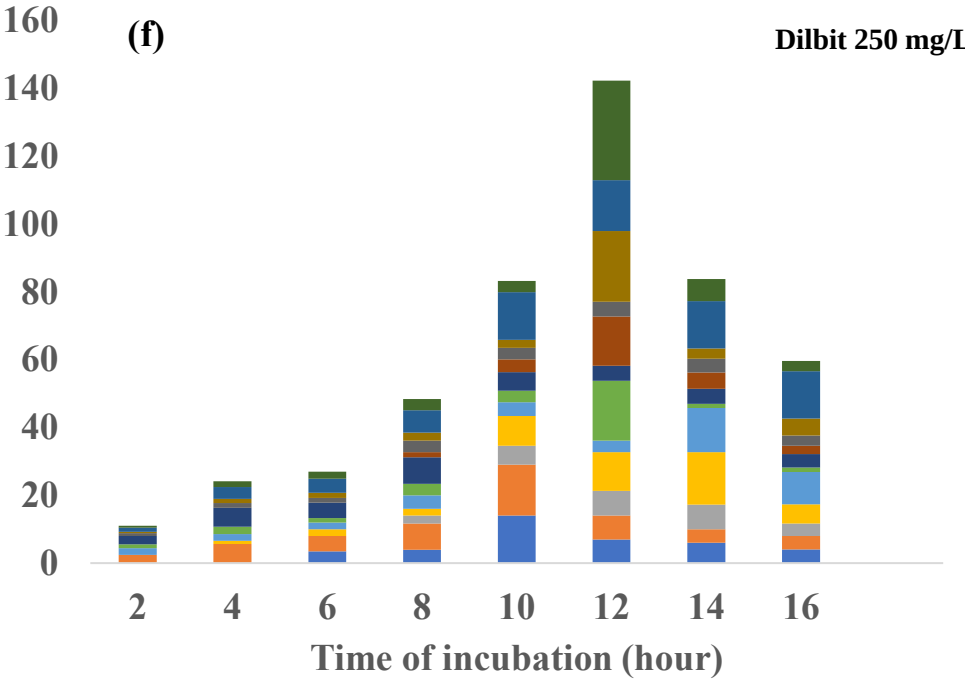
(f)
Dilbit 250 mg/I
160
140
120
100
80
60
40
20
0
2
4
6
8
10
12
14
16
Time of incubation (hour)

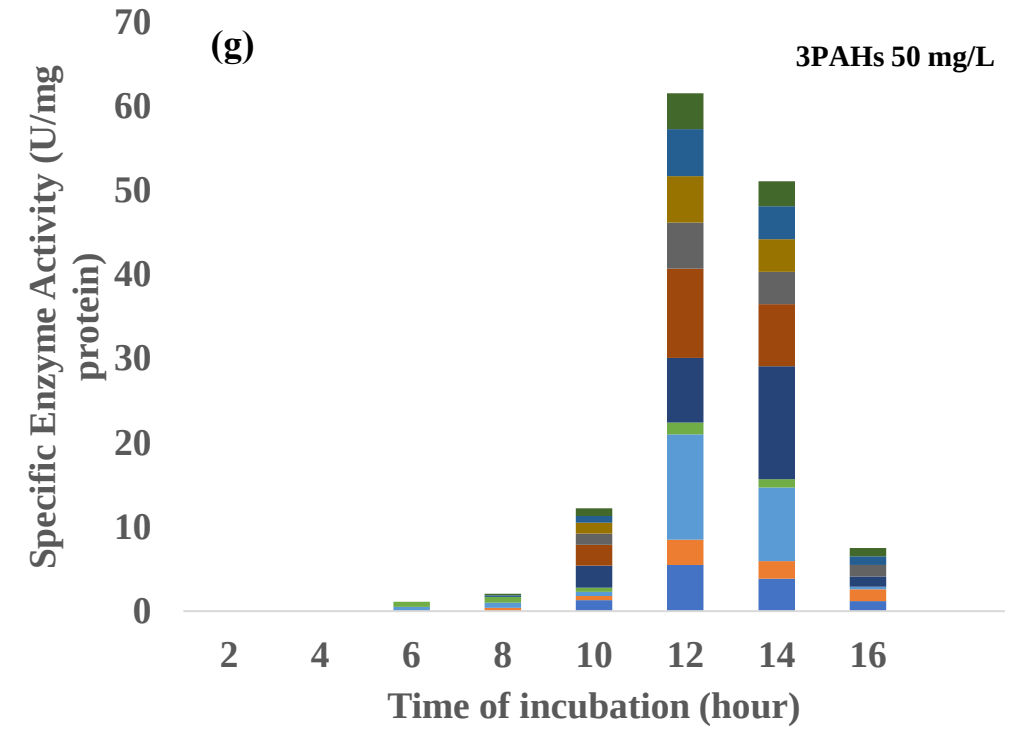
(g)
3PAHs 50 mg/L
Specific Enzyme Activity (U/mg protein)
70
60
50
40
30
20
10
0
2
4
6
8
10
12
14
16
Time of incubation (hour)

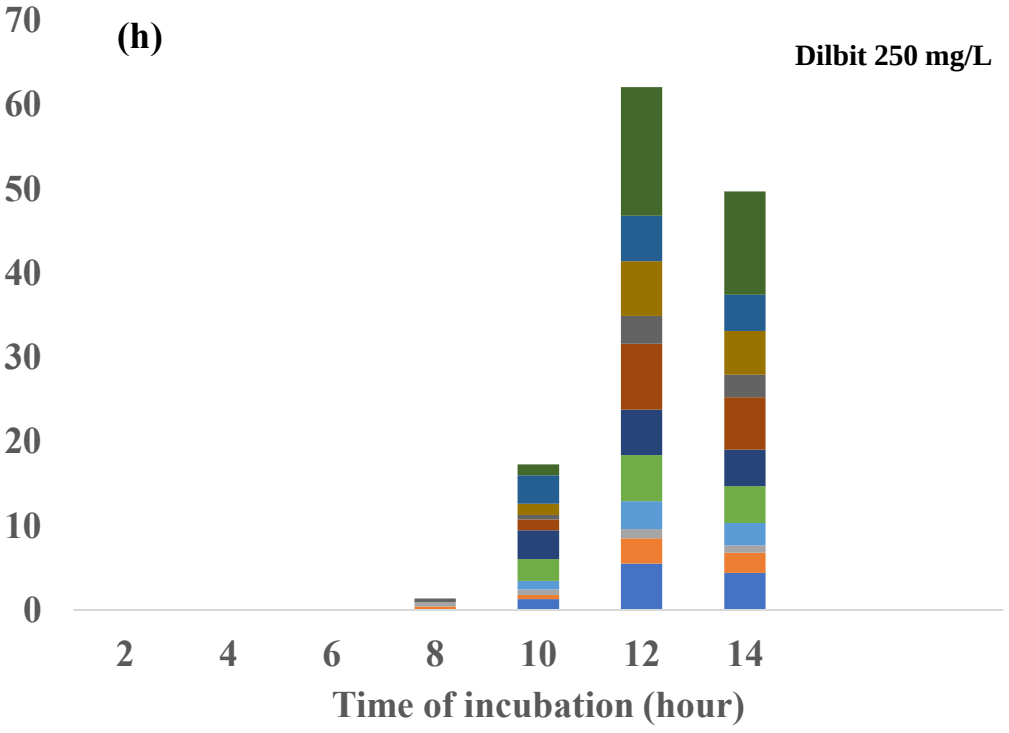
(h)
Dilbit 250 mg/L
70
60
50
40
30
20
10
0
2
4
6
8
10
12
14
Time of incubation (hour)

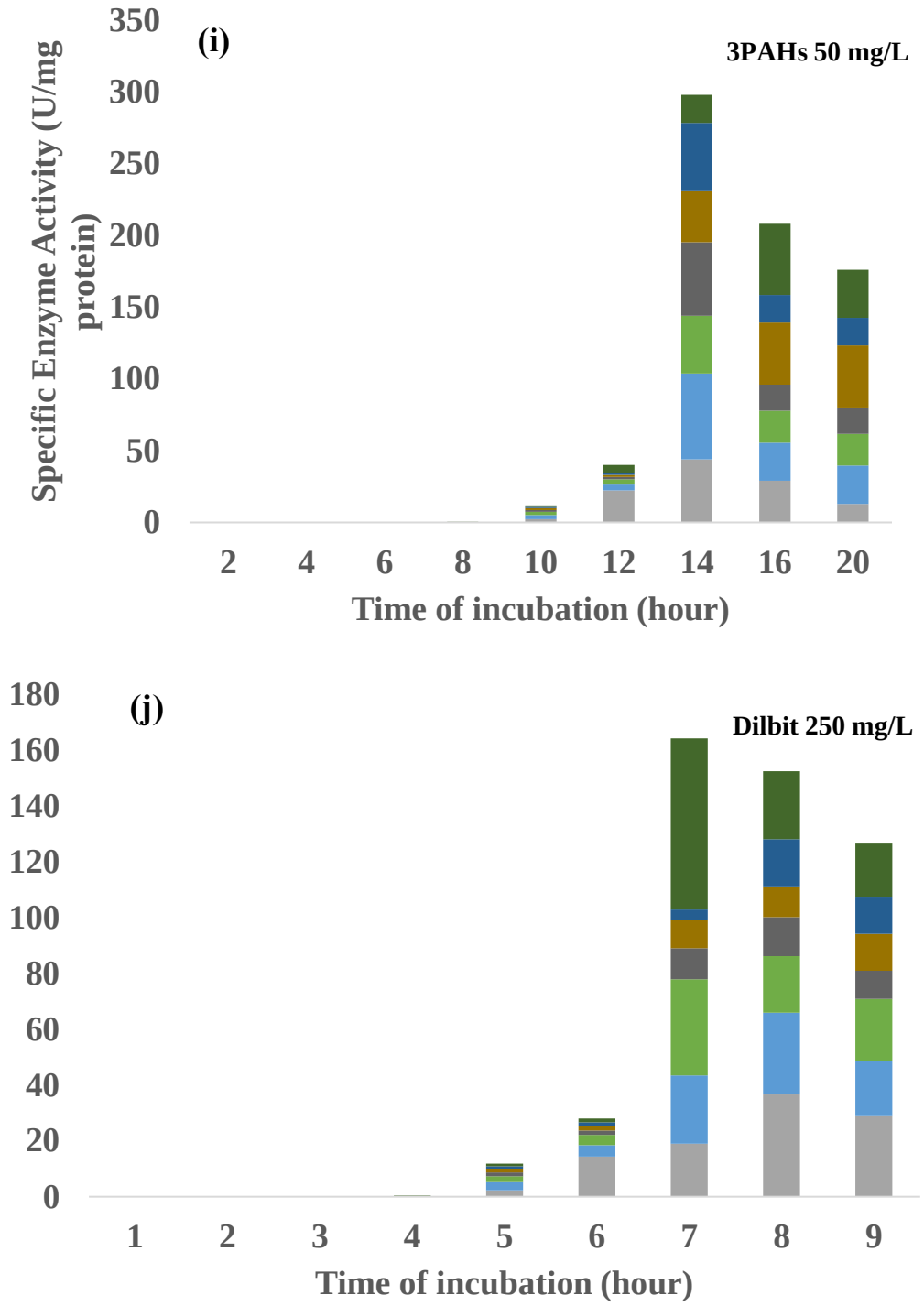

Fig. 4.1.6. Enzyme activity of different cultures inoculated on a and b) NDH, c and d) PDH, e and f) C2,3D, g and h) HY, i and J) PCAD

According to the Fig, the low value of the axial dispersion coefficient (D_{ax} = 0.35 cm^2/min) for packed soil columns is typical of a well-packed soil. In these experiments, hydraulic conductivity values indicated.(Robert et al., 2017) The transport pore volume of 25 mL based on the tracer test with Br corresponds to 50% of the total pore volume and means that there is a need to inject 125 mL of the protein solution to flood the entire soil column. (Diffusion dominated flow)

Mass distribution of pyrene in the column

The retardation factor is a commonly used indicator for illustrating the movement of fluid through fixed-bed column systems. (Davoodi et al., 2021) Our model fitting curve method determined the $K_{f\,enzyme} = 0.43\ ((mg/g)(L/mg))^{0.89}$ and $R_f = 4.1$ value for a relative concentration of 0.5 of enzyme mixture that indicated the adsorption from liquid phase onto the surface of soil. Therefore, the isotherm of adsorption was studied for enzyme solution onto contaminated soil particles in a batch process to obtain an initial estimate of soil adsorption capacity and the interaction between soil, pollutant, and enzyme during bioremediation. Figure 4.1.7 shows the results of the multicomponent Freundlich adsorption models for the three sets of experimental data obtained for pyrene.

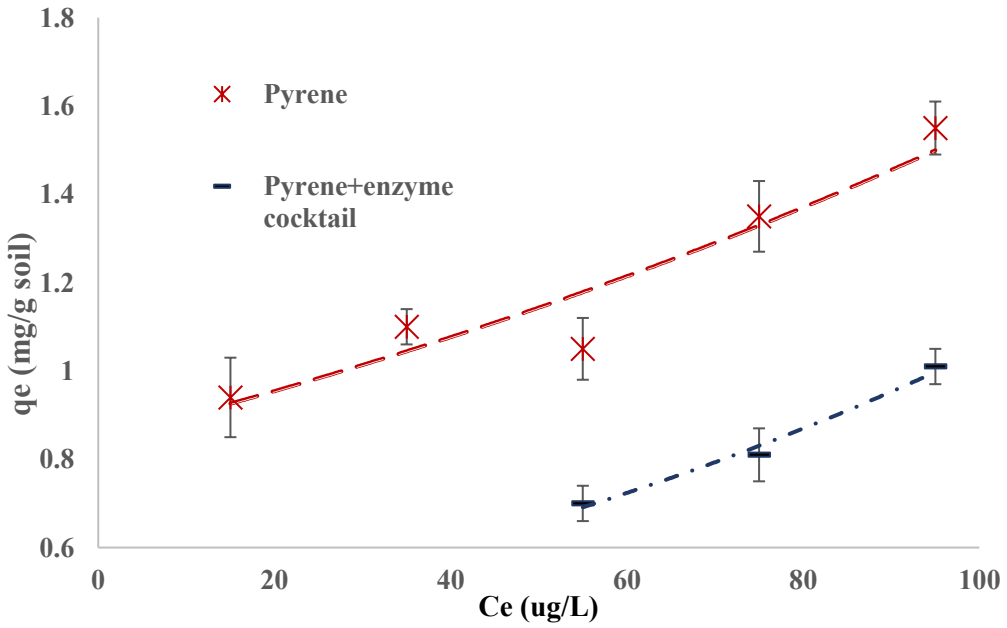

Fig. 4.1.7. Plots of predicted and experimental multicomponent Freundlich isotherm fits for pyrene for single compound, and mixture of pyrene and enzyme cocktail enzyme at 15 ℃

Table A.9 shows the parameters for the multicomponent adsorption isotherm for each component, K_{fi}, n_i, and a_{ij}. Using the obtained coefficient of determination (R^2), it was concluded that the multicomponent adsorption Freundlich isotherm model appropriately fits the data. In the presence of enzyme solutions, the competitive adsorption coefficients (interaction parameter) obtained for the components in the system were lower than zero. The hypothesis that a higher enzyme content in the solution leads to higher adsorption of pyrene is also rejected. At a 5% level of significance for 1 degree of freedom for the $\chi 2$ distribution (Abdehagh et al., 2016), the tabulated value of χ 2 is: 3.84 and the obtained value of χ 2 observed = 5.74 using Eq.4. As mentioned previously, pyrene sorption was observed to be dependent on the amount of organic matter in each soil, as well as the clay mineralogy of the soil and DRM isotherm explain the pyrene behaviour. However, in the presence of an enzyme, the isotherm that best explains the behavior of pyrene in samples is Freundlich isotherm model. This fact can be explained in several ways. Langmuir theory that is linear part of DRM, is the theoretical base for other theories, such as the linear theory. In this model, adsorption occurs within a monolayer, the surface of the adsorption site is flat, and there are a fixed number of identical active sites without competition between the molecule's adsorbent. In the presence of enzyme cocktails, the nature of the adsorption sites might change or the great competition between pyrene and proteins for finite number of sorption sites resulted in the change in mechanism and sorption capacity of adsorbent. Clay minerals have a large surface area, which provides functional groups, such as hydrophobic -Si-O-Si- groups on the tetrahedral silicate (Si-O) sheets that can facilitate interactions between clay minerals, organic enzyme molecules and pyrene by hydrophobicity.(Smith and Bailey, 1963) In this regard, the reduction in pyrene adsorbed mass in liquid unfolding enzyme solutions may be explained by the displacement of the pollutants from solid adsorbents caused by the adsorption of a fraction of the protein. Table 4.2.2 presents the mass distribution of pyrene in soil samples with a soil water content of 1 g / 3.5 g dry soil.

Table 4.1.2. Mesurement and calculation of pyrene mass balance in different phases for soil samples at the soil water content of 1 g H_2O/3.5 g Dry Soil.

	Total pyrene			
	Control without enzyme mixture		Enzyme/soil/pyrene system	
	Calculated (mg)	Measured (g/kg soil)	Calculated (mg)	Measured (g/kg soil)
Free phase M_{free}	2.5	0.9	10.1	NA
Liquid phase M_{water}	4.5×10^{-5}	0.002	3.4×10^{-2}	0.023
Solid phase M_{soil}	27.5	2.1	19.4	1.1
Air phase M_{air}	2.1×10^{-6}	NA	2.1×10^{-6}	NA

[E] M_{free} calculated using Eq. (6) where M_{total} = 30 mg

[a] Total added 30 mg pyrene–17 g soil.

[b] $M_{soil} = m\, K_f\, Ce^{\,1/n}$

[c] $M_{air} = H\ S_{water}$ where H is p-xylene's Henry's constant,1.4×10^{-3} atm m^3/mol and ideal gas law, $n = PV_{air}/RT$, where $V_{air} = 5$ mL and T = 15℃.

[e] $M_{water} = S_{water}\ V_{water}$ where $V_{water} = 5$ mL.

[f] Not available.

30 mg/17 g soil

[g] mg/kg soil.

[h] mg/L.

Pyrene removal

To simulate *in-situ* enzyme application, pyrene and Dilbit contaminated soil was bioremediated in soil columns (140 mL) by injecting enzyme cocktails. In Figure 4.1.8, the bar chart graph illustrates (a) residual (adsorbed) pyrene after 2nd injections and (b) the removal of pyrene by means of biodegradation, solubilization and water flushing.

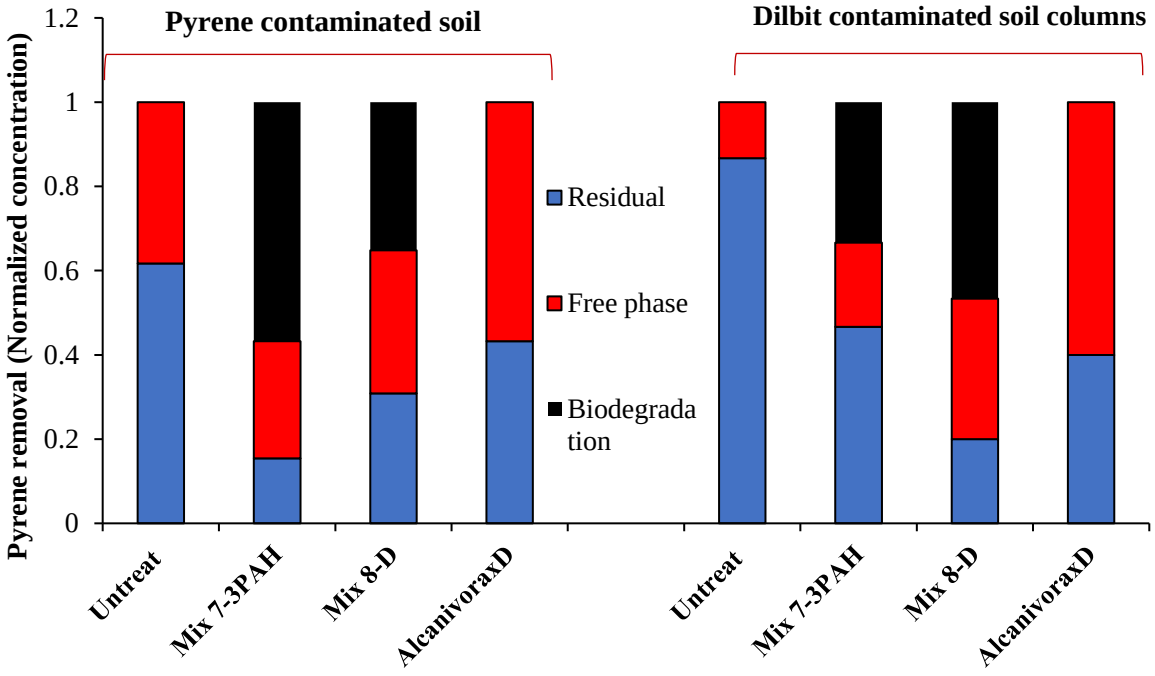

Fig. 4.1.8. pyrene removal after 2nd injection

As can be seen in Figure 4.1.8, adsorption capacity of Dilbit contaminated soil for pyrene significantly increased. This was due to the fact that the adsorbed oil molecules served as a base layer on which further non-polar molecules such as pyrene could be adsorbed, thereby further reducing substrate bioavailability and pyrene biodegradation rates (Davoodi et al., 2019; Miri et al., 2021a).

Untreated soil columns showed a high concentration of undegraded (residual) pyrene (> 70% for Dilbit contaminated site) even after water washing. This showed that biodegradation and solubilization enhanced the pyrene removal. Pyrene removal efficiency followed the order: Mix 7-PAH for pyrene contaminated soil column (84%) > Mix 8-D for Dilbit contaminated soil column (79 % residual) > *AlcanivoraxD* cell extract for Dilbit contaminated soil column (56 %) > *AlcanivoraxD* cell extract for pyrene contaminated soil column (54%). The final pyrene removal efficiency trend was similar to the degradation in the batch test.

It has been demonstrated in several research studies that compounds with low solubility and high adsorptive properties may be improved in their bioavailability by adding solubilizers, such as surfactant flushing method. To determine which portion of removal is due to degradation and oil washing, autoclaved *AlcanivoraxD* was applied in addition to Mix 7-PAH and Mix 8-D. The solubility test study showed that pyrene solubility in the presence of autoclaved Mix 7-PAH, Mix 8-D, *AlcanivoraxD* -water system was around 3.1, 4.3 and 4.7-fold higher than the solubility of pyrene in water. Thus, for example, in the case of *AlcanivoraxD*, the injected solutions can flow into the water channel and increase the recovery of contaminant (33%) compared to untreated column mainly from the action of washing oil (Figure 4.1.8).

Degradation kinetics of p-xylene in the column soil

Table 4.1.3 shows the pyrene concentration in soil samples from pyrene and Dilbit contaminated soil columns in time 0 and after 3 weeks (3W) and 6 weeks (6W) of incubation for column and flask tests. In the present study, around 73 and 55 % of pyrene removal occurred after 3 weeks for pyrene and Dilbit contaminated soils in the presence of Mix7-3PAHs and Mix8-D and pyrene contaminated soil; however, the rate of corresponding removal in column test decreased to around 50 and 30%, respectively. These pyrene removal rates for flask test were around 1.3 and 1.4-fold higher than the pyrene removal rates in the column test. A possible influencing factor to our knowledge was stirring strength so that on stirring modes for batch tests resulted in the stripping of the adsorbed or crusted contaminants.

Table 4.1.4 shows the comparison between batch test and column test degradation study in terms of kinetic constant, degradation efficiency and overall degradation rate. Zero-order reaction was obtained for untreated soil columns and columns treated by *AlcanivoraxD*. However, first order reaction was observed for soils treated with enzyme solutions. In the case of pyrene contaminated soil columns, the kinetic constant for the column test showed a decrease of 22 %, 27% and 33% for Mix7-3PAHs, Mix8-D and *AlcanivoraxD*, respectively. However, in the case of Dilbit contaminated 58%, 33% and 39% decreases were observed for Mix7-3PAHs, Mix8-D, respectively.

The low removal efficiency of pyrene in untreated soil can be attributed to the removal of pyrene in the liquid and free organic phases by water flooding.

Table 4.1.3. Pyrene concentration in soil samples from pyrene/Dilbit contaminated soil columns in time 0 and after 3 weeks (3W) and 6 weeks (6W) of incubation. Each sample was analyzed in triplicate.

Sample Nr	Description	Pyrene contaminated column test		Dilbit contaminated column test	
		Pyrene Concentration (mg/g)	Biodegradation %	Pyrene Concentration (mg/g)	Biodegradation %
1	Autoclaved soil column (3W)	2.2 ± 1 [a]	-	2.4 ± 2 [a]	-
		2.9 ± 2 [b]		2.5 ± 4 [b]	
		2.1 ± 2 [c]		2.3 ± 3 [c]	
2	Autoclaved soil column (8W)	2.5 ± 4 [a]	-	2.7 ± 1 [a]	-
		2.8 ± 2 [b]		2.5 ± 3 [b]	
		2.2 ± 1 [c]		2.6 ± 2 [c]	
3	Untreated soil column (time 0)	2.4 ± 1 [a]	-	2.5 ± 1 [a]	-
		2.2 ± 4 [b]		2.3 ± 4 [b]	
		2.0 ± 3 [c]		2.2 ± 3 [c]	
4	Untreated soil column (3W)	2.7± 4 [a]	12.5	2.4± 1 [a]	3.2
		2.1 ± 3 [b]		2.3 ± 2 [b]	
		1.6 ± 0 [c]		2.0 ± 3 [c]	
5	Untreated soil column (6W)	2.0 ± 2 [a]	25.9	2.3 ± 2 [a]	13.1
		1.8 ± 3 [b]		2.2 ± 3 [b]	
		1.5 ± 4 [c]		1.9 ± 4 [c]	
6	Treated soil column with Mix 7-3PAHs (3W)	1.5 ± 2 [a]	49.7	1.7 ± 2 [a]	27.5
		1.3 ± 1 [b]		1.6 ± 1 [b]	
		0.9 ± 4 [c]		0.7 ± 4 [c]	
7	Treated soil column with Mix 7-3PAHs	0.6 ± 1 [a]	84.1	1.2 ± 1 [a]	51.1
		0.5 ± 2 [b]		0.9 ± 1 [b]	

Samples from [a]: head (depth of 1-2cm), [b]: middle *dept of ((depth of 7-8cm) and [c]: bottom (depth of 12-13cm) of soil column.

4.1.4 Conclusion

This study demonstrated that enzymatic bioremediation was a promising tool for heavy molecular weight PAHs removal from highly contaminated soil. As a result of the biodegradation tests, it was found that the whole-cell mixture requires specific dosing for contamination and dwell times in order to be effective. Nevertheless, the obtained enzyme cocktail effectively removed target PAHs during the initial application for a different dose of contamination The production of enzymes involved in multiple-substrate transformation was also improved by the multi-culture of four psychrophilic bacteria. Due to the variety of metabolic reactions and interactions that a microbial consortium offers over monocultures, it is possible to undertake complex metabolic tasks. In the case of pyrene, a cocktail including enzymes of the pyrene catabolism pathway (ring oxidation, ring fission) for phenanthrene-3,4-diol (3,4-Dihydroxyphenanthrene) formation obtained from URS-10 were used. These ring oxidation or fission products were degraded using URS-5 and URS-8 by releasing enzymes of phenanthrene catabolism pathway (ring oxidation, ring fission) for catechol or phthalic acid formation. The biosurfactant and enzymes of catechol pathway for Acetyl-CoA formation obtained from URS-6 would be the role of this strain affecting the enhancement of biodegradation of pyrene. To simulate *in-situ* enzyme application, pyrene and Dilbit contaminated soil was bioremediated in soil columns and flask tests by injecting enzyme cocktails from most promising consortia (Mix7-3PAHs and Mix8-D). Around 73, 56 % (pyrene contaminated soils) and 36 and 44% (Dilbit contaminated soils) 3 weeks after injection with Mix7-3PAHs and Mix8-D in flask test; however, the rate of corresponding removal in column test decreased to around 50 30%, 27 and 36 % for pyrene and Dilbit contaminated soils, respectively. Microbial community analysis of Mix7-3PAHs and Mix8-D showed the synergistic activity exist between URS-10 and *Alcanovorax* that resulted in superior ability to utilize a higher concentration of pyrene. This synergistic effect and high concentration of pyrene dioxygenase in Mix8-D may also explain the better performance of Mix8-D for Dilbit contaminated soil. The high concentration of pyrene dioxygenase in Mix8-D can be attributed to this synergistic effect.

BRIDGE-2

Batch test experiments showed that the cocktail of selected could degrade 3 PAHs in soil p samples within 48h Three different *in-situ* applications for produced enzyme cocktail mixtures were proposed in this study including jellyfish like process, soil column test and continuous fixed bed columns packed with enzyme loaded aerogels. *The next step was to prepare different compartments of jellyfish like device and test produced cocktail enzyme for in-situ bioremediation of anthracene contaminated column water to confirm the potential application of the enzyme cocktail.* Based on biodegradation studies, a synergistic effect between membrane adsorption, enzymatic degradation, and ultrafiltration was proposed for the removal of anthracene from the column of water.

PART 2

4.2 Simulation of novel jellyfish type of process for bioremediation application

Seyyed Mohammadreza Davoodi[1], Saba Miri[1], Satinder Kaur Brar[1*], Emile Knystautas[2], Richard Martel[3]

[1] Department of Civil Engineering, Lassonde School of Engineering, York University, North York, Toronto, Ontario Canada M3J 1P3.

[2] Département de Physique, de génie physique et d'optique, Université Laval, Québec G1V 0A6, Canada

[3] INRS-ETE, Université du Québec, 490, Rue de la Couronne, Québec, Canada G1K 9A9

(*Phone: 1 418 736 2100 ext. 55228; E-mail: satinder. brar@lassonde.yorku.ca)

Chemosphere, (under review)

Abstract

A bioinspired device was fabricated as a sustainable remedial method and its performance as a membrane-enzyme reactor with cyclic ultrafiltration was investigated. As a device that targets oil below the surface of the water, this device was inspired by the long, elegant tentacles of jellyfish that use their sticky tentacles to catch oil below the surface water when they are struck by an incident. The body of the jellyfish-like device was composed of two parts: 1) Jellyfish arms: Mono and co-axial electrospinning have been utilized to synthesize the flexible parts (e.g., multilayer membrane PS-PVDF/PAN/PS-PVDF) used for immobilization of aliphatic degrading enzymes, and 2) Jellyfish tentacles: Hollow fiber membranes were selected for physical immobilization of polycyclic aromatic hydrocarbon (PAH) degrading enzymes. To study the behavior of the membrane/enzyme reactor, the hollow fiber enzyme reactor with pulsation was operated by recycling an enzyme solution to assess ultrafiltration efficiency. A mathematical model was suggested to describe the experimental data obtained in this study to predict the effectiveness of the reactor for PAH removal. When testing the performance of the jellyfish-like device, those equipped with nanofibers with an oil sorption capacity of ($10. \pm 0.7$ g Dilbit/g fiber) were more effective at removing oil particles before they touched the hollow fiber membrane surface. Moreover, the reaction rate measured in a free soluble enzyme and a recirculating immobilized enzyme solution exhibited a slight difference in the kinetic parameter, K_m (0.03 and 0.021 mM) due to the internal diffusional resistance. Based on biodegradation studies, a synergistic effect between membrane adsorption, enzymatic degradation, and ultrafiltration was proposed for the removal of anthracene from the column of water.

Keywords: Unconventional oil, bioremediation, bioinspired device, enzyme-mediated remediation,

Graphical Abstract

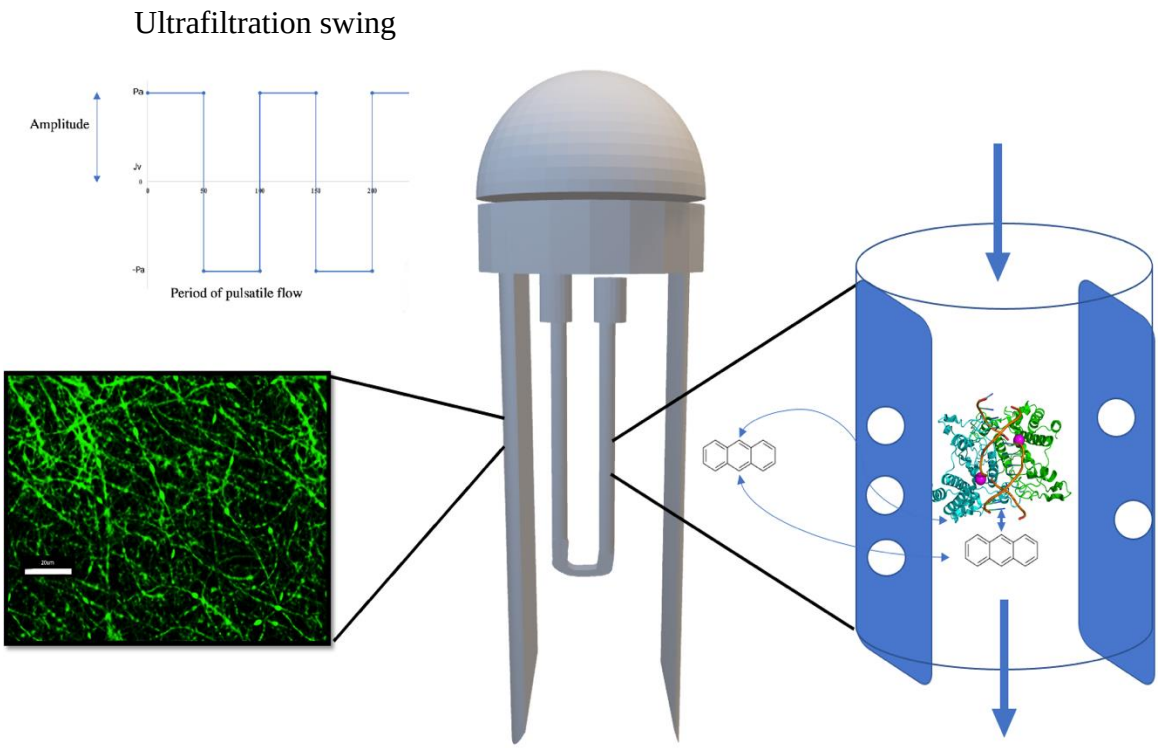

4.2.1. Introduction

An oil spill in the ocean or the sea can have devastating impacts, such as endangering human health, shutting down fisheries and hampering tourism in the region. Governments in many developed nations have organized a list of approved response tools, but a great deal of effort has been made to develop legislation to diversify those response tools by using different novel approaches for remediation of the open ocean marine environment with some focus on the freshwater environment (Davoodi et al., 2020; Forth et al., 2021; Hein, 2006; Mapelli et al., 2017).

Field data shows that following oil spills from wells or tankers, floating oil slicks covered thousands of square kilometers of the surface ocean; and chemical dispersants are applied to these slicks to disperse the oil constituents into the upper water column (Forth et al., 2021). Thus, the removal of free phase hydrocarbon out of the water column is an imperative measurement to avoid oil contamination of aquatic resources. The development of devices/processes to target oil below the water surface has also attracted the attention of researchers due to the complications that started to emerge recently. For example, the explosion in tar sands productions in Western Canada means increasing amounts of heavy crude oil making its way to the American Midwest via the Great Lakes (Hein, 2006). For these types of scenarios, it is necessary to capture the plumes of oil in the deep-water and limit the impact of the oil on the seafloor.

Hydrocarbon-polluted marine environments can be remediated using biotechnological methods, such as biosurfactant amendments, biostimulation, and bioaugmentation (Mapelli et al., 2017). However, it is regulated in countries that have strict legislation regarding the environment, such as Canada, that forbids the majority of chemical and biological products to be added to the sea (King et al., 2020). To carry out bioremediation in a controlled process that does not damage nature, two potential solutions have been presented including: (1) the development of devices

collecting contaminants (free phase oil, or dissolved and dispersed hydrocarbon) and degradation agents in one place; (Warner et al., 2018a) and (2) the use of biochemicals such as enzyme-based formulations to achieve fast biodegradation of the spilled oil safely with no environmental risk.

Most recently, enzymatic bioremediation has been studied as a rapid method of removing environmental contaminants to address unresolved issues, but because of the high costs associated with isolating, purifying, and reusing enzymes, their practical application has been limited (Davoodi et al., 2020). To improve enzyme function, an enzyme in immobilized form is preferred. Among the immobilization methods, encapsulation and physical immobilization could achieve high enzyme activity and stability (Niu et al., 2013). Physical confinement of enzymes by using semipermeable membranes has already found promising applications in food, and the environment, such as biomacromolecule hydrolysis. For example, hollow-fiber devices are currently available to address limitations for enzymatic bioremediation by providing a ready means for the physical immobilization of enzymes (Dai et al., 2011). It also offers several advantages such as simplicity, versatility, capability for co-immobilizing several enzymes, inherently large ratio of surface area to volume, and the absence of enzyme leakage (with properly chosen fibers) (Chambers et al., 1976). The use of soluble enzymes in hollow-fiber reactors has been studied by applying different configurations (Kawakami et al., 1980). The enzyme solution can be placed as a stationary fluid in the shell or the lumen compartment of hollow fibers. The preferred technique for physical immobilization of enzymes by hollow fibers is to slowly recirculate the enzyme in the shell or lumen compartment, in such a way that the enzyme solution passes through small reservoirs (Rony, 1971).

A great deal of effort has been made to fabricate novel devices/processes that demonstrate a synergistic effect upon membrane separation, adsorption and enzyme catalysis for aquatic removal of organic compounds (Chen et al., 2019). Although membrane technology has primarily been applied for pollutant removal in closed membrane reactor systems, applications for the open

natural water system for large-scale bioremediation of contaminated surface waters are possible (Zhang and Jiang, 2019; Zhu et al., 2020). The potential of immobilized enzymes to address challenges for membrane fouling in water purification and the potential of membrane systems to protect the enzyme from the environment surrounding are examples of the bio-catalytic membrane that take advantage of reaction- separation integration for continuous filtration and water purification in open natural water system (Meng et al., 2020). For example, Zhu et.al studied gravity-driven biomimetic membranes (GDBM) for water purification in the open natural water systems. GDBM has a layer composed of laccase and carrier material on a microfilter. One advantage of the proposed system was the excellent permeable structure that resulted in very low hydrostatic height needed to provide sufficient filtration driving force, meanwhile, membrane fouling rate was kept at a low level (Zhu et al., 2020).

This study aims to investigate the practical application of enzyme-mediated bioremediation for the removal of the model substrate (i.e., anthracene) from surface water, comprising three key objectives: a) enzyme solution preparation, b) jellyfish-like device fabrication, and c) confinement of enzyme solutions in hollow fibre/multilayer nanofibrous membrane systems. The jellyfish-like device draws inspiration from the long, elegant arms of jellyfish, which use their sticky arms to catch the oil that floats beneath the surface of the water when they accidentally fall into it. Each device is composed of a recirculation reservoir (e.g., jellyfish bell), sheets of electrospun nanofibers immobilized with aliphatic degrading enzymes, and hollow fiber membranes used for the physical immobilization of PAH degrading enzymes.

4.2.2. Materials and methods

Chemical and bacterial strains

The strains used for bioremediation of synthesized oil-water mixture are *Alcanivorax borkumensis* SK2 (DSM 11573), and newly isolated *Pseudomonas* URS-6. To fabricate jellyfish-like device arms, polyacrylonitrile (PAN, Mw = 150,000 g/mol), Polyvinylidene (PVDF, Mw = 180,000 g/mol) and polystyrene (PS, Mw= 250,000 g/mol) were purchased from Scientific Polymer

Product Company (USA), Sigma-Aldrich and Arcos, respectively. *N*, *N*′-Dimethyl-Formamide (DMF), and hydroxylamine hydrochloride (99.5%) were supplied by Fisher Scientific (USA). Tetrahydrofuran (THF), acetone (99.5%), nicotinamide hypoxanthine dinucleotide (sodium salt), polyethyleneimine (PEI, 50 kDa) were purchased from Sigma-Aldrich Trading Co., Ltd. Biochar was supplied by Pyrovac Inc. (Canada) Carboxyfluorescein succinimidyl ester (CFSE)-based CellTrace™ CFSE Cell Proliferation Kit were purchased from Invitrogen. The proposed methodology has been divided into three stages as shown in Figure 4.2.1. Unconventional oil e.g., Dilbit used in this study was prepared from Syncrude coke-feed bitumen, which had been extracted from Athabasca oil sands.

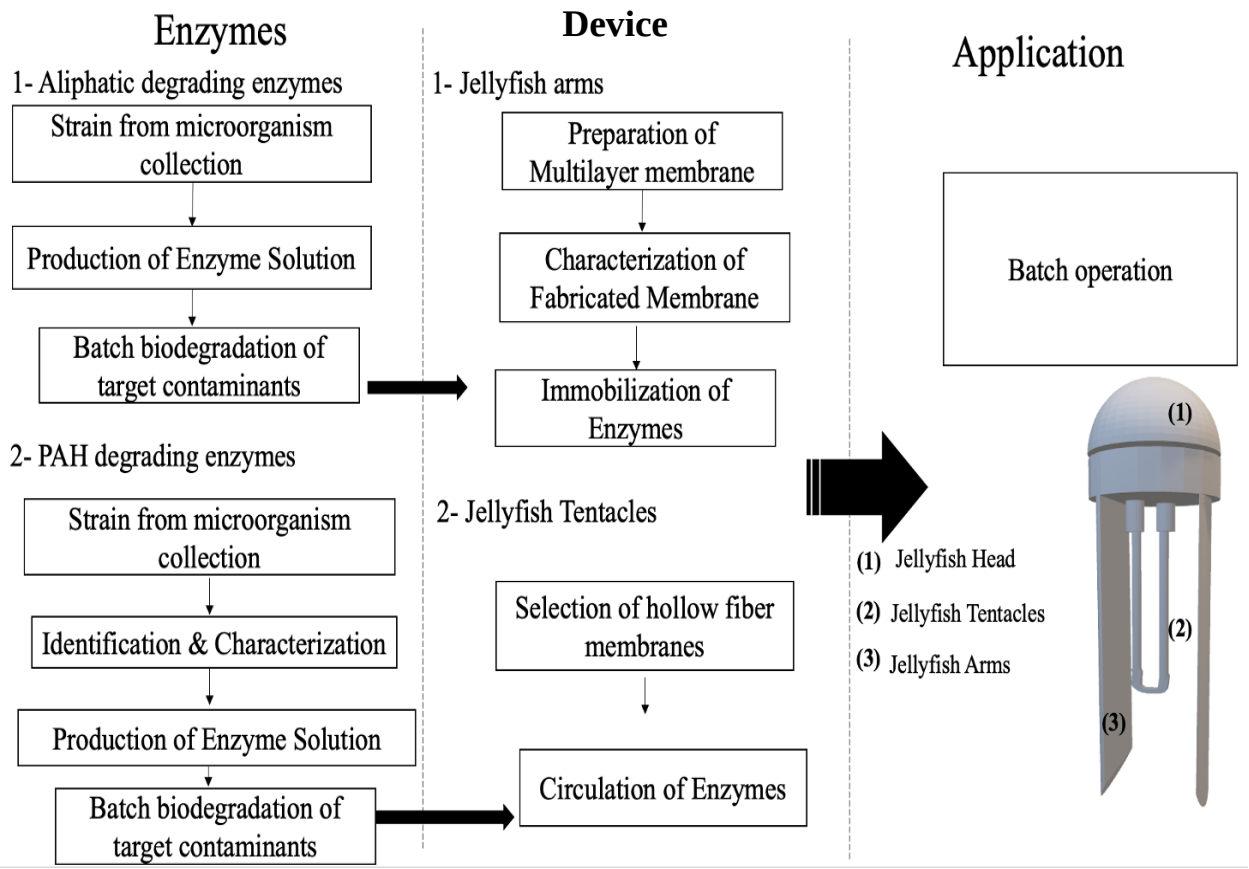

Fig. 4.2.1. Research plan for the jellyfish-like device

Aliphatic degrading enzyme study

The strain used in this study for aliphatic enzyme production was *Alcanivorax borkumensis* SK2 (DSM 11573). More detailed information on enzyme production, determination and immobilization is provided in in our in-progress article (Davoodi et al. 2022). In brief, *Alcanivoracx borkumensis* was cultivated in a liquid medium by inoculating the flasks containing seawater media using lyophilized powder and the flasks were then incubated in an orbital shaker at 27 ±1 ℃ for 4 d. Later, 150 μL of the medium was incubated in nutrition broth (NB)-agar plates at 27 ±1 ℃ and the plates were stored 27 ±1 ℃ for future use. The fermentation experiment at NB growth media supplemented with different concentrations of motor oil 5W20 (5%, 15%, and 25% v/v) was conducted in shake flasks using a 3 percent inoculum volume of pre-culture. Cultured *A. borkumensis* grown on motor oil was used to obtain cell extracts containing aliphatic degrading compounds. After incubation for enzyme production, lipase, esterase and alkane hydroxylase activity was monitored by spectrophotometric as described in the supplementary information (Section 1S). To confirm the presence of target enzymes in the crude cocktail obtained from *A.borkumensis*, the liquid chromatography-Tandem mass spectrometry (LC-MS/MS) was carried out.

PAH degrading enzyme study

Isolation and identification of PAH degrading bacteria from contaminated sediments

The strain used for the production of PAH degrading enzyme solutions is newly isolated *Pseudomonas* URS-6 from the coastal marine environment. Isolation and characterization of *Pseudomonas* URS-6 as well as production, characterization and identification of the target enzyme were described in detail in our in-progress article (Davoodi et al. 2022). In brief, 0.5 g of the impacted sediments was transferred in a crimp sealed 150 mL-serum bottles containing 25 mL of sea salt-defined media (SSM) with crude oil (200 mg/l) as the sole carbon source and incubated for a month at 4 °C. For enzyme extraction, cells were harvested from the media after culturing by centrifugation (16,000 rpm for 4 min at 4 °C). The pellets with the biomass were resuspended in phosphate buffer, pH 8, and then sonicated on ice using an Ultrasonifier (Branson Ultrasonics Corporation, Danbury, CT, USA) at 22 and 30 kHz frequencies of ultrasounds for 10 min to obtain intracellular enzymes. Cell extract obtained from *Pseudomonas* URS-6 was used to check enzyme activity for a key enzyme that transforms the target pollutant by initial attack at the 9,10- positions

(Moody et al., 2001). Because there was no accumulation of intermediates during the degradation of anthracene (Davoodi et.al 2022), the rate-limiting step might be the initial ring oxidation. Thus naphthalene dioxygenase activity was studied to determine the performance of immobilized enzyme. Naphthalene dioxygenase (ND) activity was assayed based on the formation of indigo at 500 nm per time unit. An enzyme reaction was carried out using 5 μL of indole 100 mM as a substrate in the presence of cellular lysates in DMF.

Analytical methods

Anthracene is a tricyclic aromatic hydrocarbon found in high concentrations in the upper water column under floating oil following the oil spill (Forth et al., 2021). A prototypical PAH, anthracene is used to determine factors that affect the biodegradation potential of PAH in the environment (Moody et al., 2001). The release of anthracene into the water following the crude oil spill and its biodegradation in the presence of pre-selected strain and obtained enzymes solutions were confirmed by GC-MS (Agilent model 6890 GC, 5973 MSD) analyses which were carried out at 0, 3, 7 d of incubation as described elsewhere (Li et al., 2021b).

Preparation and characterization of the jellyfish-like device

Jellyfish arms

Multilayer membrane systems were synthesized through the electrospinning technique consisting of a multilayer structure (PS-PVDF/PAN/PS-PVDF) being independently electrospun one after the other. In more detail, the enzyme cocktail obtained from *A. borkumensis* SK2 was encapsulated in modified polyacrylonitrile (PAN) membrane which at the same time is protected by two hydrophobic skin polyester-polyvinylidene fluoride (PS-PVDF) membranes (Lin et al., 2013) (Zhang et al., 2010).

Middle and skin layers of membrane

The middle hydrophilic layer was fabricated via mono and co-axial electrospinning. The skin layer of multilayer systems are hydrophobic consisting of two different polymeric components polystyrene (PS) and polyvinylidene fluoride (PVDF) and nano-biochar particles were simultaneously fabricated into one mat using one-step two-nozzle electrospinning (Jiang et al., 2015). More detailed information on PAN membrane fabrication as well as PAN membrane modification and enzyme immobilization is provided in the supplementary information (Section 1S)

Selection and characterization of hollow fiber membranes for circulation of enzymes

Spectrum® modified poly(ether sulfone) mPES hollow fibers with a molecular weight of (MWCO) of 10,000 Da (D02-E010-05-N, Spectrum Labs, USA) were used for multiple enzyme and cofactor immobilization. Since the molecular weight of PAH substrates is about 169 and the molecular weight of the studied enzymes is more than 49,000 Da (Davoodi et.al 2022), Spectrum® mPES membrane appeared appropriate for this study. Moreover, thin-skinned hydrophilic modified polyethersulfone (mPES) hollow fibers are void-free and anisotropic in a structure that provides high relative hydraulic permeability and flux rates at a maximum pressure of 30 psi. Hydrophilic neutrally charged Spectrum® mPES hollow fiber minimized non-specific protein binding as well as fouling by hydrophobic molecules (Yu et al., 2011). The hollow fiber ultrafiltration module consisted of 10 fibers with an internal diameter of 1.0 mm, a length of 45 cm, a wall thickness of 0.1 mm and a total surface area was 58 cm^2.

After selecting the membrane, the second step was to ensure that these membrane modules were intact. To do so, the diffusion test method was applied to evaluate its integrity. More detailed information on the systematic exploration of membrane hollow-fibers characteristics including the permeation of substrate and the retention ratio of the co-enzymes is provided in the supplementary information (Section 4S).

Application of the jellyfish-like device

To study the benefit of using hollow fiber modules for enzyme-catalyzed reactions, the performance of a hollow fiber system based on simple mathematical models has been examined experimentally in filtration and degradation of the model substrate in water. Ultrafiltration oscillation is induced in the beaker side of the reactor by introducing a pulsatile flow to the hollow fiber lumen as well as by maintaining outflow from the lumen at the average value of the pulsatile inflow rate. Ultrafiltration is the difference between the inlet and outlet flow rates.

For kinetic analysis of such a vertical reactor, a fundamental view of the cyclic operation in the reactor was provided by lumping the system into two compartments and using generalized phenomenological transport equations in an ultrafiltration membrane. These also give some notion about the order of magnitude of parameters that reactor performance is acceptable. The solutions contained in the enzyme compartment (II) and the substrate compartment (I) are assumed to be fully mixed. Figure 4.2.2 shows a schematic of the hollow-fiber reactor system.

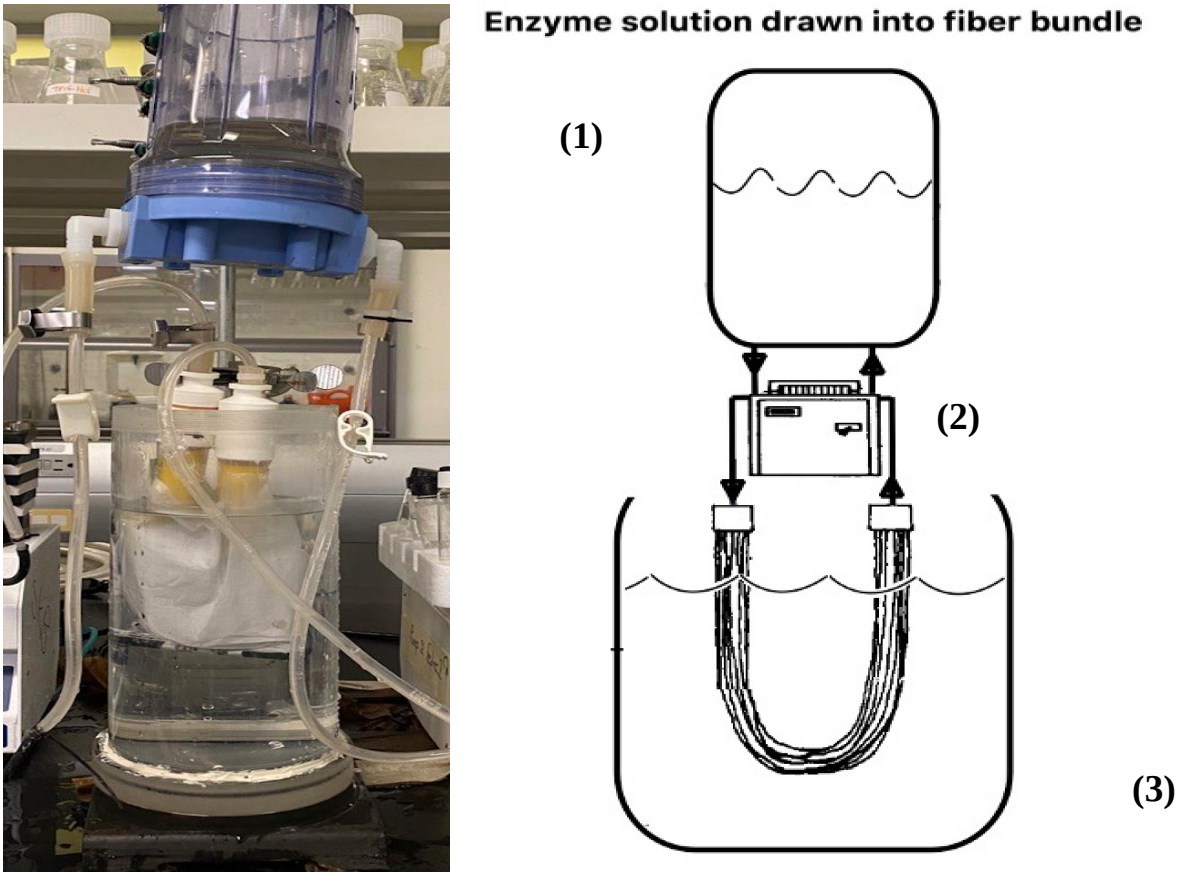

Fig. 4.2.2. Hollow fiber beaker device for enzymatic reaction:(1) enzyme reservoir, (2) inlet and outlet of the peristaltic pump, (3) hollow fiber module dioxygenas

To set a material balance around the two regions separated by ultrafiltration membrane, the transport equation may be written according to Kedem and Katachalsky (Kleinhans, 1998)

$$J_s = P_m(S_I - S_{II}) + \sigma J_w f(S_I, S_{II}) \quad (1)$$

$$J_w = P_a \sin(wt) \quad \text{or} \quad P_a\, g(t) \quad (2)$$

Where $P_a, P_m, \sigma, S_I, S_{Ii}, J_s$, and J_w refer to unltrafiltration velocity (cm/min), membrane permeability (cm min^{-1}), sieving coefficient, solute concentration (mg l^{-1}) in compartment I and II, substrate, and water flux, respectively. The sieving coefficient ($\sigma = \frac{C_{filtrate}}{C_b}$) in the absence of concentration polarization can be 1 (Fournier, 2017). Eq.(2) means the arbitarary variation of recirculation flowrate in the lumen side with sin and square-wave ultrafiltration swing). Mass balance for the substrate in compartments I and II, respectively, are given in Eqs. 3 and 4:

$$\frac{d(V_I S_I)}{dt} = -AJ_s + Q(S_{I0} - S_I) \quad (3)$$

$$\frac{d(V_{II} S_{II})}{dt} = AJ_s - V_{II}\frac{V_{max} S_{II}}{k_m + S_{II}} \quad (4)$$

Where A and Q are mass transfer area of hollow fiber membrane (cm^2) and volumetric flowrate (cm^3). For sine-wave ultrafiltration swing, Eq .(3) and (4) can be transformed into dimensionless forms by using the following dimensionless variables:

$$S_1 = \frac{S_I}{S_{I0}} \quad \tau = wt \quad \widetilde{K}_m = \frac{K_m}{S_{IO}} \quad \lambda^2 = \frac{V_{max} V_{II}}{S_{IO} A P_m} \quad \partial = \frac{V_{II0}}{V_{I0}} \quad W = \frac{\omega V_{I0}}{TAP_m} \quad F = \frac{V_{I0}}{TAP_m}$$

$$Le = \frac{Qe}{P_m A} \quad T = \frac{2\pi}{W}$$

$$V_1 \frac{d(S_1)}{d\tau} - L_e d \sin\tau = -(S_1 - S_2) - \sin\tau\, f(S_1, S_1) L_e d + Ls(1 - S_1) \quad (5)$$

$$V_2 \frac{d(S_2)}{d\tau} + L_e d \sin\tau = (S_1 - S_1) + \sin\tau\, f(S_1, S_1) L_e d - \frac{\lambda^2 S_2}{\widetilde{K}_m + S_2} \quad (6)$$

Where

$$V_1 = \partial W - L_e d\ (1 - cos\ \ \tau)$$

$$V_2 = \partial W + L_e d\ (1 - cos\ \ \tau)$$

F and W are dimensionless frequency for square and sine wave pulsations. $Le\ d$ and d are the difference between the outlet and the inlet flowrates appear as ultrafiltration and the fraction of average outlet velocity. Eq. (5) and (6) were solved numerically using Runge-Kutta scheme to study reactor performance with ultrafiltration swing. The experiments were performed in duplicates.

4.2.3. Results and Discussion

Performance of immobilized enzymes

Aliphatic degrading enzymes

The growth curves of *A.borkumensis* on NB and different concentrations of motor oil are shown in Figure 4.2.3. The control in this experiment was the seawater medium supplemented with 5% (v v^{-1}) of motor oil which was reported as the optimal substrate concentration in other studies (Kadri et al., 2018c). As shown in Figure 4.2.3, the result from cell count in culture induced with 15% of motor oil was approximately 2.2 times higher than the control indicating that NB should be applied to achieve enough biomass for enzyme production. Moreover, the best growth was obtained between 40-50h for the *A.borkumensis* growth on NB and 50-60 h for the standard medium. The analysis of the residual concentration of the motor oil by GC-FID as a function of incubation time is shown in Figure 4.2.3. The increase in motor oil concentration from 15 to 25% v v^{-1} resulted in a significant decrease in cell count that can be explained by the high concentration of inducers and continuous high level of expression (25% of Dilbit) might cause a drain or metabolic burden on the cell's energy resource leading to inhibition of cell growth.

Literature that studied the growth of different hydrocarbonoclastic bacteria on the various concentrations of carbon sources, reported that despite a higher bacterial growth for the specific concentrations of inducers or carbon sources, the degradation of target contaminant might decrease for some strains. (Mishra and Singh, 2012) The effect of various concentrations of motor oil on biodegradation kinetics was also investigated. Results are presented in Table 4.2.1. showed the first-order kinetic model using linear regression. For 15% of motor oil, about 38h biodegradation with the highest k value compared to other concentrations of motor oil demonstrated that efficiency of biodegradation and subsequent enzyme production enhanced in the presence of 15% motor oil. The results of 3-hydroxy acyl-CoA dehydrogenase, lipase, and esterase-specific activity at the end of fermentation are presented in Figure 4.2.3 (b). There was a significant increase in cell growth resulting in higher production of 3-hydroxy acyl-CoA dehydrogenase (27.6 U mg^{-1}), esterase (73.7 U mg^{-1}) and lipase (79.1 U mg^{-1}) were noticed compared to the control especially when the concentration of motor oil increased from 5 to 15% (v v^{-1}).

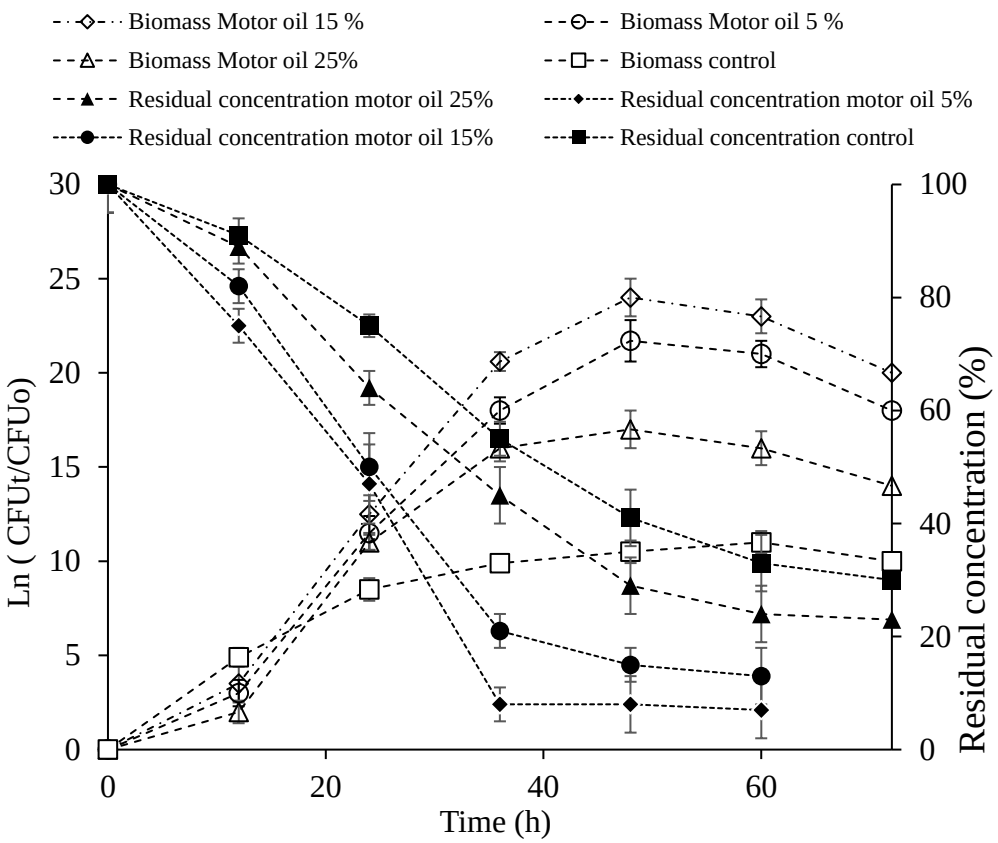
Biomass Motor oil 15 %
Biomass Motor oil 5 %
Biomass Motor oil 25%
Biomass control
Residual concentration motor oil 25%
Residual concentration motor oil 5%
Residual concentration motor oil 15%
Residual concentration control
Ln (CFUt/CFUo)
Residual concentration (%)
Time (h)
0
5
10
15
20
25
30
0
20
40
60
80
100

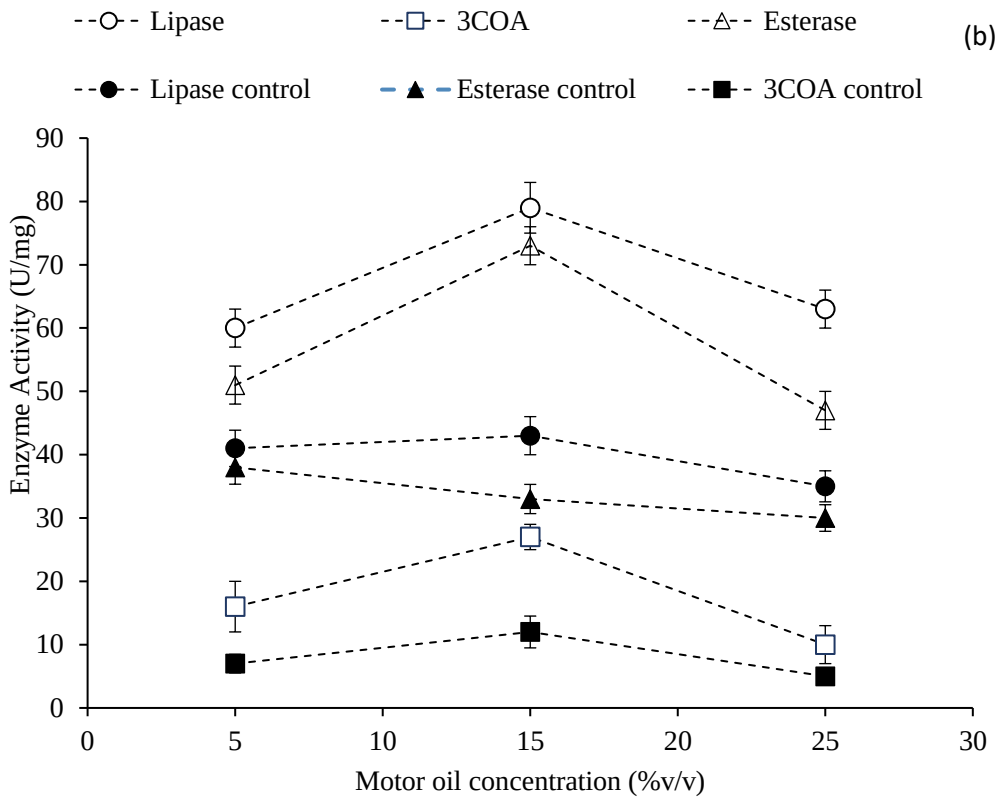

Fig. 4.2.3. Colony-forming units of *A. borkumensis* grown on NB supplemented with 5, 15 and 25% motor oil and residual concentration (TPH) profile of motor oil (b): Effect of different motor oil concentrations on the production of enzymes

Table 4.2.1. Specific degradation constant and correlation coefficient during degradation of motor oil

Motor oil concentration (%)	Treatment duration (h)	Degradation rate (%)	K (h^{-1})	R^2
15	36	93	2.1	0.93
5	48	87	1.9	0.91
25	60	76	1.6	0.9
Control	60	67	1.4	0.97

Efficiency of enzyme immobilization within the electrospun matrix

Table 4.2.2 shows total protein loading, specific activity and their yield on multilayer systems. Results suggest that the encapsulated enzymes were active after the electrospinning processing. As can be seen in Table 4.2.2, even though PS-PVDF/coPAN-EN gave the highest immobilization yield for total protein (87.5%), the total protein loading capacity of PS-PVDF/monPAN-EN was about 13 times more than PS-PVDF/coPAN-EN. PS-PVDF/monPAN-EN also gave a higher immobilization yield for lipase (85.7%), esterase (86.6%) and 3-hydroxy acyl-CoA dehydrogenase (85.9%). Thus, PS-PVDF/monPAN-EN system was applied for further study and practical application in the jellyfish-like device.

Also, it was observed that for unmodified PS-PVDF/monPAN-EN, less than 15% of enzymes were immobilized. This can be attributed to the binding onto the activated surfaces of the membrane driven by the hydrogen bonding of amine structures in the proteins toward amine and hydroxyl structures in the amidoxime-modified PAN membrane. The results showed that the leaching of enzymes from PS-PVDF/coPAN-EN and PS-PVDF/monPAN-EN were less than 16% after 48 h

of incubation which in turn results in stability and subsequent reusability of the immobilized enzymes in an aquatic medium. Thus, comparing the leached enzyme immobilized in the multilayer and modified PAN electrospun fibers showed that the hydrophobic layers protected encapsulated enzymes and significantly decreased the leached percentage.

Table 4.2.2. Immobilization of 3-hydroxy acyl-CoA dehydrogenase, esterase and lipase on fabricated membranes

Matices	Total protein loaded (μg/ml)	Total protein loading yield (%)	Lipase activity (U/mg protein)	Lipase immobilization yield (%)	Esterase activity (U/ml)	Esterase immobilization yield (%)	3-hydroxyacyl-CoA dehydrogenase specific activity (U/ml)	3-hydroxyacyl-CoA dehydrogenase immobilization yield (%)	leached Lipase (%)	leached esterase (%)	leached 3-hydroxyacyl-CoA dehydrogenase (%)
PS-PVDF/coPAN-EN [1]	18.4± 1.1	87.5± 0.7	10.8± 0.3	72.8± 4.6	11.2±1.1	70.1±0.4	3.3±0.1	75.0±0.7	9.7±1.6	11.4±0.3	14.9±0.9
Unmodified PS-PVDF/coPAN-EN[2]	17.3± 2.8	77.1± 0.2	13.1± 0.2	91.5± 5.4	10.8±4.2	66.7±0.2	4.9±0.3	74.3±0.8	8.3±0.2	11.5±0.9	36.7±1.5
PS-PVDF/monPAN-EN[3]	248.2± 10.2	42.4± 3.8	60.1± 6.8	85.7± 3.8	63.1±1.9	86.6±0.3	19.3±0.9	85.9±0.1	10.3±0.7	17.8±0.3	15.6±2.5
Un modified PVDF/monPAN-EN[4]	48.9±2.4	7.5± 1.7	11.3± 2.6	14.1± 0.1	8.3±0.4	10.5±0.9	2.2±0.2	0.9±0.2	52.5±2.6	64.8 ±1.6	49.7±4.9
monPAN-EN [5]	269.9± 3.8	48± 4.3	52 ± 1.3	60.1± 3.4	60.9±0.5	52.5±0.1	13.4±0.4	44.1±1.9	28.7±0.8	33.9±1.9	35.2±2.9
Unmodified monPAN-EN[6]	50.6± 1.9	8.8± 0.8	8.4± 0.3	10.1± 0.8	5.4±0.1	7.9±0.2	2.1±0.3	13.1±1.7	95.1±0.8	98.4±2.1	94.6±4.4

[1] Multilayer membrane system (Skin layer: Polyester-polyvinylidene fluoride (PS-PVDF) membranes/Middle layer: Co-axial modified polyacrylonitrile (PAN) fibers immobilized with an enzyme cocktail

[2] Multilayer membrane system (Skin layer: Polyester-polyvinylidene fluoride (PS-PVDF) membranes/Middle layer: Co-axial unmodified polyacrylonitrile (PAN) fibers immobilized with an enzyme cocktail

[3] Multilayer membrane system (Skin layer: Polyester-polyvinylidene fluoride (PS-PVDF) membranes/Middle layer: Co-axial unmodified polyacrylonitrile (PAN) fibers immobilized with an enzyme cocktail

[4] Mono-axial modified polyacrylonitrile (PAN) fibers immobilized with an enzyme cocktail

[5] Mono-axial unmodified polyacrylonitrile (PAN) fibers immobilized with an enzyme cocktail

Alkane compound removal and stability of immobilized enzymes

Table 4.2.3 shows removal half-life, the reaction rate constant and the removal rate of hexadecane by free and immobilized enzymes. These results were used to reassess the catalytic activity of free and immobilized enzymes. The degradation test for samples after 40 h, showed that the highest removal of hexadecane adsorbed and catalyzed by 0.5 g enzyme immobilized between PS/PVDF membrane reached 76%. Meanwhile, the highest removal of hexadecane catalyzed by 0.5 g enzyme immobilized on modified PAN reached 64%. These results indicate that the hydrophobic membrane surface outperformed the hydrophilic PAN surface. Even though the activities of immobilized enzymes are lower than that of free enzymes (Table 4.2.3), the higher removal efficiencies and reaction rate constant for immobilized enzymes (Table 4.2.3) might be due to the adsorption of contaminants on the membrane. As a consequence, free enzymes can quickly lose their activity when exposed to an aqueous solution, resulting in a low degradation efficiency (Alonso-González et al., 2020). Comparing enzymes immobilized between PS/PVDF membrane showed that the highest removal of hexadecane was achieved using mono-axial PAN fibers which can be attributed to the diffusion limitations that affected the entire process for co-axial PAN fibers. For both types of multilayer membranes, third-order kinetics were applied to study the synergy effect of adsorption and enzymatic degradation of hexadecane; however, the specific kinetics for a complex system such as PS-PVDF/coPAN-ENZ requires further investigation. Due to the higher removal efficiency obtained using PS-PVDF/monPAN-EN, mono-axial electrospinning was applied to fabricate the middle hydrophilic layer.

Table 4.2.3. Half-life, the reaction rate constant for free enzymes and multilayer system

	Removal half-life (h)	Reaction rate constant (dm^6 $mmol^{-2}$ h^{-1})	Hexadecane removal (%)
Free enzymes	17.7	0.025	53± 4.1
monPan-ENZ [1]	0.029	5.15	64± 2.3
PS-PVDF/monPan-EnZ [2]	0.003	45.1	76± 1.9
coPan-ENZ [3]	0.128	1.3	59± 3.1
PS-PVDF/coPan-ENZ [4]	0.0425	3.9	62± 4.6

[1] Mono-axial polyacrylonitrile (PAN) fibers immobilized with enzyme cocktail

[2] Multilayer membrane system (Skin layer: Polyester-polyvinylidene fluoride (PS-PVDF) membranes/Middle layer: Mono-axial polyacrylonitrile (PAN) fibers immobilized with enzyme cocktail

[3] Co-axial polyacrylonitrile (PAN) fibers immobilized with enzyme cocktail

[4] Multilayer membrane system (Skin layer: Polyester-polyvinylidene fluoride (PS-PVDF) membranes/Middle layer: Co-axial polyacrylonitrile (PAN) fibers immobilized with enzyme cocktail

The stability of the enzymes as reaction biocatalysts is important for biotechnological processes. However, the depletion of enzyme activity and denaturation of enzymes are both natural processes that occur over time. Fortunately, the immobilization method can lead to increased enzymes' stability toward deactivation by restricting the freedom of macromolecules and increasing the structural rigidity of the protein. Dai *et. al.* (2011) studied the development of core-shell nanofibers for enzyme immobilization in the degradation of PAHs (Dai et al., 2011). They showed that a hydrophobic polymer shell protected the laccase from the influence of the external surroundings and enhanced the operational stability of the enzyme by retaining 70% o initial activity. Figure 4.2.4 shows the residual activity of free and immobilized enzymes stored at 15 °C ± 1. The lipase, esterase and 3-hydroxy acyl-CoA dehydrogenase immobilized in the middle layer preserved around 50.7%, 57.1 %, and 49.6 % of their initial activities; however, the free enzymes retained only 19.2% ,15.1% and 4.4 % of their initial activities, respectively. An important reason for this enhancement is that enzyme immobilization inhibits conformational changes, which prevents denaturation and increases stability (Miri et al., 2021b).

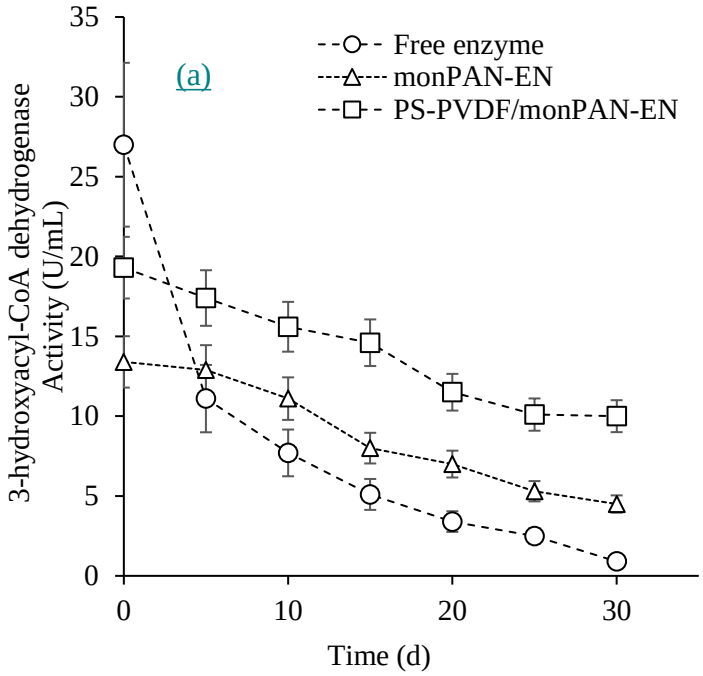
(a)
Free enzyme
monPAN-EN
PS-PVDF/monPAN-EN
3-hydroxyacyl-CoA dehydrogenase Activity (U/mL)
Time (d)
0
5
10
15
20
25
30
35
0
10
20
30

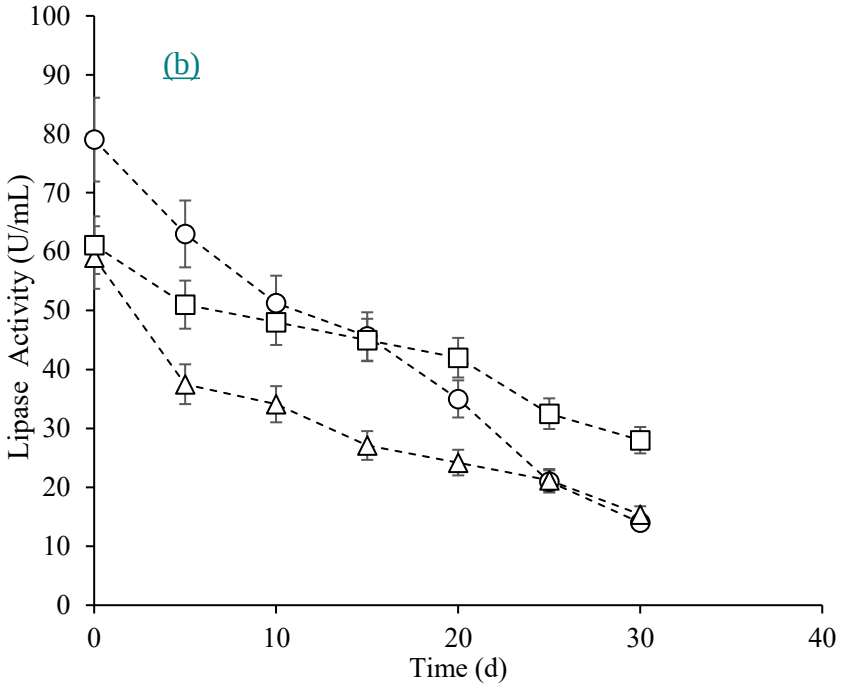
(b)
Lipase Activity (U/mL)
Time (d)
0
10
20
30
40
50
60
70
80
90
100
0
10
20
30
40

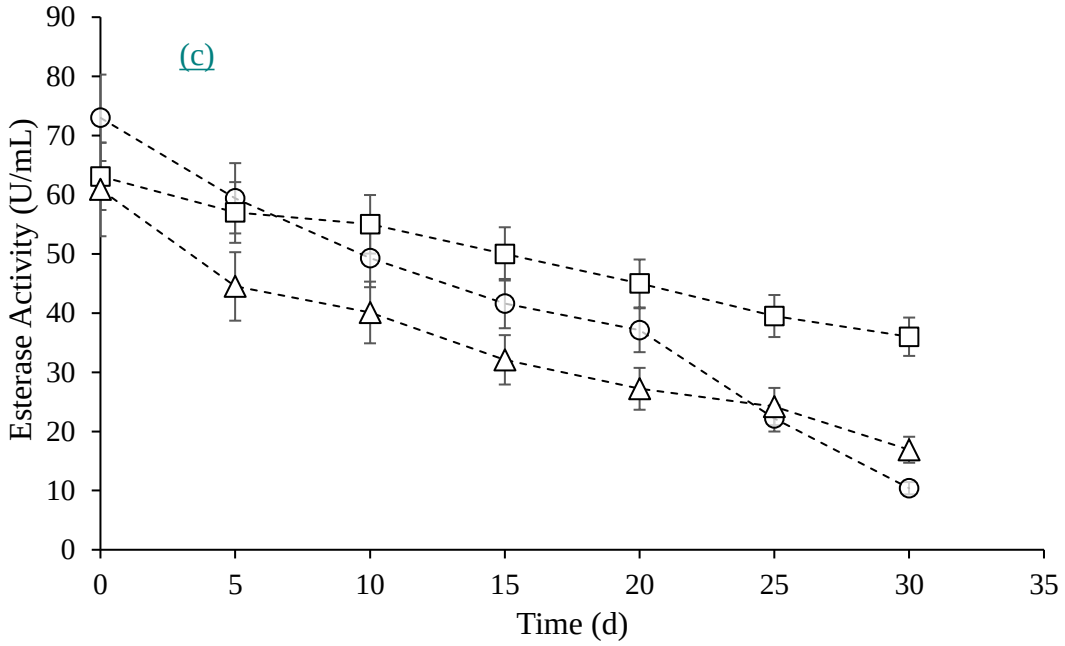

Fig. 4.2.4. Effect of time on the activity of the crude enzymes: (a) 3-hydroxy acyl-CoA dehydrogenase; (b) Lipase and (c) esterase

PAH degrading enzymes

Cell extracts from newly isolated *Pseudomonas* URS-6 showed high activity of naphthalene dioxygenase, which is the key enzyme involved in the initial attack on anthracene after which anthracene is converted to metabolites. The initial reactions leading to the degradation of anthracene are catalyzed by multicomponent dioxygenases that include both atoms of oxygen in the nucleus of the PAH to produce cis-dihydrodiol (Fuenmayor et al., 1998; Moody et al., 2001). Spectrophotometer readings of indigo production by cell extract showed an activity of 34.7 $\pm$ 0.5 U/mg protein where 1 unit converts 1 indole μmol/min to equimolar indigo at room temperature. The enzyme showed optimum activity at pH 7.8 and at a 150 mM NaCl concentration at 15 ℃.

Kinetic parameters

Reaction rates at various substrate concentrations were measured in free solution and at a recirculating flow rate of 200 mL/min. The Lineweaver-Burk equation was applied to calculate K_m

of soluble enzyme and hollow fiber immobilized enzyme through the linear fitting. The observed values for the anthracene relate to a multienzyme system of target enzymes. Two parallel control experiments with inactivated enzyme and without solution circulation were also run in the same conditions to distinguish between adsorption and biodegradation for anthracene removal. As shown in Figure 4.2.5, the hollow fiber immobilized enzyme (0.021 mM) was slightly higher than that of the soluble enzyme (0.03 mM) which might be attributed to the internal diffusion resistance.

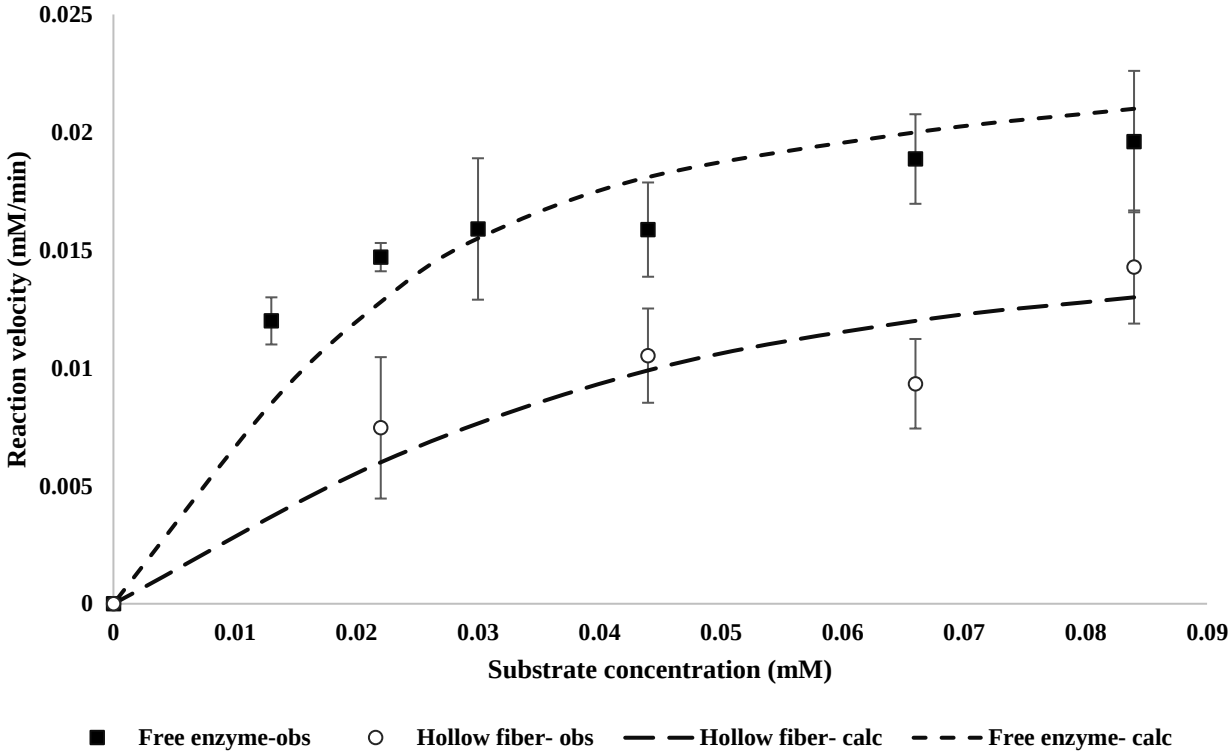

4.2.5. Michaelis-Menten plot for comparison of activities with various concentrations of hexadecane in hollow fibers and free solution (corresponding to the naphthalene dioxygenase-specific activity of 34.7 ±0.5 U/mg of total protein) at 15 ℃ Fig.

Anthracene is a stable molecule that can be degraded by complex chemical processes. The obtained cell extract circulating in hollow fiber membrane contains key enzymes for attacking the

aromatic systems when target pollutant is transferred to the lumen side. For naphthene 1,2-dioxygenase to be able to attack anthracene's lateral ring, it needs NADH, from which a vicinal diol is formed and two hydrogens will be added to the ring (Parales et al., 2000). Thus, continuous retention of native NADH in an enzyme membrane reactor for anthracene biodegradation is proposed to enhance the stability of the enzyme. Figure 4.2.6 shows the enzyme activity-time profiles for test solutions containing enzyme cocktail 0.2 mM PEI which were circulated through the lumen of hydrophilic modified polyethersulfone (mPES) hollow fiber beaker containing 500 mL of 20 mg^{-1} anthracene in 150 mM saltwater, pH 6.8.

Each day saltwater was removed from the beaker and replaced with fresh substrate solution. A parallel control experiment with native enzyme solution was also run. As shown in Figure 6, the enzyme solution (corresponding to the naphthalene dioxygenase-specific activity of 34.7 $\pm$0.5 U/mg of protein) containing 0.2 mM PEI retained 90% activity for 4 d whereas the free soluble enzyme rapidly deteriorated. Enhanced stability of enzyme circulating in hollow fiber membrane can be attributed to the continued retention of the coenzyme NADH in the presence of PEI and membrane system. Moreover, the stability enhancement resulting from the addition of PEI might be attributed to the entrapment of coenzyme inside the lumen. Thus, it appears feasible to combine in this way the stability advantage of the immobilized enzyme with the semi-permeability properties of hollow fibers (Chambers et al., 1976). As can be seen in Figure, it can be safely assumed the enzyme activity remains constant during three-day period of the experiment.

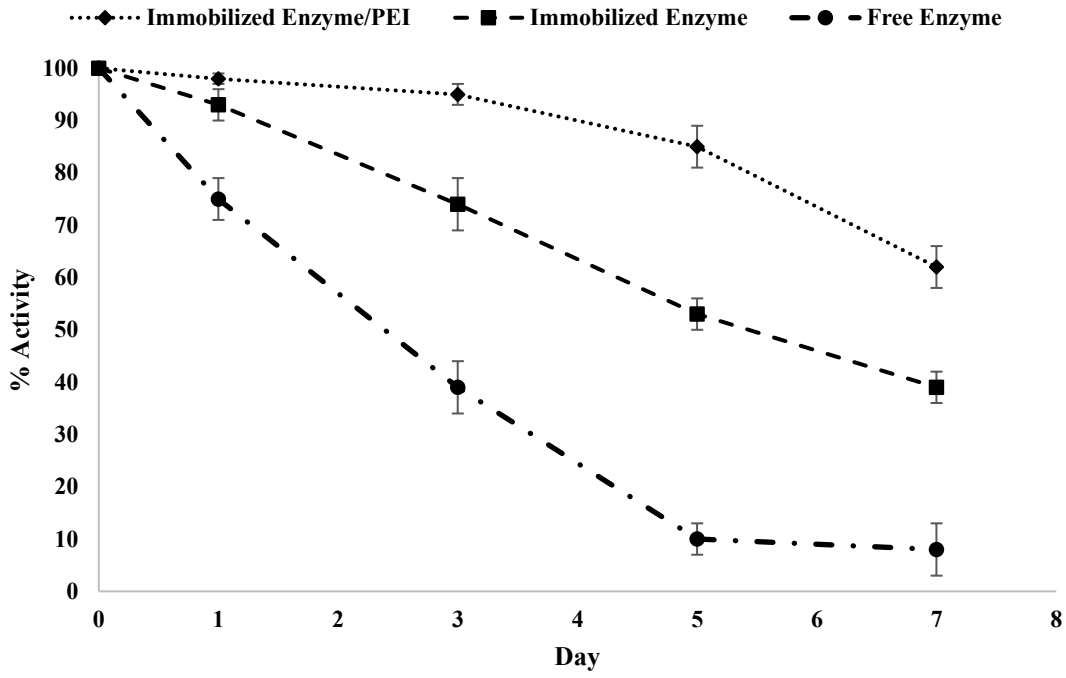

Fig. 4.2.6. The enzyme activity profiles as a function of time as they are circulated within the lumen at 15 ℃

Characterization of device compartment

As mentioned previously, jellyfish may have a thing to teach us. A jellyfish's body is symmetrical and consists of three parts: the umbrella, the oral arms, and the stinging tentacles (Yu et al., 2019). Electrospinning has been utilized to synthesize the flexible parts e.g., oral arms. It serves as membrane adsorbers that facilitate the mass transfer of target substrates from the aqueous phase to membranes.

The idea behind designing the tentacles is to have hollow fibers immobilized enzymes that are impermeable to the enzymes but permeable to contaminants resulting in simultaneous adsorption and detoxification of contaminants.

Characterization of the fabricated membrane (Jellyfish arms)

Figure 4.2.7 shows the SEM images of the composite and neat skin layers. Most of the nanofibers were uniform in size and shape and the use of a plate as a collector resulted in randomly oriented fibers, which favours membrane fabrication because of the required mechanical strength in all directions. All of the fibers were nonwoven and porous with very little bead-on-string formation. Beads should not form on the fibers, since the beads may weaken the mechanical properties of the mat and serve as stress points. The neat PVDF nanofibers had diameters in the range of 200-300 nm (Figure 4.2.7 a). A neat PS fiber, on the other hand, exhibited a diameter of 900 nm to 1.5 mm (Figure 4.2.7 a), which is several orders of magnitude larger than PVDF nanofibers. In other words, PVDF nanofibers offer a large surface area and small fiber diameters. There was no evidence of beads-on-string formation in the bicomponent composite mats, i.e., PS/PVDF (Figure 4.2.7). This also shows the entrapment of biochar particles with the average diameter of 5 μm among fibersfibres in PVDF/PS.

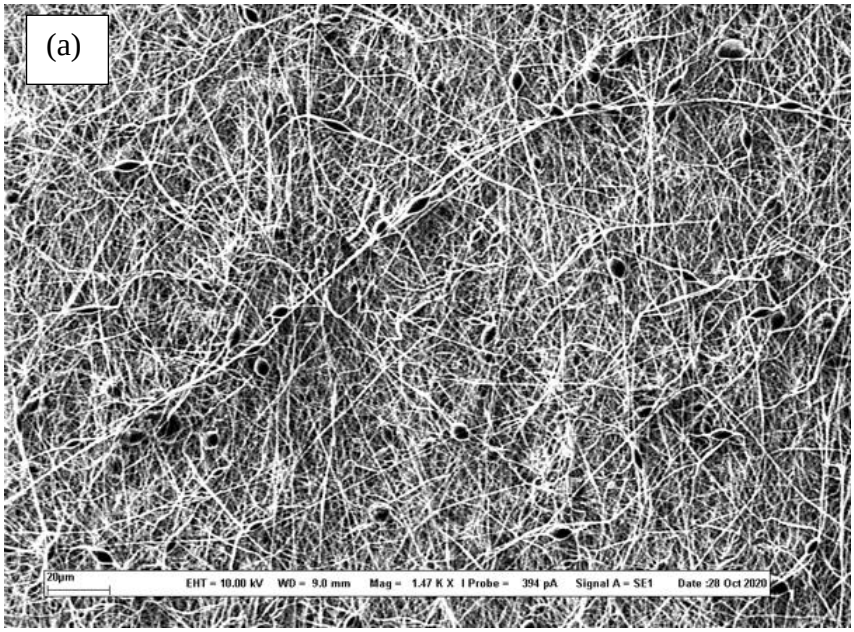
(a)
20µm
EHT = 10.00 kV WD = 9.0 mm Mag = 1.47 K X I Probe = 394 pA Signal A = SE1 Date :28 Oct 2020

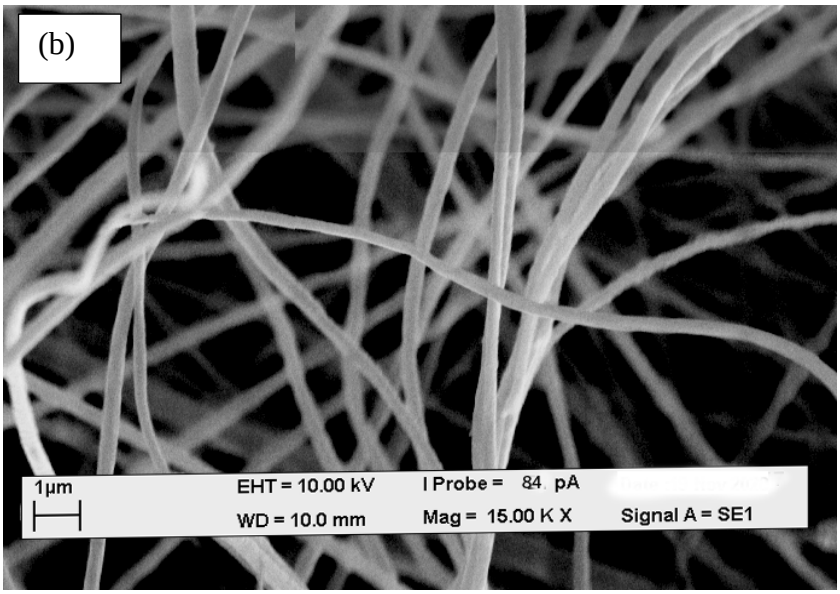
(b)
1µm
EHT = 10.00 kV
WD = 10.0 mm
I Probe = 84 pA
Mag = 15.00 K X
Signal A = SE1

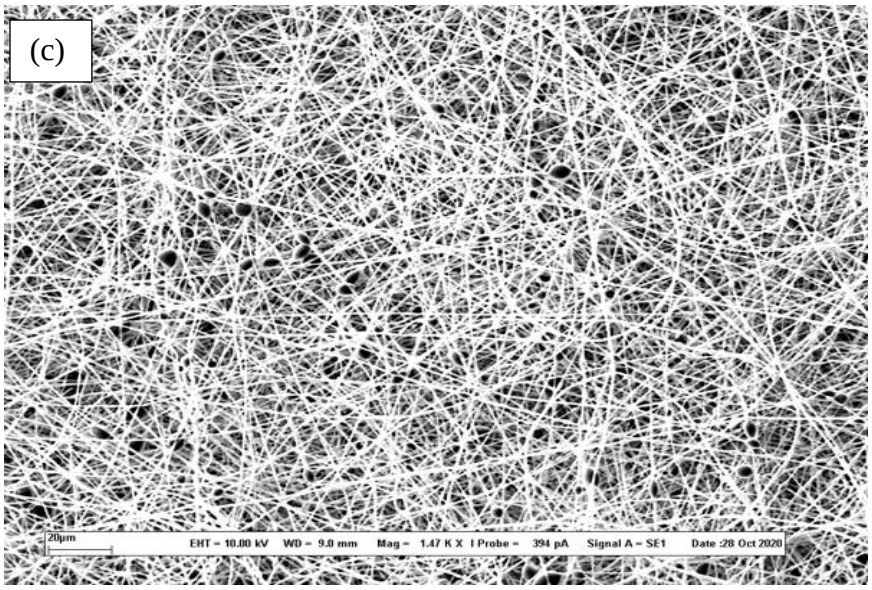
(c)
20µm
EHT = 10.00 kV WD = 9.0 mm Mag = 1.47 K X I Probe = 394 pA Signal A = SE1 Date :28 Oct 2020

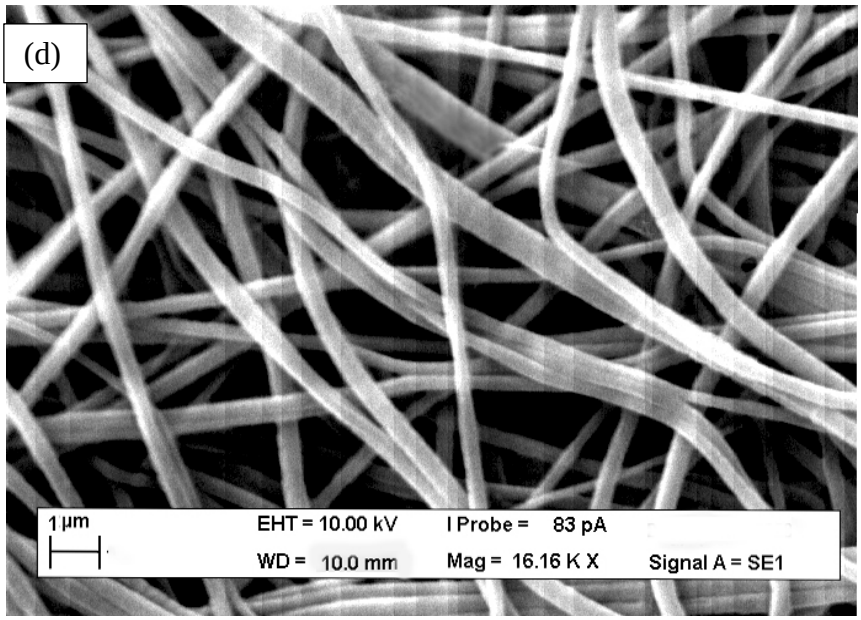
(d)
1 µm
EHT = 10.00 kV
I Probe = 83 pA
WD = 10.0 mm
Mag = 16.16 K X
Signal A = SE1

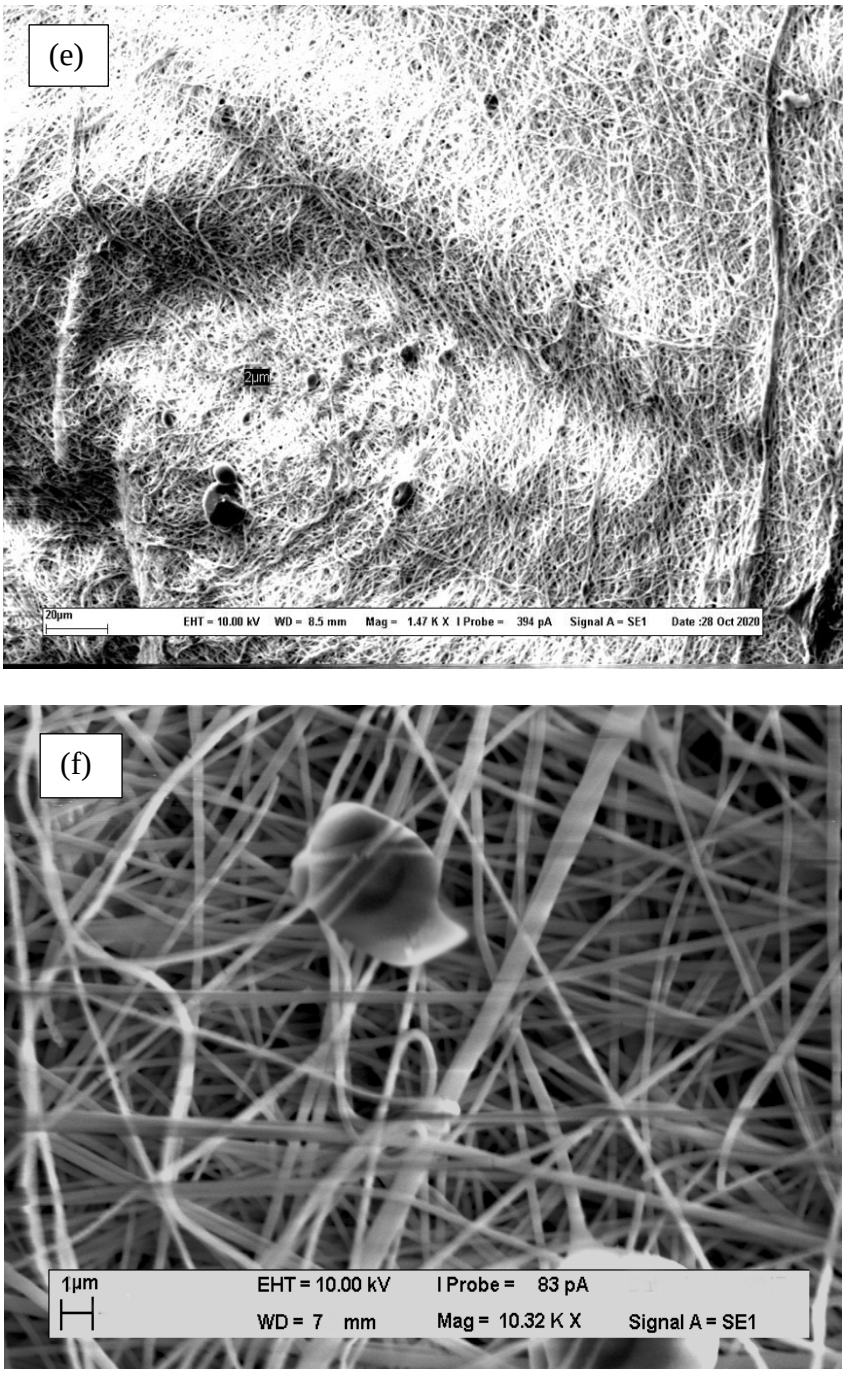

Fig. 4.2.7. SEM images of the electrospun fibers of (a) and (b) PVDF (fiber diameter: 200-300 nm); (c) and (d) PS (fiber diameter: 900 nm to 1.5 mm); and (f) PVDF/PS-Biochar 1%

Figure 4.2.8. shows SEM images of the middle layer fabricated via mono and co-axial electrospinning using rotatory drum collector. Figure 4.2.8 illustrates that, when the cylindrical collector rotates fast enough, around 10,000 rpm, nanofibers can be pulled along its perimeter and aligned within the cylinder.

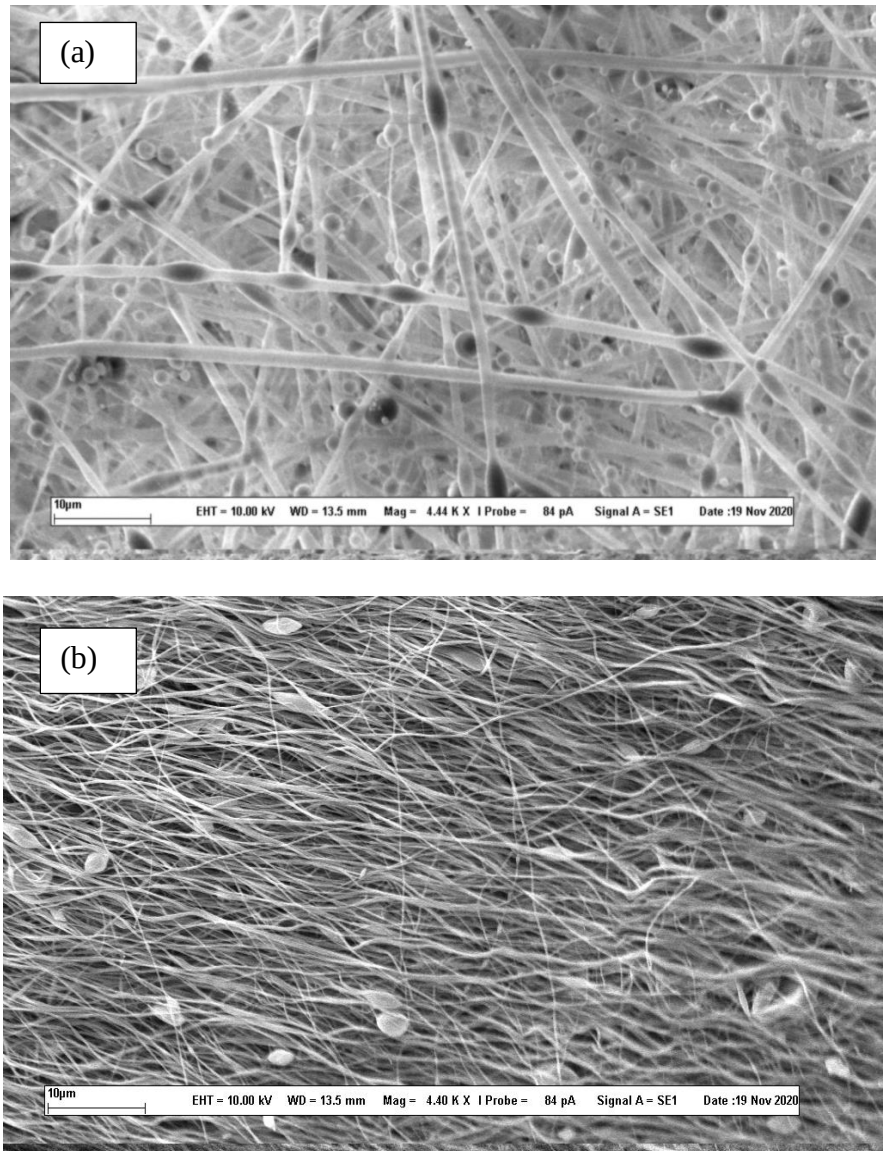

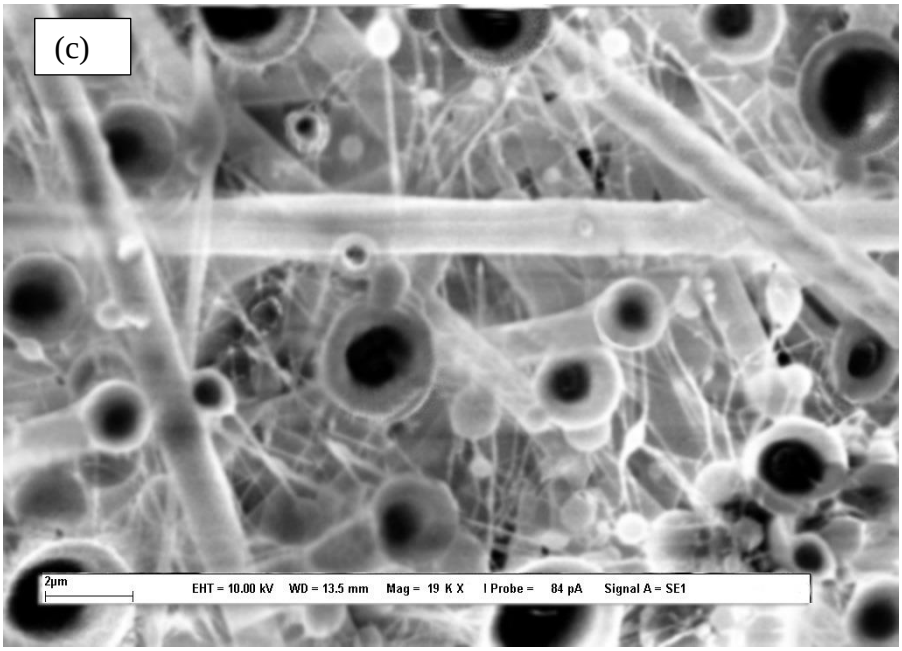

Fig. 4.2.8. SEM images of aligned co (a) and mono-axial (b) PAN fibers. (c) cross-section views of hollow nano-fiber (The appropriate entrapment of enzyme withinn the core of hollow nanofibers)

Through *in situ* encapsulation during coaxial electrospinning, it was possible to place enzymes inside the hollow nanofibers. A confocal laser scanning microscope (CLSM) was used to verify the uniform dispersion of the enzyme cocktail within the hollow nanofibers. (Figure 4.2.9).

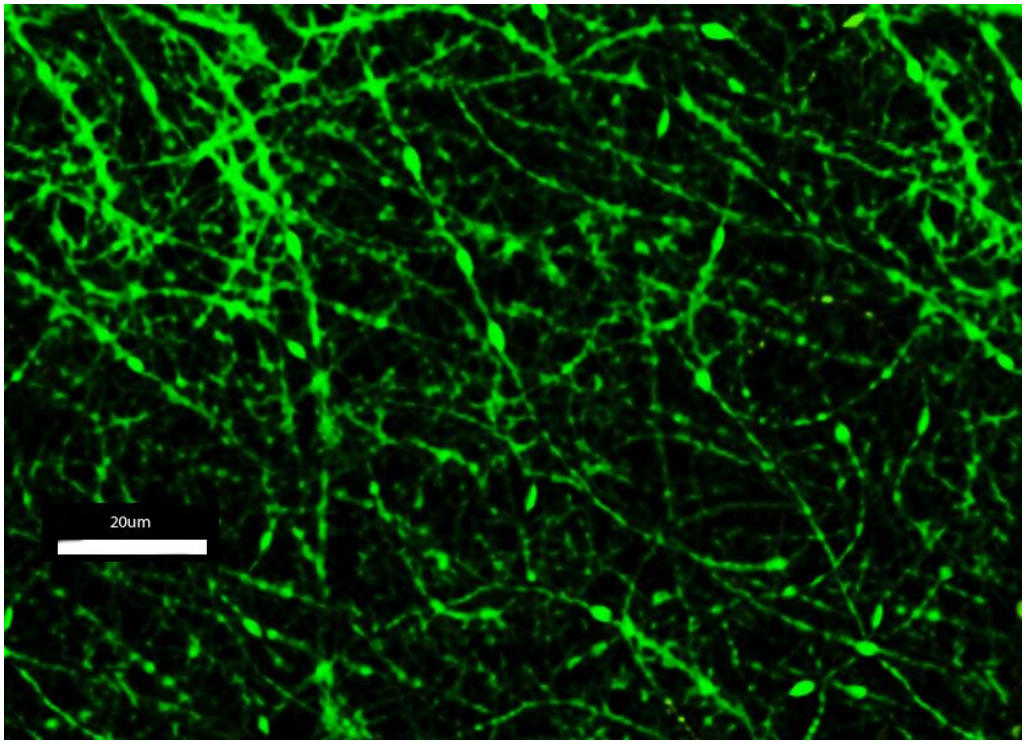

Fig. 4.2.9. Confocal microscopy images of CFSE-labelled enzyme cocktail capsulated within core-shell electrospun fibers (Uniform dispersion of enzyme solution within hollow nanofibers)

The chemical structure of PAN nanofibers in the middle layer was changed after modification and enzyme immobilization as confirmed by FT-IR presented in Figure 4.2.10. As can be seen in this Figure, the FT-IR spectra of PAN and the activated PAN demonstrate several peaks of functional groups. The most distinctive bonds of the nitrile groups (C≡N stretch; 2260 cm^{-1}) were shown in the FT-IR spectrum of PAN fibers. Following the chemical reaction of the matter, the intensity of the nitrile peak (2260 cm^{-1}) decreased and instead the characteristic peaks for the functional groups appeared at around 990 (N-H bond), 1390 (C-N stretch), 1600 (C-N bend), 1670 (C=N stretch) and 3300-3700 (O-H) cm $^{-1}$ 11. After enzyme immobilization, two peaks were observed in the FTIR spectrum of modified monPAN-EN which can be attributed to amide I (the vibration of the C=O bonds) and amide II (a combination of N-H vibration and C-N stretching in protein backbone) at 1565 and 1648 cm^{-1}, respectively. Thus, FTIR spectroscopy shows differences between the

samples including the enzyme solution and those without the enzymes making it easy to identify the encapsulated enzymes. Figure 4.2.10 shows the FT-IR spectra of the skin layer (PVDF/PS-biochar1%), PS, PVDF and biochar particles. As can be seen, PDF/PS- Biochar 1% spectrum is similar to the spectrum of the multilayer system.

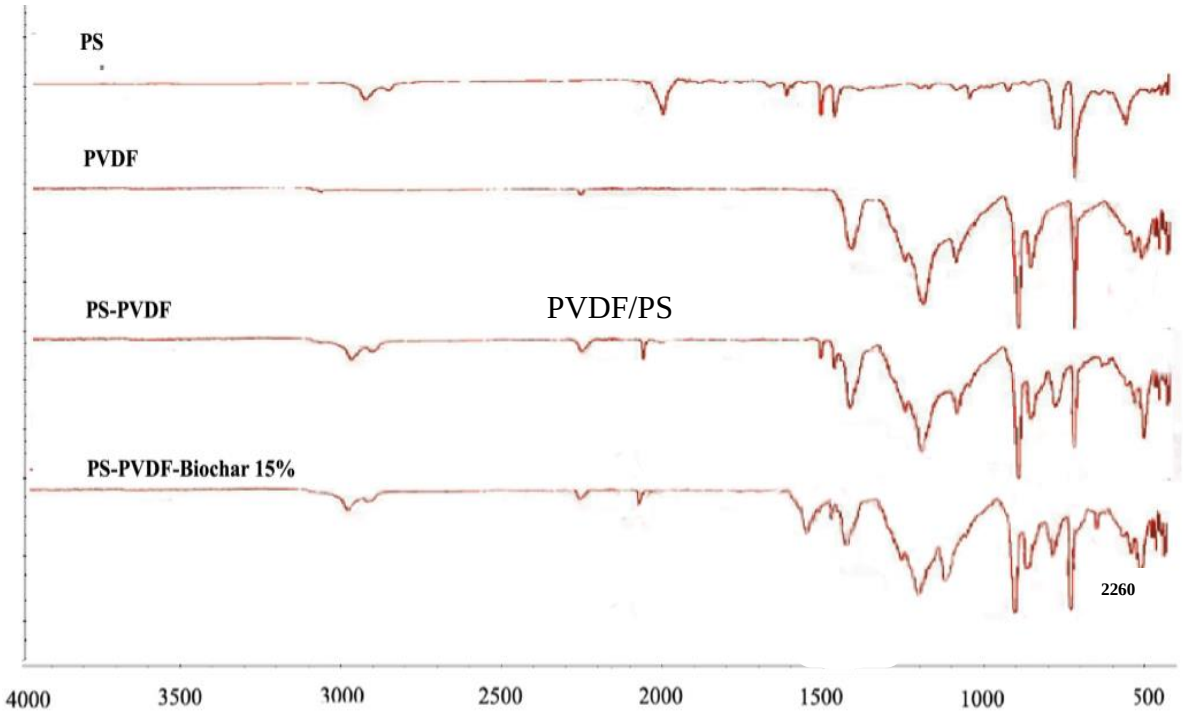

Fig. 4.2.10. IR spectra (FT/IR-410 Spectrometer) of skin layer

The fabricated electrospun nanofibers are used in this prototype as sorbents; thus, for sorbents to be compressed, they should possess a good mechanical property. Table 4.2.4 represents the mechanical parameters of electrospun nanofibers, including the representative stress-strain, Young's modulus, tensile strength, and elongation at break. As shown in Figure 4.2.11, after a sudden increase in pressure, PS nanofibers experienced a plastic behavior and a sluggish extension mode. These fibers have shown good hydrophobicity and good sorption capacity; however, the poor mechanical properties might cause a problem during the pick-up after oil absorption in the open water. Neat PVDF and PAN fibres showed a steep linear increase in the first 100 % strains, and then it reached a plateau until failure. Membranes made of PVDF have a wider elastic range and a steeper slope than those made from PAN and multilayer systems. As the PVDF sample had a greater plastic deformation and a higher mechanical strength in comparison with the rest of the membranes, the PVDF improved the mechanical properties of PS nanofibers and, thus, the mechanical properties of multilayer membranes. In other words, using the multilayer membranes fabricated by the two nozzle electrospinning process, the composite mats have been able to balance the strength of the individual components. Multilayer membrane generally shows an intermedia behavior between the PVDF, PAN and the PS. Two measurements were made of each sample, because measurements were difficult (sample breakage)

Table 4.2.4. Tensile parameters

	Young's modulus (N)	Maximum stress (N)	Strain at break (%)
PAN	7.41±0.13	55±1	67.9±3.1
PS	1.98±0.23	11.9±1.1	11.91±1
PVDF	4.78±1.09	67±3	150.9±4
PS-PVDF-biochar/monPAN-ENZ	3.93	50	103.4

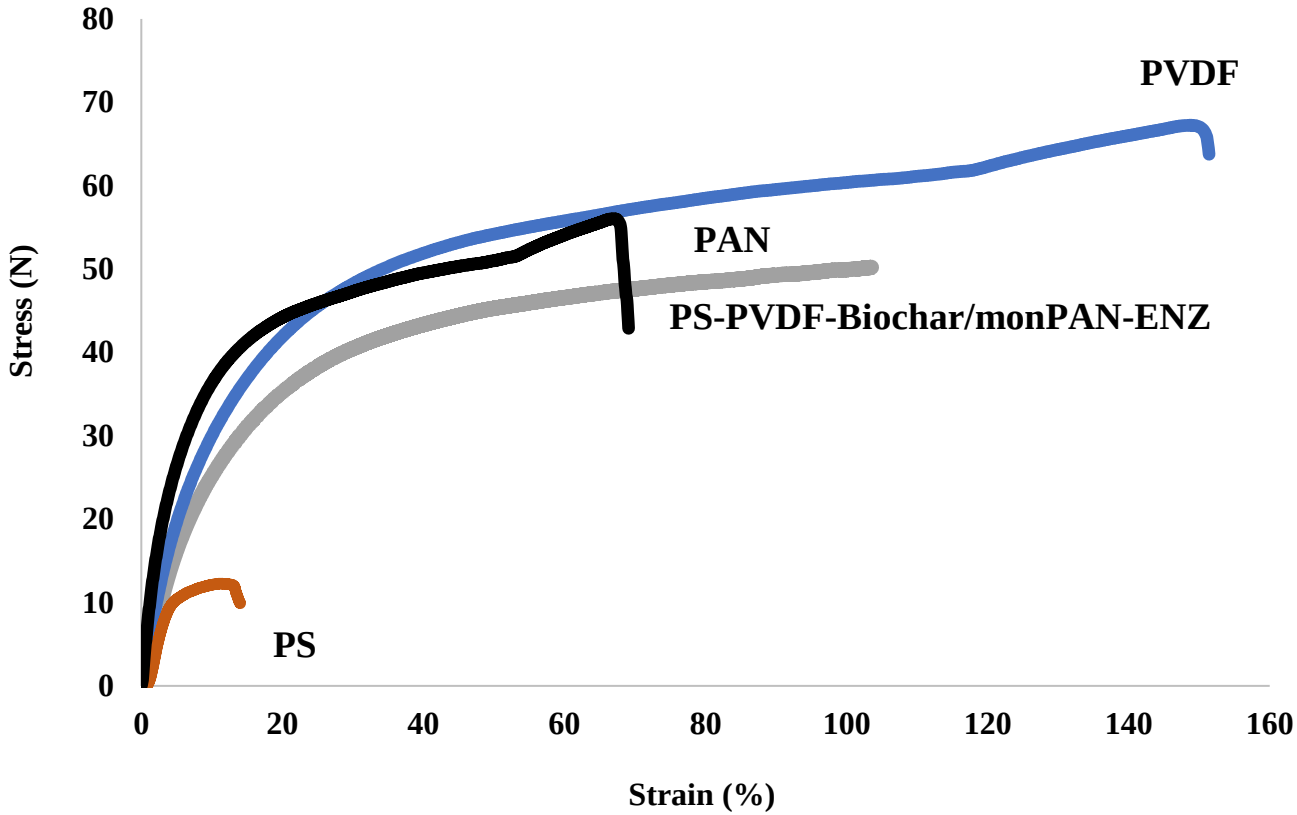

Fig. 4.2.11. Stress-strain curves (Multilayer membrane showing an intermedia behavior between the PVDF, PAN and the PS)

Characterization of the selected hollow fiber membrane (jellyfish tentacles)

The measured diffusion specification less than 2 SCCM/0.1 m^2 area showed that the selected module was intact. Figure 12 shows the plot of PAH model substrate (anthracene) concentration change in the internal recirculated solution vs the reciprocal flow rate to yield the quantity in Eq. (8).

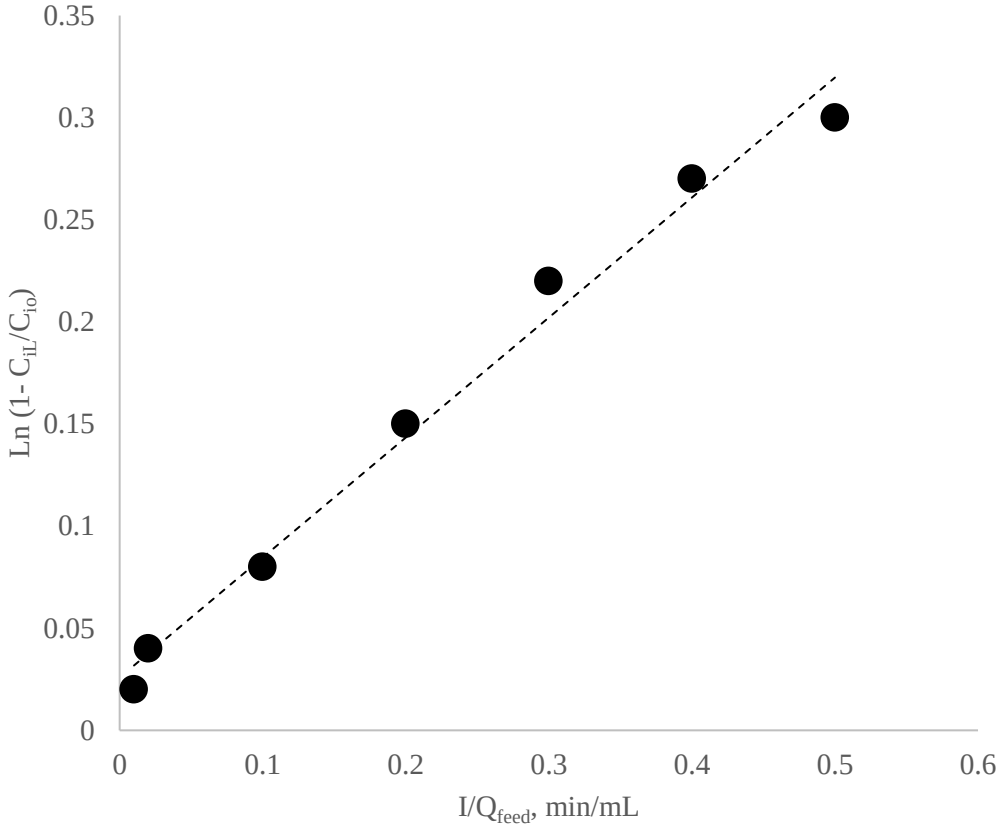

Fig. 4.2.12. Permeation data for naphthalene through hollow fiber in a single-fibre reactor at 15 ℃

The ratio of permeation coefficient for anthracene used as model substrate ($\times 10^{-3}\ s^{-1}$) to ultrafiltration velocity (5×10^{-3} -$7\times 10^{-3}\ cm^2 s^{-1}$) obtained in this section will be applied to determine the conversion rate of the substrate at different experimental conditions. The other important permeability characteristic of selected membranes under experimental conditions is

coenzyme retention that affect the performance of hollow fiber immobilized enzymes. The selected membrane reactor system benefits a high recycling speed (pumping rate from 0.2 mL/min to 200 mL/min) and it was assumed that in this reactor there are no steric problem for interactions between enzymes and coenzymes, and there is a force convection transport through the membrane of substrate. Figure 4.2.13 shows the retainment ratio of NAD+ retainment ratios in the presence of different concentration of NaCl and PEI.

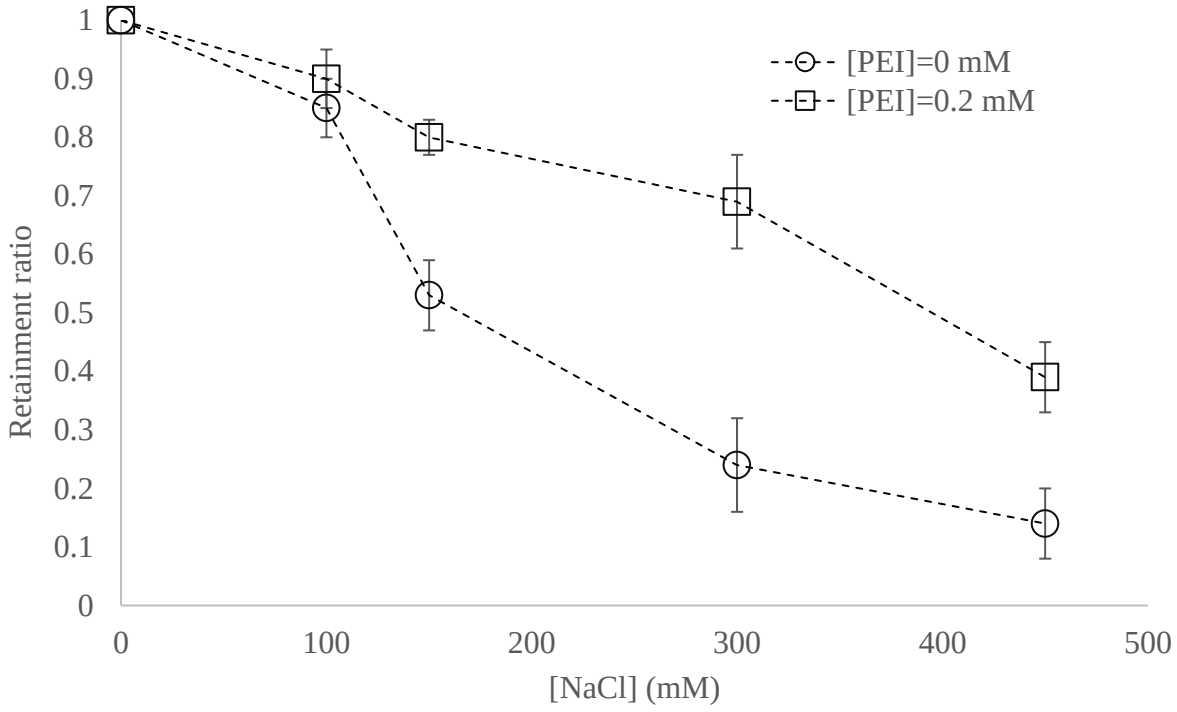

Fig. 4.2.13. Effect of PEI concentration on the retainment ratio of NAD+ in presence of different millimolar concentration of NaCl at 15 ℃

As shown in Figure 4.2.13, polyethyleneimine (PEI), a high molecular weight polymer, was present in the reaction medium, which resulted in improved retention ratios for the native coenzyme when NaCl concentrations were between 100-300 mM. The other consequence of the presence of PEI is the viscosity increase in the enzyme solution and subsequently a decrease of the

permeation flux. Our result shows that a 10% decline of flux with respect to the enzyme solution was determined by presence of 0.2 mM concentration of PEI.

Cyclic operation in membrane/enzyme reactor

The operation of a hollow fiber enzyme reactor in batch mode was studied to determine the effectiveness of ultrafiltration swing with respect to the amplitude and period of pulsatile flow. For the reactor operated in batch mode, the parameter L is set to zero. To compare the case with different parameters, performance equations were simplified as follows:

$$V_1 \frac{d(S_1)}{d\,\tau} = Le\ d\ (S_1 - f(\tau))\ \ \sin\ (\tau) \qquad (7)$$

$$V_2 \frac{d(S_2)}{d\,\tau} = -\ Le\ d\ (S_2 - f(\tau)) \sin\ (\tau)\ - \frac{\lambda^2 S_2}{\tilde{K}_m + S_2} \qquad (8)$$

In this analysis $\tilde{K}_m$ was set to 1. Figure 4.2.14 shows the simulation results of the anthracene concentration in compartments I and II decreasing with time for two different amounts of enzyme loading on the lumen side (changing λ^2). Initial substrate concentration is assumed to be 1mM, λ = 3.3, 16.5 and 33 corresponding to the enzyme activity of 4.7,1.5, and 0.47 U, respectively levels used experimentally. During the batch operation, when the ultrafiltration swing occurs, the parameter Le is larger than zero and the contribution by diffusion is negligible. As can be seen in Figure 14, increasing the enzyme concentration increases substrate concentration decay, both experimentally and theoretically. Moreover, substrate concentration in compartment I decays faster in the case of high λ which is the measure of reaction rate over diffusion rate. At λ^2 = 33, substrate concentration in the enzyme side nearly equals zero as the enzyme load increases; however, at λ^2 = 3.3 the decay does not follow the exponential decline curve. As can be seen in Figure 14, after 200 seconds ($\sim \mathbf{18.6}$) of circulating the enzyme solution (λ^2 = 33), 100% of anthracene in 1.5 L of 4.6 mg/l was removed from the beaker side. The good agreement between

predicted and measured rates means that the model well describes the recirculated hollow fiber reactor with ultrafiltration swing.

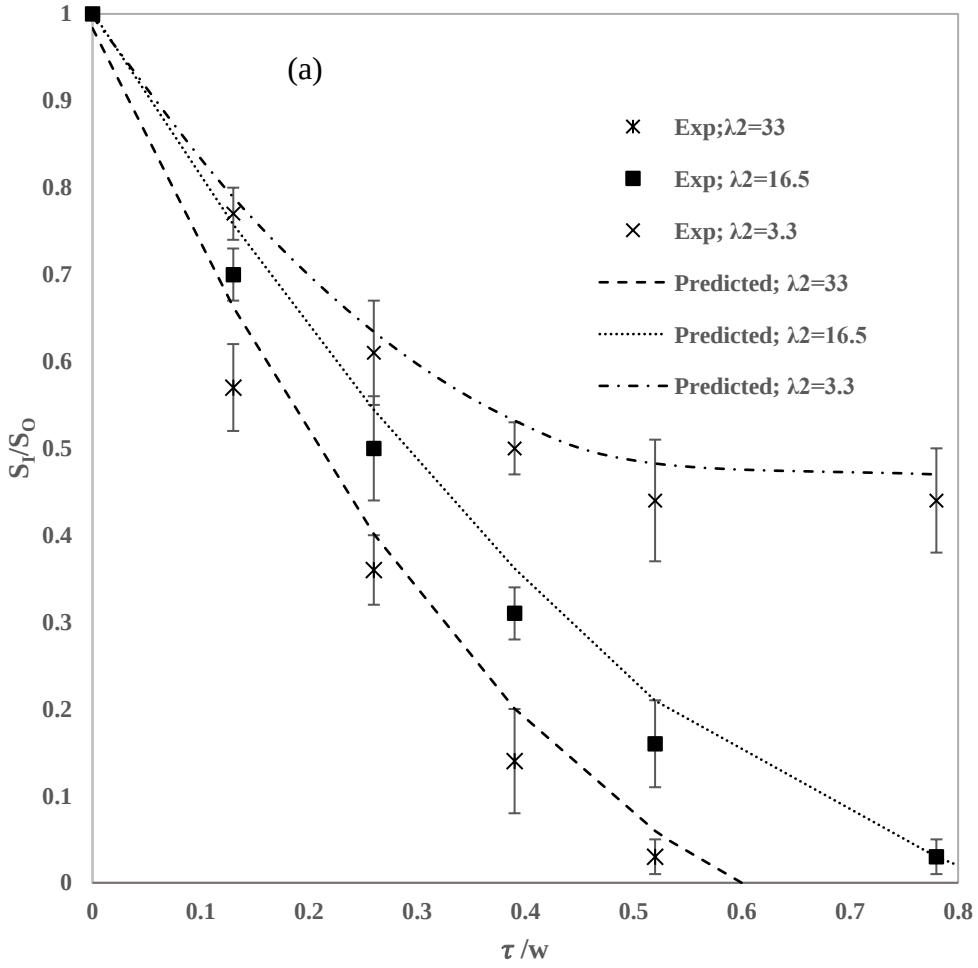

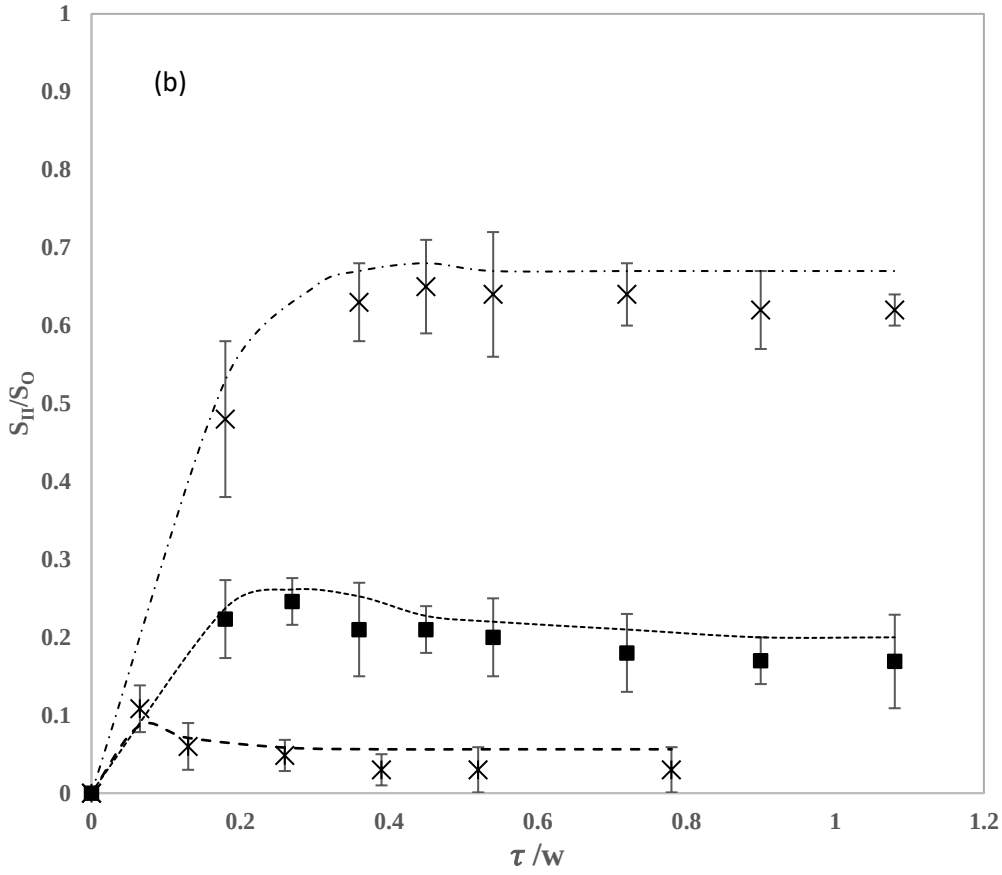

Fig. 4.2.14. Normalized concentration of anthracene in compartment (a) I and; (b) II at various λ^2. (W = 31, $\sigma = 1$, *Le* = 6, e change= 49 mL/(1/2T), Amplitude of inlet pulsatile flow 37 mL/min, 15 ℃)

The effect of amplitude of ultrafiltration swing (mL/min) and period of inlet pulsatile flow (s) was also examined in Figure 4.2.15 by studying the dependency of concentration decay on *Le* and *W*. The decay slope (e.g., $\frac{L_e}{2\pi W}$) is steeper as *Le* increases and W decreases because it results in a high-volume change in each compartment and the substrate reacts with the enzyme more easily.

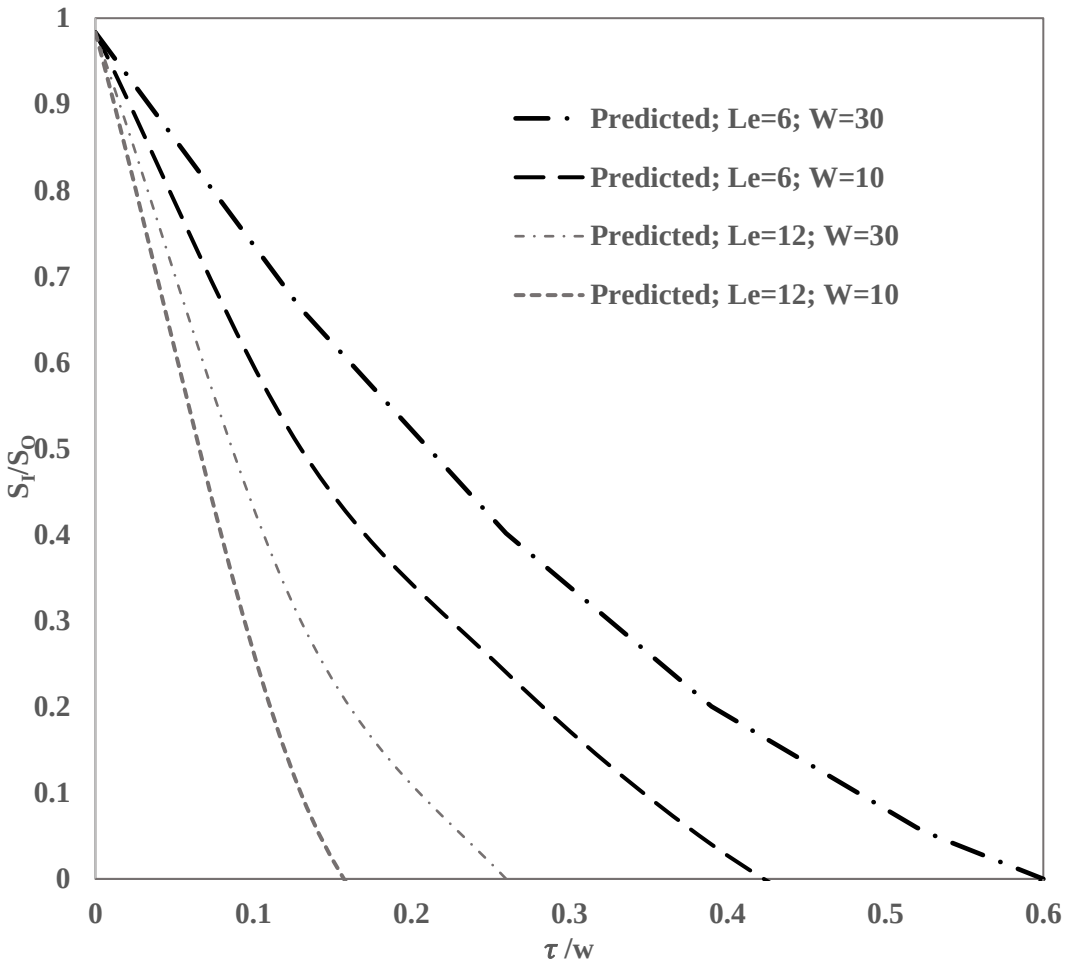

Fig. 4.2.15. Normalized concentration of anthracene in compartments I (λ^2=100; $\sigma = 1$, volume change= 49 mL/(1/2T), Amplitude of inlet pulsatile flow 37 mL/min, T = 45 s)

Removal/adsorption capacity is one of the main factors to compare the capability of different tools and processes for collecting or removing contaminants. The ratio of the volume of the treated water over the hollow fiber membrane surface area (A), can be applied to determine the maximum removal capacity of the system (Table 4.2.5). A greater V/A ratio and initial concentration of contaminant enhance the mass transfer driving force and lead to greater qm.

Table 4.2.5. PAH adsorption capacities of various tools (adsorbents and jellyfish-like device) and processes (adsorption and simultaneous ultrafiltration and biodegradation

Tool/Process	Contaminant	Initial concentration (mg/L)	V/m (L/g) or V/A (L / cm^2)	Surface area (cm^2/g)	qm (mg/g)	Refs
Jellyfish like device	Anthracene	4.5	0.06 L/cm^2	105	4.7	This work
Activated carbon (Soybean stalk)	Naphthalene	10	3.2 L/g	287	30	(Kong et al., 2011)
	Acenaphthene	3			8	
	Phenanthrene	1			3	
Activated carbon (Petroleum coke)	Naphthalene	0.25 - 6.5	1 L/g	925	12.5	(Yuan et al., 2010)
	Phenanthrene				4.3	
	Pyrene				1.5	

Performance of Jellyfish like device

To investigate the effect of electrospun nanofibers on the performance of the reactor system, it has been applied in a recycled hollow fiber enzyme reactor containing oil-water emulsion (e.g., water, anthracene, and lubricant oil) in compartment I (Figure 4.2.16). Figure 4.2.16 shows the removal of the substrate with and without using electrospun nanofibers. The addition of lubricant oil and the behavior of the emulsion filtration with the hydrophilic membranes when the emulsion passes through the membrane might change the apparent ultrafiltration velocity (cm min $^{-1}$) and volume change in each compartment.

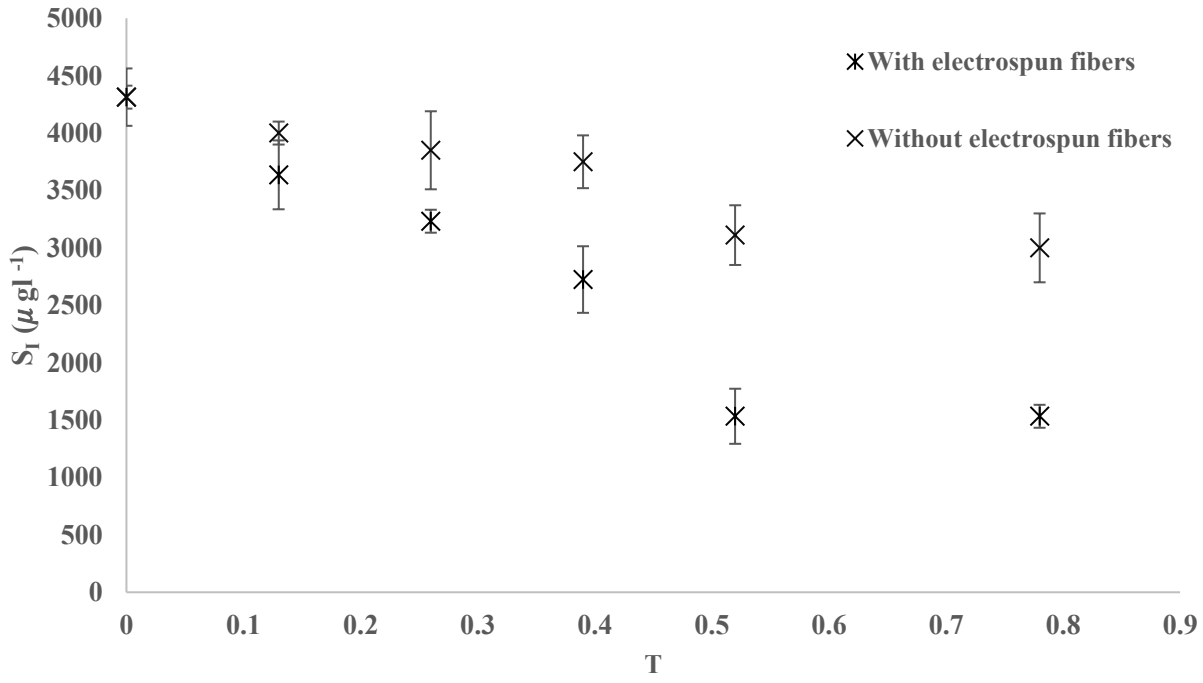

Fig. 4.2.16. Decrease of total anthracene concentrations with time for the device with and without electrospun fibers

Table 4.2.6 shows the volume change and the amplitude of inlet pulsatile flow change for different initial concentrations of lubricant oil for different systems.

Table 4.2.6. Effect of oil concentration and electrospun fibers on volume change

	Lubricant oil concentration % (v v^{-1})	Amplitude of inlet pulsatile flow (mL/min)	Volume change (mL/T/2)
With electro spun fibers	2.5	25 ± 5	37.6
	5.0		31.1
Without electro spun fibers	2.5		25.4
	5.0		21.4

The jellyfish-like device equipped with electrospun nanofibers with an oil sorption capacity of (10.8 can benefit the removal of oil particles loading before oil drops get to the surface of the membranes.

A great deal of effort has been made to decrease the tendency of membrane fouling through the application of different techniques to improve membrane properties (e.g., pore size, hydrophilicity, etc.) or pre-treatment of feed stream (e.g., flocculation and microfiltration (MF)). Thus, it is important to take care of the particle loading before the feed gets to the membrane units (Zuo and Wang, 2013).

The lack of devices and processes for large-scale bioremediation in marine cleanup represents an opportunity to monopolize the market. In this study, the feasibility of using an innovative process and tool for surface water cleanup was studied. However, further work is necessary to develop the device for large-scale application by taking into account major criteria for large-scale design and manufacturing, as well as economic evaluation of the technology.

4.2.4. Conclusion

The application of a jellyfish-like device for the removal of target contaminants from the aqueous environment was studied. The aliphatic degrading cocktail enzymes obtained from *A. borkumensis* were immobilized onto a homemade multilayer membrane system (PS-PVDF-biochar/PAN/ PS-PVDF-biochar) synthesized through an electrospinning technique. More specifically, the enzymes were encapsulated inside the hydrophilic modified PAN membrane, which was in turn protected by two hydrophobic PS-PVDF membranes. The PAHs degrading enzymes recycling in hollow fiber membranes were obtained from newly isolated *Pseudomonas* URS-6 from the coastal marine environment.

The Cyclic operation of hollow fiber enzyme reactor with and without electrospun membranes was studied in batch mode given dimensionless variables including dimensionless frequency (W), Damkohler number (λ^2), and dimensionless flow rate (Le). A general model containing convective flux for the reactor was confirmed by experiments and it theoretically shows the effect of dimensionless parameters on the contaminant concentration decay in the substrate compartment. The experimental results showed that after 200 seconds ($\sim \mathbf{18.6}$) of circulating the enzyme solution (W=31, λ^2 = 33), 100% of anthracene in 1.5 L of 4.6 mg/l was removed from the beaker side. The performance of the membrane/enzyme reactor was enhanced in the presence of electrospun fiber by decreasing the tendency of membrane fouling and increasing the volume change in the enzyme compartment by 48 %. Further experiments (e.g., pilot-scale test using a larger prototype and production of enzymes on larger scales) are under investigation to study the performance of the proposed device in continuous mode and evaluate this method for practical application. Additionally, other techniques, such as the use of crosslinking agents, will be

examined to prevent enzyme molecules from shedding into the hollow fiber nanopores to further improve the half-life of enzyme molecules circulating on the lumen side.

BRIDGE-3

Batch test experiments showed that the cocktail of selected could degrade 3 PAHs in soil p samples within 48h. *The next step was to prepare appropriate support (modified polyimide aerogel) for enzyme immobilization and test produced cocktail enzyme for in-situ bioremediation of anthracene (model substrate) contaminated water to confirm the potential application of the enzyme cocktail.* Enzyme loaded-aerogel as a fixed-bed column for the removal of polycyclic aromatic hydrocarbons provides novel insight into the application of aerogel base materials for water treatment and PAH removal with possibilities of scaling up for larger applications.

PART 3

4.3 Continuous fixed-bed column studies to remove polycyclic aromatic hydrocarbons by degrading enzymes immobilized on polyimide aerogels

Seyyed Mohammadreza Davoodi[1], Saba Miri[1], Satinder Kaur Brar[1*], , Richard Martel[2]

[1] Department of Civil Engineering, Lassonde School of Engineering, York University, North York, Toronto, Ontario Canada M3J 1P3.

[3] INRS-ETE, Université du Québec, 490, Rue de la Couronne, Québec, Canada G1K 9A9

(*Phone: 1 418 736 2100 ext. 55228; E-mail: satinder. brar@lassonde.yorku.ca)

Ecotoxicology and Environmental Safety

Abstract

The main sources of polycyclic aromatic hydrocarbons, entering aquatic environments are industrial discharges, petroleum spills, combustion of fossil fuels, urban runoff, and atmospheric deposition. For the biodegradation of polycyclic aromatic hydrocarbons (PAH), the use of biocatalysts, such as enzymes, is an environmentally friendly method. Despite this, it is necessary to immobilize the enzymes in order to facilitate their recovery and reusability, as well as to prevent their loss. Using covalent bonding, PAH degrading enzymes were immobilized on modified polyimide aerogels. Covalent immobilization of enzymes on modified polyimide aerogels resulted in around 9- and 6-fold lower enzyme leaching for naphthalene and catechol 2,3 dioxygenase enzymes compared to enzyme immobilization using adsorption. The Fourier Transform Infrared Spectrum (FTIR) confirmed the enzyme immobilization and aerogel modification. The effects of flow rate, size of aerogels and inlet concentration of anthracene on removal efficiency of pollutants were examined. Using the derived model as a basis for prediction, in terms of removal efficiency, the highest result was achieved to be 84.01% at flow rate of 22 mL min^{-1}, initial concentration of 34 mg L^{-1} and aerogel size 2 cm while under these conditions, the removal efficiency was experimentally measured to be 87.14 %. Enzyme loaded-aerogel as a fixed-bed column for the removal of polycyclic aromatic hydrocarbons provides novel insight into the application of aerogel base materials for water treatment and PAH removal with possibilities of scaling up for larger applications.

Keywords: polycyclic aromatic hydrocarbons; Enzymatic bioremediation; Fixed-bed columns

4.3.1. Introduction

There is a frequent threat of environmental contamination, OF including contamination of water bodies and soils by oil spills. This is particularly relevant for both the United States and Canada where the transportation of unconventional oils and traditional petroleum over long distances inland is accomplished by railways and pipelines. Moreover, during oil exploration, wastewater is generated that contains dissolved and dispersed oil, grease, salts, heavy metals, and other organic and inorganic substances (Zabbey and Olsson, 2017). Many aromatic hydrocarbons, polycyclic aromatic hydrocarbons, and heterocyclic compounds are present in petroleum products. Researchers have traditionally assessed the toxic effects of oil by measuring the concentration of polycyclic aromatic hydrocarbons (PAHs) since PAHs are often regarded as the most toxic fraction of oil. As a result, many water samples collected from the field during and after the oil spill were analyzed for these compounds (Davoodi et al., 2020).

Biocatalysts such as enzymes have an important role to play in industrial processes, biosensors, and biofuel cells (Çakmakçı et al., 2014). Good enzyme stability is a key requirement for these applications. The in vitro development of enzymatic cascade reactions has been inspired by biodegradation processes, in which multiple enzymes work together. The multi-enzyme immobilization could enhance the overall efficiency and specificity of the reaction, omitting the need to isolate intermediate products. The multi-enzyme immobilization recently been demonstrated on a few substrates such as magnetic particles. Our rationale is that ideal immobilization materials should be cost-effective, trap enzymes under mild conditions, allow easy substrate access, prevent enzyme leaching, and provide enzyme protection. Unfortunately, most of the above materials do not meet all these criteria (Kadri et al., 2018a). Most recently, Miri *et.al* studied the effectiveness of co-immobilization of cold-active enzymes involved in the biodegradation of monoaromatic hydrocarbons on micro/nano biochar particles. They showed that the immobilization of toluene dioxygenase and catechol 2,3 dioxygenase enhanced their storage and operational stability (Miri et al., 2021b).

Generally, it is necessary to develop an efficient method of immobilizing enzymes to facilitate their recovery and reusability while avoiding their loss (Simón-Herrero et al., 2019). Enzymes can be immobilized by several methods, including covalent, adsorption, crosslinking, encapsulation,

and entrapment (Rodríguez-Delgado and Ornelas-Soto, 2017). Most commonly, covalent attachment is used to prevent enzyme leaching and improve enzyme stability. Compared to other methods of immobilization, it is more stable within the reaction system and provides strong attachment. To maintain high activity, the structure of enzyme must be protected from the severe reaction conditions (Zucca and Sanjust, 2014). In addition, stable enzyme-matrix interactions are necessary as well as effective enzyme-matrix binding by increasing the affinity between the functional groups on the support and the enzymes (Zdarta et al., 2018b). Simón-Herrero *et.al* proposed the laccase-loaded polyimide aerogels for carbamazepine biodegradation to facilitate enzyme recovery and reusability (Simón-Herrero et al., 2019).

To achieve effective enzyme immobilization, support materials must be chemically and thermally stable, high affinity to biomolecules, insoluble in reaction conditions, biocompatible, contain reactive functional groups, regenerating and reusable, and readily available and affordable (Zdarta et al., 2018a). As inorganic supports are known to have several limitations, such as low affinity to enzymes, limited biocompatibility, and the limited possibility to create various organic materials and geometrical shapes such as synthetic polymers have increasingly been used as supports. Moreover, synthetic polymers have some advantages such as being tailored to meet the needs of specific enzymes and processes, they have some advantages. Many functional groups are present in these materials, such as trialkyl amines and hydrophobic alkyl groups, as well as epoxy, carboxyl, carbonyl hydroxyl, amine, and diol groups, facilitating enzyme binding and surface functionalization (Zdarta et al., 2018b). Nanoparticles can also be used to encapsulate enzymes. For example, Kadri et.al reported the entrapment of crude alkane hydroxylase and lipase enzymes into chitosan nanoparticles by the ionotropic gelatin method. However, nanoparticles may not be suitable for enzyme encapsulation due to their less porous structure, enzymes may have difficulty accessing substrates. However, polyimide aerogels have excellent thermal and mechanical properties, polyimide may be suitable support material for the enzyme immobilization (Murphy, 2016). Considering the benefits of polyimide aerogels as support materials for enzyme immobilization, they may be a promising alternative. Furthermore, the polyimide aerogels can be produced using an environmentally friendly freeze-drying process.

In this study, covalent immobilization of PAH degrading enzymes on modified polyimide aerogels was studied and the application of prepared immobilized enzymes in a fixed bed column was examined. The effect of inlet concentration and flowrate parameters upon the removal of target

pollutants was discussed to achieve an estimation of optimum values of the operational variables for efficient removal of pollutants through the fixed bed column.

4.3.2. Materials and Methods

Chemicals

This study used Poly (pyromellitic dianhydride-co-4,4′-oxydianiline) amic acid solution from Sigma-Aldrich to conduct the experiment. Glutaraldehyde (25%), methanol, and ethylenediamine were purchased from Sigma-Aldrich. The following analytical/microbiological grade chemicals were all purchased from Fisher Scientific (Ontario, Canada) for enzyme preparation: dichloromethane, tryptic soy broth/agar (TSB, TSA), KNO_3, NaCl, Ca_2CO_3, Na_2HPO_4, KH_2PO_4, NaOH, and HCl, yeast extract. Nutrient broth (NB) medium was purchased from Sigma-Aldrich Co. (USA). The strains used for enzyme production are newly isolated *Pseudomonas* URS-5, URS-6, URS-8 and *Rhodocucus* URS-10 (Davoodi et al.).

Production of the enzymes

PAH degrading enzymes were produced via multi-culture of psychrophilic *Pseudomonas*, and *Rhodococcus* strains as reported in previous work (Davoodi et al.). In brief, 50 mgL^{-1} of anthracene solution in methanol was mixed with autoclaved at 120 $\pm$1 ℃ nutrition broth in 50 mL Erlenmeyer flasks. After that, the inducers were inoculated with consortia including URS-6,8,10 incubated at 15 $\pm$1 ℃ for 2 days. For enzyme extraction, cells were harvested from the media after culturing by centrifugation (16,000 rpm for 4 min at 4 °C). The pellets with the biomass were resuspended in phosphate buffer, pH 6.5, and then sonicated on ice using an Ultrasonicator (Branson Ultrasonics Corporation, Danbury, CT, USA) at 22 and 30 kHz frequencies of ultrasounds for 10 min to obtain intracellular enzymes.

Preparation of polyimide aerogels

A solution of triethylamine (TEA) was first prepared in deionized water, before being stirred in an ultrasound bath. The TEA-water solution was then added with 3 wt % dried poly (amic acid) PAA, and the solution was stirred for a few minutes. Using the laboratory freeze-dryer, trays were filled with PAA/TEA-water solution, and they were then frozen at 60 °C and then sublimed under a vacuum to obtain PAA aerogel. Polyimide aerogel was obtained by thermal imidizing PAA aerogel

in a vacuum oven. The color has changed from white to bright yellow. The Fourier Transform Infrared Spectrum (FTIR) was used to confirm the thermal imidization.

Polyimide aerogel surface modification

In accordance with previous studies on polyimide aerogels, modifications were made to them (Simón-Herrero et al., 2019). Polyimide aerogels (1 g) were aminated by immersing in a 10% w/v solution of ethylenediamine in methanol for 1 hour. To remove residual ethylenediamine, the modified aerogel was immediately washed with methanol. In order to completely remove methanol from the modified aerogel, it was removed from the oven after 24 hours of drying at 60°C. Polyimide surface modification is illustrated in Fig 3.

Immobilization of enzyme on polyimide aerogel

At room temperature (20 ± 3º C) under vigorous stirring, surface-modified polyimide aerogels were immersed in a glutaraldehyde solution (25%). Then, distilled water was used to remove the unreacted glutaraldehyde from the aerogels. As a second step, glutaraldehyde-activated polyimide aerogels were dried at 60 °C for ten hours. Polyimide aerogels activated with glutaraldehyde were suspended in citrate-phosphate buffer (pH 6.0) containing a known amount of enzyme in 50 mL flasks. At room temperature, the covalent immobilization process was carried out over a period of 12 hours while shaking at 450 rpm. Figure 4.3.1 illustrates the process of immobilizing enzymes on polyimide aerogels. In addition to determining the enzyme activity in the supernatant, the activity of the enzyme was measured on immobilized polyimide aerogels.

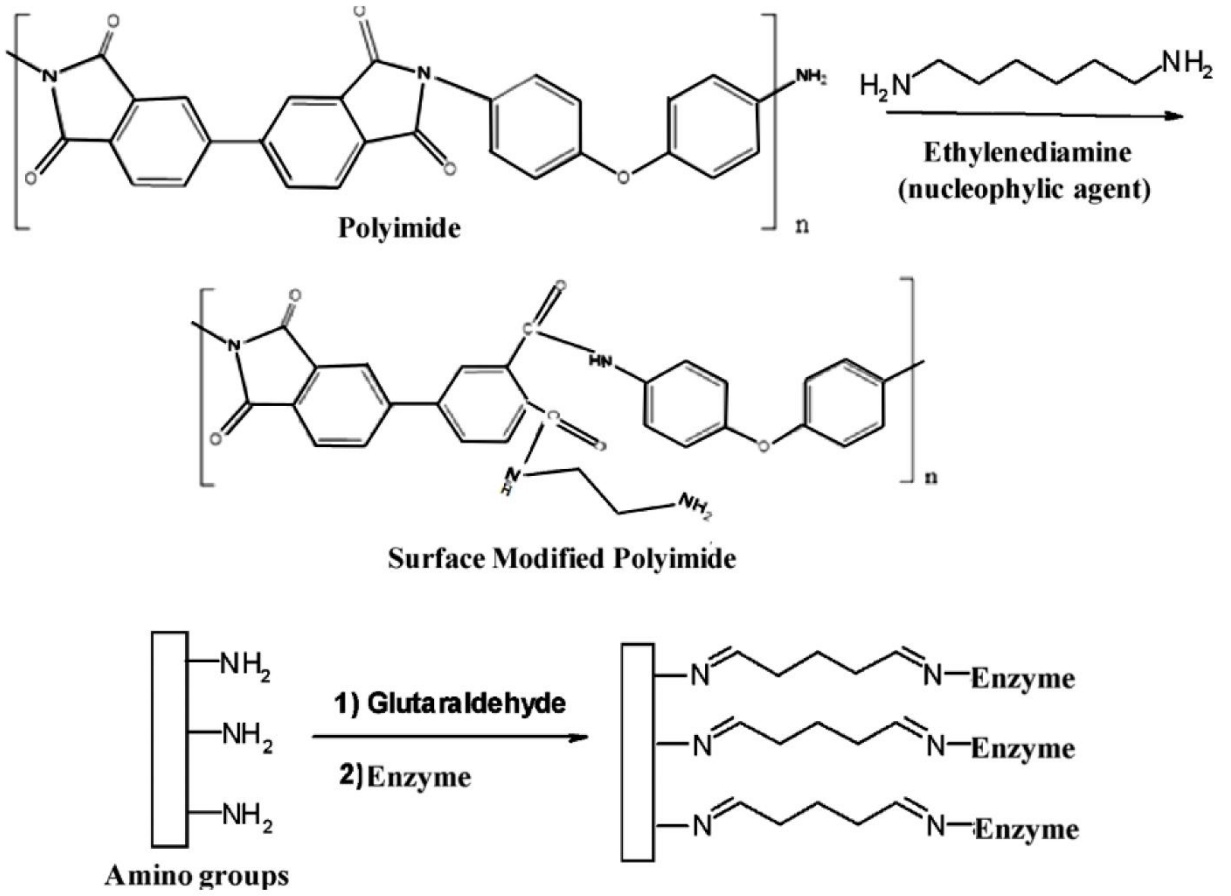

Fig. 4.3.1. Polyimide membrane surface modification followed by enzyme immobilization

For comparison, target enzymes were immobilized using adsorption. For this purpose, known amounts of enzyme solution were added to the citrate-phosphate buffer (pH 6.0) in which 1 g polyimide aerogels were suspended. For a period of 12 hours, the specimen was immobilized with shaking at 450 rpm at room temperature.

Enzyme assay

To obtain the enzyme solution for immobilization in polyimide aerogel, the crude extracts produced from promising consortia included intracellular enzymes (i.e., naphthalene dioxygenase (NDH), catechol 2,3 dioxygenase (C2,3D)) were characterized (Kadri et al., 2018a; Kadri et al., 2018b; Kadri et al., 2018c) by the spectrophotometric method as described in our previous work (Davoodi et al.). In brief, the activity of naphthalene dioxygenase was estimated by determining the formation of indigo at 500 nm per time unit. An enzyme reaction was carried out using 5 μl of indole 100 mM as a substrate in the presence of free enzyme solution or 1 g modified polyimide

aerogels after enzyme immobilization on its surface (separate tubes) and the reaction was performed at 15 ºC.

After measuring the activity of free and immobilized enzymes, immobilization and protein loading yields were determined for the evaluation of immobilization efficiency using Eqns. (1), and (2) as given below (Miri et al., 2021b):

$$Protein\ loading\ yield\ (\%) = \frac{Amount\ of\ protein\ loaded}{Amount\ of\ protein\ introduced} \times 100 \quad (1)$$

$$Immobilization\ \ yield\ (\%) = \frac{Amount\ of\ enzyme\ loaded}{Amount\ of\ enzyme\ introduced} \times 100 \quad (2)$$

Using 35 mg of immobilized enzymes in 1 mL of sodium phosphate buffer (pH 7.0), continuous stirring was performed for 48 hours. An enzyme activity test was performed by centrifuging the mixture at 16,000 g at 4°C, followed by the analysis of the supernatant (Davoodi et al.).

Anthracene degradation by NDH and C2,3D immobilized on polyimide aerogels

A batch test was conducted in contaminated water to evaluate the behavior of enzymes loaded on polyimide aerogels as materials to remove PAHs (i.e., anthracene) from aqueous media. In a 50-mL flask, a known amount of immobilized enzyme on polyimide aerogel was dispersed in 20 mL of anthracene solution (20 mg/L) and stirred at 200 rpm for 30 hours since previous tests indicated that after 24 hours, the removal rate was negligible. After decanting the supernatant (10 min and 11, 000 ×g), PAHs removal efficiency was determined using the initial and final aqueous phase concentrations. Additionally, 5 mL of methanol was mixed with the samples, and then they were sonicated for ten minutes for 10 minutes, and a 250-rpm incubation was carried out at room temperature for 8 hours to desorb PAHs from immobilized enzymes on polyimide aerogels.

Fixed bed column system (FBCS)

To study the degradation rate of anthracene by enzyme-bound aerogel, a continuous FBCS was planned and built. Test columns were composed of Teflon tubes with an inside diameter of 51 mm and a length of 151 mm. Figure 4.3.2 illustrates a schematic diagram of an FBC system. As can be seen in the Figure, there is a small tube located at the center of the spiral baffle that extends the entire length of the column and baffle. In the FBCS, PAH-contaminated effluent was pumped at a constant flow rate. As a result of an experimental design based on the response surface method (RSM), the impact of initial anthracene concentration was investigated, aerogel size and flow rate during the continuous degradation process.

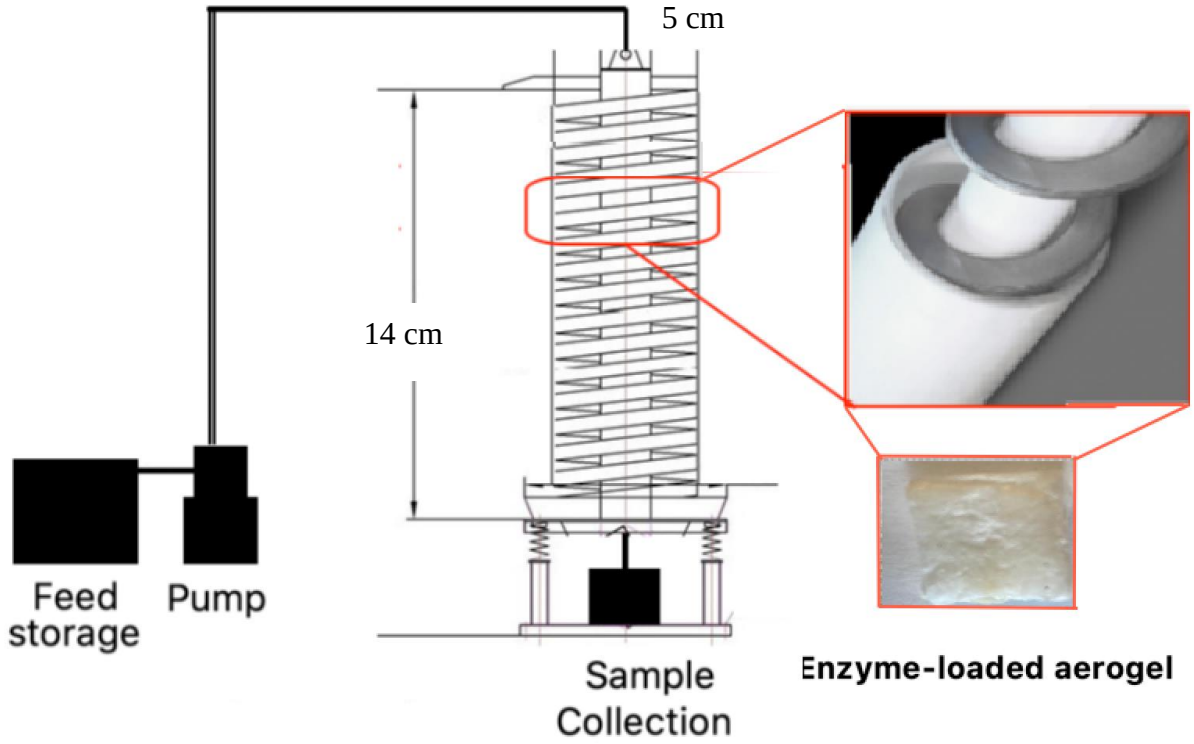

Fig. 4.3.2. Schematic diagram of fixed-bed column

Removal capacity is the FBC analysis by mathematical equations

The anthracene removal efficiency of the enzyme-loaded aerogel and capacity of aerogels were studied by measuring both the influent (C_0) and effluent concentrations of the target pollutant as a function of time, breakthrough point ($\frac{C_{t,out}}{C_o} = 0.5$) and saturated point $\left(\frac{C_{t,out}}{C_o} = 0.95\right)$. The breakthrough time is calculated by numerically integrating the area above the breakthrough curve Eq. (3)

$$m_{removal} = \frac{Q_f C_o}{m_B} \int_{t=0}^{t=t_{total}} (1 - \frac{C_{t,out}}{C_o})\, dt \qquad (3)$$

Where m_B represents mass adsorbent. During each experimental run, the breakthrough curve is derived from the concentration versus time data collected during the experiment. An investigation of the performance of a fixed bed treatment column was conducted using a breakthrough curve. This curve is a plot of the duration of the test against the anthracene concentration in the effluent stream of target contaminant dispersed in water (Davoodi et al., 2021).

Experimental design

The Response Surface Methodology (RSM) was used to optimize experimental conditions and reduce the number of experiments. Experiments were conducted based on the Box-Behnken (BBD) method with three independent variables, coded at three levels between − 1, 0, and + 1. In comparison to other experimental designs, BBD is often considered to be more efficient. BBD method is one of these methods, which is a quadratic design based on incomplete three-level design. Using this method, it is possible to estimate the value of the features in a quadratic model, designing the necessary experiments, and provide the values of the characters. Based upon the repetition of the center point and the hypothetical points at the midpoint of each side of the cube, this design might be described as a cube design with points at the midpoint of eachside. As a result of this design, it is possible to model the response by fitting a second-order polynomial, which can be expressed as follows:

$$Y = \beta_0 + \sum \beta_i X_i + \sum \beta_{ii} X_i^2 + \sum \beta_{ij} X_i X_j \quad (4)$$

This model consists of a constant and a linear coefficient, a binary interaction coefficient, and an interaction coefficient between the input variables Xi and Xj (Zhong and Wang, 2010). Based on Eq.5, the above equation can be expressed as a matrix:

$$Y=bX+\varepsilon \quad (5)$$

It is calculated by formulating the parameter Y as a vector of the measured values, along with the parameters X as a vector of independent variables. Matrix b is the coefficient matrix, and the parameter X represents the vector of the errors in the experiment. Using the matrix method, Eq.6 can be solved as follows:

$$b = (X'X)^{-1}X'Y \quad (6)$$

X' represents the transposition of X, and $(X'X)^{-1}$ represents the inverse of the matrix (X'X) (Aslan and Cebeci, 2007). As a result of the Box-Behnken method, Eq. 7 is used to determine the number of experiments.

$$N = w^2 + w + n \quad (7)$$

W represents the number of test factors, and n represents the number of iterations around the center point. Coded values are related to real values in the following manner:

$$x_i = \frac{X_i - X_0}{\Delta X_i} \quad (8)$$

In the example, χ_i and X_i are the encoded and real independent values, X_0 is the real value of the independent variable at the center point, and ΔXi is the step change of Xi (Amenaghawon et al., 2013). In order to estimate pure error, the experiment was conducted with three central points in 15 runs. As shown in Table 4.3.1, the BBD was employed to determine the relationship between the obtained results of removal efficiency and operational variables including inlet concentration (X_1), aerogel size (X_2), and flow rate (X_3).

Following the development of the model, a sensitivity analysis should be conducted to determine how different values of these parameters affect the output. As illustrated in the following equations, the sensitivity of removal efficiency can be determined by considering the change in the value of operating parameters including aerogel size, flow rate and initial concentration from ± 2 % to $\pm 30\%$.

$$Sen_1(\%) = \left| \frac{Removal\ efficiency\ (Aerogel\ size \pm 30\%, F, C_O) - Removal\ efficiency\ (Aerogel\ size, F, C_O)}{Removal\ efficiency\ (Aerogel\ size, F, C_O)} \right| \quad (9)$$

Characterization of aerogels

For the analysis of chemical interactions in polyimide aerogels following surface modification and enzyme immobilization, FT-IR spectra were recorded with a Nicolet IS50 FT-IR Spectrometer from Thermo Scientific (USA) (Simón-Herrero et al., 2019).

Analytical methods

The tricyclic aromatic hydrocarbon anthracene was found in high concentrations in the upper water column under floating oil following the spill (Forth et al., 2021). In order to determine the factors that affect the biodegradation potential of PAHs in the environment, anthracene is used as a prototypical PAH (Moody et al., 2001). GC-MS analyses (Agilent model 6890 GC, 5973 MSD) were conducted on specific days following the crude oil spill to confirm the release of anthracene into the water as well as the biodegradation of anthracene in the presence of pre-selected strains and enzyme solutions as described elsewhere (Li et al., 2021a).

Statistical analyses

To evaluate the effect of independent variables on response performance (anthracene removal efficiency), and to predict the optimal response value, Design Expert® software Trial

Version11.0.3.0 (Stat-Ease Inc., Minneapolis, MN, USA) was employed as an RSM based on the Box-Behnken design (Miri et al., 2022).

4.3.3. Result and Discussion

Figure 4.3.3 illustrates the FT-IR spectra of PAA, polyimide, aminated polyimide, glutaraldehyde-attached polyimide, and enzyme-immobilized polyimide.

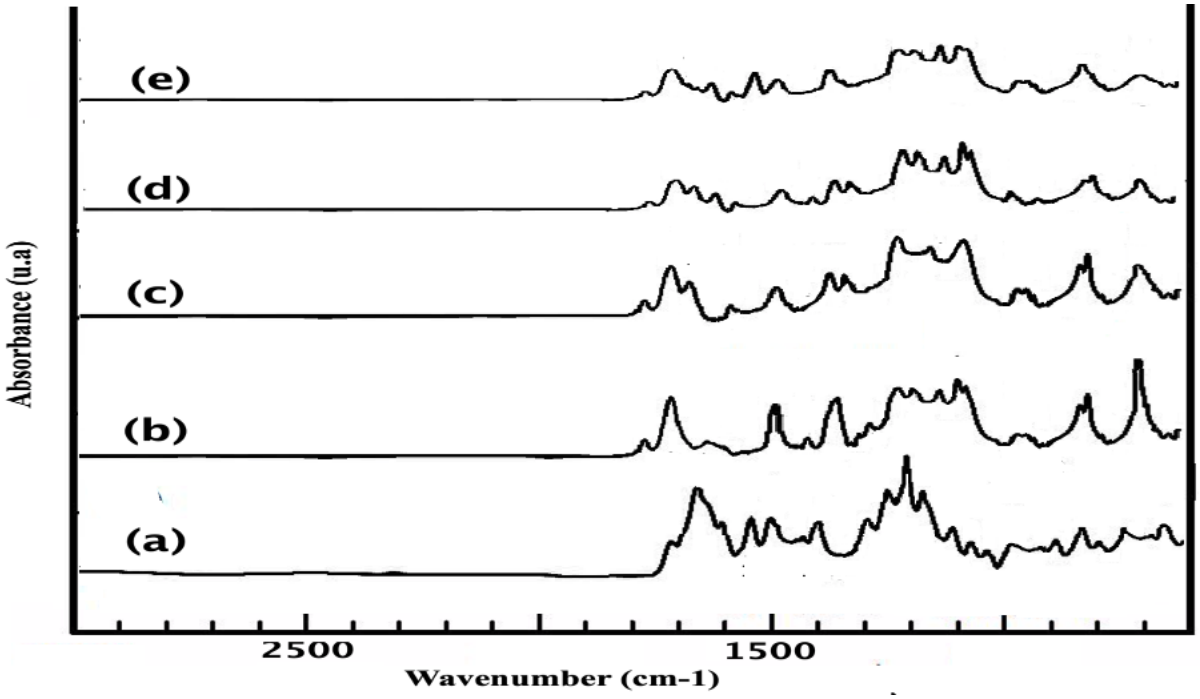

Fig. 4.3.3. FTIR spectra of a) PAA b) Polyimide aerogel; c) Aminated polyimide aerogel; d) Aminated polyimide aerogel activated with glutaraldehyde and e) Enzyme Immobilized on polyimide aerogel

At 1685 cm^{-1}, PAA displays the characteristic NHCO peak. A characteristic imide absorption band has been observed in polyimides after imidization at 740 cm^{-1}, 1368 cm^{-1} and 1780 cm^{-1} representing imide IV (bending vibration of cyclic C=O), imide II (C-N stretching vibration), and stretching vibration of cyclic C=O (imide I), respectively (Fig.3. (b)) (Kim et al., 2013). The amination reaction between ethylenediamine and the polymeric support material, and the subsequent creation of amino groups resulted in the formation of new peaks at 1690 cm^{-1} as can be seen in Figure 4.3.3. (c). During the formation of polyimide, reaction between amine nucleophilic agent and electrophilic imide group, leading to the opening of the imide ring and the formation of an amide (Çakmakçı et al., 2014). As a next step, glutaraldehyde was used to activate

amino groups on the surface of polyimide to facilitate enzyme bonding. This spectrum indicates amide bonds formation because of imide rings cleavage on polyimide surface and the reaction between HMDA's amine groups with the carboxyl group of the imide ring at 1650 cm^{-1} (cracking) and 1546 cm^{-1} (bending) (Çakmakçı et al., 2014). An imide peak is observed in the spectrum of aminated polyimide aerogels activated with glutaraldehyde. This peak was attributed to the interaction between amino groups and glutaraldehyde. In addition to the carbonyl band disappearing after immersion in glutaraldehyde, a new peak was observed at 1659 cm^{-1} after the sample was exposed to glutaraldehyde. As a result of the reaction between glutaraldehyde and free amine groups, It was believed that this band was caused by newly formed imine groups (Schiff-base).

The amide I and II bands of enzymes immobilized on polyimide aerogel were observed at 1510 cm^{-1}. The amide I at 1650 cm^{-1} was primarily attributed to stretching vibrations C=O and the amide II at 1510 cm^{-1} was attributed to stretching vibration CN and bending vibration NH in loaded enzymes. Consequently, amination, activation, and immobilization have been successfully accomplished (Simón-Herrero et al., 2019).

Enzyme immobilization on polyimide aerogel

As mentioned previously, the strains used for enzyme production are newly isolated *Pseudomonas* URS-5, URS-6, URS-8 and *Rhodocucus* URS-10 as described in detail in our previous work (Davoodi et al.) . The cell extracts obtained from co-culture contains four different types of enzymes involved in PAHs degradation including dioxygenase, hydroxylase, aldehyde dehydrogenase, decarboxylase (Miri et al., 2022). In this study, the performance of immobilization of two key enzymes including naphthalene and catechol 2,3 dioxygenase were studies. Cell extract from newly isolated strains showed high activity of naphthalene and catechol 2,3 dioxygenase. Naphthalene dioxygenase is the key enzyme involved in the initial attack (upper pathway) on anthracene after which anthracene is converted to metabolites (ring oxidation products). Catechol dioxygenase is able to open the ring with an oxidative cleavage and produce ring cleavage products (lower pathway) (Parales et al., 2000).

A variety of immobilization methods were used to immobilize PAH degrading enzymes onto polyimide aerogels. Table 4.3.1 shows loading of total protein, specific activity and their yield for adsorption and covalent methods. Results suggest that the bound enzymes were active after the immobilization. As can be seen in Table 4.3.1, covalent immobilization gave the highest

immobilization yield for total protein. Also, it was observed that for adsorption immobilization, less than 23% of the total protein was immobilized. The leaching of enzymes from covalently immobilized enzymes was less than 13% for both target enzymes after 1 h of incubation in turn results in immobilized enzyme stability and subsequent reusability in aquatic media. Thus, comparing the leached enzyme immobilized in modified and unmodified polyimide aerogels showed that covalent bonding prevents leaching and improves enzyme stability (Miri et al., 2021b; Simón-Herrero et al., 2019).

Table 4.3.1. Immobilization of naphthalene and catechol 2,3 dioxygenase on polyimide aerogel

Immobilized method	Total protein loaded (μg/ml)	Total protein loading yield (%)	Naphthalene dioxygenase activity (U/mg protein)	Naphthalene dioxygenase immobilization yield (%)	Catechol dioxygenase activity (U/ml)	Catechol dioxygenase immobilization yield (%)	leached naphthalene dioxygenase (%)	leached catechol dioxygenase (%)
Adsorption	9.1± 0.5	23.1± 1.5	22.8± 1.0	10.2± 0.8	15.1±0.8	28.1±1.3	81.7±1.2	69.4±1.6
Covalent	53.1± 1.3	71.3± 0.2	41.2± 0.1	74.9± 2.3	29.1±1.9	71.1±0.8	9.1± 0.5	12.1±0.5

Storage stability

Residual activities of free and immobilized enzymes were determined for up to 16 days at 20 °C. An important aspect of ensuring a long shelf life of an enzyme is its ability to maintain its stability during storage. Enzymes in their free form are generally unstable during storage, and their activity gradually decreases (Miri et al., 2021a; Miri et al., 2022; Miri et al., 2021b). Fig 4.3.4 presents the results. The results indicated that the immobilized enzymes on polyimide aerogels demonstrated better storage stability than corresponding free enzymes after 16 days of storage. Naphthalene and catechol 2,3 dioxygenase activity were reduced by 19% and 27% for immobilized enzymes and 60% and 73% for free enzymes during the first storage period (6 days). In addition, free naphthalene, and catechol 2,3 dioxygenase have shown a 96% and 81 %reduction in activity after 16 days of storage, while immobilized enzymes shows a 58% and 39% reduction in activity after 16 days.

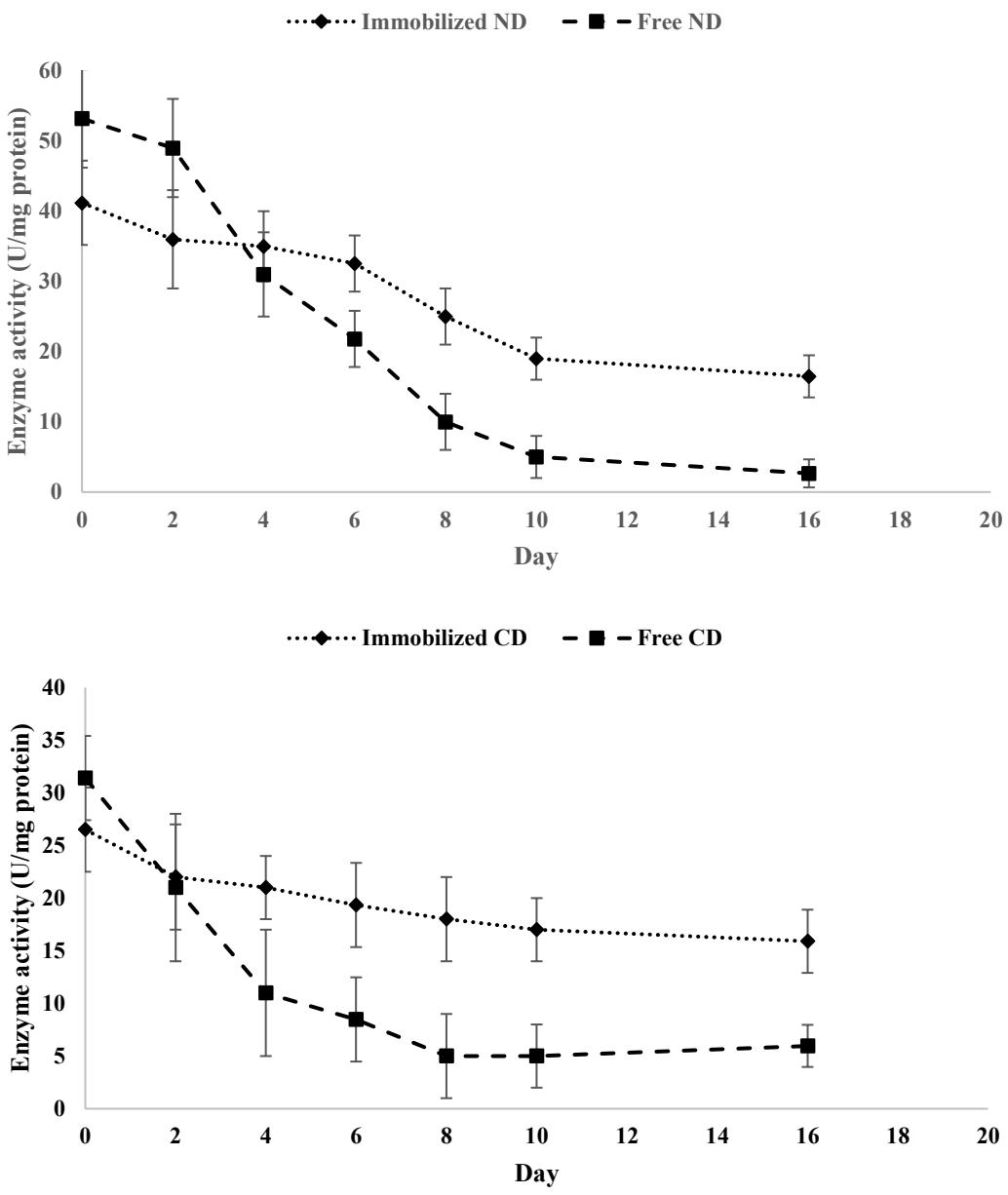

Fig. 4.3.4. Effect of time on activity of free and immobilized: (a) naphthalene dioxygenase and, (b) catechol dioxygenase.

Effect of operating parameters on breakpoint time

Effect of inlet concentration

The influence of influent PAH concentration (10, 30, 50 mg L^{-1}) upon the degradation efficiency of the fixed bed column containing the aerogel specimens was examined. As illustrated in Figure 4.3.5a, an increase in the inlet anthracene concentration from 10 to 30 mg L^{-1}, which can influent contact time, results in the increase in removal capacity of the column from 4.9 to 27.3 mg g^{-1}. In this case, the probability of contaminant contacting enzymes increased with an increase in initial anthracene concentrations, and the driving force and the rate at which anthracene passed across the boundary layer from the bulk solution to the particle surface. However, to avoid many contaminants in the outlet at high concentrations of anthracene that resulted in a lot of unused capacity, 30 mg L^{-1} was considered as desired concentration (Davoodi et al., 2021; Lonappan et al., 2019).

Effect of flow rate

The contact time between the surface of enzyme loaded aerogels and the solute is determined by this parameter; thus, it plays an important role in the design of a fixed bed column. Figure 4.3.5. illustrates the effect of flow rate on the breakthrough curve following the arrival of contamination and retardation of anthracene following the plug flow pulse (Davoodi et al., 2021). Two phenomena usually occur as the flow rate decreases: 1) the flow was travelling less quickly, so it would be delayed, and 2) the column becomes saturated after breakpoint time (Davoodi et al., 2021). Based on our results, the breakpoint time decreased from 432 to 245 min as the feed flow rate increased from 15 to 25 $mLmin^{-1}$, while the removal capacity decreased from 27 to 21 mgg^{-1} (22% decrease).

Effect of aerogel size

For columns with a constant flow rate of 15 ml min^{-1} and initial anthracene concentration of 10 mg l^{-1}, Figure 4.3.5 illustrates the effect of enzyme-loaded aerogel size on the distribution of anthracene concentration at effluent and arrival time. The cubic aerogels are considered 2, 3 or 4 cm in length.

Changing the particle size might have a significant impact on the amount of surface area that can be achieved and number of loaded enzymes. Our results showed that as the size of cubic aerogels decreased the breakpoint time increased from to min and the breakthrough curve steepness

increased which is favorable for fixed bed columns. the probability of contaminant contacting enzymes increased with an increase in initial anthracene concentrations.

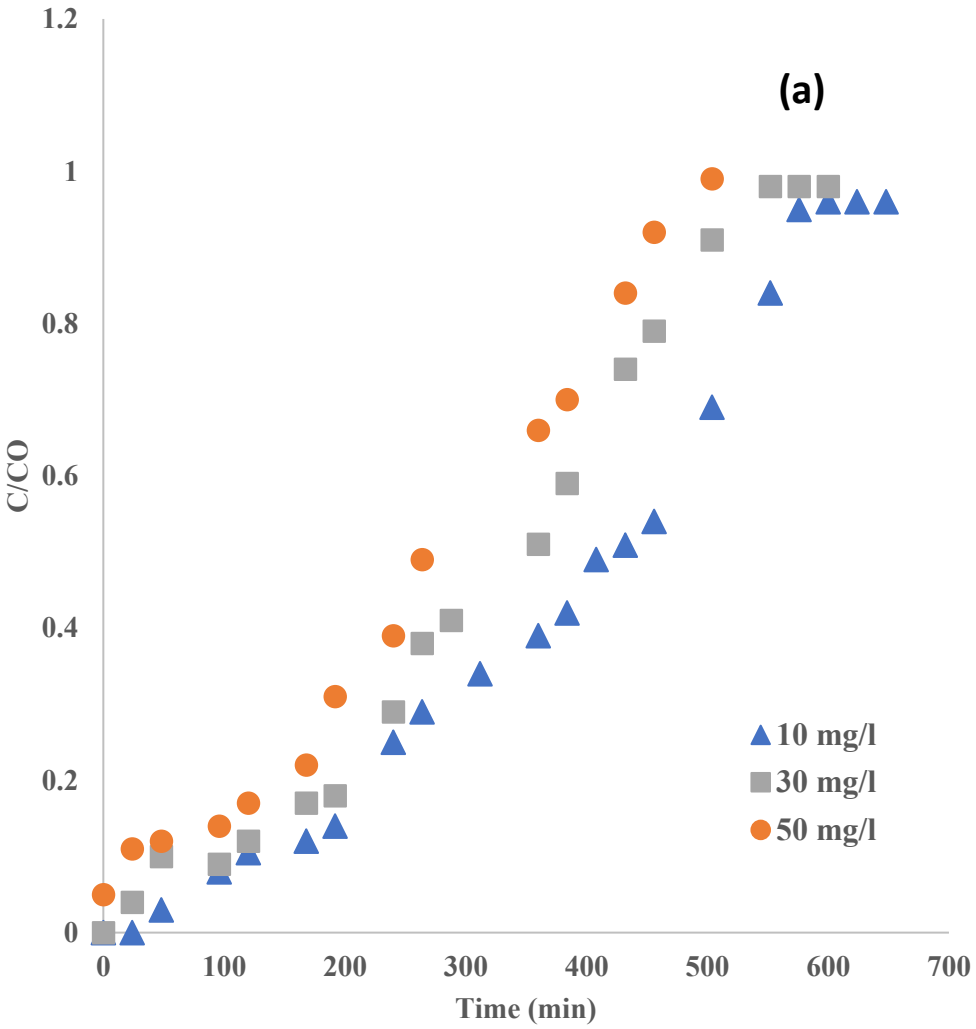
(a)
1.2
1
0.8
0.6
0.4
0.2
0
C/CO
0
100
200
300
400
500
600
700
Time (min)
10 mg/l
30 mg/l
50 mg/l

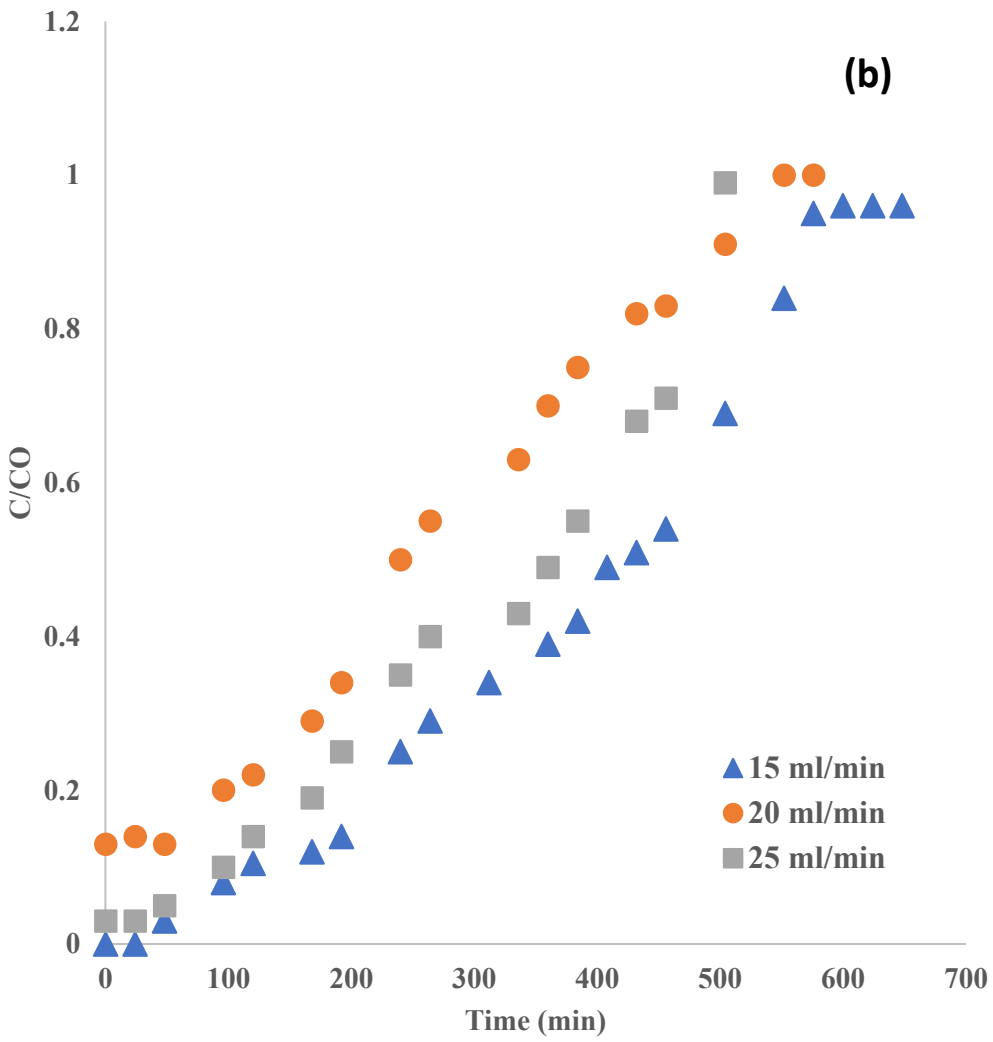
(b)
1.2
1
0.8
0.6
0.4
0.2
0
C/CO
0
100
200
300
400
500
600
700
Time (min)
15 ml/min
20 ml/min
25 ml/min

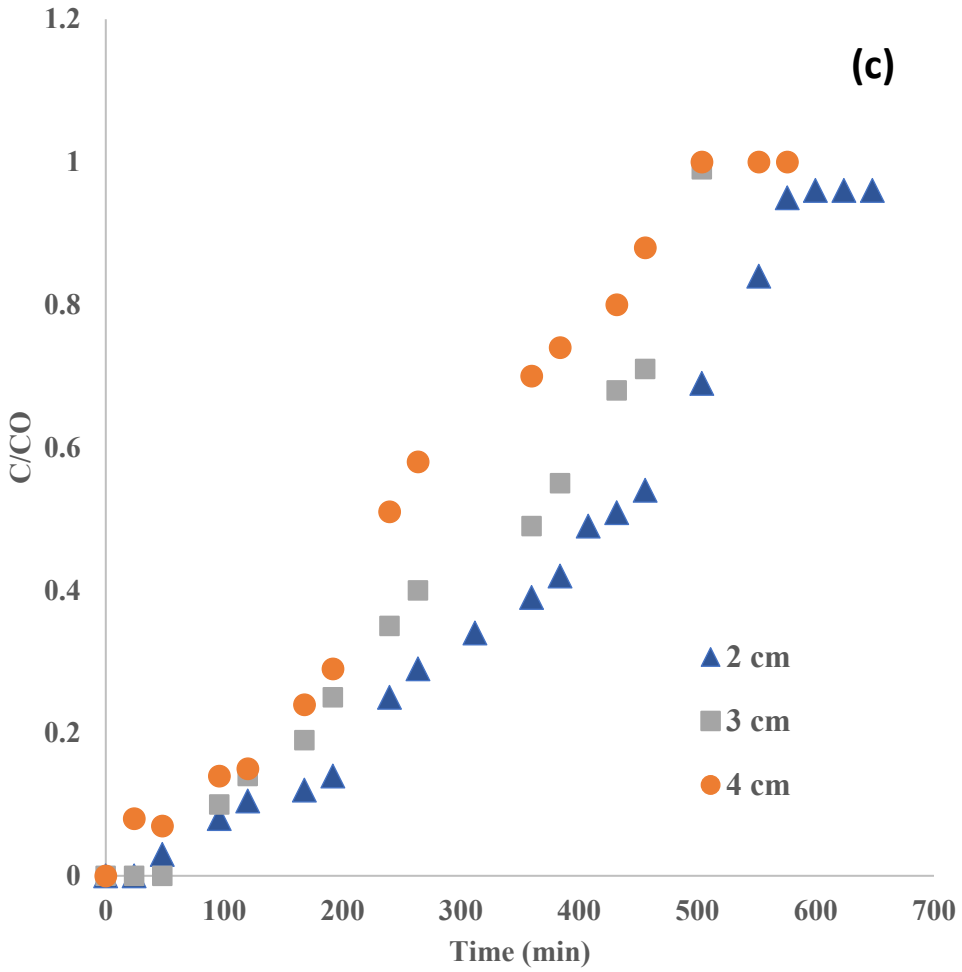

Fig. 4.3.5. Effect of: (a) initial inlet anthracene concentration (aerogel size 2 cm and flow rate 15 mL min^{-1}); (b) flow rate (aerogel size 2 cm and influent concentration 10 mg L^{-1}); (c) aerogel size (influent concentration 10 mg L^{-1} and flow rate 15 mL min^{-1}) on the breakthrough curve for anthracene removal using enzyme-loaded aerogel

Design of Experiment

Table 4.3.2 presents the actual and coded values of 15 experimental runs related to the Box-Behnken design method.

Table 4.3.2. Box-Behnken design with experimental run results and corresponding actual and coded values

Experiments	X_1	X_2	X3	Response
	Initial Concentration (mg L^{-1})	size	Flow Rate (mL min^{-1})	Anthracene removal Efficiency (%)
1	0 (30)	+1 (4)	-1 (15)	61.4
2	+1 (50)	+1 (4)	0 (20)	55.9
3	0 (30)	+1 (4)	+1 (25)	40.5
4	-1 (10)	+1 (4)	0 (20)	56.9
5	+1 (50)	-1 (2)	0 (20)	74.4
6	0 (30)	-1 (2)	-1 (15)	81.3
7	-1 (10)	-1 (2)	0 (20)	67.3
8	0 (30)	-1 (2)	+1 (25)	50.4
9	+1 (50)	0 (3)	+1 (25)	39.2
10	+1 (50)	0 (3)	-1 (15)	66.3
11	-1 (10)	0 (3)	+1 (25)	50.9
12	-1 (10)	0 (3)	-1 (15)	61.5
13	0 (30)	0 (3)	0 (20)	78.6
14	0 (30)	0 (3)	0 (20)	80.5
15	0 (30)	0 (3)	0 (20)	79.8

Using a quadratic polynomial model, the mathematical relationship between the response (ion removal efficiency %) and three independent variables (inlet anthracene concentration, size and flow rate) was simulated. Eq.7 was derived from the model based on the second-order polynomial equation (Eq. (10)).

$$Removal\ efficiency\ (\%) = 269.1\ x_1 - 0.75\ x_2 - 2.5\ x_3 + 0.01\ x_1 x_2 + 0.2\ x_1 x_{3+} 0.12 x_2 x_3 - 21.1 {x_1}^2 - 505.15 \quad (10)$$

Using the analysis of variance (ANOVA) and R^2, the gained quadratic equation was determined by the best fitting of experimental data (Mourabet et al., 2012). ANOVA analysis is a prominent step in the BBD method which is presented in Table 4.3.3.

Table 4.3.3. Effect of oil concentration and electrospun fibers on volume change ANOVA results obtained from design of experiment

Source	Sum of Squares	Mean Square	F-value	p-value
Model*	3873.2	399.3	288.13	< 0.0001
X_1- Initial Concentration (mg L^{-1})	299.1	306.1	110.49	0.0002
X_2-Aerogel size	329.3	331.9	102.70	0.0002
X_3-Flow rate	150.1	125.4	242.04	< 0.0001
$X_1 \times X_2$	6.1	6.9	3.55	0.0316
$X_1 \times X_3$	8.4	5.6	6.19	0.0453
$X_2 \times X_3$	6.9	8.3	5.66	0.1043
X_1^2	0.0201	0.0191	0.0103	< 0.0001
X_2^2	2704.1	2937.2	1453.3	0.6943
X_3^2	0.2840	0.2732	0.2402	0.4091
Residual	8.33	1.77		
Lack of Fit**	4.89	1.80	2.55	0.5114
Pure Error	1.48	0.9103		
Correlation Total	3810.29			

* significant ** not significant

There is a reasonable connection between the response and the parameters, as indicated by the F and P-values, and the parameter and response data agree. There was a greater than 0.001 F-value for the model (288), indicating that the model is significant. Since flow rate has an F-value of 242, which is higher than the F-value of the two other variables, flow. rate is more effective in influencing the output response. Significant model terms are those with a P-value less than 0.05; however, when it is greater than 0.1, the model is insignificant. The table indicates that the variables (initial concentration, aerogel size, flow rate, initial concentration *aerogel size, initial concentration*flow rate, aerogel size* flow rate) were significant with very small P-values(p=0.05). Considering the P-value of 0.51, there appears to be a lack of fit in the model,

which indicates that the difference between the pure error and the P-value is not significant. In the correlation total and residual values, the sum of each column is represented by the correlation total and the difference between the experimental and predicted data is represented by the residual value (Chen and Wang, 2004).

Using the models, the anthracene removal efficiency was predicted within the experimental range with an R^2 value of 0.989, which was in good agreement with the predicted R^2. Based on the adjusted R^2 value of 0.978, only 0.43% of the variation is not explained by input variables (Ma et al., 2018). For a reasonable agreement, the adjusted and predicted R^2 should be within approximately 0.20 of each other. Otherwise, either the data or the model may be flawed. There is a reasonable agreement between the predicted and adjusted R^2 (Mei et al., 2016). As an indicator of the degree of precision, the coefficient of variation (%) was 3.98%. An experiment with a relatively low coefficient of variation indicates that the experiment was highly reliable. As indicated by the reported standard deviation (1.09), the values are close to average, that is, their dispersion is low. According to this study, the derived model's adequacy precision is 55.19, indicating it is suitable for application within the design space (Song et al., 2018). Fig 4.3.6 compares the actual and anticipated data. As can be seen, for the initial concentration of 30 mg l^{-1}, there is a low deviation from experimental values, usually less than 5 and 2.5 %

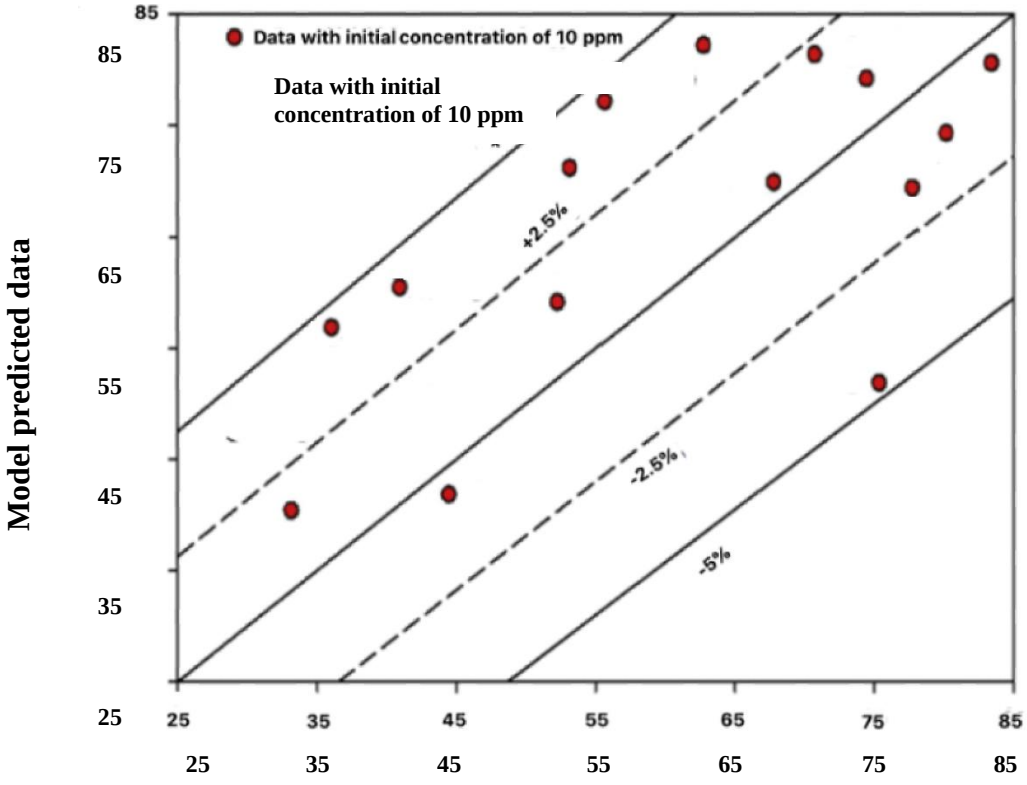

Fig. 4.3.6. Deviation b[illegible] Experimental Data [illegible]erimental data

Effect of operating parameters on the anthracene removal

Three-dimensional diagrams (Figure 4.3.7) illustrate the combined impacts of operating variables on anthracene removal efficiency. Figures 7a and 4b showed the variation of removal efficiency upon variation of flow rate from 15 to 25 ml min^{-1}. The removal efficiency decreased with increasing inlet flow rate from 22 to 30 mL min^{-1}. Additionally, the highest removal efficiency is obtained at a flow rate of 22 mL min^{-1}. Based on Figures 4.3.7b and c, the removal efficiency decreased as the inlet concentration of anthracene increased, with a maximum removal efficiency at an initial concentration of 34 mg L^{-1}.

(a)

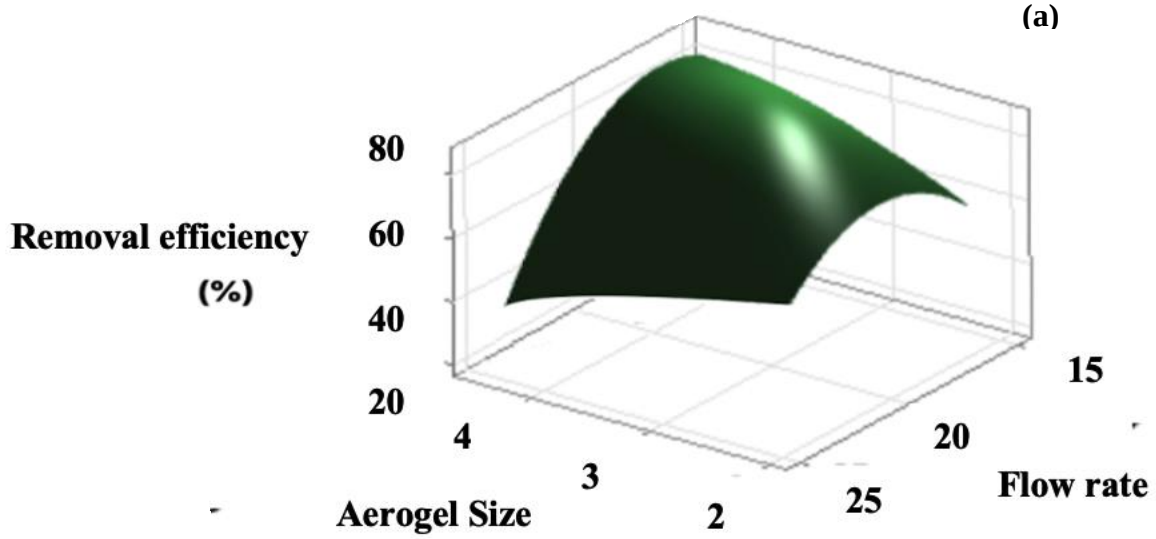
Removal efficiency
(%)
80
60
40
20
4
3
2
Aerogel Size
15
20
25
Flow rate

(b)

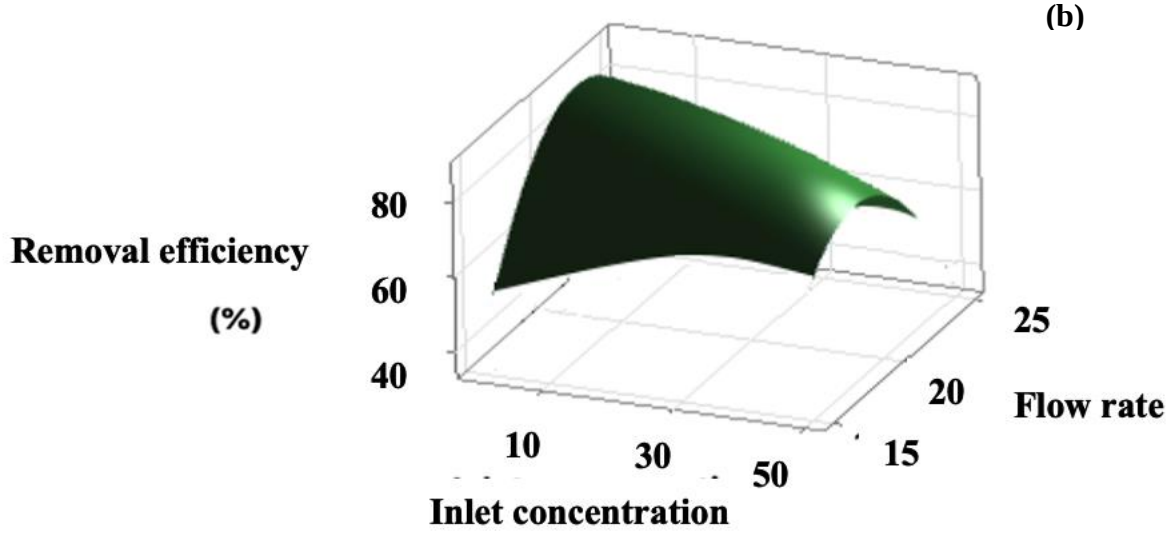
Removal efficiency
(%)
80
60
40
10
30
50
Inlet concentration
25
20
15
Flow rate

(c)

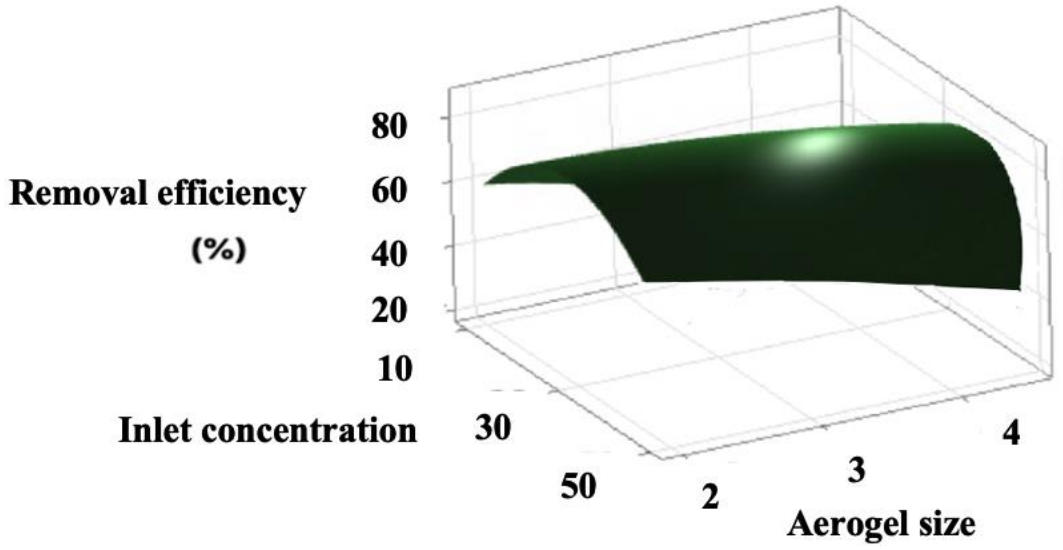

Fig. 4.3.7. Removal efficiency of anthracene based on the: (a) Aerogel size and flow rate, inlet concentration= 10 mg L^{-1} (b) Inlet concentration and flow rate, aerogel size = 2 cm (c) Inlet concentration and aerogel size, flow rate= 15 mL min^{-1}

A sensitivity analysis was performed on the correlation obtained for removal efficiency (%) to determine the effect of parameters (size of aerogel, inlet concentration, and flow rate). As can be seen in Figure 4.3.8., by decreasing the value of flow rate toward 25 mL min^{-1} and decreasing the contact time, considerable changes in the value of removal efficiency can be observed. As mentioned previously, removal efficiency is more sensitive to the flow rate in comparison to aerogel size and inlet concentration of anthracene and as the flow rate increases removal efficiency changes more significantly.

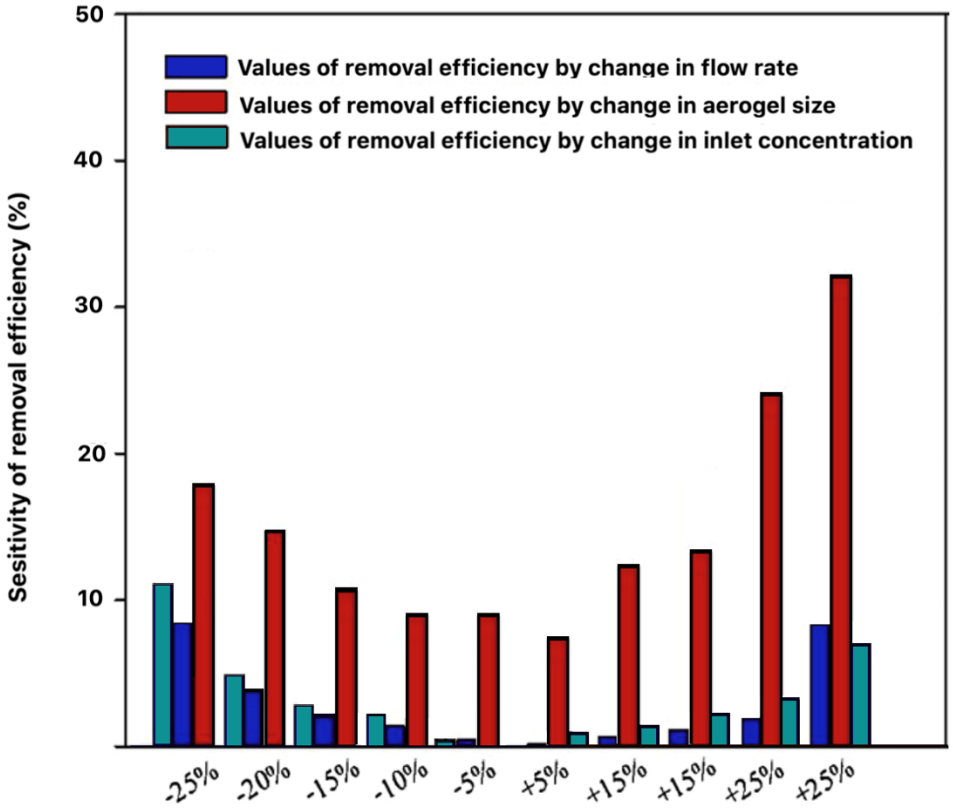

Fig. 4.3.8. Change in removal efficiency

4.3.3. Conclusion

In this paper, experimental study was presented that examines the continuous removal of polycyclic aromatics from water bodies in a fixed-bed column system using an aerogel made of polyimide. Firstly, an investigation was conducted on the covalent immobilization of PAH degrading enzymes on modified polyimide aerogels. Furthermore, the application of prepared immobilized enzymes in fixed bed columns was investigated and the effect of aerogel size,

pollutant concentration and flowrate parameters on the removal of target pollutants was examined to determine the optimum parameter values for efficient removal of pollutants using fixed bed columns using the BBD model. Finally, sensitivity analysis was performed on the correlation obtained for removal efficiency (%) to determine the effect of parameters (size of aerogel, inlet concentration, and flow rate). Our results showed that flow rate is more effective in influencing the output response. Moreover, according to the predictions of the derived model, the highest removal efficiency was achieved at a flow rate of 22 mL min^{-1}, an initial concentration of 34 mg L^{-1}, and an aerogel size of 2 cm, however, the removal efficiency was experimentally measured at 87.14 % under these conditions.

CHAPTER FIVE: CONCLUSIONS, AND RECOMMENDATIONS

5.1. CONCLUSIONS

From the obtained results, the following conclusions can be drawn:

1. The aftermath of unconventional oil accidents and the numerous pipeline projects for the transport of bitumen oil and Bakken highlight the lack of preparedness of cities and governments to deal with unconventional oil emergencies. Because bioremediation is considered slow process and effective for confined contaminated areas, physicochemical treatment processes are necessary for removing contaminants as pre-remediation to constrain the spread of oil and accelerate the bioremediation and detoxification. *The modified dolomite exhibited the highest oil sorption capacity in oil-water mixtures, making it suitable for use in fixed columns used as pretreatment for bioremediation systems. Because the adsorption was favorable in fixed bed column systems, the design parameters were obtained for large scale columns by using small scale experiments.*
2. Unconventional oil contaminated soils and water contain high concentration of polyaromatic hydrocarbons such as anthracene, and pyrene; thus, the PAH degrading bacteria were isolated from contaminated soils to produce PAH degrading enzymes. The production of enzymes involved in multiple-substrate transformation was improved by the multi-culture of four psychrophilic bacteria. *Due to the variety of metabolic reactions and interactions that a microbial consortium offers over monocultures, it is possible to undertake complex metabolic tasks*.
3. Pyrene dioxygenase, naphthalene dioxygenase, catechol-2,3-dioxygenase, 1-hydroxy-2-naphthoate hydroxylase, and protocatechuic acid (PCA) 3,4-dioxygenase enzymes have a matching product. They acted in symphony to degrade pyrene. Their unique kinetic behavior permits them to achieve rapid degradation of p-xylene at low temperatures (<15°C). *No specific product was produced after the complete action of the enzyme cocktail that confirmed the degradation of pyrene (70%) within three days in highly contaminated soil* $(\sim 3\ mg\ pyrene/gsoil)$ *samples at 15°C.*
4. To mimic *in-situ* application of enzyme mixture, bioremediation of pyrene-contaminated soil was carried out in soil column (140 mL) tests. Our results showed that the favorable mixing conditions in the flask test resulted in higher removal efficiency. *Around 73 and 56 % pyrene*

removal were obtained after 3 weeks injection with Mix7-3PAHs and Mix8-D in flask test; however, the rate of corresponding removal in column test decreased to around 50 and 30%, for pyrene contaminated soils.

5. One of the major challenges in the practical and commercial application of oxygenases for water treatment is their inherent instability. Based on our studies, modified polyimide aerogels were suitable to support enzyme immobilization (naphthalene dioxygenase and catechol dioxygenase). Using covalent bonding, PAH degrading enzymes were immobilized on modified polyimide aerogels. *Covalent immobilization of enzymes on modified polyimide aerogels resulted in around 9- and 6-fold lower enzyme leaching for naphthalene and catechol 2,3 dioxygenase enzymes compared to enzyme immobilization using adsorption..*
6. A bioinspired device was fabricated as a sustainable remedial method. The potential of membrane systems to protect the produced cocktail enzyme from the environment surrounding was investigated to take advantage of reaction-separation integration for filtration and water purification in the water system. Based on biodegradation studies, a synergistic effect between membrane adsorption, enzymatic degradation, and ultrafiltration was proposed for the removal of anthracene from the column of water. *In addition to the circulation of PAH degrading enzymes in hollow fiber lumens, aliphatic degrading enzymes confined in multilayer nanofibrous membrane systems play an important role in the removal of oily compounds.*

5.2.REMARKS

Hypothesis No.	HYPOTHESES	REMARKS
1	Dolomite is a locally available material, and the surface modification of dolomite sorbent particles can be carried out to obtain sorbents for Dilbit and Bakken oil removal.	Esterification reaction can be used for hydrophobic functionalization of dolomite via a simple and economic one-step synthetic approach to enhance sorbent selectivity and effectiveness in the removal of spilled unconventional oil from water surfaces. Kinetic study showed the heterogeneous adsorption sites on the sorbent's surface of dolomite.
2	Both packed and fluidized bed treatment columns of low-cost chemical hydrophobic sorbents for removing unconventional oil from laboratory synthetic oil-in-water emulsions would ensure a proper interpretation of the laboratory results and determine the efficiency of adsorption of contaminant.	A model was also developed to predict the fixed and fluidized bed experimental results based on kinetic and equilibrium batch measurements of the modified dolomite and the stabilized o/w emulsion. The results showed that the breakthrough curves in fluidized bed adsorbent are different than those obtained from fixed bed adsorbent due to axial mixing occurring in the solid and liquid phase.

3	Formulation of synthetic bacterial (Indigenous PAH degrading bacteria) consortia to produce cocktail enzyme mixture with higher activity can enhance the effectiveness of enzymatic bioremediation methods for land-based oil spill.	Several combinations of the pre-selected strains were used to create most prompting consortium for enzyme production. In the unique prepared formulation, the addition of biosurfactant produced by *Alcanivorax borkumensis* and activator (Fe_3SO_4) enhanced the operational stability and effectiveness of prepared solution as discussed in chapter 4, part 1.
4	A synergistic effect between membrane adsorption, enzymatic degradation, and ultrafiltration can be applied for the removal of anthracene from the column of water using jellyfish like device	To study the practical application of enzyme-mediated bioremediation for the removal of the model substrate (i.e., anthracene) from surface water, jellyfish like device can be applied. This device can adsorb and degrade dispersed oily compounds using their sticky arms and catch PAHs that float beneath the surface of water by hollow fiber membranes with recirculating enzymes (jellyfish tentacles).

5	Immobilization of target enzymes on polyimide aerogels can enhance the degradability of residual unconventional oil in the water. Moreover, a continuous fixed-bed process might be employed to resolve potential problems regarding the large-scale application of aerogel.	Multi-immobilization of PAH degrading enzymes on modified polyimide aerogel improved their anthracene biodegradation in water. Also, immobilization enhanced their storage stability at 15 ± 1 ºC for 16 days as discussed in chapter 4, part 3.

To demonstrate that polyaromatic hydrocarbons can be effectively bioremediated, the following objectives have been investigated.

5.3. FUTURE RECOMMENDATIONS

Though the project objectives were successfully performed and disseminated in form of published articles, still limitations persist and hence future recommendations.

A. Global Objective 1: As listed in the objective section, global objective 1 states "Synthesize low-cost hydrophobic dolomite sorbent for oil spill clean-ups: as well as Kinetic modeling and isotherm study". A major limitation of this objective lies in the effect of dolomite on the value of the pH of water. U*nder high temperatures and high salinity conditions, organoclay is commercially recommended for use as a stabilizer for water-in-oil emulsions. It is also possible to use other low-cost sorbents, such as modified Dilbit, if they are compatible with that operating condition.*

B. Global Objective 2: As listed in the objective section, global objective 2 states "The feasibility of packed and fluidized bed treatment columns of hydrophobic dolomite granules for removing unconventional oil from laboratory synthetic oil-in-water emulsion". Modified dolomite has a low porosity and surface area, which results in the need to use small particles in the columns, which may affect hydraulic conductivity. The bio-regeneration of saturated dolomite particles and challenges such as incomplete regeneration and microbial fouling can be studied in future. *It would*

also be preferable to conduct a fixed bed column packed with bio-regenerated granular modified dolomite

C. Global Objective 3: As listed in the objective section, global objectives 3 is related to "feasibility of enzymatic biodegradation of Polyaromatic Hydrocarbons contaminated soil using cold-active enzymes: A soil column study". Through these objectives, to study *in-situ* application for enzymatic bioremediation of contaminated soil, cocktail of the enzyme mixture including major enzymes involved in PAH biodegradation (i.e., pyrene dioxygenase, naphthalene dioxygenase, catechol-2,3-dioxygenase, 1-hydroxy-2-naphthoate hydroxylase, and protocatechuic acid (PCA) 3,4-dioxygenase enzymes) were produced and characterized. However, another "possible" limitation associated with this objective is the presence of other proteins or enzymes that may indirectly contribute to the biodegradation of model substrate (i.e., pyrene). An example would be ferrodoxins, which are iron-sulphur proteins involved in the transfer of electrons during a variety of metabolic reactions. Although LC-MS-MS was used to determine the proteins in the enzyme mixture, more precise approaches such as next-generation sequencing technologies may be used to determine each individual protein. In the case of transcriptomics studies, based on genomics, it is possible to provide information about the response of selected isolates to a variety of substrates. By analyzing the enzyme mixture, it will be possible to determine its precise composition. The other major limitation of this objective is the use of immobilized enzymes for *in-situ* application to soil matrixes. There is a technical possibility that the injection of micro-sized solids could clog injection wells. In order to determine the type and depth of the fluid injected into the soil matrix, further studies will be necessary.

D. Global Objective 4: Global objective 4 is related to "Investigate involved enzymes in PAHs (i.e., anthracene) biodegradation and potential application for the contaminated column of water". Through these objectives, the cocktail of enzyme mixtures including major enzymes involving in anthracene biodegradation (i.e., naphthalene dioxygenase) was produced for circulation in the lumen of jellyfish tentacles (i.e., hollow fibre membranes). Moreover, aliphatic degrading enzymes obtained from *Alcanivorax borkumensis* were immobilized in jellyfish arms (i.e., multilayer membrane systems (PVDF-PS/PAN/PVDF-PS)) to catch dispersed oily compounds from the water column and avoid their contact with jellyfish tentacles. *Further experiments (e.g., pilot-scale test using a larger prototype and production of enzymes on larger scales) can be carried out to study the performance of the proposed device in continuous mode and evaluate this method for*

practical application. Additionally, other techniques, such as the use of crosslinking agents, should be examined to prevent enzyme molecules from shedding into the hollow fiber nanopores to further improve the half-life of enzyme molecules circulating on the lumen side.

D. Global Objective 5: As listed in the objective section, global objectives is related to "The feasibility of a continuous fixed-bed column to remove polycyclic aromatic hydrocarbons by degrading enzymes immobilized on polyimide aerogels". The major limitation of this objective lies in the use of immobilized enzymes for *in situ* application to the water treatment. In this study cofactor-requiring enzymes were applied that present a unique problem. *Therefore, other immobilization techniques for cofactor immobilization should also be investigated.* Extracellular enzymes such as peroxidases and laccases are usually applied for immobilization and water treatment, which demonstrate strong oxidative abilities and low specificity. However, fungal oxidases, such as laccase, are not able to efferently attack un-functionalized aromatic compounds.

BIBLIOGRAPHY

1-109., E. C. F. R. A. F. W. E. I. U. L.

Abarghani, A., et al., 2018. Organofacies study of the Bakken source rock in North Dakota, USA, based on organic petrology and geochemistry. International Journal of Coal Geology. 188**,** 79-93.

Abdehagh, N., et al., 2016. Multicomponent adsorption modeling: isotherms for ABE model solutions using activated carbon F-400. Adsorption. 22**,** 357-370.

Abdulkadir, I., et al., 2016. A rapid method of crude oil analysis using FT-IR spectroscopy. Nigerian Journal of Basic and Applied Sciences. 24**,** 47-55.

Abolafia, J. C., J.; Harrison, A.; Hensley, J.; Kim, D.; Ko, W.-M.; Le, M.; Manivannan, H.; Rivera Rubio, L.; Sarker, P. Using Enzymatic Combinations to Reduce Asphaltene Aggregation. 2018.

Agamuthu, P., et al., 2013. Bioremediation of hydrocarbon contaminated soil using selected organic wastes. Procedia Environmental Sciences. 18**,** 694-702.

Agarry, S. O., K., Biodegradation of Bitumen in Soil and Its Enhancement by Inorganic Fertilizer and Oxygen Release Compound: Experimental Analysis and Kinetic Modelling. J Microbial Biochem Technol S 2014, 4, 2.

Ahmad, A., Hameed, B., 2010. Fixed-bed adsorption of reactive azo dye onto granular activated carbon prepared from waste. Journal of hazardous materials. 175**,** 298-303.

Albadarin, A. B., et al., 2012. Kinetic and thermodynamics of chromium ions adsorption onto low-cost dolomite adsorbent. Chemical Engineering Journal. 179**,** 193-202.

Alcalde, M., et al., 2006. Environmental biocatalysis: from remediation with enzymes to novel green processes. TRENDS in Biotechnology. 24**,** 281-287.

Alonso-González, M., et al., 2020. Developing active poly (vinyl alcohol)-based membranes with encapsulated antimicrobial enzymes via electrospinning for food packaging. International Journal of Biological Macromolecules. 162**,** 913-921.

Altschul, S. F., et al., 1990. Basic local alignment search tool. Journal of molecular biology. 215**,** 403-410.

Amenaghawon, N., et al., 2013. Application of Box-Behnken design for the optimization of citric acid production from corn starch using Aspergillus niger. British Biotechnology Journal. 3**,** 236.

Asadpour, R., et al., 2014. Enhancing the hydrophobicity of mangrove bark by esterification for oil adsorption. Water Science and Technology. 70**,** 1220-1228.

Aslan, N., Cebeci, Y., 2007. Application of Box–Behnken design and response surface methodology for modeling of some Turkish coals. Fuel. 86**,** 90-97.

ASTM Committee D-2 on Petroleum Products, L. F., Lubricants, 2011. Standard test method for acid number of petroleum products by potentiometric titration. ASTM international.

ASTM, D., 2007. Standard test method for particle-size analysis of soils.

ASTM, F.-S. T. M. f. S. P. o. A., in: Annual Book of ASTM Standards,ASTM Committee on Standards, West Conshohocken, PA,1998.

Atlas, R. M. A., J.; Bej, A. K., Polar microbiology: the ecology, biodiversity and bioremediation potential of microorganisms in extremely cold environments. CRC Press: 2009.
Ausuri, J., et al., 2021. Assessment of the degradation potential and genomic insights towards phenanthrene by Dietzia psychralcaliphila JI1D. Microorganisms. 9**,** 1327.
Ayala, M., et al., 2007. The prospects for peroxidase-based biorefining of petroleum fuels. Biocatalysis and Biotransformation. 25**,** 114-129.
Ayawei, N., et al., 2017. Modelling and interpretation of adsorption isotherms. Journal of Chemistry. 2017.
Ayotamuno, M., et al., 2006. Petroleum contaminated ground-water: Remediation using activated carbon. Applied Energy. 83**,** 1258-1264.
Bacosa, H. P., Inoue, C., 2015. Polycyclic aromatic hydrocarbons (PAHs) biodegradation potential and diversity of microbial consortia enriched from tsunami sediments in Miyagi, Japan. Journal of hazardous materials. 283**,** 689-697.
Balashova, N., et al., 2001. Purification and characterization of a salicylate hydroxylase involved in 1-hydroxy-2-naphthoic acid hydroxylation from the naphthalene and phenanthrene-degrading bacterial strain Pseudomonas putida BS202-P1. Biodegradation. 12**,** 179-188.
Bandura, L., et al., 2017. Application of mineral sorbents for removal of petroleum substances: A review. Minerals. 7**,** 37.
Banerjee, S., et al., 2017. Design of novel chemical solvent for treatment of waxy crude. International Journal of Oil, Gas and Coal Technology. 15**,** 363-379.
Banerjee, S. S., et al., 2006. Treatment of oil spill by sorption technique using fatty acid grafted sawdust. Chemosphere. 64**,** 1026-1031.
Banks, H., et al., 2013. Quantifying CFSE label decay in flow cytometry data. Applied mathematics letters. 26**,** 571-577.
Baquiran, J. P. T., B.; Songco, K.; Crowley, D. E., Characterization of culturable PAH and BTEX degrading bacteria from heavy oil of the Rancho La Brea tarpits. Polycyclic Aromatic Compounds 2012, 32, (5), 600-614.
Barkay, T., et al., 1999. Enhancement of solubilization and biodegradation of polyaromatic hydrocarbons by the bioemulsifier alasan. Applied and environmental microbiology. 65**,** 2697-2702.
Barros, M., et al., 2013. General aspects of aqueous sorption process in fixed beds. Mass Transfer-Advances in Sustainable Energy and Environment Oriented Numerical Modeling, InTech, Rijeka. 361-386.
Beaulieu, M., contaminés, Q. S. d. l., 2016. Guide d'intervention: protection des sols et réhabilitation des terrains contaminés. Ministère du Développement durable, de l'Environnement et de la Lutte contre ….
Bennett, G. F., Peters, R. W., 1988. The removal of oil from wastewater by air flotation: a review. Critical Reviews in Environmental Science and Technology. 18**,** 189-253.
Bezza, F. A. C., E. M. N., Biosurfactant-enhanced bioremediation of aged polycyclic aromatic hydrocarbons (PAHs) in creosote contaminated soil. Chemosphere 2016, 144, 635-644.
Bookstaver, M., et al., 2015. Interaction of Alcanivorax borkumensis with a Surfactant Decorated Oil–Water Interface. Langmuir. 31**,** 5875-5881.
Boonchan, S., et al., 2000. Degradation and mineralization of high-molecular-weight polycyclic aromatic hydrocarbons by defined fungal-bacterial cocultures. Applied and environmental microbiology. 66**,** 1007-1019.

Boonchan, S. B., M. L.; Stanley, G. A., Degradation and mineralization of high-molecular-weight polycyclic aromatic hydrocarbons by defined fungal-bacterial cocultures. Applied and environmental microbiology 2000, 66, (3), 1007-1019.

Borisova, A. S., et al., 2018. Correlation of structure, function and protein dynamics in GH7 cellobiohydrolases from Trichoderma atroviride, T. reesei and T. harzianum. Biotechnology for biofuels. 11**,** 1-22.

Borisova, R. B., Isolation of a Rhodococcus soil bacterium that produces a strong antibacterial compound. East Tennessee State University, 2011.

Bouchez, M., et al., 1999. Efficiency of defined strains and of soil consortia in the biodegradation of polycyclic aromatic hydrocarbon (PAH) mixtures. Biodegradation. 10**,** 429-435.

Bradford, M. M., 1976. A rapid and sensitive method for the quantitation of microgram quantities of protein utilizing the principle of protein-dye binding. Analytical biochemistry. 72**,** 248-254.

Brakstad, O. G. L., S.; Ribicic, D.; Netzer, R., Biodegradation of petroleum oil in cold marine environments. In Psychrophiles: From Biodiversity to Biotechnology, Springer: 2017; pp 613-644.

Brassington, K. J., 2008. New insights into the biotransformation of weathered hydrocarbons in soil.

Butler, J. D., et al., 2013. A novel passive dosing system for determining the toxicity of phenanthrene to early life stages of zebrafish. Science of the Total Environment. 463**,** 952-958.

Çakmakçı, E., et al., 2014. Immobilization of alpha-amylase on aminated polyimide membrane: Preparation, characterization, and properties. Starch-Stärke. 66**,** 274-280.

Cambiella, A., et al., 2006. Treatment of oil-in-water emulsions: Performance of a sawdust bed filter. Journal of Hazardous Materials. 131**,** 195-199.

Chambers, R., et al., [23] Physical immobilization of enzymes by hollow-fiber membranes. Methods in enzymology. Elsevier, 1976, pp. 291-317.

Chen, J., et al., 2020. Enhanced oil adsorption and nano-emulsion separation of nanofibrous aerogels by coordination of pomelo peel-derived biochar. Industrial & Engineering Chemistry Research. 59**,** 8825-8835.

Chen, J. P., Wang, L., 2004. Characterization of metal adsorption kinetic properties in batch and fixed-bed reactors. Chemosphere. 54**,** 397-404.

Chen, W., et al., 2019. Biomimetic dynamic membrane for aquatic dye removal. Water research. 151**,** 243-251.

Cheu, S. C., et al., 2016. Separation of dissolved oil from aqueous solution by sorption onto acetylated lignocellulosic biomass—equilibrium, kinetics and mechanism studies. Journal of Environmental Chemical Engineering. 4**,** 864-881.

Clegg, R. J. M. t. e. a. e. o. m. U. o. B., 2015.

Cobanli, S. G., C.; King, T.; Robinson, B.; Ryan, S.; Fortin, N.; Wohlgeschaffen, G.; Mason, J.; Thamer, P.; McIntyre, E., In Field Studies to Monitor Indigenous Microbial Respiration to Determine the Potential Biodegradation of Naturally and Chemically Dispersed Crude Oil, Condensate and Diluted Bitumen. In Poster at 38th Arctic and Marine Oil Spill Program (AMOP), 2015.

Cobas, M., et al., 2013. Development of permeable reactive biobarrier for the removal of PAHs by Trichoderma longibrachiatum. Chemosphere. 91**,** 711-716.

Coene, E., et al., 2018. A numerical model for the performance assessment of hydrophobic meshes used for oil spill recovery. International Journal of Multiphase Flow. 99**,** 246-256.
Crank, J., 1979. The mathematics of diffusion. Oxford university press.
Cremaldi, J. C., et al., 2015. Interaction of oil drops with surfaces of different interfacial energy and topography. Langmuir. 31**,** 3385-3390.
Crini, G., Badot, P.-M., 2010. Sorption processes and pollution: Conventional and non-conventional sorbents for pollutant removal from wastewaters. Presses Univ. Franche-Comté.
Crosby, S., et al., 2013. Transporting Alberta oil sands products: defining the issues and assessing the risks.
da Silva, M. L. B., Alvarez, P. J., 2010. Indole-based assay to assess the effect of ethanol on Pseudomonas putida F1 dioxygenase activity. Biodegradation. 21**,** 425-430.
Dai, Q., Chung, K. H., 1995. Bitumen—sand interaction in oil sand processing. Fuel. 74**,** 1858-1864.
Dai, Y., et al., 2011. Laccase-carrying electrospun fibrous membranes for adsorption and degradation of PAHs in shoal soils. Environmental science & technology. 45**,** 10611-10618.
Dai, Y. Y., L.; Niu, J., Laccase-carrying electrospun fibrous membranes for adsorption and degradation of PAHs in shoal soils. Environmental science & technology 2011, 45, (24), 10611-10618.
Das, N., Chandran, P., 2011. Microbial degradation of petroleum hydrocarbon contaminants: an overview. Biotechnology research international. 2011.
Das, S., Dash, H. R., 2017. Handbook of metal-microbe interactions and bioremediation. CRC Press.
Das, S. D., H. R., Handbook of Metal-microbe Interactions and Bioremediation. CRC Press: 2017.
Datta, R., et al., 2017. How enzymes are adsorbed on soil solid phase and factors limiting its activity: A Review. International agrophysics. 31**,** 287.
Daughney, C. J., 2000. Sorption of crude oil from a non-aqueous phase onto silica: the influence of aqueous pH and wetting sequence. Organic Geochemistry. 31**,** 147-158.
Davoodi, S. M., et al., 2021. Performance of packed and fluidized bed columns for the removal of unconventional oil using modified dolomite. Fuel. 285**,** 119191.
Davoodi, S. M., et al., Simulation of Novel Jellyfish Type of Process for Bioremediation Application. Available at SSRN 4140189.
Davoodi, S. M., et al., 2020. Bioremediation of Unconventional Oil Contaminated Ecosystems under Natural and Assisted Conditions: A Review. Environmental Science & Technology. 54**,** 2054-2067.
Davoodi, S. M., et al., 2019. Hydrophobic dolomite sorbent for oil spill clean-ups: Kinetic modeling and isotherm study. Fuel. 251**,** 57-72.
de Santiago-Martín, A., et al., 2015. Oil spill in Lac-Mégantic, Canada: Environmental monitoring and remediation. Int J Water Wastewater Treat. 2.
Deshpande, R. S., Biodegradability of Diluted Bitumen (Dilbit). University of Cincinnati, 2016.
Deshpande, R. S., et al., Comparative study on rate of biodegradation of diluted bitumen and conventional oil in fresh water. International Oil Spill Conference Proceedings, Vol. 2017. International Oil Spill Conference, 2017, pp. 2256-2267.

Deshpande, R. S. S., D.; Techtmann, S.; Conmy, R. N.; Santo Domingo, J. W.; Campo, P., Microbial degradation of Cold Lake Blend and Western Canadian select dilbits by freshwater enrichments. Journal of hazardous materials 2018, 352, 111-120.

Deziel, E. P., G.; Villemur, R.; Lepine, F.; Bisaillon, J., Biosurfactant production by a soil Pseudomonas strain growing on polycyclic aromatic hydrocarbons. Appl. Environ. Microbiol. 1996, 62, (6), 1908-1912.

Diagboya, P. N., et al., 2018. Concentration-dependent and simultaneous sorption and desorption of pyrene and fluorene on major soil minerals in sub-Saharan Africa. Applied Clay Science. 153**,** 257-264.

Díaz Sanz, J., Bioremediation of urban soils polluted with non-conventional petroleum in the Canadian context. 2015.

Dollhopf, R., Durno, M., Kalamazoo River\Enbridge Pipeline Spill 2010. International oil spill conference proceedings (IOSC), Vol. 2011. American Petroleum Institute, 2011, pp. abs422.

Domínguez, A. M., J.; Inguanzo, M.; Pis, J., Investigations into the characteristics of oils produced from microwave pyrolysis of sewage sludge. Fuel Processing Technology 2005, 86, (9), 1007-1020.

Doshi, B., et al., 2018. A review of bio-based materials for oil spill treatment. Water research. 135**,** 262-277.

Duan, B., et al., 2006. A nanofibrous composite membrane of PLGA–chitosan/PVA prepared by electrospinning. European Polymer Journal. 42**,** 2013-2022.

EIA, U., 2008. US Energy Information Administration. International Energy Outlookt. 11**,** 1-3.

EIA, U., US Crude Oil Production to 2025: Updated Projection of Crude Types. US Energy Information Administration Washington, DC, 2015.

El Fantroussi, S., Agathos, S. N., 2005. Is bioaugmentation a feasible strategy for pollutant removal and site remediation? Current opinion in microbiology. 8**,** 268-275.

Elanchezhiyan, S. S., et al., 2018. Effective adsorption of oil droplets from oil-in-water emulsion using metal ions encapsulated biopolymers: Role of metal ions and their mechanism in oil removal. International journal of biological macromolecules. 112**,** 294-305.

Emam, E. A., 2013. Modified activated carbon and bentonite used to adsorb petroleum hydrocarbons emulsified in aqueous solution. Am J Environ Prot. 2**,** 161-169.

Estell, D., et al., 1986. Probing steric and hydrophobic effects on enzyme-substrate interactions by protein engineering. Science. 233**,** 659-663.

Farahbakhsh, K., Smith, D., 2004. Estimating air diffusion contribution to pressure decay during membrane integrity tests. Journal of membrane science. 237**,** 203-212.

Fard, A. K., et al., 2016. Enhancing oil removal from water using ferric oxide nanoparticles doped carbon nanotubes adsorbents. Chemical Engineering Journal. 293**,** 90-101.

Feller, G., Gerday, C., 2003. Psychrophilic enzymes: hot topics in cold adaptation. Nature reviews microbiology. 1**,** 200-208.

Fetter, C. W., et al., 1999. Contaminant hydrogeology. Prentice hall Upper Saddle River, NJ.

Fielding, E., et al., 2010. The National Transportation Safety Board: A model for systemic risk management. Available at SSRN 1695781.

Filler, D. M. V. S., D. R.; Leigh, M. B., Remediation of frozen ground contaminated with petroleum hydrocarbons: feasibility and limits. In Permafrost soils, Springer: 2009; pp 279-301.

Fini, M. N., et al., 2019. The effect of water matrix, feed concentration and recovery on the rejection of pesticides using NF/RO membranes in water treatment. Separation and Purification Technology.

Forth, H. P., et al., 2021. Use of Correlated Water Sample Chemistry and Synthetic Aperture Radar Footprints to Estimate Oil Concentrations in the Upper Water Column during the Deepwater Horizon Oil Spill. ACS Earth and Space Chemistry.

Fournier, R. L., 2017. Basic transport phenomena in biomedical engineering. CRC press.

Fuenmayor, S. L., et al., 1998. A gene cluster encoding steps in conversion of naphthalene to gentisate in Pseudomonas sp. strain U2. Journal of Bacteriology. 180**,** 2522-2530.

Gan, Q., Soil Quality Fertility Determination in Precision Agriculture and Bitumen Residue Determination in Oil Sand Tailings by Fourier Transform Infrared Spectroscopy Coupled with Chemometrics. McGill University Libraries, 2017.

Gao, H. Z., J.; Lai, H.; Xue, Q., Degradation of asphaltenes by two Pseudomonas aeruginosa strains and their effects on physicochemical properties of crude oil. International Biodeterioration & Biodegradation 2017, 122, 12-22.

García-Sánchez, M., et al., 2018. A comparative study to evaluate natural attenuation, mycoaugmentation, phytoremediation, and microbial-assisted phytoremediation strategies for the bioremediation of an aged PAH-polluted soil. Ecotoxicology and environmental safety. 147**,** 165-174.

García-Sánchez, M. K., Z.; Mercl, F.; Aranda, E.; Tlustoš, P., A comparative study to evaluate natural attenuation, mycoaugmentation, phytoremediation, and microbial-assisted phytoremediation strategies for the bioremediation of an aged PAH-polluted soil. Ecotoxicology and environmental safety 2018, 147, 165-174.

Gaur, N. N., K.; PydiSetty, Y., Recent advances in the bio-remediation of persistent organic pollutants and its effect on environment. Journal of Cleaner Production 2018.

Gilbert, D., et al., 2015. Endocrine activity of persistent organic pollutants accumulated in human silicone implants—Dosing in vitro assays by partitioning from silicone. Environment international. 84**,** 107-114.

Gisi, D., 2017. In situ remediation of contaminated marinesediment: an overview. Environmental science and pollution research international.

Glogauer, A., et al., 2011. Identification and characterization of a new true lipase isolated through metagenomic approach. Microbial cell factories. 10**,** 1-15.

Gomari, K. R., Hamouda, A., 2006. Effect of fatty acids, water composition and pH on the wettability alteration of calcite surface. Journal of petroleum science and engineering. 50**,** 140-150.

Gordon, D., 2012. Understanding unconventional oil. Carnegie Endowment for International Peace.

Gordon, G., et al., 2018. Oil spill effects on soil hydrophobicity and related properties in a hyper-arid region. Geoderma. 312**,** 114-120.

Grant, S., The Kalamazoo River Spill: Pipelines, Politics, and Economies of Knowledge. 2014.

Gruszecka-Kosowska, A., et al., 2015. An analysis of the chemistry, mineralogy and texture of waste dolomite powder used to identify its potential application in industry. Geology, Geophysics and Environment. 41.

Gurav, R. L., H.; Ma, J.; Tang, J.; Liu, Q.; Zhang, H., Degradation of n-alkanes and PAHs from the heavy crude oil using salt-tolerant bacterial consortia and analysis of their catabolic genes. Environmental Science and Pollution Research 2017, 24, (12), 11392-11403.

Hein, F. J., 2006. Heavy oil and oil (tar) sands in North America: An overview & summary of contributions. Natural Resources Research. 15**,** 67-84.

Heitkamp, M. A., et al., 1988. Pyrene degradation by a Mycobacterium sp.: identification of ring oxidation and ring fission products. Applied and Environmental Microbiology. 54**,** 2556-2565.

Hentati, D. C., A.; Hadrich, F.; Frikha, I.; Rabanal, F.; Sayadi, S.; Manresa, A.; Chamkha, M., Production, characterization and biotechnological potential of lipopeptide biosurfactants from a novel marine Bacillus stratosphericus strain FLU5. Ecotoxicology and environmental safety 2019, 167, 441-449.

Hernández-López, E. L., et al., 2016. Biotransformation of petroleum asphaltenes and high molecular weight polycyclic aromatic hydrocarbons by Neosartorya fischeri. Environmental Science and Pollution Research. 23**,** 10773-10784.

Hernández-López, E. L. P., L.; Huerta-Saquero, A.; Mouriño-Pérez, R.; Vazquez-Duhalt, R., Biotransformation of petroleum asphaltenes and high molecular weight polycyclic aromatic hydrocarbons by Neosartorya fischeri. Environmental Science and Pollution Research 2016, 23, (11), 10773-10784.

Hoang, A. T. B., X. L.; Pham, X. D., A novel investigation of oil and heavy metal adsorption capacity from as-fabricated adsorbent based on agricultural by-product and porous polymer. Energy Sources, Part A: Recovery, Utilization, and Environmental Effects 2018, 40, (8), 929-939.

Hodson, P. V., 2017. The toxicity to fish embryos of PAH in crude and refined oils. Archives of environmental contamination and toxicology. 73**,** 12-18.

Hosokawa, R., et al., 2009. Autochthonous bioaugmentation and its possible application to oil spills. World Journal of Microbiology and Biotechnology. 25**,** 1519-1528.

Hossain, S. Z., et al., 2017. Laboratory study of mass transfer from diluted bitumen trapped in gravel. Environmental Science: Processes & Impacts. 19**,** 1583-1593.

Hosseinpour, N., et al., 2013. Asphaltene adsorption onto acidic/basic metal oxide nanoparticles toward in situ upgrading of reservoir oils by nanotechnology. Langmuir. 29**,** 14135-14146.

Hua, Y., et al., 2018. Effect of evaporative weathering and oil-sediment interactions on the fate and behavior of diluted bitumen in marine environments. Part 1. Spill-related properties, oil buoyancy, and oil-particulate aggregates characterization. Chemosphere. 191**,** 1038-1047.

Huang, H., et al., 2018. Environmental and Economic Implications of the Biogeochemistry of Oil Sands Bitumens. Hydrocarbons, Oils and Lipids: Diversity, Origin, Chemistry and Fate. 1-19.

Huang, X., Lim, T.-T., 2006. Performance and mechanism of a hydrophobic–oleophilic kapok filter for oil/water separation. Desalination. 190**,** 295-307.

Itodo, A., Itodo, H., 2010. Sorption energies estimation using Dubinin-Radushkevich and Temkin adsorption isotherms. Life Science Journal-Acta Zhengzhou University Overseas Edition. 7**,** 31-39.

Ivshina, I. B., et al., 2015. Oil spill problems and sustainable response strategies through new technologies. Environmental Science: Processes & Impacts. 17**,** 1201-1219.

Jardine, J., et al., 2018. Screening of potential bioremediation enzymes from hot spring bacteria using conventional plate assays and liquid chromatography-Tandem mass spectrometry (Lc-Ms/Ms). Journal of environmental management. 223**,** 787-796.

Ji, X., et al., 2014. Enabling multi-enzyme biocatalysis using coaxial-electrospun hollow nanofibers: redesign of artificial cells. Journal of Materials Chemistry B. 2**,** 181-190.
Jiang, Z., et al., 2015. Removal of oil from water using magnetic bicomponent composite nanofibers fabricated by electrospinning. Composites Part B: Engineering. 77**,** 311-318.
Jouanneau, Y., Meyer, C., 2006. Purification and characterization of an arene cis-dihydrodiol dehydrogenase endowed with broad substrate specificity toward polycyclic aromatic hydrocarbon dihydrodiols. Applied and environmental microbiology. 72**,** 4726-4734.
Jouanneau, Y., et al., 2006. Characterization of a naphthalene dioxygenase endowed with an exceptionally broad substrate specificity toward polycyclic aromatic hydrocarbons. Biochemistry. 45**,** 12380-12391.
Kadri, T., et al., 2018a. Nanoencapsulation and release study of enzymes from Alkanivorax borkumensis in chitosan-tripolyphosphate formulation. Biochemical Engineering Journal. 137**,** 1-10.
Kadri, T., et al., 2018b. Ex-situ biodegradation of petroleum hydrocarbons using Alcanivorax borkumensis enzymes. Biochemical Engineering Journal. 132**,** 279-287.
Kadri, T., et al., 2018c. Bench-scale production of enzymes from the hydrocarbonoclastic bacteria Alcanivorax borkumensis and biodegradation tests. Journal of biotechnology. 283**,** 105-114.
Kadri, T., et al., 2018d. Production and characterization of novel hydrocarbon degrading enzymes from Alcanivorax borkumensis. International journal of biological macromolecules. 112**,** 230-240.
Kawakami, K., et al., 1980. Performance of a hollow fibre beaker device for continuous enzymic reactions. Enzyme and Microbial Technology. 2**,** 295-298.
Kelesoglu, S., et al., 2012. Adsorption of naphthenic acids onto mineral surfaces studied by quartz crystal microbalance with dissipation monitoring (QCM-D). Energy & Fuels. 26**,** 5060-5068.
Khan, A. A. W., R.-F.; Cao, W.-W.; Doerge, D. R.; Wennerstrom, D.; Cerniglia, C. E., Molecular cloning, nucleotide sequence, and expression of genes encoding a polycyclic aromatic ring dioxygenase from Mycobacterium sp. strain PYR-1. Applied and Environmental Microbiology 2001, 67, (8), 3577-3585.
Khan, A. R., et al., 1996. A generalized equation for adsorption isotherms for multi-component organic pollutants in dilute aqueous solution. Environmental technology. 17**,** 13-23.
Khosravi, M., Azizian, S., 2017. Preparation of superhydrophobic and superoleophilic nanostructured layer on steel mesh for oil-water separation. Separation and Purification Technology. 172**,** 366-373.
Kim, S., et al., 2013. Porous polyimide membranes prepared by wet phase inversion for use in low dielectric applications. International Journal of Molecular Sciences. 14**,** 8698-8707.
King, T. L., et al., 2020. Canadian bitumen is engineered for transport, but the type of product produced can affect spill contingency planning. Environmental Science: Processes & Impacts. 22**,** 863-872.
Kiso, Y., et al., 2001. Effects of hydrophobicity and molecular size on rejection of aromatic pesticides with nanofiltration membranes. Journal of Membrane Science. 192**,** 1-10.
Kleinhans, F., 1998. Membrane permeability modeling: Kedem–Katchalsky vs a two-parameter formalism. Cryobiology. 37**,** 271-289.
Ko, D. C., et al., 2001. Film-pore diffusion model for the fixed-bed sorption of copper and cadmium ions onto bone char. Water research. 35**,** 3876-3886.

Kolenc, R. I., W.; Glick, B.; Robinson, C.; Mayfield, C., Transfer and expression of mesophilic plasmid-mediated degradative capacity in a psychrotrophic bacterium. Applied and environmental microbiology 1988, 54, (3), 638-641.
Kong, H., et al., 2011. Removal of polycyclic aromatic hydrocarbons from aqueous solution on soybean stalk–based carbon. Journal of environmental quality. 40**,** 1737-1744.
Konnova, S. A., et al., 2016. Nanoshell assembly for magnet-responsive oil-degrading bacteria. Langmuir. 32**,** 12552-12558.
Korfiatis, G. P., Christodoulatos, C., 1993. Treatability studies as a remedial option screening tool for contaminated soils. Remediation Journal. 3**,** 395-412.
Krishnan, S., et al., 2004. o-Phthalic acid, a dead-end product in one of the two pathways of phenanthrene degradation in Pseudomonas sp. strain PP2.
Kumar, P., et al., 2020a. Removal of microcystin-LR and other water pollutants using sand coated with bio-optimized carbon submicron particles: Graphene oxide and reduced graphene oxide. Chemical Engineering Journal. 397**,** 125398.
Kumar, P., et al., 2019. Agro-industrial residues as a unique support in a sand filter to enhance the bioactivity to remove microcystin-Leucine aRginine and organics. Science of the total environment. 670**,** 971-981.
Kumar, S., et al., 2020b. Insights into the metabolism pathway and functional genes of long-chain aliphatic alkane degradation in haloarchaea. Extremophiles. 24**,** 475-483.
Kwean, O. S., et al., 2018. 4-Chlorophenol biodegradation facilitator composed of recombinant multi-biocatalysts immobilized onto montmorillonite. Bioresource technology. 259**,** 268-275.
Lacoursière, J. P., et al., 2015. Lac-Mégantic accident: What we learned. Process Safety Progress. 34**,** 2-15.
Lapointe, M.-C., et al., 2016. Effect of energetic materials wettability on their outdoor effective elution rate. Journal of Hazardous Materials. 311**,** 194-202.
Lavagna, L., et al., 2019. Hydrophobic cellulose ester as a sustainable material for simple and efficient water purification processes from fatty oils contamination. Wood Science and Technology. 53**,** 249-261.
Lee, S. Y., Consequences of microbial interactions with hydrocarbons, oils, and lipids: production of fuels and chemicals. Springer: 2017.
LeVan, M. D., et al., 1997. Adsorption and ion exchange. Energy. 16**,** 17.
Li, D.-C., et al., 2018a. Remediation of Petroleum-Contaminated Soil and Simultaneous Recovery of Oil by Fast Pyrolysis. Environmental science & technology. 52**,** 5330-5338.
Li, D.-C. X., W.-F.; Mu, Y.; Yu, H.-Q.; Jiang, H.; Crittenden, J. C., Remediation of Petroleum-Contaminated Soil and Simultaneous Recovery of Oil by Fast Pyrolysis. Environmental science & technology 2018, 52, (9), 5330-5338.
Li, X., et al., 2018b. Understanding desorption of oil fractions from mineral surfaces. Fuel. 232**,** 257-266.
Li, X. P., Y.; Hu, S.; Cheng, Y.; Wang, Y.; Wu, K.; Zhang, S.; Yang, S., Diversity of phenanthrene and benz [a] anthracene metabolic pathways in white rot fungus Pycnoporus sanguineus 14. International biodeterioration & biodegradation 2018, 134, 25-30.
Li, Y., et al., 2014. Aerobic degradation of trichloroethylene by co-metabolism using phenol and gasoline as growth substrates. International journal of molecular sciences. 15**,** 9134-9148.
Li, Z., et al., 2021a. Efficiencies of selected biotreatments for the remediation of PAH in diluted bitumen contaminated soil microcosms. Biodegradation. 32**,** 563-576.

Li, Z., et al., 2021b. Efficiencies of selected biotreatments for the remediation of PAH in diluted bitumen contaminated soil microcosms. Biodegradation. 1-14.
Lim, M., et al., 2017. OPTIMIZATION STUDIES FOR THE FLOTATION OF BUNKER OIL FROM CONTAMINATED SAND USING MICROBUBBLES. Journal of Engineering Science and Technology. 12**,** 2046-2063.
Lin, J., et al., 2013. Co-axial electrospun polystyrene/polyurethane fibres for oil collection from water surface. Nanoscale. 5**,** 2745-2755.
Lin, X., et al., 2017. Estimation of fixed-bed column parameters and mathematical modeling of breakthrough behaviors for adsorption of levulinic acid from aqueous solution using SY-01 resin. Separation and Purification Technology. 174**,** 222-231.
Liu, H. C., Y.; Du, B.; Tong, C.; Liang, S.; Han, S.; Zheng, S.; Lin, Y., Overexpression of a novel thermostable and chloride-tolerant laccase from Thermus thermophilus SG0. 5JP17-16 in Pichia pastoris and its application in synthetic dye decolorization. PLoS One 2015, 10, (3), e0119833.
Liu, J., et al., 2021. Analysis of the mechanism for enhanced pyrene biodegradation based on the interactions between iron-ions and Rhodococcus ruber strain L9. Ecotoxicology and Environmental Safety. 225**,** 112789.
Logeshwaran, P., et al., 2018. Petroleum hydrocarbons (PH) in groundwater aquifers: An overview of environmental fate, toxicity, microbial degradation and risk-based remediation approaches. Environmental Technology & Innovation. 10**,** 175-193.
Lonappan, L., et al., Chlorpyrifos Degradation by Crude Enzyme Extracts Obtained from Alcanivorax borkumensis. Integrated and Sustainable Environmental Remediation. ACS Publications, 2018, pp. 81-95.
Lonappan, L., et al., 2019. Removal of diclofenac using microbiochar fixed-bed column bioreactor. Journal of Environmental Chemical Engineering. 7**,** 102894.
Ma, H., et al., 2021. Characterizing the Host Coral Proteome of Platygyra carnosa Using Suspension Trapping (S-Trap). Journal of Proteome Research.
Ma, S., et al., 2018. Effect of ultrasound treatment on antioxidant activity and structure of β-Lactoglobulin using the Box–Behnken design. CyTA-Journal of Food. 16**,** 596-606.
Manzetti, S., 2014. Remediation technologies for oil-drilling activities in the Arctic: oil-spill containment and remediation in open water. Environmental Technology Reviews. 3**,** 49-60.
Mapelli, F., et al., 2017. Biotechnologies for marine oil spill cleanup: indissoluble ties with microorganisms. Trends in biotechnology. 35**,** 860-870.
Margesin, R., et al., 2008. Psychrophiles: from biodiversity to biotechnology. Springer.
Marouf, R., et al., 2009. Zeta potential study of thermally treated dolomite samples in electrolyte solutions. Microporous and Mesoporous Materials. 122**,** 99-104.
Marques, M., Hogland, W., 2003. Hydrological performance of MSW incineration residues and MSW co-disposed with sludge in full-scale cells. Waste Management. 23**,** 469-481.
Mathavan, G., Viraraghavan, T., 1992. Coalescence/filtration of an oil-in-water emulsion in a peat bed. Water Research. 26**,** 91-98.
Mawad, A. M., et al., 2020. Quantification of naphthalene dioxygenase (NahAC) and catechol dioxygenase (C23O) catabolic genes produced by phenanthrene-degrading Pseudomonas fluorescens AH-40. Current Genomics. 21**,** 111-118.
McGenity, T. J., 2014. Hydrocarbon biodegradation in intertidal wetland sediments. Current Opinion in Biotechnology. 27**,** 46-54.

McKay, G., et al., 1986. External mass transfer during the adsorption of various pollutants onto activated carbon. Water Research. 20**,** 435-442.
McMurray, A., et al., 2018. Annex J1: Recent pipeline accidents involving crude oil in Canada and the United States. GUIDANCE FOR THE ENVIRONMENTAL PUBLIC HEALTH MANAGEMENT OF CRUDE OIL INCIDENTS. 131.
MDDELCC, M. d. D. d., de l'Environnement et de la Lutte contre les changements climatiques. 2016.
Mei, D., et al., 2016. Optimization of CO2 conversion in a cylindrical dielectric barrier discharge reactor using design of experiments. Plasma Processes and Polymers. 13**,** 544-556.
Meng, S., et al., 2020. The role of transparent exopolymer particles (TEP) in membrane fouling: A critical review. Water Research. 181**,** 115930.
Mercer, J. W., Basics of pump-and-treat ground-water remediation technology. Robert S. Kerr Environmental Research Laboratory, Office of Research and …: 1990.
Miri, S., et al., 2021a. Psychrozymes as novel tools to biodegrade p-xylene and potential use for contaminated groundwater in the cold climate. Bioresource Technology. 321**,** 124464.
Miri, S., et al., 2022. Enzymatic biodegradation of highly p-xylene contaminated soil using cold-active enzymes: A soil column study. Journal of Hazardous Materials. 423**,** 127099.
Miri, S., et al., 2018. Recent biotechnological advances in petroleum hydrocarbons degradation under cold climate conditions: A review. Critical Reviews in Environmental Science and Technology. 1-34.
Miri, S., et al., 2019. Recent biotechnological advances in petroleum hydrocarbons degradation under cold climate conditions: A review. Critical Reviews in Environmental Science and Technology. 49**,** 553-586.
Miri, S., et al., 2021b. Sustainable production and co-immobilization of cold-active enzymes from Pseudomonas sp. for BTEX biodegradation. Environmental Pollution. 285**,** 117678.
Mishra, S., Singh, S., 2012. Microbial degradation of n-hexadecane in mineral salt medium as mediated by degradative enzymes. Bioresource technology. 111**,** 148-154.
Mohamed, A. I., et al., 2018. Use of organoclay as a stabilizer for water-in-oil emulsions under high-temperature high-salinity conditions. Journal of Petroleum Science and Engineering. 160**,** 302-312.
Mohamed, A. I., et al., 2017. Influence of surfactant structure on the stability of water-in-oil emulsions under high-temperature high-salinity conditions. Journal of Chemistry. 2017.
Moody, J. D., et al., 2001. Degradation of phenanthrene and anthracene by cell suspensions of Mycobacterium sp. strain PYR-1. Applied and environmental microbiology. 67**,** 1476-1483.
Mourabet, M., et al., 2012. Removal of fluoride from aqueous solution by adsorption on Apatitic tricalcium phosphate using Box–Behnken design and desirability function. Applied Surface Science. 258**,** 4402-4410.
Mowla, D., et al., 2013. Modeling of the adsorption breakthrough behaviors of oil from salty waters in a fixed bed of commercial organoclay/sand mixture. Chemical engineering journal. 218**,** 116-125.
Muratova, A. H., T.; Narula, N.; Wand, H., Rhizosphere microflora of plants used for the phytoremediation of bitumen-contaminated soil. Microbiological research 2003, 158, (2), 151.

Muratova, A. Y. T., O.; Hübner, T.; Kuschk, P., Studies of the efficacy of alfalfa and reed in the phytoremediation of hydrocarbon-polluted soil. Applied Biochemistry and Microbiology 2003, 39, (6), 599-605.

Murphy, C., 2016. Polyimides. Nova Science Publishers, Incorporated.

Naghdi, M., et al., 2017. Pine-wood derived nanobiochar for removal of carbamazepine from aqueous media: Adsorption behavior and influential parameters. Arabian Journal of Chemistry.

Nagy, Z., et al., 2001. β-Galactosidase of Penicillium chrysogenum: production, purification, and characterization of the enzyme. Protein expression and purification. 21**,** 24-29.

National Academies of Sciences, E., Medicine, 2016. Spills of Diluted Bitumen from Pipelines: A Comparative Study of Environmental Fate, Effects, and Response. National Academies Press.

Niu, J., et al., 2013. Adsorption and transformation of PAHs from water by a laccase-loading spider-type reactor. Journal of hazardous materials. 248**,** 254-260.

Nopcharoenkul, W. N., P.; Pinyakong, O., Diesel oil removal by immobilized Pseudoxanthomonas sp. RN402. Biodegradation 2013, 24, (3), 387-397.

Nwaogu, L. O., G.; Nwabueze, R., Degradation of diesel oil in a polluted soil using Bacillus subtilis. African Journal of Biotechnology 2008, 7, (12), 1939-1943.

Obón, J., et al., 1996. Continuous retention of native NADP (H) in an enzyme membrane reactor for gluconate and glutamate production. Journal of biotechnology. 50**,** 27-36.

Okhrimenko, D., et al., 2013. Energies of the adsorption of functional groups to calcium carbonate polymorphs: the importance of− OH and− COOH groups. Langmuir. 29**,** 11062-11073.

Olu-Owolabi, B. I., et al., 2014. Evaluation of pyrene sorption–desorption on tropical soils. Journal of environmental management. 137**,** 1-9.

Ortmann, A. C. C., S. E.; Wohlgeschaffen, G.; Thamer, P.; McIntyre, C.; Mason, J.; King, T. L., Inorganic nutrients have a significant, but minimal, impact on a coastal microbial community's response to fresh diluted bitumen. Marine pollution bulletin 2019, 139, 381-389.

Parales, R. E., et al., 1998. Substrate specificities of hybrid naphthalene and 2, 4-dinitrotoluene dioxygenase enzyme systems. Journal of Bacteriology. 180**,** 2337-2344.

Parales, R. E., et al., 2000. Substrate specificity of naphthalene dioxygenase: effect of specific amino acids at the active site of the enzyme. Journal of bacteriology. 182**,** 1641-1649.

Patel, M. S., Evaluation of Mass Transfer Rate in Column of Small Lilsx Particles. Cleveland State University, 2017.

Patowary, M., et al., 2015. A facile preparation of superhydrophobic and oleophilic precipitated calcium carbonate sorbent powder for oil spill clean-ups from water and land surfaces. RSC Advances. 5**,** 79852-79859.

Patterson, L. A., et al., 2017. Unconventional oil and gas spills: risks, mitigation priorities, and state reporting requirements. Environmental science & technology. 51**,** 2563-2573.

Peixoto, R. V., A.; Rosado, A., Petroleum-degrading enzymes: bioremediation and new prospects. Enzyme research 2011, 2011.

Peng, R.-H., et al., 2008. Microbial biodegradation of polyaromatic hydrocarbons. FEMS microbiology reviews. 32**,** 927-955.

Penning, T. M., et al., 1999. Dihydrodiol dehydrogenases and polycyclic aromatic hydrocarbon activation: generation of reactive and redox active o-quinones. Chemical research in toxicology. 12**,** 1-18.

Phillips, L. A. G., C. W.; Germida, J. J., Culture-based and culture-independent assessment of the impact of mixed and single plant treatments on rhizosphere microbial communities in hydrocarbon contaminated flare-pit soil. Soil Biology and Biochemistry 2006, 38, (9), 2823-2833.

Pintor, A. M., et al., 2016. Oil and grease removal from wastewaters: sorption treatment as an alternative to state-of-the-art technologies. A critical review. Chemical Engineering Journal. 297**,** 229-255.

Pokrovsky, O. S., et al., 1999. Dolomite surface speciation and reactivity in aquatic systems. Geochimica et Cosmochimica Acta. 63**,** 3133-3143.

Prendergast, D. P., Gschwend, P. M., 2014. Assessing the performance and cost of oil spill remediation technologies. Journal of cleaner production. 78**,** 233-242.

Price, J. S., et al., 2010. Landscape restoration after oil sands mining: conceptual design and hydrological modelling for fen reconstruction. International Journal of Mining, Reclamation and Environment. 24**,** 109-123.

Qiao, K., et al., 2019. Application of magnetic adsorbents based on iron oxide nanoparticles for oil spill remediation: A review. Journal of the Taiwan Institute of Chemical Engineers.

Qiu, H., et al., 2009. Critical review in adsorption kinetic models. Journal of Zhejiang University-Science A. 10**,** 716-724.

Quast, K., 2016. The use of zeta potential to investigate the pKa of saturated fatty acids. Advanced Powder Technology. 27**,** 207-214.

Quesada, E., et al., 1987. Growth characteristics and salt requirement of Deleya halophila in a defined medium. Current Microbiology. 16**,** 21-25.

Radović, J. R., et al., Environmental Assessment of Spills Related to Oil Exploitation in Canada's Oil Sands Region. Oil Spill Environmental Forensics Case Studies. Elsevier, 2018, pp. 401-417.

Rahman, M., Sathasivam, K. V., 2015. Heavy metal adsorption onto kappaphycus sp. from aqueous solutions: The use of error functions for validation of isotherm and kinetics models. BioMed research international. 2015.

Raji, F., Pakizeh, M., 2014. Kinetic and thermodynamic studies of Hg (II) adsorption onto MCM-41 modified by ZnCl2. Applied Surface Science. 301**,** 568-575.

Raji, F., et al., 2015. Removal of Pb (ii) from aqueous solution by mesoporous silica MCM-41 modified by ZnCl 2: kinetics, thermodynamics, and isotherms. Rsc Advances. 5**,** 37066-37077.

Refining, A. P. I. D. o., 1969. Manual on Disposal of Refinery Wastes: Volume on Liquid Wastes. American Petroleum Institute, Division of Refining.

Reid, T. C., S. R.; Droppo, I. G.; Weisener, C. G., Novel insights into freshwater hydrocarbon-rich sediments using metatranscriptomics: Opening the black box. Water Research 2018, 136, 1-11.

Ridley, C. M., 2018. Microbial Ecology of Subsurface Oil Sands Deposits in Northern Alberta, Canada.

Robert, T., et al., 2017. Impact of heterogeneous properties of soil and LNAPL on surfactant-enhanced capillary desaturation. Journal of contaminant hydrology. 204**,** 57-65.

Rodríguez-Delgado, M., Ornelas-Soto, N., Laccases: A blue enzyme for greener alternative technologies in the detection and treatment of emerging pollutants. Green Technologies and Environmental Sustainability. Springer, 2017, pp. 45-65.

Rony, P. R., 1971. Multiphase catalysis. II. Hollow fiber catalysts. Biotechnology and Bioengineering. 13**,** 431-447.
Rowbotham, T., Cross, T., 1977. Ecology of Rhodococcus coprophilus and associated actinomycetes in fresh water and agricultural habitats. Microbiology. 100**,** 231-240.
Rudyk, S., 2018. Relationships between SARA fractions of conventional oil, heavy oil, natural bitumen and residues. Fuel. 216**,** 330-340.
Sadalage, P. S., et al., 2020. Formulation of synthetic bacterial consortia and their evaluation by principal component analysis for lignocellulose rich biomass degradation. Renewable Energy. 148**,** 467-477.
Sadeghi, K. M., et al., 1992. A new bitumen recovery technology and its potential application to remediation of oil spills. Journal of Petroleum Science and Engineering. 8**,** 105-117.
Sahoo, P., Sahoo, A., 2013. Fluidization and spouting of fine particles: A comparison. Advances in Materials Science and Engineering. 2013.
Saint-Laurent, D., et al., 2018. Assessment of Hydrocarbons (C10-C50), Polycyclic Aromatic Hydrocarbons (PAHs), and Trace Metals (TMs) Contamination in the Riverbanks of the Chaudière River Three Years after the Lac-Mégantic Railway Disaster (Southern Québec, Canada). Soil and Sediment Contamination: An International Journal. 27**,** 98-119.
Salim, F., et al., 2019. Modelling permeation passive sampling: Intra-particle resistance to mass transfer and comprehensive sensitivity analysis. Environmental Science: Processes & Impacts. 21**,** 469-484.
Santos, R., et al., 2014. An overview of heavy oil properties and its recovery and transportation methods. Brazilian Journal of Chemical Engineering. 31**,** 571-590.
Schneiker, S., et al., 2006. Genome sequence of the ubiquitous hydrocarbon-degrading marine bacterium Alcanivorax borkumensis. Nature biotechnology. 24**,** 997.
Schneiker, S. d. S., V. A. M.; Bartels, D.; Bekel, T.; Brecht, M.; Buhrmester, J.; Chernikova, T. N.; Denaro, R.; Ferrer, M.; Gertler, C., Genome sequence of the ubiquitous hydrocarbon-degrading marine bacterium Alcanivorax borkumensis. Nature biotechnology 2006, 24, (8), 997.
Schreiber, L., et al., 2019. Evaluation of the natural attenuation potential of diluted bitumen by microbial communities in the Douglas Channel and Hecate Strait, British Columbia. Appl. Environ. Microbiol.**,** AEM. 00086-19.
Sekulic, M. T., et al., 2019. Surface functionalised adsorbent for emerging pharmaceutical removal: Adsorption performance and mechanisms. Process Safety and Environmental Protection. 125**,** 50-63.
Shafeeyan, M. S., et al., 2014. A review of mathematical modeling of fixed-bed columns for carbon dioxide adsorption. Chemical engineering research and design. 92**,** 961-988.
Shahsavari, E., et al., 2013. Plant residues—a low cost, effective bioremediation treatment for petrogenic hydrocarbon-contaminated soil. Science of the Total Environment. 443**,** 766-774.
Shaikhulova, S., et al., 2021. Worms eat oil: Alcanivorax borkumensis hydrocarbonoclastic bacteria colonise Caenorhabditis elegans nematodes intestines as a first step towards oil spills zooremediation. Science of The Total Environment. 761**,** 143209.
Shi, Y. H., C.; Rocha, K. C.; El-Din, M. G.; Liu, Y., Treatment of oil sands process-affected water using moving bed biofilm reactors: with and without ozone pretreatment. Bioresource technology 2015, 192, 219-227.

ShiungLam, S., Chase, H., 2015. Progress in waste oil to sustainable energy, with emphasis on pyrolysis techniques.
Sidik, S., et al., 2012. Modified oil palm leaves adsorbent with enhanced hydrophobicity for crude oil removal. Chemical Engineering Journal. 203**,** 9-18.
Silva, S. M., et al., 2013. Adsorption of carotenes and phosphorus from palm oil onto acid activated bleaching earth: Equilibrium, kinetics and thermodynamics. Journal of Food Engineering. 118**,** 341-349.
Simón-Herrero, C., et al., 2019. Immobilized laccase on polyimide aerogels for removal of carbamazepine. Journal of hazardous materials. 376**,** 83-90.
Singh, R. P., Jha, P. N., 2016. A halotolerant bacterium Bacillus licheniformis HSW-16 augments induced systemic tolerance to salt stress in wheat plant (Triticum aestivum). Frontiers in plant science. 7**,** 1890.
Singleton, D. R., et al., 2012. Heterologous expression of polycyclic aromatic hydrocarbon ring-hydroxylating dioxygenase genes from a novel pyrene-degrading betaproteobacterium. Applied and environmental microbiology. 78**,** 3552-3559.
Smith, J. V., Bailey, S., 1963. Second review of Al–O and Si–O tetrahedral distances. Acta Crystallographica. 16**,** 801-811.
Smith, K. E., et al., 2010. Passive dosing for producing defined and constant exposure of hydrophobic organic compounds during in vitro toxicity tests. Chemical research in toxicology. 23**,** 55-65.
Song, D., et al., 2018. Optimization of growth and production parameters of walnut (Juglans regia) saplings with response surface methodology. Scientific reports. 8**,** 1-10.
Speight, J. G., 2013. Enhanced recovery methods for heavy oil and tar sands. Elsevier.
Speight, J. G., 2016. Introduction to enhanced recovery methods for heavy oil and tar sands. Gulf Professional Publishing.
Stout, S., Wang, Z., 2017. Oil Spill Environmental Forensics Case Studies. Butterworth-Heinemann.
Sun, Y., et al., 2016. Purification and properties of NADH-ferredoxinNAP reductase, a component of naphthalene dioxygenase from Pseudomonas sp. strain NCIB 9816. Biotechnology. 16**,** 107-123.
Sze, I., Dagley, S., 1984. Properties of salicylate hydroxylase and hydroxyquinol 1, 2-dioxygenase purified from Trichosporon cutaneum. Journal of bacteriology. 159**,** 353-359.
Taheran, M., et al., 2017. Degradation of chlortetracycline using immobilized laccase on Polyacrylonitrile-biochar composite nanofibrous membrane. Science of The Total Environment. 605**,** 315-321.
Tamas, I., et al., 2014. The (d) evolution of methanotrophy in the Beijerinckiaceae—a comparative genomics analysis. The ISME journal. 8**,** 369.
Tamas, I. S., A. V.; He, Z.; Dunfield, P. F., The (d) evolution of methanotrophy in the Beijerinckiaceae—a comparative genomics analysis. The ISME journal 2014, 8, (2), 369.
Tamura, K., et al., 2011. MEGA5: molecular evolutionary genetics analysis using maximum likelihood, evolutionary distance, and maximum parsimony methods. Molecular biology and evolution. 28**,** 2731-2739.
Thompson, I. P., et al., 2005. Bioaugmentation for bioremediation: the challenge of strain selection. Environmental Microbiology. 7**,** 909-915.

Thornton, S., et al., Bioremediation of Hydrocarbons and Chlorinated Solvents in Groundwater: Characterisation, Design and Performance Assessment. Hydrocarbon and Lipid Microbiology Protocols. Springer, 2016, pp. 11-64.

Tomás-Gallardo, L., et al., 2006. Proteomic and transcriptional characterization of aromatic degradation pathways in Rhodoccocus sp. strain TFB. Proteomics. 6**,** S119-S132.

Transportation Safety Board of Canada Pipeline Investigation Report. 2007, P. H.

Tsai, S.-C., et al., 2008. Comparison of different methods to determine the retardation factor of 137 Cs transport through granite in column experiments. Journal of Radioanalytical and Nuclear Chemistry. 275**,** 351-354.

Turner, C., 2017. The patch: The people, pipelines, and politics of the oil sands. Simon and Schuster.

Ukotije-Ikwut, P. R., et al., 2016. A novel method for adsorption using human hair as a natural oil spill sorbent. Int. J. Sci. Eng. Res. 7**,** 1754-1765.

USEPA Dredging Begins on Kalamazoo River, E. O. S., Marshall, Michigan,; 2013a., U. S. E. P. A.

van Beilen, J. B. D., W. A.; Schmid, A.; Witholt, B., Practical issues in the application of oxygenases. Trends in biotechnology 2003, 21, (4), 170-177.

Van Hamme, J. D., Ward, O. P., 2001. Physical and metabolic interactions of Pseudomonas sp. strain JA5-B45 and Rhodococcus sp. strain F9-D79 during growth on crude oil and effect of a chemical surfactant on them. Applied and environmental microbiology. 67**,** 4874-4879.

Vijayaraghavan, K., et al., 2006. Biosorption of nickel (II) ions onto Sargassum wightii: application of two-parameter and three-parameter isotherm models. Journal of hazardous materials. 133**,** 304-308.

Voth, W., Jakob, U., 2017. Stress-activated chaperones: a first line of defense. Trends in biochemical sciences. 42**,** 899-913.

Wahi, R., et al., 2013. Oil removal from aqueous state by natural fibrous sorbent: an overview. Separation and Purification Technology. 113**,** 51-63.

Wald, J., et al., 2015. Pseudomonads rule degradation of polyaromatic hydrocarbons in aerated sediment. Frontiers in microbiology. 6**,** 1268.

Walter, U., et al., 1991. Degradation of pyrene byRhodococcus sp. UW1. Applied Microbiology and Biotechnology. 34**,** 671-676.

Wang, D., 2011. Separation of Oil and Other Organics from Water Using Inverse Fluidization of Hydrophobic Aerogels. Arizona State University.

Wang, J., et al., 2002. Sum frequency generation vibrational spectroscopy studies on protein adsorption. The Journal of Physical Chemistry B. 106**,** 11666-11672.

Wang, L., et al., 2019a. Influence of organic carbon fractions of freshwater biofilms on the sorption for phenanthrene and ofloxacin: The important role of aliphatic carbons. Science of The Total Environment. 685**,** 818-826.

Wang, T., et al., 2005. The steam reforming of naphthalene over a nickel–dolomite cracking catalyst. Biomass and Bioenergy. 28**,** 508-514.

Wang, Z., et al., 2015. Kinetic and equilibrium studies of hydrophilic and hydrophobic rice husk cellulosic fibers used as oil spill sorbents. Chemical Engineering Journal. 281**,** 961-969.

Wang, Z., et al., 2019b. Different distribution of polycyclic aromatic hydrocarbons (PAHs) between Sphagnum and Ledum peat from an ombrotrophic bog in Northeast China. Journal of Soils and Sediments. 19**,** 1735-1744.

Ware, G. W. A., L. A.; Crosby, D.; Voogt, P.; Hutzinger, O.; Knaak, J. B.; Mayer, F. L.; Morgan, D.; Park, D. L.; Tjeerdema, R. S., Reviews of environmental contamination and toxicology. Springer: 2006.

Warner, A., et al., Development of the Electromagnetic Boom and MOP System (EMOP). Fermi National Accelerator Lab.(FNAL), Batavia, IL (United States), 2018a.

Warner, A., et al., Development of the Electromagnetic Boom and MOP System (EMOP). 2018b.

Warner, A. C., D.; Cullen, G.; Kasper, P.; Lumpkin, A.; Nelson, J. In Development of the Electromagnetic Boom and MOP System (EMOP), 6th Int. Beam Instrumentation Conf.(IBIC'17), Grand Rapids, MI, USA, 20-24 August 2017, 2018; JACOW, Geneva, Switzerland: 2018; pp 304-308.

Weber Jr, W. J., et al., 1992. A distributed reactivity model for sorption by soils and sediments. 1. Conceptual basis and equilibrium assessments. Environmental science & technology. 26**,** 1955-1962.

Wojcieszyńska, D., et al., 2012. Properties of catechol 2, 3-dioxygenase from crude extract of Stenotrophomonas maltophilia strain KB2 immobilized in calcium alginate hydrogels. Biochemical Engineering Journal. 66**,** 1-7.

Wong, M.-L., et al., 2015. Roles of thermophiles and fungi in bitumen degradation in mostly cold oil sands outcrops. Applied and environmental microbiology. AEM. 02221-15.

Wong, M.-L. A., D.; Caffrey, S.; Soh, J.; Dong, X.; Sensen, C. W.; Oldenburg, T.; Larter, S.; Voordouw, G., Roles of thermophiles and fungi in bitumen degradation in mostly cold oil sands outcrops. Applied and environmental microbiology 2015, AEM. 02221-15.

Wu, F.-C., et al., 2009. Characteristics of Elovich equation used for the analysis of adsorption kinetics in dye-chitosan systems. Chemical Engineering Journal. 150**,** 366-373.

Wu, M. L., W.; Dick, W. A.; Ye, X.; Chen, K.; Kost, D.; Chen, L., Bioremediation of hydrocarbon degradation in a petroleum-contaminated soil and microbial population and activity determination. Chemosphere 2017, 169, 124-130.

Wu, X., 2003. Investigating the stability mechanism of water-in-diluted bitumen emulsions through isolation and characterization of the stabilizing materials at the interface. Energy & fuels. 17**,** 179-190.

Wyndham, R., Costerton, J., 1981. Heterotrophic potentials and hydrocarbon biodegradation potentials of sediment microorganisms within the Athabasca oil sands deposit. Applied and environmental microbiology. 41**,** 783-790.

Xia, F., et al., 2005. Effect of pH changes on water release values in hydrophobic interaction chromatographic systems. Journal of Chromatography A. 1079**,** 229-235.

Xie, L., et al., 2017. Mapping the nanoscale heterogeneity of surface hydrophobicity on the sphalerite mineral. The Journal of Physical Chemistry C. 121**,** 5620-5628.

Xu, R., et al., 2013. Laccase immobilization on chitosan/poly (vinyl alcohol) composite nanofibrous membranes for 2, 4-dichlorophenol removal. Chemical engineering journal. 222**,** 321-329.

Younis, S. A., et al., 2017. Modeling and Optimization of Oil Adsorption from Wastewater Using an Amorphous Carbon Thin Film Fabricated from Wood Sawdust Waste Modified with Palmitic Acid. Environmental Processes. 4**,** 147-168.

Yu, J., et al., 2019. Design and attitude control of a novel robotic jellyfish capable of 3D motion. Sci. China Inf. Sci. 62**,** 194201:1-194201:3.

Yu, Q., et al., 2011. Anti-fouling bioactive surfaces. Acta biomaterialia. 7**,** 1550-1557.

Yu, X., et al., 2018a. Accelerated dewatering and detoxification of oil sands tailings using a biological amendment. Journal of Environmental Engineering. 144**,** 04018091.
Yu, X., et al., 2018b. Indigenous microorganisms residing in oil sands tailings biodegrade residual bitumen. Chemosphere.
Yu, X. C., Y.; Sampaga, R.; Rybiak, S.; Burns, T.; Ulrich, A. C., Accelerated dewatering and detoxification of oil sands tailings using a biological amendment. Journal of Environmental Engineering 2018, 144, (9), 04018091.
Yuan, M., et al., 2010. Adsorption of polycyclic aromatic hydrocarbons from water using petroleum coke-derived porous carbon. Journal of Hazardous Materials. 181**,** 1115-1120.
Yuan, X., Chung, T. M., 2012. Novel solution to oil spill recovery: using thermodegradable polyolefin oil superabsorbent polymer (oil–SAP). Energy & fuels. 26**,** 4896-4902.
Zabbey, N., Olsson, G., 2017. Conflicts–oil exploration and water. Global challenges. 1**,** 1600015.
Zdarta, J., et al., 2018a. Developments in support materials for immobilization of oxidoreductases: A comprehensive review. Advances in colloid and interface science. 258**,** 1-20.
Zdarta, J., et al., 2018b. A general overview of support materials for enzyme immobilization: characteristics, properties, practical utility. Catalysts. 8**,** 92.
Zhang, H., et al., 2016. A novel film–pore–surface diffusion model to explain the enhanced enzyme adsorption of corn stover pretreated by ultrafine grinding. Biotechnology for biofuels. 9**,** 181.
Zhang, L., et al., 2010. Sandwich-structured enzyme membrane reactor for efficient conversion of maltose into isomaltooligosaccharides. Bioresource technology. 101**,** 9144-9149.
Zhang, W., Jiang, F., 2019. Membrane fouling in aerobic granular sludge (AGS)-membrane bioreactor (MBR): Effect of AGS size. Water research. 157**,** 445-453.
Zhao, B., et al., 2009. Biodegradation of phenanthrene by a halophilic bacterial consortium under aerobic conditions. Current microbiology. 58**,** 205-210.
Zhong, K., Wang, Q., 2010. Optimization of ultrasonic extraction of polysaccharides from dried longan pulp using response surface methodology. Carbohydrate polymers. 80**,** 19-25.
Zhou, J.-F., et al., 2018. Heavy hydrocarbon degradation of crude oil by a novel thermophilic Geobacillus stearothermophilus strain A-2. International Biodeterioration & Biodegradation. 126**,** 224-230.
Zhou, J.-F. G., P.-K.; Dai, X.-H.; Cui, X.-Y.; Tian, H.-M.; Xie, J.-J.; Li, G.-Q.; Ma, T., Heavy hydrocarbon degradation of crude oil by a novel thermophilic Geobacillus stearothermophilus strain A-2. International Biodeterioration & Biodegradation 2018, 126, 224-230.
Zhu, Z., et al., 2020. Gravity-driven biomimetic membrane (GDBM): An ecological water treatment technology for water purification in the open natural water system. Chemical Engineering Journal. 399**,** 125650.
Zucca, P., Sanjust, E., 2014. Inorganic materials as supports for covalent enzyme immobilization: methods and mechanisms. Molecules. 19**,** 14139-14194.
Zuo, G., Wang, R., 2013. Novel membrane surface modification to enhance anti-oil fouling property for membrane distillation application. Journal of membrane science. 447**,** 26-35.

APPENDICES

APPENDIX A. Supplementary information of section 4.1.

Isolation of PAH degrading bacteria from contaminated sediments

After 1 month of incubation of the final enrichment culture on the mixture of oils, aliquots (100 µl) of 10^{-1} -10^{-10} dilutions, in SSM were spread on agar plates (M3 and NB agar) through the conventional spread-plate technique and then incubated at 15 °C for 4 days. After that, single colonies with different morphologies were visually selected and each of them inoculated to the freshly prepared M3 or NB medium (50 mL) amended with NaCl (10%) and used as inoculum for degradation and enzyme production screening. (Borisova, 2011; Miri et al., 2021a)

A series of pyrene biodegradation tests were conducted using SSM supplemented with three PAHs (naphthalene, phenanthrene, pyrene); and among all the isolated obtained (28 strains), URS-5, URS-6, URS-8, and URS-10 were selected based on their ability to grow on pyrene. To investigate the ability of individual strains to degrade PAHs at 15 ±1°C, 6×10^9 cfu/mL (exponential phase bacteria) of each bacterial cell were spiked to each sample. All tests were performed in SSM and PAHs (naphthalene, phenanthrene, and pyrene) as the sole carbon sources. To control the freely dissolved concentration of PAHs rather than the total concentration, the PAHs were loaded on the silicone O-rings before culturing of the bacteria as described in next section. Then. the mixture was incubated at 15 ±1°C on a rotary shaker at 170 rpm. These conditions were selected based on aerobic PAH biodegradation and optimum growth using above-mentioned genera. (Miri et al., 2021b) The efficiency of PAH biodegradation was calculated by the Eq. (A1)

$$\text{Degradation (\%)} = \frac{C_n - C_O}{C_O} \times 100 \qquad \text{(A1)}$$

Where, C_O and C_n are initial and final concentration (μg/mg of silicon) of PAH in the silicone O-ring, respectively. Among a total of 18 isolates that have been obtained, four isolates, were selected based on their ability to grow on PAHs in separate and mixture substrate tests at 15 ± 1 °C. A

spectrophotometer was used to measure bacterial growth, with the optical density (OD) being measured at 600 nm (OD600nm * 1–1.2, which equals 2.0×10^9 cells/ml).

As a final step, the 16S ribosomal RNA gene was used to identify the selected colonies. The following universal primers for PCR were used to amplify the gene fragment: 1492R (5′-GGTTACCTTGTTACGACTT-3′) and 27F (5′- AGAGTTTGATCCTGGCTCAG-3′). After sequencing the amplified products, the sequences of the 16S rRNA fragments were compared with the reference ones by using the BLASTn program available in the National Center for Biotechnology Information (NCBI) database.(Altschul et al., 1990) Afterward, the phylogenetic analysis was performed utilizing the neighbor-joining algorithm that is part of MEGA 7.0 software with a total of 1000 bootstraps.(Tamura et al., 2011)

Table A1 The individual PAH degrading bacterial strains and their combinations in different synthetic consortia

Sr.No.	Codes	Isolated Bacterial Strains
a) Individual Strains		
1	URS-5	
2	URS-6	
3	URS-8	
4	URS-10	
5	Alc	
b) Consortium code		Bacterial Combination in consortia
5	Mix1	URS5+URS6+URS8
6	Mix2	URS5+URS6+URS8+Alc
7	Mix3	URS6+URS10
8	Mix4	URS6+URS10+Alc
8	Mix5	URS5+URS8+URS10
9	Mix6	URS5+URS8+URS10+Alc
10	Mix7	URS5+URS6+URS8+URS10
11	Mix8	URS5+URS6+URS8+URS10+Alc

Biodegradation versus dissolved concentration

The performance of passive dosing was determined by studying O-ring loading, substrate release into medium and equilibrium concentration in medium. During the loading of PAHs, individual PAHs were dissolved in methanol (loading solvent) to saturation level. To create the PAHs mixture, the concentration in loading solution was calculated using partitioning coefficients for each PAH from

Gilbert et.al. (2011). (Gilbert et al., 2015) It has been suggested that after the O-rings have been cleaned and dried, 50 mL of loading solution at 15*1°C be added to the 50 mL of O-rings. The O-ring was removed from each loading batch after 128 h, and they were transferred into SSM to measure O-ring (C_{test}) and freely dissolved concentration of each PAH (C_{free}) at 0.33, 0.66, 1.33, 2.66, 5.33, 12, 24,48 and 72 h. The partition coefficient between different phases ($K_{Methanol:Oring}$ *and* $K_{Oring:SSM}$) were obtained using the measured $C_{test,initial}$ and $C_{free,\ initial}$. The obtained partitioning coefficient ($K_{Oring:SSM}$) was applied to calculate the required O-ring volume to avoid depletion (< 5%) using Eq.(A2)

$$V_{Oring} = \frac{V_{MSM}}{0.05 * K_{Oring:SSM}} \qquad \text{(A2)}$$

With a 5 mL SSM and partitioning coefficients from Table.A2, the O-ring volume needed for each PAH and PAH mixture were determined (Table.S2). The initial concentrations of freely dissolved PAHs ($C_{free\ initial}$) and O-ring concentrations (C_{test}) in medium samples were calculated via the approach published by Butler et.al (2013). (Butler et al., 2013) Finally, for the determination of the losses, freely dissolved concentrations of PAHs were directly measured in medium samples to compare with calculated $C_{free\ initial}$.

Two controls were included to study biodegradation versus dissolved concentrations. First control contained 5 mL of strain inoculating suspension in passive doing vials with O-rings to account for losses through biodegradation. Second control contained 5 mL of SSM without any strain in passive dosing vials in the presence of O-ring loaded with PAHs to account for losses through volatilization.

Table.A2 shows the partition coefficients obtained from measured PAH concentrations in loading solution, MSM and O-ring. The losses of naphthalene, anthracene, phenanthrene, and pyrene through volatilization for control 1 were 19, 4, 0 and 0 %, respectively.

Table A2. Octanol-water coefficients (log K_{OW}) and solubilities for PAHs in MSM. Also initial concentrations in solution and O-ring as well as the obtained partitioning coefficients for O-ring and MSM

	Log K_{ow}	C_{MSM} mg/L	$C_{test\ initial}$ mg/L	$C_{free\ initial}$ mg/L	C_{free} mg/L	$K_{Oring:MSM}$ mg/L
Naphthalene	3.37	20.52	97.8	18.31	17.73	1402±91
Anthracene	3.92	3.11	94.1	2.98	2.66	2559±442
Phenanthrene	4.57	1.04	48.6	1.01	0.91	7420±110
Pyrene	4.88	0.08	21.3	0.08	0.08	6502±740

Figure A1 shows the release of anthracene, phenanthrene, pyrene from the silicone O-rings into the medium. These results were representative of the PAHs behaviour, with the release being sufficiently rapid so that maximum concentrations were reached less than 45 minutes for all components. For naphthalene, after about 4h, the naphthalene concentration decreased due to the volatility of this compound at 15 ± 1 °C (not shown here); thus, the volume of the applied o-ring was 5 times higher compared to the needed volume for naphthalene to buffer the losses.

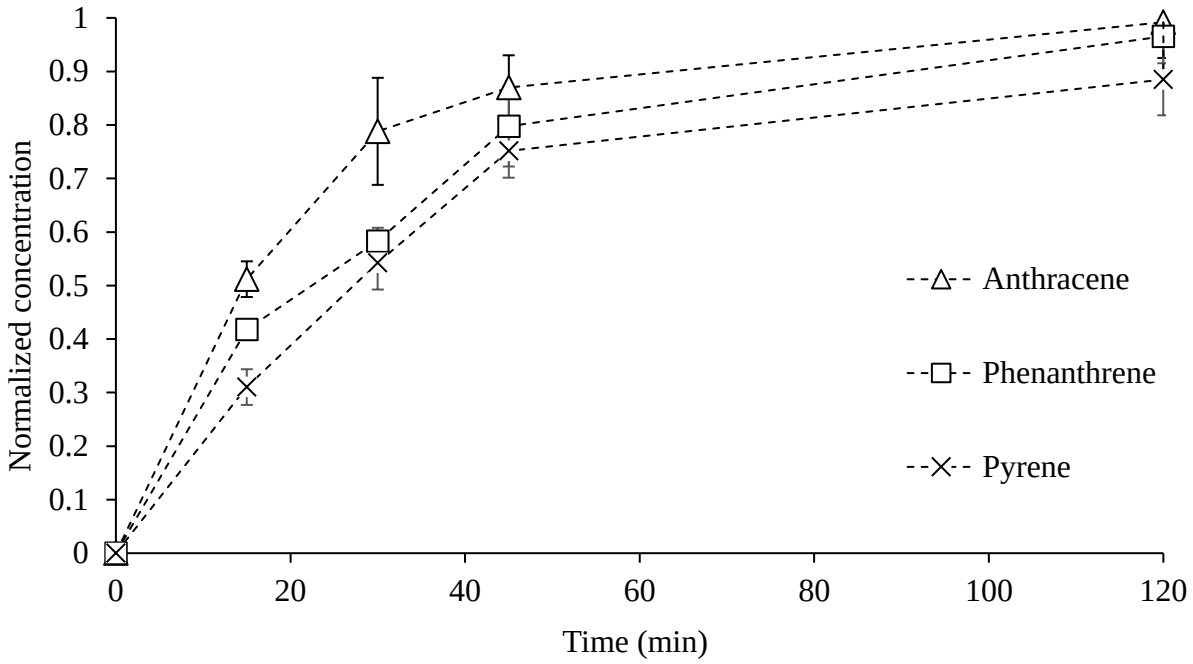

Fig.A1. Release of PAHs from silicone O-ring into 1 ml MiliQ water when shaking at 300 rpm. The data were normalized to the final saturation concentrations.

Proteomics sample preparation

In this study, 100-300µg of mini-S-Trap kit was used according to the manufacturer's instructions. Briefly, protein (250 µg) was reduced using TCEP with a final concentration of 30 mM at 60±1˚C for 15 min and alkylated with 1M IAA at room temperature for 1 h in a dark environment. Then, phosphoric acid (12.5%) was added to the samples and mixed with S-trap binding buffer (100 mM TEAB in 90% methanol, pH 7.1). The sample mixture was transferred into S-Trap microcolumns and centrifuged at 4000 *x* g until all solution was passed through. The columns were washed with S-trap binding buffer three times and 25 µL of Trypsin/Lys-C buffer with 50 mM TEAB and

trypsin (1:25:1 trypsin: protein) was added to the columns and incubated at 47˚C, 1h. The resulting peptides were eluted by elution basic buffer (50 mM TEAB), acidic buffer (0.1% formic acid in water) and organic buffer (0.1% formic acid in 80% of acetonitrile). The resulting peptides were dried at 45±1˚C and resuspended in 0.2% formic acid in water

Drop collapse assay and surface tension measurement

Using crude oil as the hydrocarbon substrate, a drop collapse assay was performed according to the method described by Bodour and Miller-Maier with slight modifications. In order to achieve the main objective of this study, crude oil was used as the substrate for this assay. One drop of 48-hour-grown culture broth was dropped onto a drop of crude oil on a glass slide. There was evidence of drop collapse. A tensiometer (K11, Kruss, Germany) was used to measure ST reduction every 24 hours up to the fifth day of culture. Isolates were screened that were capable of reducing the ST of the culture medium below 35 mN m*1 as efficient biosurfactants.

Enzyme production

Before inoculation for enzyme production, each bacterium was cultured in nutrition broth (NB) amended with NaCl (10%) at 15±1◦C and 150 rpm.(Singh and Jha, 2016) The enzyme production based on monoculture of newly isolated was carried out in serum bottles (250 mL) containing 50 mL of MSM and NB supplemented with Dilbit (500, 250 and 100 mg/L containing 7, 15, and 20 parts per million of pyrene) or mixture of 3 PAHs with $\sum 3\ PAHs = 25$, 50 and 75 mg/L. The target enzymes were also produced based on the multi-culture of newly isolated *Pseudomonas* URS-5, URS-6, URS-8, and *Rhodocucu* URS-10 as well as *Alcanivorax*. Following a specific period of incubation, the culture was centrifuged at 3810 *x* g for 20 min. The time-course experiments showed that depending on the type of enzymes and inducer, around 12 hours of incubation might be the best time when the production of enzymes is close to maximum. (Miri et al., 2022; Nagy et al., 2001) When growth reached the late exponential phase, extracellular enzymes were obtained from the supernatant extracted by centrifuging the culture washed with phosphate buffer (0.05 mM, pH 6.8) three times. Cells were harvested from the media after culturing by centrifugation (16,000 rpm for 4 min at 4 °C). The pellets with the biomass were resuspended in phosphate buffer, pH 8, and then sonicated on ice using an Ultrasonifier (Branson Ultrasonics Corporation, Danbury, CT, USA) at 22 and 30 kHz frequencies of ultrasounds for 10 min to obtain intracellular enzymes.

Enzyme assay

Naphthalene dioxygenase (ND) activity was assayed base on the formation of indigo at 500 nm per time unit. An enzyme reaction was carried out using 5 μl of indole 100 mM as a substrate in the presence of cellular lysates in DMF. A blank containing all the ingredients except for the substrate was used as a standard for measuring the absorbance of the reaction mixture at 500 nm. The specific enzyme activity was defined as the initial rate of indigo formation by plotting the increase in absorbance at the first 2 h of reaction normalized to the protein content of the sample. An indication of indigo formation was the formation of a purple product. The maximal absorbance of indigo was determined by mass spectrum at different wavelengths using a standard indigo solution dissolved in DMF. (da Silva and Alvarez, 2010)

Catechol 2,3- dioxygenase (C2,3D) and Catechol 1,2- dioxygenase (C1,2D) (not NADH requirement) activities were assayed by monitoring the production of muconic acid and 2-hydroxymuconic semialdehyde at 260 and 370 nm, respectively. Activity assays were performed in 3 mL of 50 mM sodium phosphate buffer (pH=7.0) containing 0.6 mL catechol (1 mM), 0.2 mL cellular lysates and 0.2 mL deionized water. After allowing the mixture to proceed at 15 ℃, a sub-sample was collected every 2 minutes and the results were analyzed. Enzyme activity is the amount of enzyme necessary to convert 1 mol of the substrate to muconic acid and 2-hydroxymuconic semialdehyde per unit of time. (Li et al., 2014; Liu et al., 2021) Salicylaldehyde dehydrogenase was followed by the decrease in salicylaldehyde at 255 nm ($\varepsilon = 9.74\ mM^{-1}\ cm^{-1}$) in the presence of NAD^{+1} mM, salicylaldehyde 1 mM, phosphate buffer (pH 7.4) 10 mM and the crude extract. (Miri et al., 2021a)

1-hydroxy-2-naphthoate (HNH) and salicylate hydroxylase activities were measured at 340 nm by an assay described by Balashova et al. (Balashova et al., 2001) The reaction mixture (1 ml) contained 20 mM KH_2PO_4 (pH 7.5), 100 µl cell extract, 100 µM NADH, and 50 µM 1-hydroxy-2-naphthoate or salicylate, respectively. Molar reaction coefficient at 340 nm of 5.08 and 6.22 $mM^{-1}cm^{-1}$ were used to determine the reaction of 1-hydroxy-2 naphthoate and salicylate. The rate of change in light absorption was measured at 340 nm. One unit of activity is the amount of enzyme that is needed to catalyze the conversion of one mol of NADH per minute into oxygen.(Sze and Dagley, 1984)

Protocatechuic acid (PCA) 3,4-dioxygenase enzyme assays were performed using quartz cuvettes with a 10-mm light path and UV-VIS spectrophotometer.(Tomás-Gallardo et al., 2006)

Approximately 100 to 150 mg of crude extract was added to a reaction mixture containing 50 mM Tris-HCl, pH 8.8 and 160 mM PCA. PCA 3,4-dioxygenase was followed by the decrease in PCA at 290 nm (ε = 5.11 mM^{-1} cm^{-1}). An enzyme activity unit (U) is defined as mmols of PCA transformed per minute. Using the Bradford assay kit as mentioned previously(Bradford, 1976), the total protein content of the cell can be determined.

PD and ND were precipitated at 40-50 and 20-30 % cut of ammonium sulphase for cell extract obtained from URS-10 and 6.

Initially, pyrene is oxidized to the central intermediates, including phthalic acid, by dioxygenase or monooxygenase, and then in the second step of biodegradation, phthalic acid is decomposed into inert intermediate by the ring-fission enzyme. The catalytic efficiency (K_{cat}/K_m) for naphthalene dioxygenase (ND), pyrene dioxygenase (PD) was determined to confirm the difference initial bacteria attack on pyrene after incubation of different isolates. In this regard, ND and PD were partially purified by ammonium sulfate as described in our previous work (Section S10).(Miri et al., 2022)

PD and ND catalytic parameters on pyrene and naphthalene were determined at 15◦C for the partially purified dioxygenase enzymes. Regarding the dioxygenase obtained from URS-6, a substrate-dependent oxidation of NADH was observed with two PAHs, but pyrene was the only PAHs, which was converted by the dioxygenase obtained from URS-10. To determine the substrate specificity of dioxygenase, the enzyme activity was determined in a reaction mixture (1mL) containing 50 μM of respective PAH in acetonitrile, 20 μL of partially purified enzyme, and 0.5 mM NADH in 50 mM potassium phosphate buffer pH 7.0. The oxidation of NADH was determined at 340 nm. Reactions were carried out at 15 °C in quartz cuvettes, and the adsorption at 340 nm was recorded at 0.1 s intervals over 1 min with a HP8452 spectrophotometer (Agilent Technologies, Les Ulis, France). A NADH absorption coefficient of 6,220 $M^{-1}.cm^{-1}$ was used to calculate enzymatic activity from the initial linear portion of the time course. (Jouanneau and Meyer, 2006)The enzyme activity with naphthalene or pyrene (U/mg) was taken as 100 for URS-6 and 10, respectively.

Table A3. Kinetic parameters and substrate specificity of the purified PD and ND

Enzyme	Substrate	Vmax (mM/min)	Km (mM)	Relative activity(%)
Naphthalene Dioxygenase (URS-6)	Naphthalene	17.64	2.7	100
	Pyrene	6.41	7.9	21
Pyrene dioxygenase (URS-10)	Naphthalene	0.49	6.1	< 5
	Pyrene	9.53	3.4	100

Enzyme identification

Based on enzyme activities, degradation of three PAHs and PCA analysis, the most promising consortium was selected and used to produce enzymes. In this regard, the selected consortium was grown on optimal media and incubated at optimum conditions. Following incubation, the cell extract was used to check enzyme activity. The proteins remained in the samples were identified by carrying out LC-MS/MS to confirm the presence of target enzyme in enzyme mixture obtained from multi-culture. An enzyme cocktail was prepared using the suspension trapping (S-Trap) method, as described in our previous study, to serve as a reference data set for peptide spectrum match (PSM) analysis of target enzymes.(Miri et al., 2022) In order to determine the mass of the peptides, a mass spectrometer coupled to an EASY-nLC system (Thermo Fisher Scientific, USA) was used, and the peptides were analyzed via mass spectrometry-mass spectrometry sequence analysis using an Orbitrap Elite mass spectrometer (Thermo Fisher Scientific, USA) as described in the supplementary information (Section 6). The raw data was processed using the software Proteome Discoverer (Version 2.2, Thermo Fisher Scientific, USA), then aligned them with the protein databases of UniProt (www.uniprot.org) and BLASTP (www.blast.ncbi.nlm.nih.gov). (Jardine et al., 2018; Ma et al., 2021; Miri et al., 2022)

PAH analysis in soil and water

The release of PAHs to soil following crude oil spill and its biodegradation in the presence of pre-selected strains and enzymes solutions were confirmed by GC-MS (Agilent model 6890-GC, 5973-MSD) analyses which were carried out before and after incubation. (Li et al., 2021b) Biotic and abiotic controls were used in the same conditions. The preparation of samples for GC/MS analysis was described elsewhere in detail. (Li et al., 2021b) Regarding the soil sample, the moisture content of the soil was determined, followed by the weighting of 3–5 grams of sample soil into 40-mL glass tubes (with covers), into which the internal standards (ISTDs) were prepared for addition and weighed to achieve a final concentration of 1.0 $mgmL^{-1}$ (for pyrene-D10) and 0.7 $mgmL^{-1}$ (for chrysene-D12, anthracene-D10, and acenaphthene-D10 each). The tube was filled with 2.5 grams of diatomaceous earth (DIONEXTM, Fisher Scientific, Canada). Each sample was thoroughly mixed with 20 mL of dichloromethane (HoneyWellTM, Fisher Scientific, Canada), followed by sonication for 30 minutes. A concentrated solution of five grams of silica (SiliCycle, Canada) was added to the tube, and the entire apparatus was shaken on a wrist shaker (Burrell Wrist Action

Shaker-385 oscillations/min) for 10 min. 5 mL of the supernatant was transferred into a calibrated glass tube, and then the volume was reduced to one mL (35 °C with nitrogen gas) for GC/MS analysis (1 mL/min, 35 min 300 °C,). Based upon the fact that the soil for testing was collected in the province of Quebec (Canada), the local soil PAH threshold of 0.1 $mg.kg^{-1}$ was used as a benchmark in assessing the efficacy of treatment. (Beaulieu and contaminés, 2016) The quantification was carried out using a standard curve constructed using by extraction of p-xylene spiked soil samples. The standard calibration graphs were linear with correlation coefficients (R2) being greater than 0.995. (Miri et al., 2022)

Regarding the water samples, the fermentative medium (20 mL) containing the remaining PAHs and metabolites and surrogate standards (Acenaphthene D10, Chrysene D12, Anthracene D10 each – 0.7 $\mu g \bullet mL^{-1}$, Pyrene D10 – 1.0 $\mu g \bullet mL^{-1}$; purchased from Chromatographic Specialties Inc., Canada) were added to glass tubes (50 mL with covers). After mixing, dichloromethane (20 mL) was added to each sample and mixed thoroughly for 30 minutes. 5 g of silica (SiliCycle, Canada) was added, and the tube were shaken on an oscillating shaker. 5 mL of supernatant were withdrawn and transferred in a calibrated glass tube, reduced to 0.5 mL (36°C with nitrogen gas) and then analyzed by GC/MS (1 mL/min, 35 minutes, 300°C) (Li et al., 2021b)

Enzyme stability in soil batch test

After determining the formulation of the synthetic bacterial consortia for enzyme production, to obtain information on the activation of the key enzymes by activators, the effect of Fe_3S0_4 on the activity of naphthalene, catechol and pyrene dioxygenase obtained from strains was studied. Separate batch tests were run on the columns in sealed 150 mL serum bottles with aluminium caps and rubber septa with the same conditions as soil columns (static incubation at 15°C). An enzyme mixture was mixed with 2 g of dried soil that had been contaminated with p-xylene. In this experiment, two control groups were created: (1) soil sample without any enzymatic treatment, and (2) enzyme mix without soil. Over a period of four weeks, subsamples were collected every two days to measure residual activities for ND, PD, CD, HY, PCA.

Soil characteristics

Grain size distribution and characteristics of the soil are summarized in Table A4. The size of particles between 500 µm and 2 mm was used for column tests.

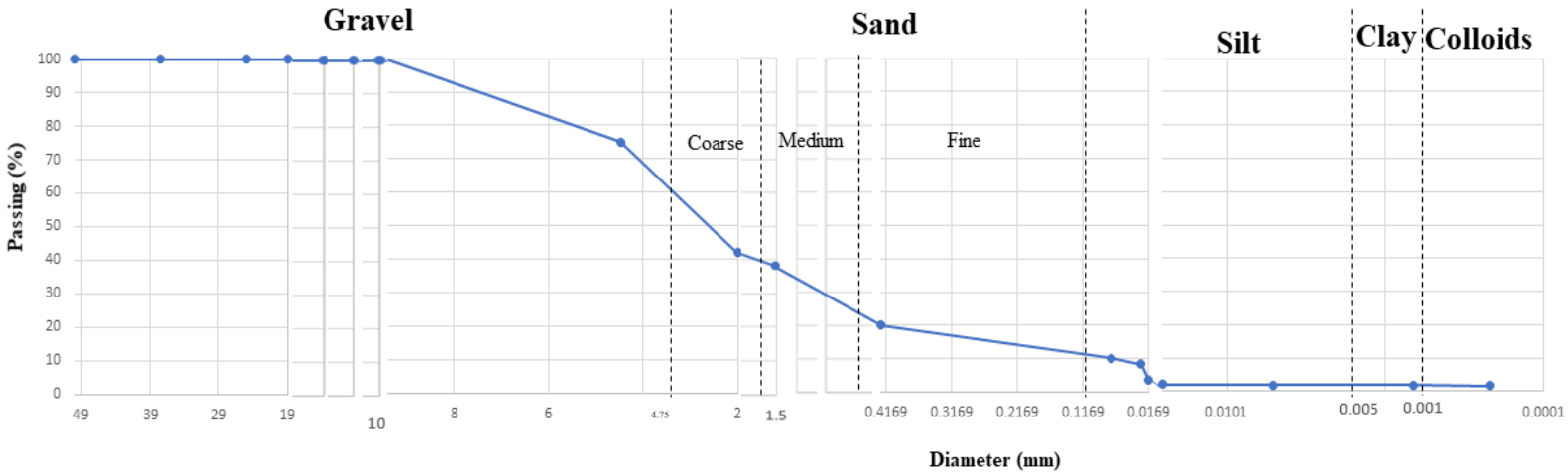

Fig. A2. Particle-size analysis of soi

Table A4. Size analysis of soil (Standard method form (ASTM, 2007))

Diameter (mm)	50	37.5	25	19	9.5	4.75	2	0.425	0.075	0.0289	0.0169	0.0121	0.0086	00.42	0.0018
Passing (%)	100	100	100	100	100	75	42	20	10.2	8.4	3.6	2.2	1.9	1.8	1.7

Table A5. Physico-chemical properties of the soil from a contaminated site.

Physico-chemical properties		
pH		6.1±0.5
Organic matter		9.5 g/kg
Porosity		0.29± 0.08
Moisture content		13.6±0.5 (% dry weight)
Water holding capacity		71±2 (%)
Total carbon		2.6±0.3 (%)
Nitrogen		0.2± 0.1 (%)
Soil type	Gravel	25.0 (%)
	Sand	64.8 (%)
	Silt	8.3 (%)
	Clay	0.1 (%)
	Colloids	1.8 (%)
The mineralogical composition from XRD crystallography	Montmorillonite	0.5
	Calcite	1.3
	Dolomite	5.4
	Aragonite	15.6
	Quartz	24.4
	Gibbsite	52.8

Table A6. Soil column treatment and experimental conditions.

Soil column No.	Experimental properties	Treatment duration	Description
1	Autoclaved soil column	3 weeks	As a sterile control for determination of natural biodegradation rate
2		6 weeks	
3	Untreated soil column	Time 0	As a control for determination of the initial concentration of contaminant and natural biodegradation rate
4		3 weeks	
5		6 weeks	
6	Treated soil column with Mix7-3PAHs*	3 weeks	Mix7-3PAHs: cell extract obtained from Mix7 incubated on solution of 3PAHs
7		6 weeks (with an enzyme injection after 3 weeks)	
8	Treated soil column with Mix8-D**	3 weeks	Mix8-D: cell extract obtained from Mix8 incubated on solution of Dilbit
9		6 weeks (with an enzyme injection after 3 weeks)	
10	Treated soil column with autoclaved *AlcanivoraxD*	3 weeks	Autoclaved *AlcanivoraxD*
11		6 weeks (with an enzyme injection after 3 weeks)	

Mass distribution of pyrene in soil

A set of equilibrium isotherm equations has been developed to explain how pyrene is fixed from a solution to the surface of soil particles. The adsorption process was described in linear form using three adsorption models: Langmuir (Eq. (A1)), Freundlich (Eq. (A2)), and Distributed reactivity model (DRM) (Eq. (A7)).

$$\frac{C_e}{q_e} = \frac{1}{bQ_o} + \frac{C_e}{Q_o} \text{ (A1)}$$

$$\log Msoil = \frac{1}{n}\log C_e + \log K_f \text{ (A2)}$$

Here, Q_o (mg/g) represents the maximum adsorption capacity of the soil; C_e the concentration of pyrene at equilibrium after sorption (mgl^{-1}); b represents the binding energy constant; K_f and n represent Freundlich isotherm constant (the capacity of the sorbent); and constant indicative of sorption intensity. These constants are calculated by regressing logarithms of the sorbed mass on soil particles ($Msoil$) and logarithms of the equilibrium pyrene concentration in the liquid phase (Ce).

The DRM describes sorption as a function of both linear and nonlinear isotherms. In this case, the linear isotherm is represented by Eqs. (A1) and (A2), and the non-linear isotherm by Eq. (A3). The DRM in Eq. (3) can be calculated by combining Eqs. (A4) and (A6). (A7).

$$Msoil = x_i K_D C_e + \sum_{i=1}^{m} (x_{nl})_i K_{F_i} C_e \text{ (A3)}$$

x_i represents the summed mass fraction of a solid phase exhibiting linear sorptions, and $(x_{nl})_i$ represents the mass fraction of a solid phase that exhibits nonlinear sorptions, $K_D$is the mass-averaged partition coefficient for the summed linear components. A Freundlich isotherm model was used for multi-component adsorption systems to investigate the effect of the presence of enzymes in the solution on the adsorption of pyrene and subsequently the distribution of pyrene in soil as described in our previous work. (Miri et al., 2022) Based on the definition of the error function (standard deviation of relative errors) described in our previous work, the minimum error distribution between the predicted isotherm and experimental data was calculated using a non-linear regression method as described in our previous work. To investigate the effect of enzyme

content on pyrene adsorption, the experimental data were analyzed statistically by hypothesis testing using the Chi-square test (χ). The null hypothesis Ho is that pyrene adsorption increases with increasing enzyme content. Alternative hypothesis Ha: enzymes decrease pyrene adsorption (Kaushal and Singh, 2017).

$$\chi^2 = \sum_{i=1}^{n} \frac{\sum(q_{calc} - q_{exp})^2}{q_{exp}} \quad \text{(A10)}$$

Where n is the number of observations in the experimental data; q_{calc} (mg/g) and q_{exp} (mg/g) are, theoretically calculated and experimental adsorption capacity at equilibrium, respectively.

Effect of inducers and consortia on enzyme activity

Naphthalene dioxygenase activity (ND)

The cell lysate from cultured *Pseudomonas* sp. URS-6, in the presence of 50 mg l^{-1} of 3PAHs solution showed high activity for naphthalene dioxygenase (34.7 U/mg protein) measured compared to other strains after 8 hours of incubation. The results from enzyme activity for different consortia and inducer showed that the highest of 43.1 and 33.5 U/mg protein naphthalene dioxygenase activity (U/mg protein) were exhibited by the consortium Mix1-3PAHs after 8 hours of incubation at 15 ˚C (Figure.S3.). Thus, results showed that Mix1 when incubated on PAHs had a better effect than any single bacteria, suggesting the strains worked synergistically to enhance the degradation efficiency.

Naphthalene dioxygenase activity for consortium incubated on Dilbit ranged from 7.5 to 33.5 and 5.4 to 9.5 U/mg protein after 12 hours of incubation in consortium with/without *Alcanovorax*, respectively. Thus, the addition of *Alcanovorax* to PAH degrading consortium enhanced the activity of ND and it reached to its optimal value after 12 hours of incubation. However, mixture of 3 PAHs proved to be the most advantageous inducer for most of the consortiums. In other words, in terms of naphthalene dioxygenase activity on tested inducers for consortiums there was a trend that 3PAHs > Dilbit.

Pyrene dioxygenase activity (PD)

Only the cell lysate from *Rhodococus* showed activity (17.4 U/mg protein) for pyrene dioxygenase after 12 hours of incubation on 3 PAHs. The pyrene dioxygenase activities by the bacteria consortia included URS-10 incubated on 3 PAHs, and Dilbit ranges from 4.1 (Mix5) to 18.3 (Mix 3) U/mg protein after 12 hour of incubation, 4.8 (Mix 5) to 24.1 (Mix 4) U/mg protein after 8 hours of incubation, respectively. The highest of 24.1 and 19.7 U/mg protein activity was estimated on 8 hours of incubation for Mix4-D and Mix8-D. Thus, in order to obtain a consortium with high activity of pyrene dioxygenase, it will be necessary to include Dilbit and *Alcanovorax*.

Catechol 2,3 dioxygenase (C2,3D)

In the environment, catechol 2,3 dioxygenase is one of the important enzymes involved in the degradation of aromatic molecules by soil bacteria. It catalyzes the incorporation of dioxygen into catechol (and its derivatives), and the cleavage of the extradiol ring to form 2-hydroxymuconate semialdehyde. The cell lysate from cultured *Pseudomonas* sp. URS-5 (30.3 U/mg protein) and URS-6 (33.1 U/mg protein), in the presence of 50 mg l^{-1} of 3 PAHs showed high activity catechol 2,3 dioxygenase measured compared to other strains after 12 hours of incubation (P-value <0.05). The highest of 35 U/mg protein extract catechol 2,3 dioxygenase activity for Mix1-3PAHs, showed that the activity of catechol 2,3 dioxygenase did not increase significantly (P-value<0.05) in consortia compared to pure cultures. Moreover, the cell lysate from pure cultures incubated on 3 PAHs showed higher activity for catechol dioxygenase (ranges from 10.2 to 33.1 U/mg protein) compared to those strains incubated on Dilbit (ranges from 6.6 to 17.4 U/mg protein). However, catechol dioxygenase activities by the bacteria consortia, Mix8-D, reached to 29.7 U/mg protein due to the synergistic effect of bacteria on the promotion of enzyme production after 12 hours of incubation.

1-hydroxy-2-naphthoate hydroxylase (HY)

Since the enzymes of the naphthalene pathway are important to catalyze the mineralization of phenanthrene and pyrene, it is apparent to test the 1-hydroxy-2-naphthoate hydroxylase activity of the consortia in order to attain the maximum degree of degradation of the pyrene. Only the cell lysate from *Pseudomonas* sp. URS-5 and URS-6 showed activity 1-hydroxy-2-naphthoate

hydroxylase after 12 hours of incubation on 3PAHs. In this study, of all the tested consortia, Mix8-D produced the highest 1-hydroxy-2-naphthoate hydroxylase activity (15.3 U/mg protein) after12 hours. Whereas Mix1-D produced the lowest activity (3.2 U/mg protein) after 12 hours of culture conditions compared to other consortia (Figure. S3a). In the case of 3 PAHs mixture, the highest of 11.9 and 14.4 U/mg protein activities were shown by Mix1 and Mix3 after 12 and 14 hours of incubation, respectively.

Protocatechuic acid 3,4-dioxygenase (PCAD)

Aerobic biodegradation of aromatic compounds generally occurs via the catabolic intermediate's catechol (1,2-dihydroxybenzene) or protocatechuate (3,4-dihydroxybenzoate) and is mediated by metabolite-specific pathways (lower pathways). Most of the metabolites, dicarboxylic aromatic acids and partially oxidized compounds, formed as a result of the utilization of growth substrates (phenanthrene, pyrene, or fluoranthene) by multibranched pathways including meta and ortho-ring-cleavage reactions, can be degraded by other strains. Thus, the enhancement of biodegradation of high-molecular-weight PAHs in the environment usually achieved by applying consortia of PAH degrading isolates or gathering enzymes responsible for PAH metabolism.

Phthalate is generally considered as a partially oxidized dead-end product if the enzymatic pathway for phthalate metabolism is not available in the system. These metabolic pathways (e.g., phthalate metabolism) can be induced by metabolites in consortiums, or the catabolic pathways for target dead-end products and metabolites of other metabolisms share some enzymatic steps that are induced by metabolites. In this study, the activity of phthalic acid dioxygenase (protocatechuic acid (3,4, dioxygenase)) was assessed. Only the cell lysate from *Pseudomonas* sp. URS-8 showed activity protocatechuic acid (3,4, dioxygenase) after 14 hours of incubation on 3 PAHs. The highest of 59.7 U/mg protein protocatechuic acid (3,4, dioxygenase) activity for Mix5-3PAHs, showed that the activity of protocatechuic acid (3,4, dioxygenase) increased significantly (P-value > 0.05) in consortia compared to pure cultures URS-8 (44.5 U/mg protein). Mix6-D produced the highest activity (61.4 U/mg protein) of PCA 3,4-dioxygenase after 14 hours. As a result of the use of Dilbit for enrichment of these bacterial strains and their subsequent culture in

these inducers containing NB media with *Alcanivorax* borkumensis, the highest PCA 3,4-dioxygenase activity may have been observed.

The results of this study also showed that the enzyme production increased in the multi-culture of selected strains. Genetically engineered microbes have been suggested for achieving preferable biodegradation pathways within a single strain of bacteria. However, it is possible to combine enzymes from different bacteria and devise multi-step catalysis for the degradation of PAHs. In addition, environmental risks associated with the release of genetically engineered organisms in the environment must be considered.(Miri et al., 2019)

Table A7 Pyrene sorption isotherm parameters for the Langmuir, Freundlich, and Distributed Reactivity Models (DRM).

DRM		Freundlich sorption model			
qT(1+nl)mg/g)	r2	qe(mg/g)	n	kf	r2
1.90	0.979	1.71	0.61	0.15	0.833

Table A8. Characterization and initial condition of the soil column experiment

Soil column No.	Column volume (cm^3)	Soil density in column [(1)] (g/cm^3)	Soil intrinsic permeability (m^2)	Pore volume (cm^3)	Hydraulic conductivity (K_w)
1	140.39	1.88	$7.5\text{-}9.2\times10^{-13}$	50±0.5	1.3×10^{-6}
2	139.37	1.79		49±0.5	1.4×10^{-6}
3	141.41	1.71		50±0.5	2.4×10^{-6}
4	140.39	1.72		50±0.5	2.2×10^{-6}
5	139.36	1.82		49±0.5	1.5×10^{-6}
6	140.39	1.78		50±0.5	2.3×10^{-6}
7	139.36	1.90		49±0.5	2.4×10^{-6}
8	139.36	1.84		50±0.5	2.5×10^{-6}
9	139.36	1.90		50±0.5	1.6×10^{-6}
10	139.36	1.81		49±0.5	2.9×10^{-6}
11	140.39	1.70		50±0.5	1.7×10^{-6}

(1) Soil density was selected based on site soil density ranging 1.7-1.9 g/cm^3.

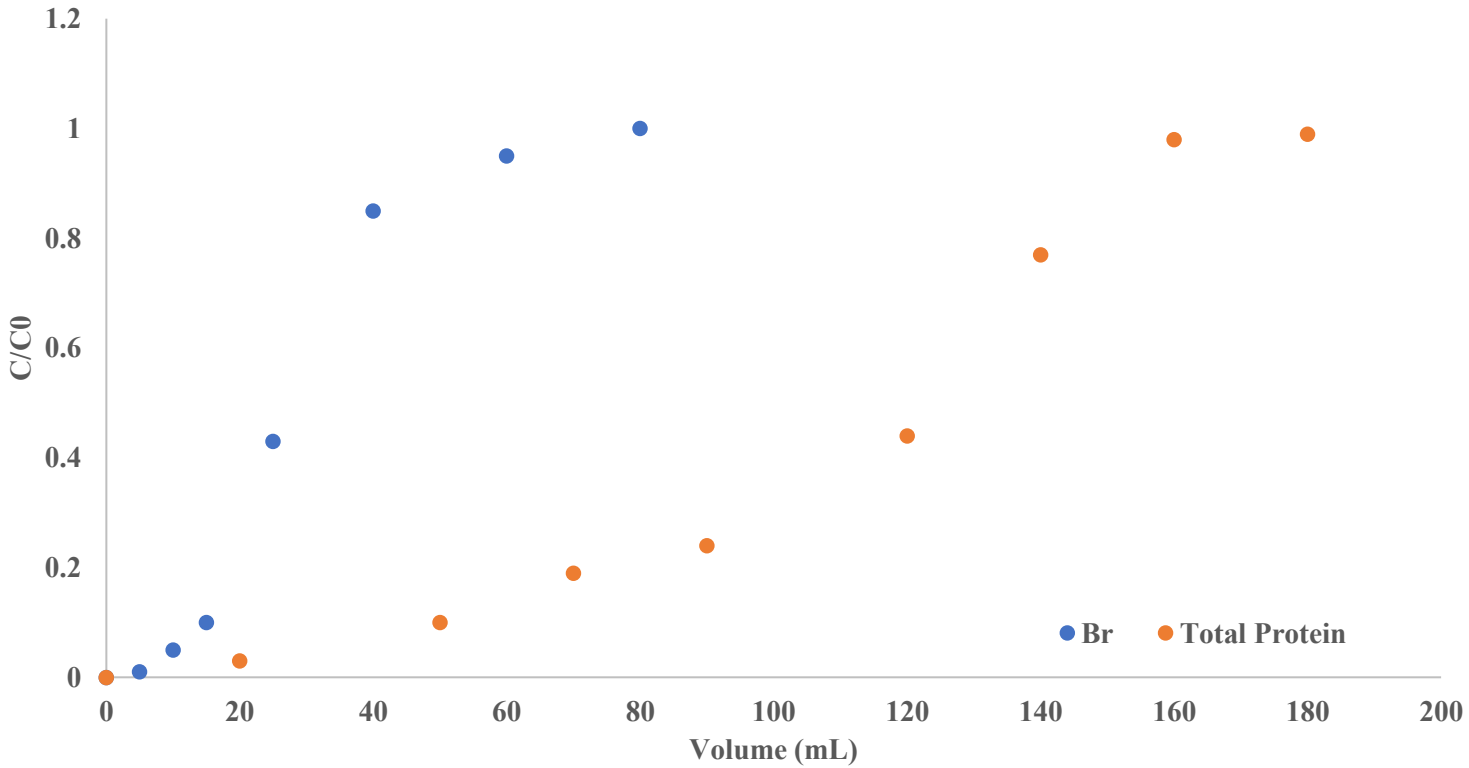

Fig. A 4. Relative concentration on the breakthrough curve for trace element (Br^-) and total protein in the effluent sample during enzyme injection.

Table A9. Parameters of the Freundlich adsorption isotherm model for the enzyme (Low-level concentration of enzyme solutions; X/10) and p-xylene individually (Kfi, n from Eq. (A5)) and as a mixture (aij from Eq.(6))

	Protein	Pyrene
K_f	0.42	0.2
n	0.85	0.58
R^2	0.9	0.94
a_{i1}	1	-0.28
a_{i2}	-	-0.43

APPENDIX B. Supplementary information of section 4.2.

Aliphatic degrading enzyme study

Enzyme assays, immobilization efficiency and kinetic parameters

To obtain the enzyme solution for immobilization in electrospun fibers, the crude extracts produced from *A.borkumensis* SK2 included extracellular and intracellular enzymes (i.e., lipase, esterase and alkane hydroxylase) were characterized (Kadri et al., 2018b; Kadri et al., 2018c; Kadri et al., 2018d). Specific enzyme activity of 3-hydroxy acyl-CoA dehydrogenase (identified by LC-MS/MS) was determined by following the rate of NADH oxidation at 340 nm in 3mL of 100 mM Tris–HCl (pH 7.5), 2 M KCl, 5 mM $MgCl_2$, 75 mM NADH, 5 mM acetoacetyl-CoA, and 1.2 mg of the crude extract or 35 mg of immobilized crude enzyme onto electrospun nanofibers. The amount of enzyme oxidizing 1 μmoL of NADH per minute under standard assay conditions was defined as one unit of 3-hydroxy acyl-CoA dehydrogenase activity (Kumar et al., 2020b).

The spectrophotometric method was also used to assess the activity of lipase and esterase produced by *A.borkumensis* SK2 as described elsewhere (Kadri et al., 2018c). In brief, the activity of lipase was estimated by determining the amount of the *p*-nitrophenol released as a result of enzymatic hydrolysis of P-nitrophenyl palmitate (p-NPP) at 410 nm. 30 mg of *p*-NPP dissolved in 10 mL isopropanol/acetonitrile (4/1 v/v) and 90 mL assay buffer containing (Tris-HCL pH 7.5, $CaCl_2$, 4% v/w Triton X-100, 0.2 % w/v gum Arabic) were incubated in a 60 °C water bath until the solution became transparent. To 2.4 mL of the prepared substrate solution, 0.1 mL free enzyme solution or 35 mg of immobilized lipase were added (to separate tubes) and the reaction was performed at room temperature. The measurements were conducted at 410 nm in duplicate and the average was reported. One unit of lipase activity was defined as 1 um of the *p*-nitrophenol liberated per minute. Calcium chloride and Triton X-100 were applied to remove the turbidity from the reaction solution. Esterase activity was determined spectrophotometrically following the hydrolysis of P-nitrophenyl butyrate (*p*-NPB) at 405 nm. 3.43 mL of substrate solution containing: 1.12 mM *p*NPB dissolved in 50 mM phosphate buffer, pH at 7.2, also containing 0.43 M

tetrahydrofuran and 0.2% (N/P) Triton X-100, was added to 0.1 mL of enzyme suspension and 35 mg of immobilized esterase onto electrospun fibers in separate tubes (Taheran et al., 2017). The hydrolysis reaction was monitored for 20 minutes to determine *p*-nitrophenol liberated per minute. The *p*-nitrophenol standard curves (plate activity) were prepared with a concentration range of 0 – 13 g/100 μL at 405 and 410 nm (Glogauer et al., 2011).

After measuring the activity of free and immobilized enzymes, immobilization and protein loading yields were determined for the evaluation of immobilization efficiency using Eqs. (B1), and (B2) as given below (Miri et al., 2021b):

$$Protein\ loading\ yield\ (\%) = \frac{Amount\ of\ protein\ loaded}{Amount\ of\ protein\ introduced} \times 100 \quad \text{(B1)}$$

$$Immobilization\ \ yield\ (\%) = \frac{Amount\ of\ enzyme\ loaded}{Amount\ of\ enzyme\ introduced} \times 100 \quad \text{(B2)}$$

Moreover, immobilization of lipase, esterase, and 3-hydroxy acyl-CoA dehydrogenase in the middle layer of electrospun fiber was studied by analyzing enzyme leaching on different matrices (Taheran et al., 2017). An immobilized enzyme leaching test was performed using 35 mg of enzymes in 1 mL of sodium phosphate buffer (pH 7.0) with continuous stirring for 1 h, 6 h, 12 h, 24 h, and 48 h. The mixture was centrifuged at 16,000 × g at 4 ◦C and then the supernatant was analyzed for enzyme activity. The leaching (%) was calculated according to Eq. (B3):

$$Leaching\ (\%) = \frac{Amount\ of\ protein\ in\ supernatant}{Amount\ of\ protein\ immobilized} \times 100 \quad \text{(B3)}$$

The kinetic model proposed by Michaelis-Menten was applied to study the behavior of enzymes immobilized in electrospun nanofibrous membranes. About 1 mL of the enzyme mixture was added, which corresponds to 70, 68 and 21 U of lipase, esterase and 3-hydroxy acyl-CoA dehydrogenase. Finally, the kinetic parameters of the hexadecane degradation by enzyme mixture was determined by measuring the initial degradation rate of the substrate at different concentration. By applying the Michaelis-Menten equation to steady-state conditions, the initial velocity of the reaction is related to the concentration of the substrate by applying Equation S4 (Lonappan et al., 2018):

$$\frac{1}{V} = \frac{Vmax\ [S]}{Km + [S]} \quad \text{(B4)}$$

where V_m , [S] and K_m are the maximum reaction rate, the substrate concentration and the constant of Michaelis-Menten, respectively. The Excel Solver add-in was used to perform the nonlinear regression analysis. A statistical weighting scheme, $[(v_{obs} - v_{calc})^2/v_{calc}]$, was applied for the calculation of weighted squared residuals, where v_{obs} represents the observed reaction rate and v_{calc} is the calculated rate based on the kinetic parameters (V_{max}, K_M). Solver's Generalized Reduced Gradient (GRG) nonlinear solving method was used to fit the kinetic parameters toward the minimized sum of residuals (Borisova et al., 2018).

Finally, to study the synergistic effect between contaminant degradation and membrane adsorption, the degradation/adsorption first and second-order kinetics relation (Dai et al., 2011)

Fabrication and characterization of multilayer membrane

Middle layer PAN membrane

Mono and co-axial electrospinning were applied to fabricate the middle hydrophobic layer. The mono-axial electrospinning of PAN fibers was carried out using a PAN/DMF solution which was electrospun at a concentration of 20 wt% in terms of solid content, and stirred with a magnetic stirrer to form a homogeneous solution (Taheran et al., 2017). PAN nanofibrous membrane was fabricated by electrospinning with a rotatory drum collector (diameter = 10 cm, length = 25 cm). A field strength of 1.54 kV/cm, a voltage of 20 kV, a flow rate of 0.4 mL/h, and a rotational speed of 4000 rpm were selected for the electric field (needle and collector voltages). In addition, the distance between the needle tip and the center of the collecting drum was 18 cm, and the needle gauge was 22. A step motor drives the nozzles to oscillate in translation in a perpendicular direction to the cylindrical collector (rotary). During electrospinning, the membrane was electrospun for 15 hours and then washed with methanol for 120 minutes in order to remove residual solvents. After being washed with distilled water, the nanofibrous membrane sample was dried for 10h at 50 °C. The whole electrospinning set-up was placed in a sealed chamber with an exhaust system, as well as a heating system.

PAN hollow nanofiber were also prepared via co-axial electrospinning. This was accomplished by dissolving PAN in DMF to obtain a final polymer concentration of 20 wt %. The core solution was prepared by mixing 2 mL ultra-pure water solution, 30 mL glycerol, and 30 mL (about 21 mg total protein) of the crude enzyme produced by *A. borkumensis ordered from DSMZ (Braunschweig, Germany).* Enzyme activity measurement showed that addition of glycerol had

not affect on the lipase and 3-hydroxyacyl-CoA dehydrogenase activity. Thus, no washing up step was performed after sample preparation. The spinneret was comprised of two needles of coaxial stainless steel.(Ji et al., 2014) In order to obtain highly aligned core-shell fibers, a PAN nanofibrous membrane was electrospun under ambient conditions (T = 21 °C) and collected using a rotary drum collector (length = 25 cm, diameter = 10 cm). In order to form a compound droplet at the tip of the needle, the core solution and shell solution were pumped through two syringe pumps with a flow rate of 1 and 0.02 mL/min, respectively. The electrospinning distance is applied with a potential of several kilovolts by means of a high voltage source. When the potential reached approximately 10 kV, the charged compound droplet formed a conical structure (Taylor cone).(1-109.; Ji et al., 2014)

Skin layer

For the preparation of skin layers, PVDF solution (20 wt%) in DMF/acetone mixed solvent at a 7:3 ratio and PS solution (20 wt%) in DMF/THF mixed solvent at a 3:1 ratio were stirred for 24 hours at 50°C and room temperature. Activated biochar was added to a polymer solution at a ratio of 1.5 % (w/w) and stirred for 48 hours. Electrospinning was performed simultaneously on two polymer solutions using two nozzles located side by side. A constant angle of 80 degrees was maintained between the two nozzle tips (Jiang et al., 2015; Lin et al., 2013). Electrospun fibers were electrospun onto a flat, grounded collector (negative) and covered with electrospun middle layers at a voltage of 11 kV (positive), with a distance of 100 mm between the nozzle tip and the collector. One syringe contained 35 mL of neat PS solution while the other syringe contained 35 mL of neat PVDF solution. Single component nanofibrous mats were fabricated using single nozzle oriented perpendicular to the collector. Table.B1. shows the sample name of fabricated membranes and the corresponding electrospinning parameters to aid in the discussion.

Table.B1. The electrospinning parameters and nanofibrous mats' corresponding names

Sample	Method	Feed rate	Electrospun volume
PS	one-nozzle		
PVDF		0.3 mL/min	35 mL
PS/PVDF	two-nozzle	PS: 0.3 mL/min	25 mL
		PVDF: 0.1 mL/min	9 mL

As part of this investigation, the activated biochar was incorporated into the skin layers to enhance the ability of the membrane to adsorb emulsified oils. Usually the oil spilled in the sea, rivers or lakes contain oil emulsion and the literature reported a high capacity of activated biochar for the removal of emulsified oil from water (Chen et al., 2020). A schematic of the electrospinning process for the preparation of fibres is illustrated in Figure B1.

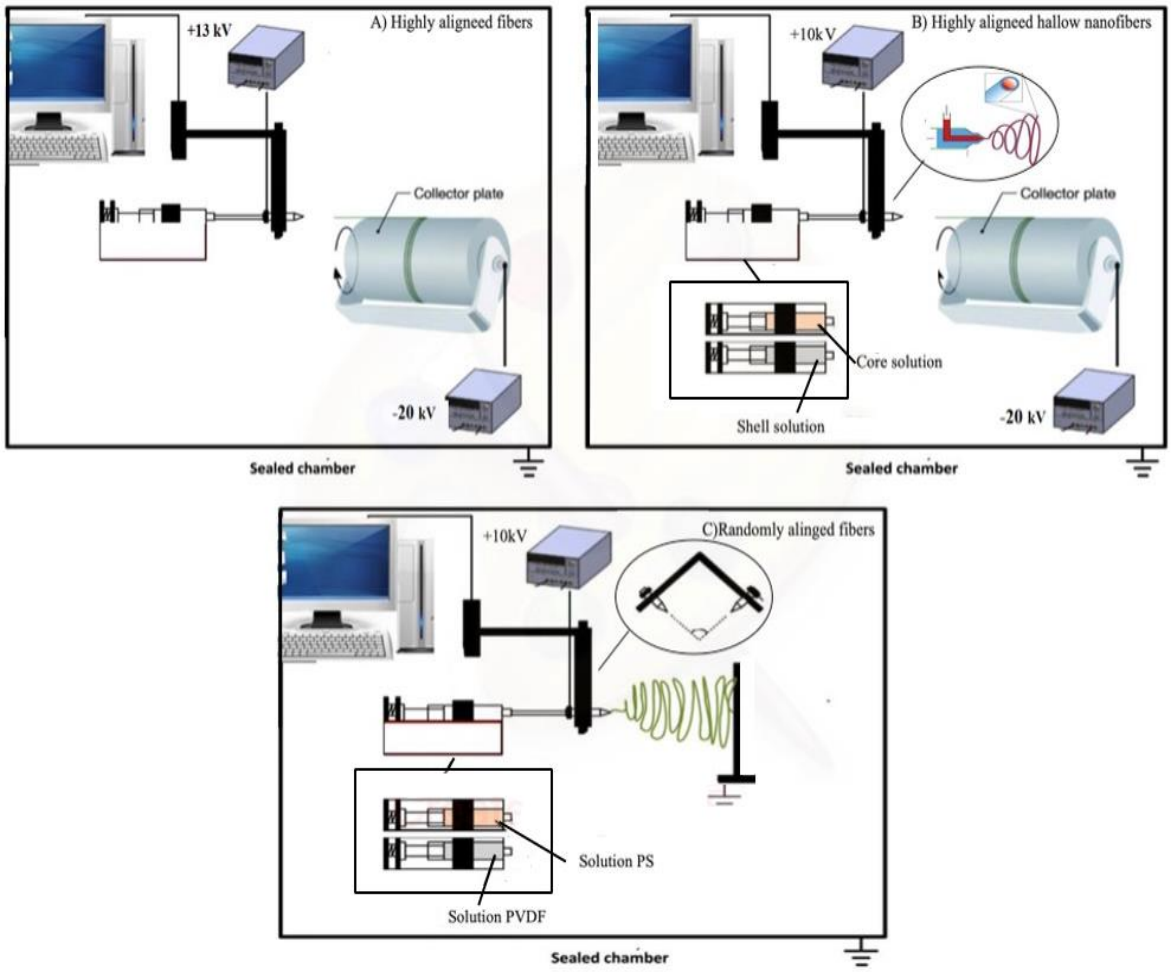

Fig.B1. Schematic illustration of the applied electrospinning set-up.

Characterization of fabricated electrospun membranes

A scanning electron microscope (SEM) (EVO-50, Zeiss, Germany) at an acceleration voltage of 10 kV was used to examine the surface morphology of the fabricated multilayer membranes. An SPI Module sputter coater was used to sputter a thin layer of gold on a small piece of the nanofibrous membrane as part of this analysis.

Fourier transform infrared-attenuated total reflectance (FTIR-ATR) spectra were recorded on a Nicolet iS50 spectrometer (Thermo Scientific, USA) in the range of 400–4000 cm^{-1} at 0.04 cm^{-1} resolution 85. The capability of fabricated membranes for adsorbing aliphatic compounds was studied on the multilayer samples. The tests for crude oil sorption capacity were carried out following the ASTM F726-60 standard (Yuan and Chung, 2012). Briefly, 10 g of oil was added to 150 mL water in a 250 mL glass bottle. The known weight of specimens was then gently placed on the oil/water mixture. The samples were retrieved using tweezers, drained for 30 seconds by hanging them in air and then weighed. The oil sorption capacity was quantified by the weight ratio as oil absorbency (g/g). At room temperature, the Instron 88215 tensile tester (load 5 kN) with a cross-head speed of 5 cm/min was used to determine the modulus of elasticity, tensile strength, and elongation at the break of the material. The data presented here are averages of three tests with a maximum error of 15 %. The dumbbell-shaped specimens standardized as DIN-53504 S3 for tensile tests were cut from the fibers (Duan et al., 2006).

To characterize the distribution of encapsulated enzymes inside the lumen of the hollow nanofibers, the crude enzyme was labelled by CFSE dye. Enzyme reactions with cellular esterases produce a stable fluorescent label (Banks et al., 2013; Shaikhulova et al., 2021). Confocal laser scanning microscopy (CLSM) was used to characterize these hollow nanofibers using a Leica TCS SP5 microscope (Leica Camera AG, Germany). The laser provided excitation of CFSE at 350 nm, and emitted fluorescent light was detected between 420 nm (Banks et al., 2013).

Hollow fibre membrane characterization

The test to measure diffusion air flow rate was carried out as described elsewhere. (Farahbakhsh and Smith, 2004) Briefly, UF membranes were wetted and pressurized with air to about 30 psi. On the shell side, valve 2 is closed and the valve 3 is opened to determine the volume of displaced air or liquid. The volume of air passing through the membrane is then measured and compared with values for diffusive airflow through an intact membrane. Figure S2 shows the setups for the membrane's diffusion flow rate determination. A diffusional flow reading higher than the specification is an indication of a non-integral filter.

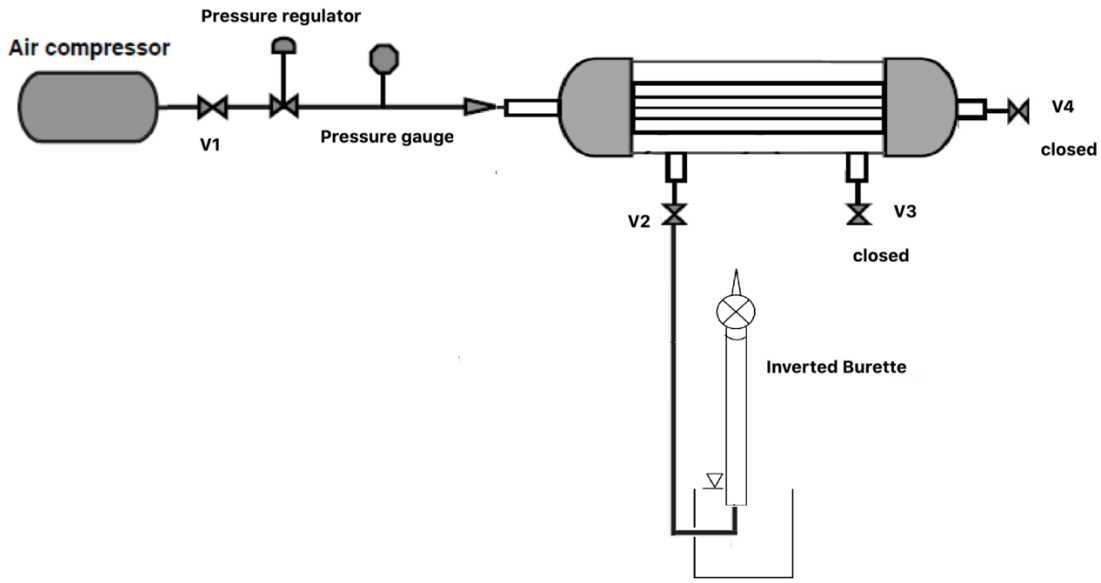

Fig.B2. The schematic diagram for measuring the diffusive air flow rates

The permeation equipment, shown schematically in Fig. S3, consisted of high-pressure liquid pumps, and the analytical instrument including a UV-visible spectrophotometer, was applied to determine retention (R) of co-enzymes (NAD^+) in continuous mode. The effect of salinity and polyethyleneimine (PEI) on NAD^+ retention ratio was also studied to determine the optimum condition for the physical entrapment of co-enzyme within the membrane. The main advantage of using PEI and enhancing of retainment ratio (R-value) for the coenzymes is that the kinetics of the enzymes does not change. (Obón et al., 1996)

Recycling-pump speed was fixed at 50 mL min^{-1} to circulate enzyme solution or co-enzyme (NADH) in 20 mM Tris-HCl buffer pH = 9. The retention of 1mM enzyme or coenzyme (NADH) inside the lumen of a hollow fibre membrane was studied by calculating the retainment ratio as follows

$$R = \frac{\ln\frac{C}{C_0}}{\ln\frac{V_O}{V}} \qquad \text{(B5)}$$

Where C, C_O , V and V_O are the solute (i.e., coenzyme) concretions and volumes of the inner solution before and after the permeation experiments. The concentration of co-enzymes (NAD^+) retained in pre-selected ultrafiltration with 10 kDa were measured via Biowave UV–vis spectrophotometer at 260 nm, respectively.

To determine the permeation coefficient for substrates, a single fibre reactor consisting of gas-liquid chromatography was applied. A mass exchanger equation was used to analyze experimental data (Eq.(6)): (Chambers et al., 1976)

$$\ln\left(1-\frac{C_{I\,(z=0)}}{C_2(z=l)}\right)=\left[\frac{-1}{\frac{1}{K_0}+\frac{a+b}{bk_i}\times\frac{(a+b)^{\ln\frac{a+b}{aa}}}{k_{i2}D_{i2}}}\right]\times\frac{1}{Q} \qquad \text{(B6)}$$

Where K_o, K_i, a, $a+b$, D_{i2} *and* K_{i2} are mass transfer coefficients for an external flowing stream, mass transfer coefficient for the internal flowing stream, the radius of the hollow region in fiber (I.D), the diffusion coefficient of permeating solute in fibre wall, and solubility of permeating solute in fibre wall respectively. The high flow rate of the internal flowing stream (100 mL/min) and vigorous agitation at 500 in a 1L flask were adjusted so that the first and second terms in the denominator of the quantity inside the brackets were small (the absence of internal and external diffusional limitation). By assuming the high mass-transfer coefficient for the external and internal flowing streams, the permeation coefficient of the substrate can be calculated (P_{i2}=$k_{i2}D_{i2}$).

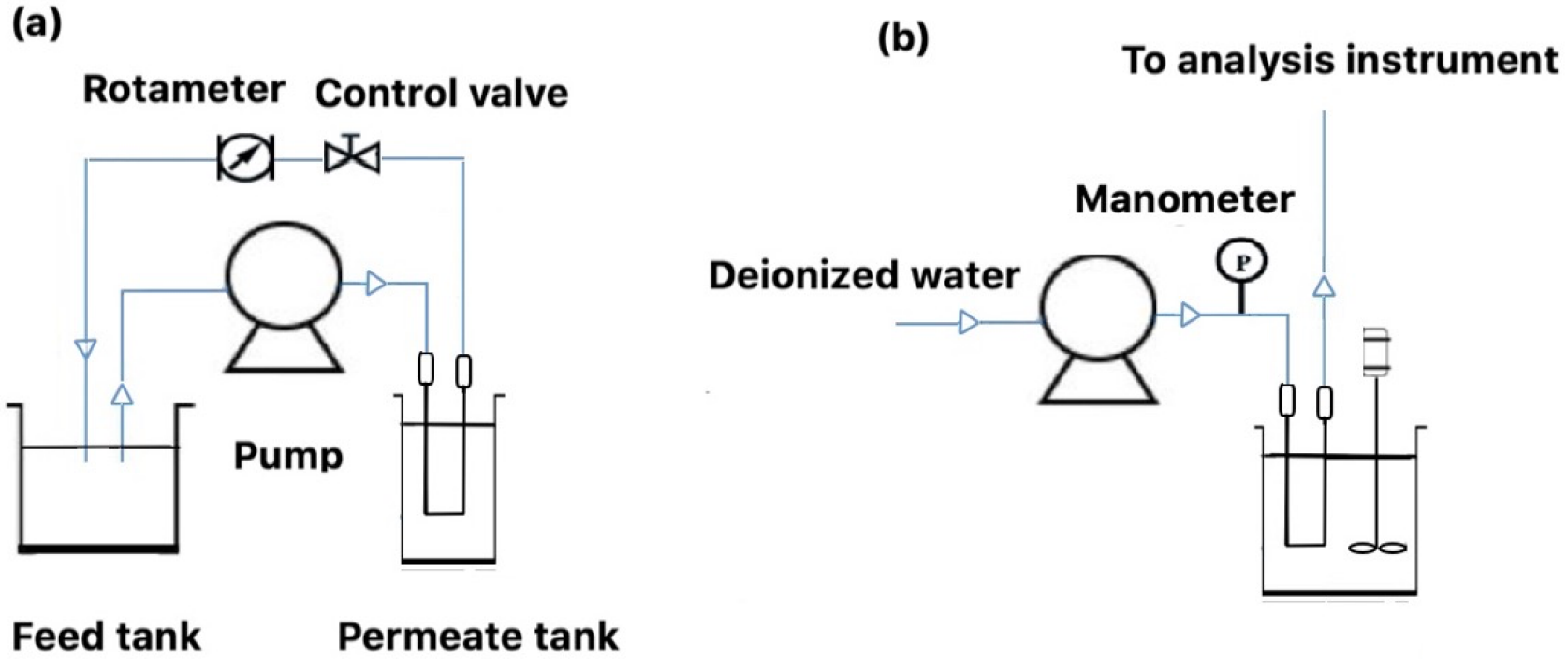

Fig.B3. Schematic illustration of a single-fibre reactor for the study of permeation: (a) substrate and; (b) co-enzyme and enzyme solution